NOVA SCHOOL OF SCIENCE & TECHNOLOGY

DEPARTMENT OF MECHANICAL AND INDUSTRIAL ENGINEERING

NUMERICAL DEVELOPMENT AND OPTIMIZATION OF THERMAL STORAGE SYSTEMS BY PHASE CHANGE

JOÃO PEDRO ALVES PÁSSARO

Master in Energy

DOCTORATE IN MECHANICAL ENGINEERING

NOVA University Lisbon
July, 2022

NOVA SCHOOL OF SCIENCE & TECHNOLOGY

DEPARTMENT OF MECHANICAL AND INDUSTRIAL ENGINEERING

NUMERICAL DEVELOPMENT AND OPTIMIZATION OF THERMAL STORAGE SYSTEMS BY PHASE CHANGE

JOÃO PEDRO ALVES PÁSSARO

Master in Energy

Adviser: José Manuel Paixão Conde
Assistant Professor, NOVA School of Science and Technology, NOVA University Lisbon

Co-adviser: Luís Manuel Rodrigues Coelho
Assistant Professor, Polytechnic Institute of Setubal

Examination Committee:

Chair: Telmo Jorge Gomes dos Santos
Full Professor, NOVA School of Science and Technology, NOVA University Lisbon

Rapporteurs: José Joaquim da Costa
Associate Professor, Faculty of Science and Technology, University of Coimbra

Eusébio Zeferino Encarnação da Conceição
Assistant Professor, Faculty of Science and Technology, University of Algarve

Adviser: José Manuel Paixão Conde
Assistant Professor, NOVA School of Science and Technology, NOVA University Lisbon

Members: Telmo Jorge Gomes dos Santos
Full Professor, NOVA School of Science and Technology, NOVA University Lisbon

José Fernando de Almeida Dias
Associate Professor, NOVA School of Science and Technology, NOVA University Lisbon

DOCTORATE IN MECHANICAL ENGINEERING

NOVA University Lisbon
July, 2022

NUMERICAL DEVELOPMENT AND OPTIMIZATION OF THERMAL STORAGE SYSTEMS BY PHASE CHANGE

Acknowledgements

Despite this document being presented as result of individual work, it would not have been possible without the support, incentive and contribution of several people.
The work displayed in this thesis was achieved thanks to European Union, Horizon 2020, Research and Innovation Programme, Grant Project TESSe2b.

I would like to thank my advisers. To Professor José Manuel Paixão Conde (FCT/UNL) for his guidance, criticism and encouragement. For sharing knowledge and his inputs concerning this work throughout this academic quest.
To Professor Luis Manuel Rodrigues Coelho (EST/IPS), for backing this work and giving me the opportunities he gave and for his support, recognition and incentive in my academic and professional life and to the advancement my academic journey.

An honourable mention to professor João Lourenço (FCT), for the help provided with the LaTex template in use to adhere to the NOVA required publication standards.

I would like to express special appreciation to NKUA's (National and Kapodistrian University of Athens) team, which were responsible for running the laboratory experiments of the pre-prototype and prototype that were used for validations and confirmation of the numeric models presented in this thesis. Additionally, my thanks must be extended to Professor Georgios Evangelakis and UOI's (University of Ioannina) team for their contributions and collaborations concerning the academic research developments of this work. As well as all the partners of the TESSe2b project.

A thank you to Carlos Simão for the opportunity to take part in the collaboration in the food industry concepts developed with this thesis and opening up a new front for investigation, development new applications for PCM and numeric work.

A very heartfelt thank you to Dr. Amândio Rebola (IPS) for sharing his knowledge and experience of numeric work with me as well as providing a lot of help with the literature

research and all his input and insight concerning this work's development and academic documented results, without which, it would not have been possible, my sincere gratitude.

To all my colleagues and friends that contributed to help me finish this work.

My sincere gratitude to my family that supported, helped me whenever, however they could in my academic progress and ultimately in all aspects of my life, especially my parents, Vitor and Idalina, that always believed in me, without whom I would not be where I am today.

Lastly but not least, I would like to thank Rita for her love, care and concern, for being understanding and always pushing me to try and be a better person. I'm fortunate to have you in my life. And to José Armelim this work ise certainly dedicated to you in the hope that will help provide you with a better and brighter future.

Abstract

The building sector accounts for a large portion of energy consumption and carbon dioxide emissions in Europe reducing buildings energy footprint can bring significant decreases in energy consumption. In this specific case, reducing the energetic footprint in residential buildings is a step in the right direction. One way of achieving this is using renewable energies, however these have unreliable production windows, often with a mismatch between production and demand. Using the technical solutions presented here, this mismatch is bridged storing energy whenever it is available to use it when need, even when not available, thermally storing the energy. It was studied the behaviour of Phase Change Materials (PMCs) in heat exchanging and thermal energy storage applications using Computational Fluid Dynamic (CFD) tools. The work presented here successfully developed several technical solutions of heat exchangers for different thermal storage systems components and applications using PCMs, specifically the heat exchangers that would allow for the maximum benefit to use from the PCMs properties in order to heat, cool and provide domestic hot water (DHW) by means of a geothermal heat pump coupled with PCM enhanced boreholes . The heat exchangers developed are to be employed in the domestic storage tanks applications and in the geothermal boreholes, thus storing renewable energy from solar and geothermal sources for domestic use. Additionally, developing heat exchangers that allow either macro or microscopic encapsulation usage of PCM to help maintain the underground soil average temperature in order to benefit from geothermal heat pump efficiency. It was concluded from these applications that a good methodology was achieved that allows for thermal storage system based on PCMs to be used in residential dwellings either already existing and retrofitted or designed specifically for new residences and successfully decrease their overall energy consumption and carbon footprint.

Keywords: CFD, PCM, heat exchanger, geothermal boreholes, storage tanks, PCM applications, building energy efficiency.

Resumo

O sector dos edifícios corresponde a uma grande porção do consumo energético e emissões de dióxido de carbono na Europa. Ajudar a reduzir a pegada energética dos edifícios pode trazer reduções significativas no consumo de energia. Neste caso, reduzir a pegada energética de edifícios residenciais é um passo na direção certa. Uma maneira de atingir este objetivo é utilizando energias renováveis. Contudo estas tendem a ter intervalos de produção pouco fiáveis, em que as fases de produção e de consumo têm um desfasamento entre si. Com as soluções técnicas apresentadas este desfasamento é minorado, armazenando termicamente a energia quando disponível para que possa ser utilizada quando necessária. Foi estudado o comportamento de Materiais de Mudança de Fase (PCM em inglês) para aplicações de permuta de calor e armazenamento térmico de energia utilizando ferramentas de simulação de Dinâmica de Fluidos Computacional (CFD em inglês).O trabalho apresentado desenvolveu várias soluções técnicas de permutadores de calor para diferentes componentes de sistemas de armazenamento térmico recorrendo a PCMs, especificamente permutadores que permitem tirar o beneficio máximo da propriedades térmicas endémicas do PCM para aquecer, arrefecer e fornecer águas quentes sanitárias (AQS) através de uma bomba de calor geotérmica combinada com furos geotérmicos otimizados com PCMs . Os permutadores de calor foram desenvolvidos para serem instalados em tanques de armazenamento e em furos geotérmicos, armazenando energia renovável solar e geotérmica para uso doméstico. Adicionalmente, procurou desenvolver-se os permutadores de calor dos furos geotérmicos de modo a permitir a utilização do encapsulamento macro ou microscópico dos PCMs procurando alcançar a manutenção da temperatura média do subsolo, de modo a beneficiar a eficiência da bomba de calor geotérmica. Pode ser concluído destas aplicações que uma boa metodologia foi desenvolvida que permite a utilização de um sistema de armazenamento térmico com base em PCMs que possa ser utilizado em edifícios residenciais, novos, ou já existentes através de uma remodelação técnica das instalações e reduzir o consumo energético dos mesmos bem como a pegada de carbono.

Palavras-chave: CFD, PCM, permutador de calor, furos geotérmicos, tanques de armazenamento, aplicações com PCM eficiência energética em edifícios.

Contents

List of Figures

List of Tables

Acronyms

CFD	Computational Fluid Dynamics
CP	Specific Heat
DHW	Domestic Hot Water
DSC	Differential Scanning Calorimetry
EPBD	Energy Performance regarding Buildings Directive
GSHP	Ground Sourced Heat Pump
HTF	Heat Transfer Fluid
HVAC	Heating Ventilation and Air Conditioning
LHS	Latent Heat Storage
LHTS	Latent Heat Thermal Storage
NEPCM	Nanoparticles Enhanced Phase Change Materials
PCM	Phase Change Materials
PRESTO	PREssure STaggering Option
RNG	Re-Normalization Group
SIMPLE	Semi-Implicit Method for Pressure Linked Equations
SIMPLEC	Semi-Implicit Method for Pressure Linked Equations-Consistent
SST	Shear Stress Transport
TES	Thermal Energy Storage

TPS Transient Plane Source

ZEB Zero-Energy Buildings

1

Introduction

1.1 Background

Climate changes, depletion of fossil fuel reserves and consequent increase in their cost became a debated theme worldwide in the last few years. The root of these problems lies with increased usage of fossil fuels in all economic sectors, with special relevance regarding emerging economies like China and India. Fossil fuels (ex: coal, oil, natural gas) are non-renewable sources, since it takes millions of years to replenish and are being consumed much faster than replenishment. Another serious consequence of using such fuels lays with their combustion that releases carbon dioxide (CO_2) and other greenhouse effect gases that contribute to climate changes, as well as several other harmful gases that cause a variety problems both for the global ecosystem and to human beings. One potential solution for these problems is to minimize the consumption of fossil fuels, adopting measures of energy efficiency and changing the energy sources of all sectors to other alternatives.

Energy efficiency is one of the most effective methods, cost wise, to secure energy supply and to reduce greenhouse effects gases emissions and other pollutants. In many ways, energy efficiency can be considered the greatest European energy resource. As such, the European Union established an objective for 2020 is to reduce 20% of primary energy consumption, comparing with previous projections, this objective was designated by the Communication Commission as "Energy 2020" being a vital step to pursue the long term goals regarding energy and climate.

The greatest potential for energy saving lies with buildings. The plan defined by Horizon 2020 affects the designated instruments to trigger the process of renewal on public and private buildings and improve their energy performance as well as the equipment used within them. It promotes an exemplar behaviour of the public sector, proposing to quicken public building renovation rate through a binding objective and introducing energy efficiency criteria on public expenses. Furthermore, it considers that energy providers are obligated to create conditions allowing for their costumers to reduce their energy consumption.[1] The primary instrument to achieve this objective on the residential sector is the Energy Performance regarding Buildings Directive (EPBD). This European directive

proposes, among other measures, introducing building energy certification in all of the European Union countries. The energy certificate is to be delivered upon the building being constructed, remodelled, sold or rented. This certificate displays the actual building energy performance on an efficiency scale from A to G. In the majority of Member-States this certificate includes customized advice to improve the buildings energy efficiency and, therefore, reduce energy consumption. This directive (2010/31/EU) concerns a code or a set of guidelines, some of those are exemplified beneath but are not restricted to them.

- 2002/91/EC directive by the European Parliament and Council, December 16^{th} 2002, regarding building energy performance was altered. New substantial changes are to be introduced, it is convenient, for clarity, to proceed with its reformulation.
- A careful, rational, and efficient energy use should include, namely, oil based products, natural gas and solid fuels that constitute essential energy sources and, simultaneously, the main sources of carbon dioxide emissions.
- EU buildings represent 40% of the total energy consumption. The sector is expanding, as such it's to be expected an increase in its energy consumption. Therefore, the energy consumption reduction and usages of energy provided by renewable sources in the building sector are important steps needed to decrease Unions energy dependency and greenhouse gas emissions. Combined with a renewable energy source, the measures taken to reduce Unions energy consumption will allow for EU to meet the Kyoto Protocol goals regarding climate changes, honouring its long term commitment to keep the global temperature rise under 2ºC and its commitment to reduce by 2020 global emissions of greenhouse gases by at least 20% in relation to 1990 levels, and by 30% should an international pact is achieved. Decreasing the energy consumption and increasing energy consumption by renewable sources has an equally important role assuring energy provisioning, promoting technological advances, opening up job opportunities and regional development, particularly in rural areas.
- It is necessary to institute concrete actions to benefit from the great unused potential for energy saving in buildings and to decrease the major differences between State-Members regarding this sectors result.
- The measures intended to improve building energy performance should consider climate conditions e locations, as well as inside environment and economic profitability. These steps should not influence other building requisites, such as accessibility, security and perceived building use.
- Building energy performance should be calculated based on a methodology that can be differentiated both by countries and by regions. This methodology concerns, besides thermal characteristics, other factors with growing influence, like heating installations and Heating Ventilation and Air Conditioning (HVAC) systems, the application of energy for renewable sources, passive heating and cooling systems,

> shading, air handling, adequate lateral light and conception of the buildings themselves. The methodology for calculating energy performance should consider the buildings energy performance year-round, and not only during the heating season. Such methodology should bear in mind ruling EU norms.[2]

An important concept regarding energy saving and efficiency is building and implementation of Zero-Energy Buildings (ZEB). The concept behind this idea is to supply all the energy needs of a building through low cost resources, available on site, non-polluting and renewable. On a stricter level ZEBs should generate enough renewable power to match or exceed their annual consumption. These buildings use energy sources like electricity and natural gas when local production is not enough to meet the needs. When the opposite happens, the electrical surplus is exported to the public grid. In some cases it is possible to discount the value from a surplus period on a consumption period, balancing out the energy usage of the building. Matching the functionality of a ZEB without a network connection it is exceedingly hard, in particular because of the difficulty of properly storing energy. Despite energy production on the buildings, some might require other energy sources like natural gas, propane or butane for cooking, heating water that is not at the desired temperature or for emergency generators. Off-grid buildings are not able to match their needs using the same systems that connected to the public grid, being unable to either consume or supply the grid's energy. Consequently, these buildings need to be installed with renewable energy production systems that are over-dimensioned to supply the needs during low production periods like in winter, but that also means that it won't be possible to sell any surplus to the public grid in high production seasons like summer.[3]
One way to improve the energy performance of a building, production wise, is to install solar panels, they can be thermal, photovoltaic, or both. This allows supplying, at least partly, two of the main energy needs of a building, electricity and heating. Another way to improve the performance is using a Ground Sourced Heat Pump (GSHP) to heat and cool the building. The stable year-round soil temperature allows for a very efficient heat pump operation contributing to decrease the energy demand when heating and cooling the building. A relatively unknown technology as since appeared with great potential applications, the Phase Change Materials (PCM) are materials that allow storing a large amount of thermal energy for convenient use at specific temperatures.
Horizon 2020 TESSe2b Project, with ten partners from eight European countries that aims to correct the mismatch between energy supply and demand in a residential building, using a combination of renewable energy sources like thermal solar panels and GSHP with PCM storage tanks all being controlled by a smart self-learning system that will adapt the overall operating conditions targeting a decrease of 30% in the buildings energy consumption. It is within this context in which this thesis is framed, the work developed here will consist mostly on sizing heat exchangers to be used in storage tanks, holding PCM, that harness energy at an useful, specific temperature to be used when needed to heat, cool and to generate Domestic Hot Water (DHW) allowing for a reduction in the energy consumption

benefiting from renewable energy sources and variable electrical tariffs.

1.2 Motivation

Early on, the development of storage for electrical energy was a technology available, however storing thermal energy, although possible, was never an easy venture with considerable restrictions and drawbacks. However, the development and improvement of techniques and technologies allowed on site energy production from renewable resources in building energy applications, aiming to mitigate or remove altogether, when possible, the ecological footprint, perfecting already available systems in order to harness energy from renewable sources, increasing their efficiency.
The work reported in this document means to open the possibility to harness, store renewable energy to heat domestic hot water, cooling, heating of a building and production processes, when readily available while using it only when needed, avoiding the discrepancy between energy accessibility and consumption.
The experimental work enables to test and study the viability of techniques, methods and systems, further developing the studies of phenomena as basis for physical-mathematical models of the simulations. Numerical work is used to study methods and conditions that would be otherwise economically and timewise unfeasible, or downright impossible to perform experimentally. However numerical work is interconnected with experimental work, since it is by such means that the work developed numerically is verified to actually perform as expected and simulated, validating results. Thus, it is with the combination of these two methodologies that technological development is achieved.
The development and increased processing capacity of computers brought a greater importance to numerical simulation tools, opening new areas of applications which have been adapted to new possibilities. Numerical work is an excellent instrument to study and optimize flow regimes and test out varied operating conditions that would be otherwise hard to reproduce or measure, enabling several simulations within a relatively small time frame with reasonable accuracy without the usual hindrances associated with experimental work.
The development of new or improved technologies to better harness renewable energies is, typically, an ongoing process, with experimental work, physical and mathematical modelling and computational fluids dynamic simulations.

1.3 Objectives

The objectives of this thesis are to present the work developed in order to find an effective solution for thermal storage resorting to PCMs, employing both numerical modelling and experimental tests, to be implemented on energy storing solutions like residential buildings thermal needs and industrial processes applying renewable energy and recovering waste

heat. The study targets specifically the heat exchangers that would allow for the maximum benefit to use from the PCMs properties in order to heat, cool and provide DHW by means of a geothermal heat pump. The heat exchangers developed are to be applied on the domestic storage tanks applications and in the geothermal boreholes, thus storing renewable energy from solar and geothermal sources for domestic use.
This work will aim to choose the appropriate PCMs based on the most appropriate properties, heat exchangers geometries, different operating conditions like work materials and water flows, inlet and outlet temperatures, etc.
Regarding the DHW application an additional objective is to minimize the volume of the storage tank while maintaining at least the same heat providing capacity as a regular, commercial, equipment.
Another objective of the thesis is to develop heat exchangers that allow either macro or microscopic encapsulation usage of PCM to help maintain the underground soil average temperature in order to benefit geothermal heat pump operative efficiency. Therefore, the primary objectives of this study are to develop:

1) Thermal storage tanks heat exchangers for heating.

2) Thermal storage tanks heat exchangers for cooling.

3) Thermal storage tanks heat exchangers for domestic hot water.

4) Geothermal heat pump borehole heat exchangers with integrated encapsulated PCM.

Altogether, the objectives come down to developing technical solutions for two applications, one application is heat exchangers for PCM storage tanks different thermal energy requirement of a dwelling, another application for boreholes heat exchangers combined with PCM that work in combination with a geothermal heat pump. In order to ascertain what are the expected ranges of thermal needs for the demosites, and respective thermal storage systems, a series of building energy simulations were run using a simulation software, EnergyPlus, to gauge what considerations need to be taken into account to meet the requirements, providing the base for the work in this thesis to be developed. These energy simulations were run outside the scope of this work.

1.4 Thesis Outline

The presented work is divided in six chapters. The objective of this work was to not only develop a working numerical methodology with known models to help develop solutions heat storage system using the latent heat of phase change of PCMs, but ultimately use this as a tool that would lead up to actually building working prototypes and eventually working full-blown commercial installation systems. These, “thermal batteries“ would then be using in combination with other already known systems, such as geothermal heat pumps and thermal solar panels, to achieve heating, cooling, and domestic hot water production

for a dwelling or applications for decreasing waste heat in industrial processes. This system would be, in concept, be able to both be installed in a new system or, alternatively, be retrofitted into an already existing system, aiming to improve the thermal performance of the system and decrease its energy consumption.

- Chapter 1 introduces the reader to the topic at hand, providing context and background, the motivation behind the work and objectives established in the scope of the work, along with the outline for the thesis.

- Chapter 2 addresses the literary review for the PCMs as they are the most preponderant and new technology brought into consideration in this work and their properties are one of the core points to achieve the final objective while other technologies are already fully established and in regular use. The chapter introduces the general inner workings of the PCM advantageous properties and defects, its classifications and types, thermophysical properties testing methods, long-term stability, applications that have been tried out combining PCMs with other technologies, techniques for enhancing the PCM in order to minimize its defects, safety issues and economic payback.

- Chapter 3 presents the mathematical theory of Computational Fluid Dynamics (CFD) models used during the development of the work presented.

- Chapter 4 explains the methodology behind the work and its processes, decisions and ponderations considered for some of the values and approaches used throughout the thesis models' constructions in order to achieve the objectives.

- Chapter 5 details and analyses the acquired results of the studied CFD parameters that were deemed relevant, including comparisons with experimental work. This section addresses the applications aimed to be developed in this work. Section 5.1 and 5.2 present a series of preliminary studies to provide a frame of reference to start from, 5.3 goes on to build on these findings to parameterise the features of the heat exchangers and actually build a pre-prototype and demosite protoypes. Section 5.4 showcases the finding concering the boreholes developments and solutions.

- Chapter 6 summarizes the overall results conclusions and findings gathered from the work developed in the thesis, addressing also themes and considerations for possible further developments.

1.5 Peer-reviewed Academic Publications

The following documents are part of the knowledge that was the result of the work developed in this thesis:

- **J. Pássaro**, A. Rebola, L. Coelho, J. Conde, G.A. Evangelakis, C. Prouskas, D.G. Papageorgiou, A. Zisopoulou, I.E. Lagaris; Effect of fins and nanoparticles in the discharge performance of PCM thermal storage system with a multi passages finned tube heat exchanger; Applied Thermal Engineering; 2022 (https://doi.org/10.1016/j.applthermaleng.2022.118569)

- **J. Pássaro**, A. Rebola, L. Coelho, J. Conde; Numeric Study of Geothermal Borehole Heat Exchanger Enhancement via Phase Change Material Macro Encapsulation; International Journal of Thermofluids, Part of special issue: Sustainable Energy and Environmental Protection 2021. (https://doi.org/10.1016/j.ijft.2022.100245)

- C. Simão, J. Murta-Pina, **J. Pássaro**, L. Coelho, R. Lopes, F. Reboredo, T. Jorge, D. Lemos; Prospects for the Improvement of Energy Performance in Agroindustry Using Phase Change Materials; Springer 2021. (https://doi.org/10.1007/978-3-030-45124-0_26)

- C. Simão, J. Murta-Pina, J. Oliveira, **J. Pássaro**, L. Coelho, D. Ferreira, F. Reboredo, T. Jorge P. Figueiredo; A Case Study for Decentralized Heat Storage Solutions in the Agroindustry Sector Using Phase Change Materials; AgriEngineering 2022. (https://doi.org/10.3390/agriengineering4010018)

2

Literature Review

This chapter will address the literary review and state-of-the-art of the technologies of relevance employed in this thesis. Generally speaking, the technologies in on themselves that are mentioned throughout this work and their related applications are recognized, ripe applications, being the thermal solar panels, geothermal heat pump and heat exchangers. All these technologies have been in commercial use for well over 30 years, the possible exception being Phase Change Materials (PCMs). While having been employed for a few decades now, PCMs have been studied for thermal storage applications for quite some time, however exploitation on a commercial, final-user level has been limited until much more recently with companies starting to apply PCMs in technical solutions. The concept behind the work approached in this document aims at combining PCMs with other previously mentioned traditional, well established technologies with the objective of obtaining a synergy, bringing each other benefits together, ultimately combining technologies that have existed for a significant time in a manner that was never considered. Since of the technologies mentioned so far, PCM is the one that bears most significance both from the new technological solution point of view and from the importance to the system here developed, the review will focus on topics concerning these materials. Differing to this are the other more matured technologies that have been applied for several years now, whose behaviour and operation is very well understood, have not had significant developments, at least for the context addressed here, as such they will not be reviewed.

2.1 Thermal Energy Storage

Recent projections predict that the primary energy consumption will rise by 48% in 2040. On the other hand, the depletion of fossil resources in addition to their negative impact on the environment has accelerated the shift toward sustainable energy sources. Renewable energies such as solar radiation, ocean waves, wind, and biogas have been playing a major role in reforming the natural balance and providing the needs of the growing population demand. However, due to the climatic intrinsic variations, the means of storing these types of renewable energy has become urgent. This has led to a need to develop efficient and

sustainable methods of storing energy. Energy storage has become an important part of renewable energy technology systems. Thermal Energy Storage (TES) is an application that stores thermal energy by heating or cooling a medium so that the energy can be used at a later time for heating and cooling applications and even power generation. The TES systems are used in buildings and in industrial processes. Advantages of using TES in an energy system include an increase in overall efficiency and better reliability, and it can lead to better economics, reductions in investment and running costs, and less pollution of the environment, i.e., fewer carbon dioxide (CO_2) emissions. Solar thermal systems, unlike photovoltaic systems with continuously improving efficiencies, are industrially mature and utilize a major part of the Sun's thermal energy during the day. Yet, they do not have enough (thermal) backup to continue operating during the low or no solar radiation hours. TES is becoming important for electricity storage in combination with concentrating solar power plants where solar heat can be stored for later electricity production when sunlight is not available. New materials are selected, characterized, and enhanced in their thermo-physical properties to serve the purpose of a 24 h operation in an efficient TES system. In Europe, it has been estimated that around 1.4 million GWh/year can be saved and 400 million tons of CO_2 emissions avoided, in buildings and in industrial sectors by more extensive use of heat and cold storage [4].

Storage density, in terms of the amount of energy per unit of volume or mass, is important for optimizing solar ratio (how much solar radiation is useful for the heating/cooling purposes), efficiency of appliances (solar thermal collectors and absorption chillers), and energy consumption for space heating/cooling room consumption. Therefore, the possibility of using PCMs in solar system applications is worth investigating. PCMs might be able to increase the energy density of small-sized water storage tanks, reducing solar storage volume for a given solar fraction or increasing the solar fraction for a given available volume. It is possible to consider thermal storage on the hot and/or cold side of the plant. The former allows the storage of hot water from the collectors (and from auxiliary heaters) to be supplied to the generator of the absorption chiller (in cooling mode) or directly to the users (in heating mode). The latter allows the storage of cold water produced by the absorption chiller to be supplied to the cooling terminals inside the building. It is usual to identify three situations as "hot", "warm", and "cold" storage based on the different temperature ranges. Typically, a hot tank may work at 80–90°C, a warm tank at 40–50°C, and a cold tank at 7–15°C.

While heat storage on the hot side of solar plants is always present (because of heating and/or DHW) production, cold storage is justified in larger plants. Cold storage is used not only to gain economic advantages from lower electricity costs (in the case of electric compression chillers) depending on the time of day but also to lower the cooling power installed and to allow more continuous operation of the chiller.

The use of thermal storage, initially, could not provide effective backup but helped the system to thermally stabilize. Consequently, thermal storage found use in solar-assisted thermal systems. Since then, studying thermal energy storage technologies as well as the

usability and effects of both sensible and latent heat storage in numerous applications increased, leading to a number of reviews.

This section is focused on TES technologies that provide a way of capitalising solar heat and reducing the energy demand of buildings. The principles of several energy storage methods and calculation of storage capacities are described. Latent Heat Storage (LHS) systems associated with PCMs for use in the solar heating and cooling of buildings, solar water heating and heat-pump systems. Finally, cool thermal energy storage will be also briefly reviewed and outstanding information on the performance and costs of TES systems are included.

Due to intermittency in availability and constant variation in solar radiation, TES found its place in thermodynamic systems. TES not only reduces the discrepancy between the demand and supply by conserving energy, but also improves the performance and thermal reliability of the system. Therefore, designing efficient and economical TES systems is of high importance. However, few solar thermal plants in the world have employed TES at a large scale. Additionally, the design of TES systems in various domestic solar applications is currently being investigated. Using a CFD approach is also a widespread method to save money, in this case, where FLUENT software is used successfully for testing and developing different engineering applications, as it allows for physical simulations to study real processes without the expenses of building prototypes and running lab experiments.The main types of thermal energy storage of solar energy are presented in (Figure 2.1). An energy storage system can be described in terms of the following characteristics:

- Capacity - defines the maximum energy that can be stored in the system and depends on the storage process, the medium, and the size of the system;
- Power - defines how fast the energy stored in the system can be discharged (and charged);
- Efficiency - is the ratio of the energy provided to the user to the energy needed to charge the storage system. It accounts for the energy loss during the storage period and the charging/discharging cycle;
- Storage period - defines how long the energy is stored and lasts (i.e., hours, days, weeks, and months for seasonal storage);
- Charge and discharge time - defines how much time is needed to charge/discharge the system;
- Cost - refers to either capacity (€/kWh) or power (€/kW) of the storage system and depends on the capital and operation costs of the storage equipment and its lifetime (i.e. the number of cycles).

Capacity, power, and discharge time are interdependent variables. In some storage systems, capacity and power can also depend on each other. Typical parameters for

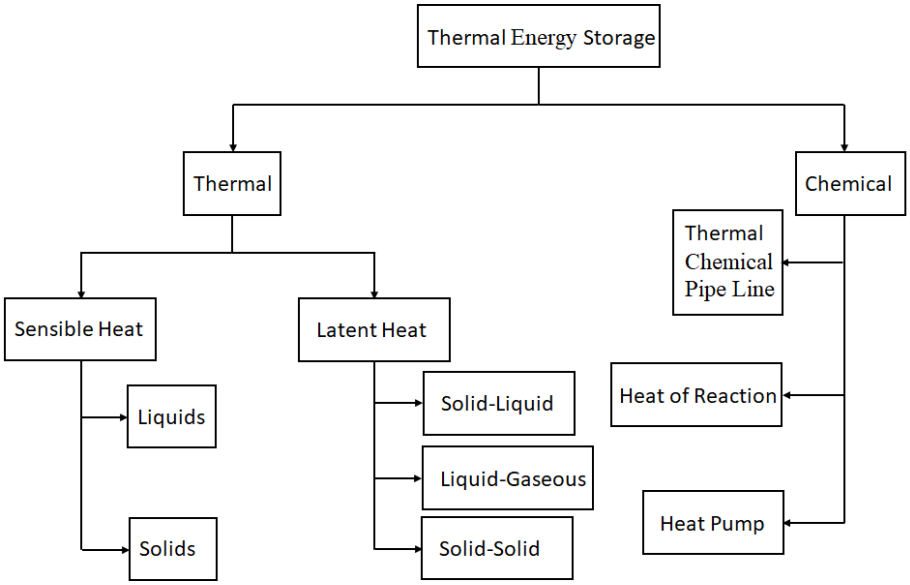

Figure 2.1: Types of thermal energy storage (TES). Picture adapted from.[5]

TES systems are shown in 2.1, including capacity, power, efficiency, storage period, and cost. High-energy storage density and high power capacity for charging and discharging are desirable properties of any storage system. It is well known that there are three methods for TES at temperatures from -40 °C to more than 400 °C: sensible heat, latent heat associated with PCMs, and thermo-chemical heat storage associated with chemical reactions (Figure 2.2) [5].

Table 2.1: Typical parameters of TES systems.

TES System	Capacity (kWh/t)	Power(MW)	Efficiency (%)	Storage Period	Cost (€/kWh)
Sensible (hot water)	10-50	0.001-10.0	50-90	days/months	0.1-10
Phase Change Material (PCM)	50-150	0.001-1.0	75-90	hours/months	10-50
Chemical Reactions	120-250	0.01-1.0	75-100	hours/days	8-100

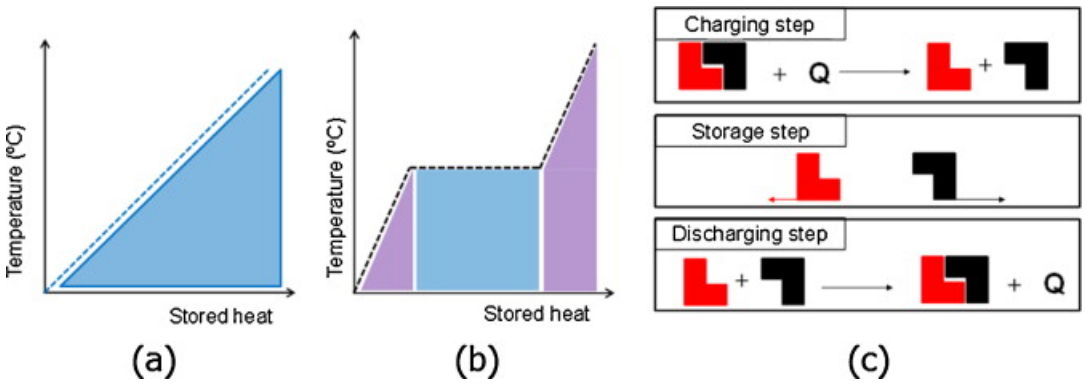

Figure 2.2: Methods of thermal energy storage: (a) sensible heat; (b) latent heat; (c) thermo-chemical reactions.[5]

2.2 Methodology

Thermal energy storage plays and important role in the good application of energy allowing for the decoupling of production and demand of energy. With applications with variable energy generation such as solar thermal systems or waste heat recovery, an appropriate thermal storage system is paramount. Thermal storage based on PCMs recently raised interest. Although the main criteria to select a PCM lies with its phase change temperature other parameters should be considered, such as: phase change latent heat, thermal conductivity and material stability. The low thermal conductivity of PCMs in particular leads to specific set of problems when using such materials since the needed energy might be available but the system will not be able to use it at the required rate. In this regard several ideas and systems have been proposed using both experimental and numerical solutions, leading to a considerable range of choices to address the matter, each with its own inherent advantages and disadvantages.

Plenty of models have been established for applications of PCMs. In most cases, simplified models and correlations functions have been developed for practical guidance in optimized designs of system using PCMs. Validation of numerical calculations should, ideally, always be performed by means of appropriate experimental data.

2.2.1 Geometry and Enhancement

Despite the excellent capacity for PCMs to store thermal energy at a desired temperature range their major drawback is, in most cases, their poor thermal conductivity that can deter actual applications for these materials. Therefore, a logical step would be to improve this property and for that, there are several methods that have various degrees of success for different types of PCMs. Some techniques rely on manipulation of the heat exchanger geometry to achieve the improvement needed to increase the overall thermal conductivity of the medium (the PCM and heat exchanger combination) using apparatus such as fins (radial and longitudinal), and porous matrixes. Other techniques use additional materials that are mixed together with the PCMs such as powders, particles of different size ratings and fibres, aiming to obtain a homogenous mixture throughout the medium. In all the mentioned cases, either the geometric features of the heat exchanger or the added material must replace a fraction of the PCM net volume.

In one study [6], lab experiments were performed with three different heat exchangers setups. One was a single copper pipe running through a PCM annulus, another was a pipe with longitudinal fins and a tube with helical fins all cases were equipped with 30 precise thermocouples spread throughout the test section. The aim being to study the heat storying density and the heat exchange power. The storage density of all the designs was close to 47,2 kWh/m^3, on average, for the charging process. The implementation of fins in the heat exchanger improved the heat exchange rate by a factor of 10 due to the increased surface area, reducing the melting time .

Darzia, Jourabian and Farhadic's work proposed a 2D enclosure, concentric annulus with the inner circular or an elliptical tube.[7] An inner elliptical tube is oriented horizontally or vertically. Two different aspect ratios of elliptical tube are considered. The outer tube is adiabatic and inner tube has a constant temperature. Different numbers of thin longitudinal fins (4, 10, 15 and 20) with length of 1.5 cm and thickness of 0.1 cm were placed on the inner tube. The net area of the enclosure (PCM zone) is 0.0049 m^2 and it is identical for all cases. During the melting process is was observable that adding copper nanoparticles to the PCM can augment the heat transfer rate resulting the acceleration of the melting process through improving the heat conduction of the mixture. To investigate the effect of adding nanoparticles, the simulation was performed inside a circular annulus filled by Nanoparticles Enhanced Phase Change Materials (NEPCM) samples having different volume fractions of copper nanoparticles. It was possible to see that the use of NEPCM sample engenders a faster growth of the solid–liquid interface. It was observed that the insertion of 2% and 4% of nanoparticles to the base PCM leads to the decrease of the full melting time by 25% and 46%, respectively. It must be emphasized that increasing the volume fraction of the nanoparticles leads to the augmentation of the viscosity of the mixture, but this influence is overcompensated by the increment in the thermal conductivity of the mixture. Although the full melting time was reduced generally by adding the nanoparticles, the melting of the PCM in the pure conduction zone beneath the hot cylinder takes unfavourably a long time from an energy-saving point of view. It can be concluded that adding nanoparticles does not improve the overall melting process and the undesirable effect of the stable heat transfer in the heat conduction dominated zone. During the solidification process the density of the solid PCM does not change sensitively with temperature. It was clear that the solid layers have identical thickness on all directions around the inner tube. Consequently, the conduction plays the dominant mode of heat transfer during the solidification process. Early on where the liquid PCM is in the direct contact with the cold wall of the inner tube, a thin layer of the solid PCM is formed around the cold tube and it then gets thicker as time passes. The thicker solid layer induces a higher thermal resistance and therefore, the solidification rate reduces temporarily. It seems that the solid front moves slightly with a faster speed by increasing the concentration of the nanoparticles, this was due to the enhancement of the thermal conductivity of the mixture by nanoparticles. It is quantitatively evident that the full solidification time is reduced by 9% and 16% by using 2% and 4% of nanoparticles. Concerning the fins effect, as stated already, in the melting part, a thin solid layer formed on the fin surfaces as well as on the cold tube at early time and then gets thicker as time passes more. Heat loss penetrates into the liquid PCM through surfaces of the fins. As expected, the solidification rate increases by adding fins. The solidification time is reduced by 28%, 62%, 75% and 85% by using 4, 10, 15 and 20 fins, respectively. So, increasing the number longitudinal fins in the solidification process is more efficient than that in the melting process because the blocking of the flow in the melted PCM and the suppression of the natural convection effect occurs simultaneously when more fins are used during the melting process.

Another work, developed by Torlak et al, with a simple shell-and-tube PCM considered, simulated a 2D approximation comparing the effect of buoyancy, or lack of it, testing the influence of natural convection on the heat transfer on the numerical work. Concerning simulations with no buoyancy the heat transfer worked by simple conduction with a relatively long phase change period and with uniform behaviour of the phase change front. While simulating with buoyancy it was possible to witness the effect of the natural convection and convection currents with a non-uniform heat transfer area and a noticeable increase in the heat transfer rate. Simulations wise, as long as only heat conduction is considered, with no buoyancy, the simulations are time-efficient. Natural convection, consequence of buoyancy, makes the coupling of momentum and energy equation stronger, leading to potentials instabilities and longer computing times [8].

A different study by Medrano et al [9], investigated the heat transfer process in five small heat exchangers working with latent a heat storage system, stating that numerical work agreed generally with the experimental results. Three different types of heat exchangers were applied in this work, a concentric single tube heat exchanger, a compact tube-fin heat exchanger and a plate heat exchanger. With this basic exchanger types five setups were built, i - simple single tube and PCM; ii - simple tube and PCM/graphite matrix medium; iii - single tube with radial fins and PCM; iv - compact coil and fins heat exchanger, and v - plate heat exchanger. Along with the heat exchanger behaviour, the effects of the water flow were evaluated. As expected, the results showed that heat transfer improved when turbulent regime was achieved in the water flow, as the total heat transfer resistance from water to PCM decreased. Using low water flow rates contributes 40-50% to the total thermal resistance, while with a turbulent regime most of the resistance is shifted to the PCM portion (90-95%). As such, the total time for both melting and solidification of the PCM is considerably shortened when the water flow is within the turbulent Reynolds value. The comparing results showed that full melting time is almost halved due to higher thermal transfer occurring in the high water flow rate. The experiments indicated that temperature difference is of great importance in the process time, the solidification process tends to spend more time to complete the phase change than the melting process, especially with lower temperature differences. This can be justified by the different nature of the heat transfer phenomena that are take place when a PCM fuses or solidifies. The convective heat transfer has a higher contribution regarding the liquefaction process and helps in decreasing the heat transfer resistance of the PCM. The exception being in charging and discharging in the heat exchangers with fins and plates, since in these cases the heat transfer takes place mostly through pure conduction, consequence of the close packing of the fins/plates. In such cases the melting and solidification process take very similar times. The experimental results revealed that, as anticipated, a concentric single tube and plate heat exchangers are not adequate solutions for real applications, particularly for the single tube heat exchanger with no fins, as the heat transfer is unacceptably low. The plate heat exchanger has the second smallest heat transfer rate, with a comparable power in the solidification process to the finned heat exchanger. However, for melting

test, the finned pipe performs better than the plate exchanger with about 100% more power. The plate exchanger is not suited as PCM heat storage not only for the low heat transfer, but mainly because it stores a very small amount of PCM and it is very heavy. In power performance, the third position was for the pipe and radial fins exchanger. The graphite matrix exchanger provided the second best solution because conduction is the main transfer mechanism through the embedded PCM matrix whereas the other cases convection plays a role, which in turn have a different nature for melting and solidification. The compact heat exchanger is by far the case with the highest heat transfer rate for both charging and discharging processes, at the worst conditions having three times the heat transfer rate of the second best heat exchanger.

2.2.2 Physical and Natural Processes

Throughout the literature, several authors mention that simulations of PCM behaviour given different considerations have different outcomes. One such example is the consideration of the effect of natural convection on the PCM. Although it takes place in a cohesive mass of material natural convection will be considerably reduced or halted with certain physical restrictions like fins and matrixes, exchanging heat mostly through conduction. Because of the computational capacity and time demands that are involved with natural convection processes calculations, simplification methods are useful for providing reasonably accurate solutions with reasonable time and computational capacity.

In transient modelling with density variation taken into consideration by Longeon et al, natural convection can be calculated with the Boussinesq approximation. The influence of the natural convection in a simplified heat exchanger with a single heating/cooling pipe used to transfer heat to a mass of PCM enclosed around is of great significance for the process especially during the charging process, with convection currents significantly increasing the heat transfer rate as the PCM phase changes from solid to liquid. On the other hand, throughout the discharge process, the liquid PCM beyond the solidification front remains mostly isothermal, avoiding the formation of natural convection. The liquid material settles homogenously in layers that transfer heat through conduction significantly reducing the transfer rate as this conduction depends on the PCM properties, this results in a considerably longer period for the discharge process to be concluded.[10]

2.2.3 Experimental Work and Numerical Solutions

With more PCM technical systems being considered for practical uses it becomes important use simulation tools to study such applications. Efforts have been made to make and standardise thermal storage systems design-to-validation protocols and performance evaluations. For these methods to work numerical solutions supported by experimental work need to be actively correlated and tested for accurate solutions to be found and employed.

A study [11] aiming to improve a thermal storage system heat transfer rate through surface area increase used to this end a numerical model that was constructed with a fixed-grid enthalpy-method based explicit finite-difference model. The geometry of the model is a submerged axisymmetric cylindrical finned pipe heat exchanger. The assumptions and conditions considered were: the system is axisymmetric; the PCM is homogenous and has isotropic properties; the PCM is gelled therefore the dominant heat transfer mechanism is conduction. Three different methods were used to integrate enthalpy. First, fixed phase change temperature. Second, measured specific heat. Third, adapted function curve. The experimental setup was an aluminium finned-tube cylindrical storage unit with T-type thermocouples distributed though the setup domain, including the inlet and outlet.

The results show that for discharging, for three different test runs, the time for the process to conclude differed less than 2% of the average time. The numerical results for the same process differed 5% from the experimental data with the exception for the scheme of the first enthalpy model. While charging the numerical results are 4% slower than the experimental values. Both processes showed a shorter time for the phase change than the experiments, attributed to thermal leaks of the experimental setup, accentuating the need for a well-insulated storage system. The numerical results have the same trend as the experimental data, with a 5% offset, validating the use of the conduction heat transfer mechanism in numerical simulations.

Another work by Castell et al used a coil inserted in a tank, which was filled with PCM. Two version were made, one with a single coil length and the other with two coils. For each configuration different flow rates were tested for the same inlet temperatures, with the inlet and outlet temperature being measured for the heat transfer fluid. The inlet temperature was kept at a constant temperature. It was verified that tanks with coiled tubes are an effective design for constant outlet temperatures and effective heat transfer rates. The constant inlet and outlet temperatures proved to have a constant effectiveness during the phase change process.[12]

A study [13] using a porous matrix mixed with PCM to enhance the heat transfer process developed a numerical model for an energy storage system, testing different porosities 95%, 90% and 85% comparing them with just PCM. The numerical results showed good agreement with other published results for melting pure PCM. A parametric study was performed to test the effects of porosity and thermal conductivity. Comparison the performance with and without the matrix showed that a matrix has a great influence on the heat transfer and melting of the PCM. It was also found that decreasing the porosity increased the melting rate but hampers the natural convective motion in the liquid phase .

In a work related with encapsulated PCMs by Hawlader, Uddin and Zhu, a combination of experiments and numerical simulations was performed for a thermal storage system. In this case, the encapsulation method used was coacervation using gelatine and acacia to trap paraffin inside. The PCM was then tested on the energy storage and release capacity; encapsulation ratio and cycles of solidification and melting to test the performance and behaviour of the encapsulation. Parallel to this, a simulation was performed where the

PCM properties were considered constant, the temperature on the encapsulation is uniform and inter-particle conduction is negligible. The k-ε turbulence model was employed. It was concluded that encapsulated PCM has a large energy storage and release capacity during the phase change. The thermal cycling showed that the PCM maintained its original geometrical profile and retained its heat storing capacity after 1000 cycles. The simulation showed that FLUENT was a suitable for simulating the system set up.[14]

2.3 Phase Change Materials (PCMs)

Since the European Union decided to reduce their greenhouse gas emission by accepting the Kyoto-protocol of the UNFCCC (United Nations Framework Convention on Climatic Change) in 1997, many serious steps have been taken. A promise was made that emissions 8% lower as the levels in 1990 would be reached in 2008–2012 and levels 20% lower in 2020 (United Nations, Kyoto protocol to the united nations framework convention on climate change, 1998). In 1999, the total energy consumption in Europe was 1780 million tons of oil equivalent, for which 35% was used in the residential and commercial sector. It became clear that reducing the energy consumption of buildings can have a major impact on the total greenhouse gas emissions in Europe.[15]

Sustainable technology offers a solution for the ever-tightening environmental building legislation, propelled by the charge to alleviate climate change and the desire for increased quality of life.

Most of the available renewable energy sources are incapable of providing constant power. To overcome this, solutions have been proposed by combining batteries, energy storage technology, with renewable energy generation. TES offers thermal energy efficiency enhancement for intermittent heat sources (e.g. solar heating). By 2050, it is predicted that over 70% of the world population will live in urban environments; thus the need for effective sustainable TES in buildings is ever increasing.[16]

Energy storage decreases the mismatch between supply and demand while improving the performance and reliability of energy systems and plays an important role in conserving the energy.[17][18] It leads to saving premium fuels and makes the system more cost effective by reducing the wastage of energy and capital cost. For example, storage would improve the performance of a power generation plant by load levelling and higher efficiency would lead to energy conservation and lesser generation cost. One of prospective techniques of storing thermal energy is the application of phase change materials (PCMs).[19]

An alternative to meet the increasing energy demand and reduce the negative environmental impacts would be to reduce energy usage in combination with higher application of environmentally friendly renewable energy technologies. These may be well-known technologies such as hydropower, wind energy and solar energy, or new emerging technologies such as ocean energy and enhanced geothermal systems to mention a few. Building integration of some of these technologies may also be found to be beneficial.[20][21][22] Several new technologies are emerging to help realize the goal of reducing energy usage in buildings.

[23][15][24][25][26][27][28][29][30][31] Some of these technologies are related to thermal insulation materials applied in the building envelope. Also part of the thermal building envelope, although not a thermal insulation material in itself, is the promising technology of phase change materials that has received considerable attention over the last decade. PCMs utilize the principle of Latent Heat Thermal Storage (LHTS) to absorb energy in large quantities when there is a surplus and releasing it when there is a deficit. Correct use of PCMs can reduce peak heating and cooling loads, i.e. reduce energy usage, and may also allow for smaller dimensions of technical equipment for heating and cooling. An added benefit is the ability to maintain more comfortable indoor environment due to smaller temperature fluctuations. Over the past few years it has been clearly shown that the interest for PCMs is increasing worldwide.[32][33][34][35][36][37][38][39][40][41][42][43][44][45] For building applications the possible areas where PCMs can be utilized are many. Some of the areas that have been studied to this day include ventilation systems, passive heating and cooling systems, floors, roofs and wallboards. PCMs can also be incorporated directly into building materials such as concrete [46] and wallboards [47], enabling them to be applied in constructions with minimal alterations to the original design.

2.3.1 Phase Change Materials in General

Phase change materials (PCMs), as the name implies, use the latent heat of phase change to control temperatures within a specific range. The thermal energy transfer occurs when, for example, a material changes from solid to liquid, or liquid to solid. This is called a change in state, or "Phase". Initially, these solid–liquid PCMs perform like conventional storage materials, their temperature rises as they absorb heat. Unlike conventional (sensible) storage materials, PCM absorbs and releases heat at a nearly constant temperature. They store 5-14 times more heat per unit volume (at a specific temperature) than sensible storage materials such as water, masonry work, or rock. A large number of PCMs can change phase in any required temperature range. When the temperature rises above a certain point (solidus temperature), the chemical bonds in the material will start to break up and the material will absorb the heat in an endothermic process where it changes state from solid to liquid. As the temperature drops below certain point (liquidus temperature), the material will undergo the reverse process giving off energy and return to a solid state. The energy used to alter the phase of the material, given that the phase change temperature is around the desired operation temperature, will lead to a more stable and homogenous operation condition, as well as cut peak cooling and heating loads.[34] Hence, phase change materials can provide an increase in heat storage capacity, especially in buildings with low thermal mass. The temperature range varies depending on the materials used as the phase change material. Some of the desired overall thermophysical, kinetic and chemical properties that should be required from phase change materials are:

- High Density;

- High latent heat per unit volume and unit weight, and high specific heat. This is desirable to gain a greater effect from latent heat storage with a small as possible volume of PCMs;
- Phase change temperature suitably matched to the application. To gain the most out of PCMs the phase change temperature must be in accordance with the climate, location of the building or the type of system where the PCM is used;
- Low vapour pressure at operational temperature. To avoid extra costs or danger of rupture because of pressure of the container, the vapour pressure should be as low as possible;
- Chemical stability and low corrosion rate. Chemically stable materials will allow for PCMs to operate at the given temperature and with the given effect for a longer period with out degradation and reduce the chances that the PCM reacts with materials that are in contact with it, i.e. increasing the lifetime of PCMs;
- Not hazardous or poisonous. To be allowed in the building sector there can be no poisonous emissions during fire or if the encapsulation is ruptured during regular use. Production of the material should also not release dangerous emissions to the environment
- Low/No flammability. Strict laws with regards to fire safety must also be fulfilled by PCMs;
- Reproducible crystallization without degradation. Much the same as chemical stability, the reproduction of crystals over thousands of phase changes without degradation is vital to attain long life-times cycles for PCMs;
- Small degree of supercooling and a high rate of crystal growth. Supercooling will alter the temperature of the phase change. An attractive PCM should have an exact phase change temperature so that the phase change is predictable to allow a material to be selected correctly for optimal design;
- Low thermal expansion coefficient throughout phase change. A large volume change will mean that the container has to allow for expansion of the PCM, thus decreasing the amount of PCM it can hold;
- High thermal conductivity. A high thermal conductivity will allow heat to disperse throughout or leave the material more rapidly, allowing the PCM to absorb or release heat at a higher rate;
- Use materials that are abundant and cheap. To make the technology more attractive and possible to use at a large scale it is important that the materials to be used are abundant and cost-effective.[48][49][44]

2.3.2 Classification of Phase Change Materials

There are several materials that can be used as PCMs. A common way to distinguish PCMs is by dividing them into organic, inorganic and eutectic PCMs. These categories are further divided based on the various components of the PCMs (Figure 2.3). (Figure 2.4) shows the difference in melting enthalpy and melting temperature for some of the most common materials used as PCMs.

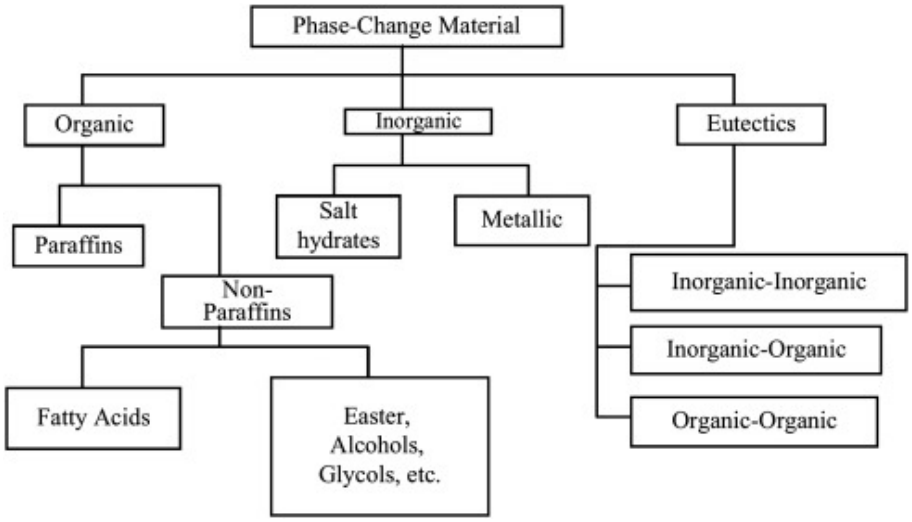

Figure 2.3: General categorization of PCMs.[50]

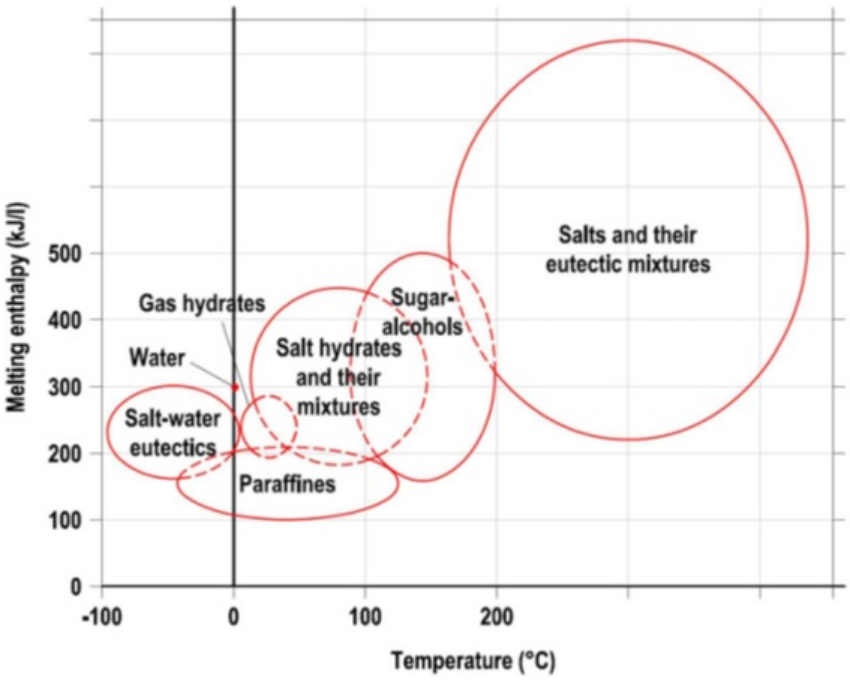

Figure 2.4: The melting enthalpy and melting temperature for the different groups of phase change materials.[49]

2.3.3 Organic

Organic phase change materials are in general chemically stable, fuse and solidify repeatedly without phase separation and consequent degradation of their fusion latent heat, self-nucleation meaning they crystallize and do not suffer from supercooling, are non-corrosive to metals, are non-toxic and have a high latent heat of fusion. Organic PCMs can be subdivided in two groups: paraffins and non-paraffins. Commercial paraffin waxes are inexpensive and usually have a reasonable thermal storage density from 120kJ/kg up to 210kJ/kg. Paraffins are available in a wide range of melting temperatures from approximately 20°C up to about 70°C, they are chemically inert, have a low vapour pressure when they melt and do not undergo phase segregation. Differential Scanning Calorimetry (DSC) has also shown that technical grade paraffin waxes do not show any indication that thermal cycling can significantly degrade its thermal performance. However, paraffins have a low thermal conductivity of about 0.2W/m.K which limits their application and has a significant volume change during the phase transition. Metallic fillers and matrix structures are used to improve the thermal conductivity, while plastic containers and different geometries of containers are used to overcome the volume change during melting and freezing. Paraffins make for attractive PCMs because:

- they have a wide and variable melting point range;
- they have a relatively high heat of fusion;
- they show no supercooling;
- they are chemically stable and recyclable;
- they show good compatibility with other materials (for mixtures).[16][51]

The non-paraffin organics include a wide selection of organic materials such as fatty acids, esters, alcohols and glycols. They have generally excellent melting and freezing properties, but are about three times more expensive than paraffins.[52][53] Of most interest in this group are the fatty acids or palmitoleic acids, which have melting points in a relatively low temperature range, have a high latent heat of fusion, undergo small volume changes during phase transition and do not undergo supercooling during freezing. Most common useful fatty acids are divided in 6 groups: caprylic, capric, lauric, myristic, palmitic and stearic with respectively 8 up to 18 carbon atoms per molecule. Their melting points are in the range between 16 and 65°C and freezing points between 17 and 64°C, with a heat of fusion between 155 and 180kJ/kg. However, there is a lack of materials with phase transition around the comfort temperature of 21°C.[34]

2.3.4 Inorganic

Inorganic PCMs in general have a rather high heat of fusion, good thermal conductivity, are cheap and non-flammable. However, most of them are corrosive to most metals,

undergo supercooling and undergo phase decomposition. Most common inorganic PCMs are hydrated salts.

Hydrated salts are attractive materials for thermal energy storage due to their relatively high storage density of about 240kJ/kg, their relative high thermal conductivity of about 0.5W/m.K and their reasonable cost compared to paraffin waxes. Additionally, the high storage density of hydrated salts is hard to maintain during cycling, hydrated salts will melt congruently with formation of lower salts, which makes the process irreversible and results in a decreasing storage capacity.[52]

Hydrated salts consist of an alloy of inorganic salts and water enabling a cost effective PCM due to easy availability and low cost. The phase change transformation involves hydration or dehydration of the salts in a process that resembles typical melting and freezing. The salt hydrate may either melt to a salt hydrate containing less water or to an anhydrous form where salt and water is completely separated.[54] Hydrated salts suited for commercial use suffer from incongruent melting. This is a typical problem for hydrated salts as the melting process in many cases leads to the salt releasing water and turning into a salt in its anhydrous from, or a different salt. The density of the anhydrous salt may be higher, causing it to sink to the bottom of the container. When the temperature reaches the freezing point, the salt will be stacked at the bottom and some salt will be unable to reabsorb the water. Hence, the total volume of salt that can undergo phase change has decreased, and the effectiveness of the PCM is reduced.[55]

Three types of the behaviour of the melted salts can be identified: congruent, incongruent and semi-congruent melting.

1. Congruent fusion takes place when the anhydrous salt is completely soluble in its hydrating water at the melting temperature.

2. Incongruent fusion takes place when the salt is not entirely soluble in its water of hydration at the melting point.

3. Semi-congruent melting the liquid and solid phases in equilibrium during a phase transition is of different melting composition because of conversion of the hydrate to a lower-hydrated material through loss of water.

The major problem in using salt hydrates as PCMs is that most of them, which are judged suitable for use in thermal storage, melt incongruently. As n moles of hydrating water are not sufficient to dissolve one mole of salt, the resulting solution is supersaturated at the melting temperature. This culminates in an irreversible melting–freezing of the salt hydrate goes on decreasing with each charge–discharge cycle. Another important problem common to salt hydrates is that of supercooling. At the fusion temperature, the rate of nucleation is generally very low. To achieve a reasonable rate of nucleation, the solution has to be supercooled and hence energy instead of being discharged at fusion temperature is discharged at much lower temperature. Adding chemicals can prevent the nucleation of lower salt hydrates, which preferentially increases the solubility of lower salt

hydrates over the original salt hydrates with higher number of water moles. The problem of incongruent melting can be tackled by one of the following means: (i) by mechanical stirring, (ii) by encapsulating the PCM to reduce separation, (iii) by adding thickening agents it keeps the solid salts from setting by holding it in suspension, (iv) by using excess water so that the melted crystals do not generate a supersaturated solution, (v) by chemical modification of the composition of the system and turning incongruent material into congruent.[54][56][57][58][59][60]

To overcome the problem of salt segregation and supercooling of salt hydrates, it has been suggested using a rolling cylinder heat storage system. The system consists of a cylindrical vessel mounted horizontally with two sets of rollers. A rotation rate of 3 rpm produced sufficient motion of the solid content (i) to create effective chemical equilibrium, (ii) to prevent nucleation of solid crystals on the walls, and (iii) to assume rapid attainment of axial equilibrium in long cylinders. Some of the advantages of the rolling cylinder method are: (i) complete phase change, (ii) latent heat released was in the range of 90-100% of the theoretical latent heat, (iii) repeatable performance over 200 cycles, (iv) high internal heat transfer rates, (v) freezing occurred uniformly.[61][62]

Metallics, on the other hand, have not yet been seriously considered for PCM technology because of weight penalties. However, when volume is a consideration, they are likely candidates because of the high heat of fusion per unit volume. They have high thermal conductivities, so fillers with added weight penalties are not required. The use of metallics poses a number of unusual engineering problems. A major difference between the metallics and other PCMs is their high thermal conductivity.[19]

Inorganic salts are favourable as PCMs due to their:

- High heat of fusion;
- High thermal conductivity (around 0.5W/m.K);
- Low volume change;
- Low cost.[51][35]

2.3.5 Eutectics

Eutectic mixtures or eutectics, i.e. a mixture of multiple solids in such proportions that the melting point is as low as possible, have in general sharp melting points and its volumetric storage density is slightly higher than that of organic compounds. However, limited data is available on their thermal and physical properties. Eutectics may be divided in 3 groups according to the materials of which they consist: (i) organic-organic, (ii) inorganic–inorganic and (iii) inorganic–organic eutectics. Pure acids and their eutectic compounds are characterized by a single peak in DSC (Differential Scanning Calorimetry) thermograms, which is sharp and well-defined. Binary systems of fatty acids may form a single eutectic point for both melting and freezing, but mixtures with up to four peaks have been noticed. The

eutectic binary systems showed melting points between 18 and 51°C and freezing points between 16 and 51°C, with a heat of fusion between 120 and 160kJ/kg.[63][64] A eutectic is a melting composition of a minimum of two or more components, each of which fuses and solidifies congruently. During the crystallization phase, a mixture of the components is formed, hence acting as a single component. The components freeze to an intimate mixture of crystals and melt simultaneously without separation.[65]

Eutectics can be mixtures of organic and/or inorganic compounds. This gives room for a wide variety of combinations that can be tailored for specific applications. Of organic eutectic mixtures, the most commonly tested consist of fatty acids. Some organic eutectics that have been studied include capric acid/myristic acid, lauric acid/stearic acid, myristic acid/palmitic acid and palmitic acid/stearic acid and capric acid/lauric acid. The most common inorganic eutectics that have been investigated consist of different salt hydrates.[21][66][67] The benefits of eutectic mixtures are their ability to obtain more desired properties such as a specific melting point or a higher heat storage capacity per unit volume. Though it has been given significant interest over the last decade by researchers, the use of eutectic PCMs for use in latent storage heating systems is not as established as pure compound PCMs. Hence, thermophysical properties of eutectics is still a field for further investigations as many combinations have yet to be tested and proved.
The advantages and drawbacks for organic, inorganic and eutectic PCMs are compared and summarized in Table 2.2.[55]

Table 2.2: Overview of Advantages and Drabacks for PCMs.

Organic		**Inorganic**		**Eutetics**	
Advantages	Drawbacks	Advantages	Drawbacks	Advantages	Drawbacks
-No supercooling	-Flammable	-High volumetric latent heat storage capcity	-Corrosive to metals	-Sharp melting points	-Limited data on thermophysical properties for many combinations
-No phase segregation	-Low thermal conductivity	-Higher thermal conductivity than organic PCMs	-Supercooling	-Properties can be tailored to match requirements	-High cost
-Low temperature pressure	-Low volumetric latent heat storage capacity	-Low cost	-Phase segregation		
-Large temperature range		-Non-flammable	-Congruent melting		
-Self-nucleating		-Sharp phase change	-High volume change		
-Compatible with conventional construction materials					
-Chemically stable					
-Recyclable					
-High heat fusion					

2.3.6 Characterization Methods for Phase Change Materials

A variety of analytical methods can be used to characterize the thermal properties of materials such as PCMs, the following section approaches some of these techniques.

2.3.6.1 Differential Scanning Calorimetry (DSC)

Differential scanning calorimetry measures the amount of heat required to keep a substance at a given temperature. [51]Tests vary temperature linearly with time.[68] PCM samples are tested against a reference sample (with known thermal properties). The product of a DSC test is a curve displaying the heat flux versus temperature or time. The resulting DSC curve reveals solidification and melting temperatures along with the latent heat value. The drawbacks of DSC are the accentuated super-cooling effects reported due to small sample sizes and thus poor nucleation effects.[69] Large-scale and small-scale tests were compared to validate a differential scanning calorimeter (DSC) test as standard for the measurements of PCM performances. A DSC is an instrument that measures the heat capacity of small material samples with a typical size of 6.3mm in diameter. For PCMs, the DSC gives the melting and freezing curves and the associated heat transfers. The principle of the test is to keep a temperature equilibrium between the test sample and a reference sample, i.e. mostly certified Indium metal, that is heated or cooled at a constant rate. The excess heat absorbed or emitted by the test sample is recorded as a function of the time and the total heat transition of the test sample between two temperatures is retrieved by integrating this recorded excess heat.[70][63][64][71] The comparison between large-scale and small-scale tests shows that both vary with only 8.7% and the DSC test underestimates the results compared to the large-scale tests.[70] This indicates that small-scale differential scanning calorimetry can adequately predict the performance of PCM enhanced products when installed in full-scale applications: expensive large-scale testing is thus not required until the products are well along in development.[70][72][73]

2.3.6.2 Differential Thermal Analysis (DTA)

Similar to DSC, differential thermal analysis keeps the heat flux as a constant and monitors the difference in temperature change between the reference and test samples. Thermal properties, including thermal conductivity, are then calculated from the temperature differences.[51] A simple variation of DTA tested samples with an accuracy of 5% when compared with DSC results.[69] DTA produces time versus temperature graphs, graphically presenting the heat transfer rate at a variety of temperatures.[74] Small sample sizes used in testing may misrepresent the thermo-physical performance of a given material when operating in bulk units. Further limitations of DSC and DTA are the expense and their inability to measure multiple samples simultaneously.[75]

2.3.6.3 T-history Method

A simplified T-history method has been developed with results comparable to DSC and DTA [51]. In this method the test samples are placed in test tubes equipped with thermocouples connected to a data logger. The samples are heated and cooled in water baths for a set time period. From temperature versus time curves, the thermal properties of the sample can be obtained. With a reported accuracy of 10% with literature data for the samples tested. [75] The process has since been refined to correct some assumptions in the initial method and widen the operation envelope.[76][77] Despite this being a simple method and it is useful for characterising bulk PCM, giving a more realistic representation of applied performance, many still rely on DSC and DTA to characterise the performance of the heat storage technology.

2.3.6.4 Dynamic Heat Flow Apparatus

The dynamic heat flow apparatus method is based on the traditional heat flowmeter apparatus method, which is used to determine steady-state heat transfer properties, thermal conductivity and thermal resistance of flat slab specimens. The traditional heat flow apparatus method is already used in accordance with standards such as EN 12667, ISO 8301 and ASTM C518 to determine these properties for traditional insulation materials. When performing a dynamic heat flow test, the plates on each side of the specimen to be tested are held at the same temperature, and both plates are changed to a different temperature, whereas different temperatures are used in normal heat flow tests. By using the dynamic method, results were found to be more accurate when testing PCMs. Kosny, found that dynamic properties such as heat capacity profiles, peaks of melting and solidification cycles and amount of supercooling were relatively similar to those measured by DSC.[78]

2.3.6.5 Dynamic Hot Box

The dynamic hot box method can be used to simulate changes in temperature on the climate side of a test specimen, particularly concerning building elements with PCM. From this, the dynamic thermal characteristics of a building component can be found. When testing PCMs it is important to get as correct picture as possible of their dynamic properties. With the dynamic hot box, the temperature is held constant until a steady-state is reached, then the temperature on one side is changed and results are measured until a new steady-state has been reached.[55]

2.3.6.6 Dynamic Guarded Hot Plate

A recent study investigated the possibility of using a dynamic guarded hot plate apparatus to determine the specific heat capacity as a function of the temperature for PCM incorporated concrete. The study describes the experimental set-up and proposes various methods

to calculate the specific heat capacity of PCM concrete. The advantage of this method is the possibility to attain a very small heating rate, which can imitate the temperature increase in real building constructions. That is, simulating realistic thermal conditions of the PCM in actual use. Though the study focuses on PCM concrete, it is pointed out that this experimental set-up could also be used on various other PCM composites.[79]

2.3.6.7 M-value

Phase change materials are added to structures and lead to an increase in thermal mass. As PCMs have a specific temperature range, they have also been referred to as "smart thermal mass". However, the phase change temperature of a PCM is not always absolute. It may happen over a small temperature interval and differ between melting and freezing. This is a cause for confusion as there is no standard which specifies in which part of the phase change process this value should be stated. A new energy performance label for PCMs has been mentioned. The M-value, which should express the phase transition related enthalpy change of the PCM within a standardized range so that all values given for a PCM can be evaluated on an equal basis.[80]

2.3.6.8 Transient Plane Source (TPS)

N. Soares et al performed a systematic characterisation of thermophysical properties of ten commercial paraffin-based PCMs with the Transient Plane Source (TPS) method, comparing the gathered data with commercial datasheets. It concluded that information on the thermal conductivity is very scarce in the catalogues. The k-values higher than 0.2 $W/m \cdot °C$ should be considered for modelling in particular in the solid phase. Moreover, different k-values should be used for the solid and liquid phases. Another conclusion is that the TPS method provides reliable input on the variation of the heat capacity with temperature for solid and liquid PCMs. It was concluded that the majority of the PCMs exhibits slightly lower melting/solidification peak temperatures than those declared in the commercial catalogues. Furthermore, the measured enthalpies of fusion are quite lower than those provided by the manufacturer. Finally, it was concluded that the reference cp-value of 2 $J/g \cdot °C$ does not fit all the PCMs (as claimed by some manufacturers).[81]

2.3.7 Long-term Stability Considerations of Phase Change Materials

As a melting/freezing cycle occurs thousands of times, some phase change materials may have the tendency to deteriorate overtime. Gradual breakdown of the material will end up reducing the amount of latent heat storage per phase transition and may also affect the phase change temperature, and hence reduce the overall energy performance. Such deterioration is particularly common in inorganic PCMs, and to some extent in less pure organic PCMs. It is important that future possible PCMs are tested with regard to their ageing over time. As of today there is no standard method to do this. An aim for the

future should be to develop a standard testing scheme which all commercial grade PCMs will have to follow when stating the lifetime of their products [55]. Paraffins have shown good thermal stability. For fatty acids the purity plays an important role. Industrial grade fatty acids may experience changes in its thermal behaviour over time and should be tested by accelerated ageing. Most studies have shown that the thermal stability of salt hydrates is poor due to phase separation and supercooling. However, the thermal stability may be improved to a certain extent by introducing gelled or thickened mixtures and suitable nucleating materials.[82][83]

2.3.8 Phase Change Material Applications

PCMs thermal properties makes them a ideal for several applications of varied areas of application ranging from simple thermal bottles to spacecraft applications, the following section focuses primarily on general potential applications.

2.3.8.1 Free Cooling

Free cooling systems with PCMs work by storing outdoor coolness (e.g. during the night) and release the coolness indoors during the day. The PCM can then be used during the day to absorb the heat from e.g. passing air in a ventilation system or water in a pipe system, and stored as latent heat, to cool the building in the day when temperatures are higher and the need for cooling arises. These systems work as long as the ambient temperature allows the PCM to freeze and melt over the day, i.e. the ambient temperature must be above the phase change temperature during the day and below during the night.[84]

2.3.8.2 Peak Load Shifting

Peak loads that hit during the day put pressure on the electrical grid and also lead to the need for heating, ventilation and air conditioning (HVAC) systems being dimensioned for higher heating or cooling loads. Ultimately, this could lead to a need for more power generation facilities being built. By shifting the peak load away from the peak hours of electrical demand using PCMs, the peak load may be divided throughout the day reducing the highest peaks. Figure 2.5 illustrates how the peak maybe both reduced and shifted by the use of PCMs. From the studies reviewed, peak cooling load reductions ranging from 10 to 57% with no or simple control strategies were found. The greatest reductions were found in cases where the PCM was compared against an insulated lightweight construction, while the lowest reduction was found when comparing against structures containing more mass, e.g. concrete. However, the cost saving potential of these systems could be further improved if more sophisticated load shifting control strategies were developed.[85][86]

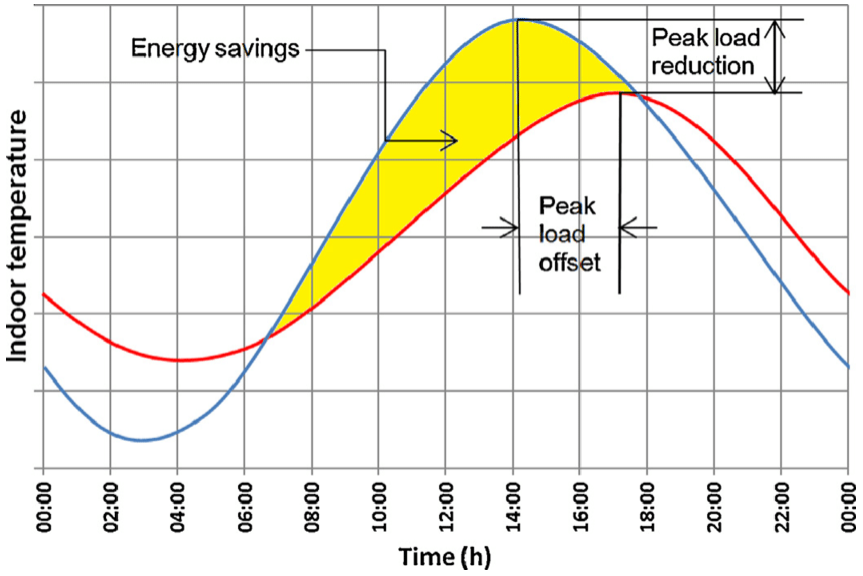

Figure 2.5: Illustration of peak load offset and peak load reduction .[87]

2.3.8.3 Thermal Comfort Control

Though PCMs show potential for energy savings, another important factor to highlight is the benefits PCMs may have towards increasing the overall indoor thermal comfort. When temperatures increased up to 20°C there was an increase in working performance. However, when temperatures increased above 23°C there was a decrease in productivity. Maintaining a steady temperature around the comfort zone for longer periods without relying on HVAC systems may be possible with PCMs. With PCMs installed temperature fluctuations are reduced. The focus should be placed on selecting a PCM within the desired melting/freezing point so temperatures stay stable around the comfort temperature. This will benefit the indoor climate in two ways. First, the temperature will be held more stable, reducing the feelings of thermal discomfort due to temperature fluctuations throughout the day. Second, the peak temperature will be reduced and should not reach a temperature which leads to increased thermal discomfort. Another possible benefit of PCMs can be that they lead to a more uniform temperature between surfaces and air temperature, reducing thermal discomfort from radiative heat [88][89]. It should be noted though that, there are several factors that can affect thermal comfort such as metabolic rate, clothing insulation, air temperature, mean radiant temperature, air speed, relative humidity and natural ventilation and only some of these factors can be influenced by PCM usage. In 1970 Fanger created the PMV/PPD model, which uses empirical research on skin temperature and heat-balance equations to describe comfort. On a seven-point scale from cold (-3) to hot (+3), individuals are asked to rate their thermal sensations in standard thermal comfort questionnaires. The Predicted Mean Vote (PMV) of a group of participants is determined using Fanger's equations for a given set of air temperature, mean radiant temperature, relative humidity, air speed, metabolic rate, and garment insulation. [90] The comfort zone

is determined by the combinations of the six parameters for which the PMV is within the advised limits (-0.5<PMV<+0.5), with PMV equal to zero denoting thermal neutrality. [91] Despite the fact that forecasting a population's thermal perception is a crucial step in figuring out what conditions are pleasant, it is more useful to think about whether or not people will be satisfied. Fanger created a different formula to connect the PMV to the anticipated percentage of dissatisfied customers (PPD). This connection was established by research that polled participants in a controlled environment, such as a chamber. [90]

2.3.8.4 Solar Energy Storage

PCMs hold the ability to store energy given off by the sun. Where solar cell panels can produce energy during hours of solar radiation, PCMs can store some of the excess energy and release it at a more needed time of the day. This can be combined with different energy distribution systems such as a heat pump. For PCMs to best utilize the solar energy it is important that the surfaces are positioned in areas where they can fully absorb the energy coming from the sun, e.g. wallboards or PCM windows. PCM incorporated into concrete floors is an example of a position which poorly utilizes the possible energy gains from the sun as such floors are covered with other materials in most traditional structures.[55]

2.3.8.5 Passive Building Systems

Passive building systems and their use have attained the most interest as of yet. For passive applications, PCMs are integrated into the building envelope to increase the thermal mass. This is especially beneficial in lightweight constructions, which suffer from low thermal inertia. A known issue for these buildings are large temperature fluctuations in the summer due to excessive overheating caused by a lack of thermal mass. This is especially the case in cold climates where buildings have been built according to passive house standards, often involving large amounts of insulation to reduce heating loads in the winter. The materials incorporating PCMs will melt during the day time and solidify during night time. This will help rooms from overheating during the daytime in warm months and may also reduce the need for heating during night time in the winter. An issue that has been brought up is the importance of getting passive PCM systems to completely discharge during night time in warm periods. If the PCM is not able to completely solidify, the effectiveness of the system may be considerably reduced. This point makes PCMs more effective in climates with large daily variation in temperatures. For areas where the discharge does not happen naturally, cool air has to be supplied during night time to reset the PCMs completely.

Examples of integration of phase change materials for buildings passive systems:

- Walls;
- Floors;
- Roofs;

- Windows and shutters;
- Concrete;
- Thermal insulation materials;
- Furniture and indoor appliances;
- Retrofitting;
- PCM Trombe Wall.[55]

Al-Yasiri and Szabó showed that when employing PCM in buildings constructive elements like wall or roofs, in cooling season/weather, it should be place as far as possible from the inside living space, thus being placed on the outer boundaries of the building envelope to prevent heat emittance towards the living space. For heating season/weather the PCM should be placed closer to the living space in order to supply back stored heat in little loss.[92]

Gergiou et al examined how retrofitting buildings with PCM coatings affected their thermal performance. The results revealed that, for the conditions at the testing site, the optimal location of the PCM in the building's structure is on external outer wall, regardless of the orientation. The study addressed masonry buildings which is a common typology in Europe, helping gauge the expectations and limitations of the PCM use.[93]

2.3.8.6 Active Building Systems

The storage capability of PCMs can be integrated into systems such as solar heat pump systems, heat recovery systems and floor heating systems. Such systems can be combined to attain a peak load reduction. However, if they are made even more effective they can achieve further savings through reduced electrical demand for HVAC systems. An example of such systems is latent energy storage systems (LES) or latent heat storage (LHS), resembling the system considered for the work developed in this thesis.[94]

2.3.8.7 Phase Change Materials Enhancement

A problem that has been addressed throughout the available literature is the low thermal conductivity for many promising PCMs (around 0.15 - 0.2 W/m.K) for organic PCMs and around 0.5 W/m.K for inorganic salts). Low thermal conductivity reduces the rate of heat absorption or heat release throughout the PCM, i.e. reducing the effectiveness at which it can store and release thermal energy. This may lead to a system which does not fully utilize the full latent heat storage of PCM materials. Recently, graphite based PCM systems and metal foams have been getting increased attention. One solution that has been investigated includes adding of a material with a high thermal conductivity to the PCM. A material that has been investigated for this purpose is various carbon-based nano-fillers. Though the results are varying, the increase in thermal conductivity has increased

between 65 and 336% in such studies. Another solution is to add the PCM to a material with a porous structure and a high thermal conductivity (Figure 2.6). Investigations on graphite foam composites and metal foams based on aluminium have been conducted. Graphite foam composites have shown potential for creating a structure with high thermal conductivity (ranging from 230 to 570 times higher than the original PCM). Note that adding a new material to the PCM and creating a composite material reduces the total latent heat storage ability per unit weight due to the adding of new particles. The energy uptake and release of the system may improve, but as of yet, this comes at the cost of less thermal heat storage per unit weight.[95][96][97][98][99][100][101][102]

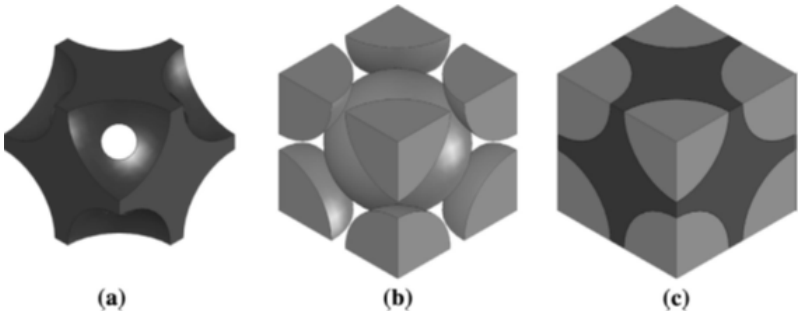

Figure 2.6: Illustration of (a) graphite foam, (b) PCM material, and (c) graphite foam and PCM composite.[103]

2.3.9 Safety and Environment

The safety requirements for materials used in buildings are crucial points for the PCMs to fulfil. PCMs should not be toxic or flammable. However, for many organic PCMs flammability and possible release of toxic fumes during combustion have been an issue. Solutions have been made to counter this issue, such as ignition resistant microcapsules for PCMs and the adding of fire retardants. Hence, it is of significance that manufacturers of PCMs for building applications are required to give reliable information about the fire performance of their products.[104]

New materials that may be suitable for use as PCMs are continuously being investigated. As mentioned earlier, it is critical that PCMs for use in buildings are not hazardous or poisonous in anyway. This also includes during production and handling after a PCM's useful lifetime. It is important that possible new materials are evaluated with regard to waste from the production and necessary treatment when they are to be disposed. As there may be many different chemicals in use in PCMs, environmental assessments could be conducted to avoid unknown pollutants of any kind.[55]

2.3.10 Economics and Payback

Though the theory behind PCMs shows that they have the ability to reduce temperature fluctuations in buildings, there has been no study to prove an increase in overall thermal

comfort or productivity. A way of measuring the effect and number of full cycles in different environments is needed. To fully utilize the effect of PCMs an overview of how they perform in different climates are needed. Ideally, a PCM should undergo a full phase change cycle once a day. However, the lack of guidelines for selecting PCMs for various climates is a source for uncertainty when used for building applications and systems. It would be preferable, if a detailed overview of the effect that could be expected for various PCMs in various climates was developed. It has been pointed out that it is difficult to select a PCM that functions optimally for every season and location. From all the experiments and simulations reviewed in this study, one of the most important factors for implementing PCM enhanced materials is found to be selecting the correct phase change temperature. Other crucial aspects are the difficulty of selecting the correct PCM for specific climates and that the effect of PCMs will vary with varying climate conditions over the year. The selection of a PCM based on a specific phase change temperature in one climate region will not be appropriate for another. Important factors that govern the selection of a PCM include phase change temperature, local climate, type of PCM and design and orientation of the system/building. Although every project t in such context has been deemed to increase energy efficiency and thermal comfort, monitoring projects from real life situations should be conducted and evaluated so the beneficial effects of PCMs can be documented and shared.[105][106][107]

As PCMs offer a decrease in overall energy usage, in many cases through minimal interference with the original structure, it is highly relevant to know the expected payback time of the initial investment. So far little research has been carried out on this topic. This may be due to several factors. The most important one being that there is still a lack of knowledge on how PCMs actually perform in real life constructions in all sorts of various climates. There is still much uncertainty regarding the overall effect of PCMs. Showing the long-term economic benefits of selecting PCMs may help to increase the interest among customers to use PCMs. Should the results of such analyses show unfavourable pay-back times, it may also help to drive the research and development forward towards more cost-efficient solutions.[55]

3

CFD Theory

This chapter presents a brief overview of the mathematical theory for the governing equations that solve the different phenomena of the used models. The main models used throughout the simulation work of this thesis concern heat transfer, fluid flows in laminar, transition, and turbulent regimes, and solidification and melting processes.

The following section will address the mathematical theory of the model used by the simulation software Fluent v17.1, from Ansys. The equations displayed here show only the models used in the simulations done in the course of this work, not being the intention here to go into too deep details regarding mathematical models provided by Ansys Fluent Theory Guide besides the content relevant for the numerical work.

3.1 Continuity and Momentum Equations

Regarding all flows, ANSYS Fluent solves conservation equations for mass and momentum. For flows involving heat transfer, an additional equation for energy conservation is solved. Additional transport equations are also solved when the flow is turbulent.[108]

3.1.1 Mass Conservation Equation

The equation for conservation of mass, or continuity equation, can be written as follows:

$$\frac{\partial \rho}{\partial t} + \nabla \cdot (\rho \vec{\nu}) = S_m \tag{3.1}$$

Equation 3.1 is the general form of the mass conservation equation and is valid for incompressible as well as compressible flows. The source S_m represents the rate of mass added to the continuous phase and any user-defined sources. For 2D axisymmetric geometries, the continuity equation is given by

$$\frac{\partial \rho}{\partial t} + \frac{\partial}{\partial x}(\rho \nu_x) + \frac{\partial}{\partial r}(\rho \nu_r) + \frac{\rho \nu_r}{r} = S_m \tag{3.2}$$

where x is the axial coordinate, r is the radial coordinate,ν_x is the axial velocity, and ν_r is the radial velocity.[108]

3.1.2 Momentum Conservation Equations

Conservation of momentum in an inertial (non-accelerating) reference frame is presented as:

$$\frac{\partial}{\partial t}(\rho\vec{\nu}) + \nabla\cdot(\rho\vec{\nu}\vec{\nu}) = -\nabla p + \nabla\cdot(\bar{\bar{\tau}}) + \rho\vec{g} + \vec{F} \tag{3.3}$$

where p is the static pressure, $\bar{\bar{\tau}}$ is the stress tensor, and $\rho\vec{g}$ and $\vec{F}$ are the gravitational body force and external body forces, respectively. $\vec{F}$ also contains other model-dependent source terms such as porous-media and user-defined sources. The stress tensor $\bar{\bar{\tau}}$ is given by:

$$\bar{\bar{\tau}} = \mu\left[(\nabla\vec{\nu} + \nabla\vec{\nu}^T) - \frac{2}{3}\nabla\cdot\vec{\nu}I\right] \tag{3.4}$$

where μ is the molecular viscosity, I is the unit tensor, and the second term on the right hand side is the effect of volume dilation.
For 2D axisymmetric geometries, the axial and radial momentum conservation equations are given by

$$\begin{aligned}\frac{\partial}{\partial t}(\rho\nu_x) + \frac{1}{r}\frac{\partial}{\partial x}(r\rho\nu_x\nu_x) + \frac{1}{r}\frac{\partial}{\partial r}(r\rho\nu_r\nu_x) = -\frac{\partial p}{\partial x} + \frac{1}{r}\frac{\partial}{\partial x}\left[r\mu(\left(2\frac{\partial\nu_x}{\partial x} - \frac{2}{3}(\nabla\cdot\vec{\nu})\right)\right] \\ + \frac{1}{r}\frac{\partial}{\partial r}\left[r\mu\left(\frac{\partial\nu_x}{\partial r} + \frac{\partial\nu_r}{\partial x}\right)\right] + F_x\end{aligned} \tag{3.5}$$

and

$$\begin{aligned}\frac{\partial}{\partial t}(\rho\nu_r) + \frac{1}{r}\frac{\partial}{\partial x}(r\rho\nu_x\nu_r) + \frac{1}{r}\frac{\partial}{\partial r}(r\rho\nu_r\nu_r) = -\frac{\partial p}{\partial r} + \frac{1}{r}\frac{\partial}{\partial r}\left[r\mu\left(2\frac{\partial\nu_r}{\partial x} - \frac{2}{3}(\nabla\cdot\vec{\nu})\right)\right] \\ + \frac{1}{r}\frac{\partial}{\partial x}\left[r\mu\left(\frac{\partial\nu_r}{\partial x} + \frac{\partial\nu_x}{\partial r}\right)\right] - 2\mu\frac{\nu_r}{r^2} + \frac{2}{3}\frac{\mu}{r}(\nabla\cdot\vec{\nu}) + \rho\frac{\nu_z^2}{r} + F_r\end{aligned} \tag{3.6}$$

where

$$\nabla\cdot\vec{\nu} = \frac{\partial\nu_x}{\partial x} + \frac{\partial\nu_r}{\partial r} + \frac{\nu_r}{r} \tag{3.7}$$

with ν_z being the swirl velocity.[109]

3.2 Turbulence

This section provides theoretical background about the turbulence models available in ANSYS Fluent that were used throughout the thesis.

3.2.1 Transition k-kl-ω Model

The k-kl-ω transition model is used to predict boundary layer development and calculate transition onset. This model can be used to effectively address the transition of the boundary layer from a laminar to a turbulent regime.[110]

Transport Equations for k-kl-ω Model The k-kl-ω model is considered to be a three-equation eddy-viscosity type, which includes transport equations for turbulent kinetic energy (k_t), laminar kinetic energy (k_L), and the inverse turbulent time scale (ω).

$$\frac{Dk_T}{Dt} = P_{k_t} + R + R_{NAT} - \omega k_T - D_T + \frac{\partial}{\partial x_j}\left[\left(\nu + \frac{\alpha_T}{\alpha_k}\right)\frac{\partial k_T}{\partial x_j}\right] \tag{3.8}$$

$$\frac{Dk_L}{Dt} = P_{k_L} - R - R_{NAT} - D_L + \frac{\partial}{\partial x_j}\left[\nu\frac{\partial k_L}{\partial c_j}\right] \tag{3.9}$$

$$\begin{aligned}\tfrac{D_\omega}{Dt} = C_{\omega 1}\tfrac{\omega}{k_T}P_{k_T} + \left(\tfrac{C_{\omega R}}{f_W} - 1\right)\tfrac{\omega}{k_T}(R + R_{NAT}) - C_{\omega 2}\omega^2 \\ + C_{\omega 3} f_\omega \alpha_T f_W^2 \tfrac{\sqrt{k_t}}{d^3} + \tfrac{\partial}{\partial x_j}\left[\left(\nu + \tfrac{\alpha_T}{\alpha_\omega}\right)\tfrac{\partial \omega}{\partial x_j}\right]\end{aligned} \tag{3.10}$$

The inclusion of the turbulent and laminar fluctuations on the mean flow and energy equations via the eddy viscosity and total thermal diffusivity is as follows:

$$\overline{-u_i u_j} = \nu_{TOT}\left(\frac{\partial U_i}{\partial x_j} + \frac{\partial U_j}{\partial x_i}\right) - \frac{2}{3}k_{TOT}\delta_{ij} \tag{3.11}$$

$$\overline{-u_i \theta} = \alpha_{\theta,TOT}\frac{\partial \theta}{\partial x_i} \tag{3.12}$$

The effective length is defined as

$$\lambda_{eff} = MIN(C_\lambda d, \lambda_T) \tag{3.13}$$

where λ_T is the turbulent length scale and is defined by

$$\lambda_T = \frac{\sqrt{k}}{\omega} \tag{3.14}$$

and the small scale energy is defined by

$$k_{T,s} = f_{ss} f_W k_T \tag{3.15}$$

$$f_W = \frac{\lambda_{eff}}{\lambda_T} \tag{3.16}$$

$$f_{ss} = exp\left[-\left(\frac{C_{ss}\nu\Omega}{k_t}\right)^2\right] \tag{3.17}$$

The large scale energy is given by

$$k_{T,l} = k_T - k_{T,s} \tag{3.18}$$

Note that the sum of Equation 3.15 and Equation 3.18 yields the turbulent kinetic energy k_T. The turbulence production term generated by turbulent fluctuations is given by

$$P_{k_T} = \nu_{T,s} S^2 \tag{3.19}$$

where the small-scale turbulent viscosity is $\nu_{T,s}$

$$\nu_{T,s} = f_\nu f_{INT} C_\mu \sqrt{k_{T,s}\lambda_{eff}} \tag{3.20}$$

and

$$C_\mu = \frac{1}{A_0 + A_S(S/\omega)} \tag{3.21}$$

$$f_\nu = 1 - exp\left(-\frac{\sqrt{Re_{T,s}}}{A_\nu}\right) \tag{3.22}$$

A damping function defining the turbulent production due to intermittency is given by

$$f_{INT} = MIN\left(\frac{k_L}{C_{INT}k_{TOT}}, 1\right) \tag{3.23}$$

$$Re_{T,s} = \frac{f_W^2 k_T}{\nu\omega} \tag{3.24}$$

In Equation 3.9, P_{k_L} is the production of laminar kinetic energy by large scale turbulent fluctuations, such that

$$P_{k_L} = \nu_{T,l} S^2 \tag{3.25}$$

The large-scale turbulent viscosity $\nu_{T,1}$ is modeled as

$$\nu_{T,1} = MIN\left\{\nu^*_{T,1}, \frac{0.5(k_L + k_{T,1})}{S}\right\} \tag{3.26}$$

where

$$\nu^*_{T,1} = f_{\tau,1} C_{11}\left(\frac{\Omega\lambda^2_{eff}}{\nu}\right)\sqrt{k_{T,1}}\lambda_{eff} + \beta_{TS} C_{12}\varphi_{NAT} d^2\Omega \tag{3.27}$$

The limit in Equation 3.26 binds the realizability such that it is not violated in the two-dimensional developing boundary layer. The time-scale-based damping function $f_{\tau,1}$ is

$$f_{\tau,1} = 1 - exp\left[-C_{\tau,s}\frac{k_{T,1}}{\lambda^2_{eff}\Omega^2}\right] \tag{3.28}$$

where β_{TS} from Equation 3.27 is

$$\beta_{TS} = 1 - exp\left(-\frac{MAX(\varphi_{NAT} - C_{TS,crit}, 0)^2}{A_{TS}}\right) \tag{3.29}$$

$$\varphi NAT = \frac{d^2\Omega}{\nu} \tag{3.30}$$

Near-wall dissipation is given by

$$D_T = 2\nu\frac{\partial\sqrt{k_T}}{\partial x_j}\frac{\partial\sqrt{k_T}}{\partial x_j} \tag{3.31}$$

$$D_L = 2\nu \frac{\partial \sqrt{k_L}}{\partial x_j} \frac{\partial \sqrt{k_L}}{\partial x_j} \tag{3.32}$$

In Equations 3.8 to Equation 3.10, R represents the averaged effect of the breakdown of streamwise fluctuations into turbulence during bypass transition:

$$R = C_R \beta_{BP} k_L \omega / f_w \tag{3.33}$$

β_{BP}, which is the threshold function controls the bypass transition process:

$$\beta_{BP} = 1 - exp\left(-\frac{\varphi_{BP}}{A_{BP}}\right) \tag{3.34}$$

$$\varphi_{BP} = MAX\left[\left(\frac{k_T}{\nu\Omega} - C_{BP,crit}\right), 0\right] \tag{3.35}$$

The breakdown to turbulence due to instabilities is considered to be a natural transition production term, given by

$$R_{NAT} = C_{R,NAT} \beta_{NAT} k_L \Omega \tag{3.36}$$

$$\beta_{NAT} = 1 - exp\left[-\frac{MAX\left(\varphi_{NAT} - C_{NAT,crit}/f_{NAT,crit}, 0\right)}{A_{NAT}}\right] \tag{3.37}$$

$$f_{NAT,crit} = 1 - exp\left(C_{NC}\frac{\sqrt{k_L}d}{\nu}\right) \tag{3.38}$$

The use of ω as the scale-determining variable can lead to a reduced intermittency effect in the outer region of a turbulent boundary layer, and consequently an elimination of the wake region in the velocity profile. From Equation 3.10, the following damping is defined as

$$f_\omega = 1 - exp\left[-0.41\left(\frac{\lambda_{eff}}{\lambda_T}\right)^4\right] \tag{3.39}$$

The total eddy viscosity and eddy diffusivity included in Equation 3.11 and Equation 3.12 are given by

$$\nu_{TOT} = \nu_{T,s} + \nu_{T,l} \tag{3.40}$$

$$\alpha_{\theta,TOT} = f_W\left(\frac{k_T}{k_{TOT}}\right)\frac{\nu_{T,s}}{Pr_\theta} + (1 - f_W)\, C_{\alpha,\theta}\sqrt{k_T}\lambda_{eff} \tag{3.41}$$

The turbulent scalar diffusivity in Equations 3.8 to Equation 3.10 is defined as

$$\alpha_T = f_\nu C_{\mu,std}\sqrt{k_{T,s}\lambda_{eff}} \tag{3.42}$$

$$k_{TOT} = k_T + k_L \tag{3.43}$$

A compressibility effects option, similar to the one in the $k-\varepsilon$ model is available for the k-kl-ω model. By default, this compressibility effects option is turned off.

Model Constants The model constants for the k-kl-ω transition model are listed below [110]:

$$A_0 = 4.04, A_S = 2.12, A_\nu = 6.75, A_{BP} = 0.6, A_{NAT} = 200, A_{TS} = 200, C_{BP,crit} = 1.2,$$

$$C_{NC} = 0.1, C_{NAT,crit} = 1250, C_{Int} = 0.75, C_{TS,crit} = 1000, C_{R,NAT} = 0.02,$$

$$C_{11} = 3.4e-6, C_{12} = 1.0e-10, C_R = 0,12, C_{\alpha.\theta} = 0.035, C_{SS} = 1.5,$$

$$C_{\tau,1} = 4360, C_{\omega 1} = 0.44, C_{\omega 2} = 0.92, C_{\omega 3} = 0.3, C_{\omega R} = 1.5,$$

$$C_\lambda = 2.459, C_{\mu,std} = 0.09, Pr_\theta = 0.85, \sigma_k = 1, \sigma_\omega = 1.17$$

3.2.2 Transition SST Model

The Transition Shear Stress Transport (SST) model (also known as the γ-Re$_\theta$ model) is based on the coupling of the SST k-ω transport equations with two other transport equations, one for the intermittency and one for the transition onset criteria, in terms of momentum-thickness Reynolds number. An Ansys empirical correlation (Langtry and Menter) has been developed to cover standard bypass transition as well as flows in low freestream turbulence environments. Additionally, an option has been included to allow entering user-defined empirical correlation, which can then be used to control the transition onset momentum thickness Reynolds number equation.[108]
While this model was used in the following work, it was only applied nominally up until the results shown in Figure 5.49, being then disregarded in favour of the k-kl-ω model that provided seemingly better results for transition flows in the work cases displayed here, thus it will not be further elaborated upon.

3.2.3 Standard k-ε

The following presents the standard, Re-Normalization Group (RNG), and realizable k - ε models. All three models have similar forms, with transport equations for k and ε . The major differences in the models are as follows:

- the method of calculating turbulent viscosity;
- the turbulent Prandtl numbers governing the turbulent diffusion of k and ε;
- the generation and destruction terms in the ε equation.

The transport equations, the methods of calculating turbulent viscosity, and model constants are presented separately for each model. The features that are essentially common to all models follow, including turbulent generation due to shear buoyancy, accounting for the effects of compressibility, and modeling heat and mass transfer.

Two-equation turbulence models allow the determination of both, a turbulent length and time scale by solving two separate transport equations. The standard k-ε model in ANSYS Fluent falls within this class of models and has become the workhorse of practical engineering flow calculations in the time since it was proposed by Launder and Spalding. Robustness, economy, and reasonable accuracy for a wide range of turbulent flows explain its popularity in industrial flow and heat transfer simulations. It is a semi-empirical model, and the derivation of the model equations relies on phenomenological considerations and empiricism.

The standard k-ε model [111] is a model based on model transport equations for the turbulence kinetic energy (k) and its dissipation rate (ε). The model transport equation for k is derived from the exact equation, while the model transport equation for ε was obtained using physical reasoning and bears little resemblance to its mathematically exact counterpart.

In the derivation of the k-ε model, the assumption is that the flow is fully turbulent, and the effects of molecular viscosity are negligible. The standard k-ε model is therefore valid only for fully turbulent flows.

As the strengths and weaknesses of the standard k-ε model have become known, modifications have been introduced to improve its performance. Two of these variants are available in ANSYS Fluent: the RNG k-ε model [112] and the realizable k-ε model [113].

Transport Equations for the Standard k-ε Model The turbulence kinetic energy, k, and its rate of dissipation, ε, are obtained from the following transport equations:

$$\frac{\partial}{\partial t}(\rho k) + \frac{\partial}{\partial x_i}(\rho k u_i) = \frac{\partial}{\partial x_j}\left[\left(\mu + \frac{\mu_t}{\sigma_k}\right)\frac{\partial_k}{\partial_{x_j}}\right] + G_k + G_b - \rho_\varepsilon - Y_M + S_k \tag{3.44}$$

and

$$\frac{\partial}{\partial t}(\rho \varepsilon) + \frac{\partial}{\partial x_i}(\rho \varepsilon u_i) = \frac{\partial}{\partial x_j}\left[\left(\mu + \frac{\mu_t}{\sigma_\varepsilon}\right)\frac{\partial_\varepsilon}{\partial x_j}\right] + C_{1\varepsilon}\frac{\varepsilon}{k}(G_k + C_{3\varepsilon}G_b) - C_{2\varepsilon}\rho\frac{\varepsilon^2}{k} + S_\varepsilon \tag{3.45}$$

In these equations, G_k represents the generation of turbulence kinetic energy due to the mean velocity gradients. G_b is the generation of turbulence kinetic energy due to buoyancy. Y_m represents the contribution of the fluctuating dilatation in compressible turbulence to the overall dissipation rate. $C_{1\varepsilon}$, $C_{2\varepsilon}$ and $C_{3\varepsilon}$ are constants. σ_k and σ_ε are the turbulent Prandtl numbers for k and ε, respectively. S_k and S_ε are user-defined source terms.

Modelling the Turbulent Viscosity The turbulent (or eddy) viscosity, μ_t, is computed by combining k and ε as follows:

$$\mu_t = \rho C_\mu \frac{k^2}{\epsilon} \tag{3.46}$$

where C_μ is a constant.[114]

Model Constants The model constants $C_{1\varepsilon}$, $C_{2\varepsilon}$, C_μ, σ_k and σ_ε have the following default values:

$$C_{1\varepsilon} = 1.44, C_{2\varepsilon} = 1.92, C_\mu = 0.09, \sigma_k = 1.0, \sigma_\varepsilon = 1.3$$

These default values have been determined from experiments for fundamental turbulent flows including frequently encountered shear flows like boundary layers, mixing layers and jets as well as for decaying isotropic grid turbulence. They have been found to work fairly well for a wide range of wall-bounded and free shear flows. Although the default values of the model constants are the standard ones most widely accepted, they can be changed if needed.[111]

3.2.4 RNG k-ε

The RNG k-ε model was derived using a statistical technique called renormalization group theory. It is similar in form to the standard k-ε model, but includes the following refinements:

- The RNG model has an additional term in its equation that improves the accuracy for rapidly strained flows;
- The effect of swirl on turbulence is included in the RNG model, enhancing accuracy for swirling flows;
- The RNG theory provides an analytical formula for turbulent Prandtl numbers, while the standard k-ε model uses user-specified, constant values;
- While the standard k-ε model is a high-Reynolds number model, the RNG theory provides an analytically derived differential formula for effective viscosity that accounts for low-Reynolds number effects. Effective use of this feature does, however, depend on an appropriate treatment of the near-wall region.

These features make the RNG k-ε model more accurate and reliable for a wider class of flows than the standard k-ε model. The RNG-based k-ε turbulence model is derived from the instantaneous Navier-Stokes equations, using a mathematical technique called "renormalization group" (RNG) methods. The analytical derivation results in a model with constants different from those in the standard k-ε model, and additional terms and functions in the transport equations for k and ε.[115]
While this model was used in the following work, it was only applied nominally before the results shown in Figure 5.49, being then disregarded in favour of the standard k-ε model that provided seemingly better results for turbulent flows in the work cases displayed here, as such it will not be further elaborated upon.

3.2.5 Realizable k-ε

The realizable k-ε model differs from the standard k-ε model in two important ways:

- The realizable k-ε model contains an alternative formulation for the turbulent viscosity.
- A modified transport equation for the dissipation rate, ε, has been derived from an exact equation for the transport of the mean-square vorticity fluctuation.

The term "realizable" means that the model satisfies certain mathematical constraints on the Reynolds stresses, consistent with the physics of turbulent flows. Neither the standard k-ε model nor the RNG k-ε model is realizable.[113]
While this model was used in the following work, it was only applied nominally before the results shown in Figure 5.49, being then disregarded in favour of the standard k-ε model that provided seemingly better results for turbulent flows in the work cases displayed here, thus it will not be further elaborated upon.

3.2.6 Modeling Turbulent Production in the k-ε Models

The term G_k, representing the production of turbulence kinetic energy [108] , is modeled identically for the standard, RNG, and realizable k-ε models. From the exact equation for the transport of k, this term may be defined as

$$G_k = -\rho\overline{u_i' u_j'}\frac{\partial u_j}{\partial x_i} \tag{3.47}$$

To evaluate G_k in a manner consistent with the Boussinesq hypothesis,

$$G_k = \mu_t S^2 \tag{3.48}$$

where S is the modulus of the mean rate-of-strain tensor, defined as

$$S \equiv \sqrt{2S_{ij}S_{ij}} \tag{3.49}$$

3.2.7 Effects of Buoyancy on Turbulence in the k-ε Models

When a nonzero gravity field and temperature gradient are present simultaneously, the k-ε models in ANSYS Fluent account for the generation of k due to buoyancy G_b, and the corresponding contribution to the production of ε.[108] The generation of turbulence due to buoyancy is given by

$$G_b = \beta g_i \frac{\mu_t}{Pr_t}\frac{\partial T}{\partial x_i} \tag{3.50}$$

where Pr_t is the turbulent Prandtl number for energy and g_i is the component of the gravitational vector in the i^{th} direction. For the standard and realizable k-ε models, the default value of Pr_t is 0.85. The coefficient of thermal expansion, β, is defined as

$$\beta = -\frac{1}{\rho}\left(\frac{\partial \rho}{\partial T}\right)_p \tag{3.51}$$

3.2.8 Convective Heat and Mass Transfer Modelling in the k-ε Models

In ANSYS Fluent, turbulent heat transport is modeled using the concept of Reynolds analogy to turbulent momentum transfer. The "modelled" energy equation is therefore given by

$$\frac{\partial}{\partial t}(\rho E) + \frac{\partial}{\partial x_i}\left[u_i\left(\rho E + p\right)\right] = \frac{\partial}{\partial x_j}\left(k_{eff}\frac{\partial T}{\partial x_j} + u_i(\tau_{ij})_{eff}\right) + S_h \tag{3.52}$$

where E is the total energy, k_{eff} is the effective thermal conductivity, and $(\tau_{ij})_{eff}$ is the deviatoric stress tensor, defined as

$$(\tau_{ij})_{eff} = \mu_{eff}\left(\frac{\partial u_j}{\partial x_i} + \frac{\partial u_i}{\partial x_j}\right) - \frac{2}{3}\mu_{eff}\frac{\partial u_k}{\partial x_k}\delta_{ij} \tag{3.53}$$

The term involving $(\tau_{ij})_{eff}$ represents the viscous heating, and is always computed in the density-based solvers. Additional terms may appear in the energy equation, depending on the physical models used. For the standard and realizable k-ε models, the effective thermal conductivity is given by

$$k_{eff} = k + \frac{C_p\mu_t}{Pr_t} \tag{3.54}$$

where k, in this case, is the molecular thermal conductivity. The default value of the turbulent Prandtl number is 0.85.[108]

3.2.9 Boussinesq Approach

The Boussinesq hypothesis is used in the Spalart-Allmaras model, the k-ε models, and the k-ω models. In the case of the Spalart-Allmaras model, only one additional transport equation (representing turbulent viscosity) is solved. In the case of the k-ε and k-ω models, two additional transport equations (for the turbulence kinetic energy, k, and either the turbulence dissipation rate, ε, or the specific dissipation rate, ω) are solved, and μ_t is computed as a function of k and ε or k and ω.[108] Another advantage of the Boussinesq hypothesis is, variations in fluid properties other than density ρ are ignored, and density only appears when it is multiplied by g, the gravitational acceleration.[116]

3.2.10 Natural Convection and Buoyancy-Driven Flows Theory

When heat is added to a fluid and the fluid density varies with temperature, a flow can be induced due to the force of gravity acting on the density variations. Such buoyancy-driven flows are termed naturalconvection (or mixed-convection) flows and can be modeled by ANSYS Fluent. The importance of buoyancy forces in a mixed convection flow can be measured by the ratio of the Grashof and Reynolds numbers:

$$\frac{Gr}{Re^2} = \frac{g\beta\Delta TL}{\nu^2} \tag{3.55}$$

When this number approaches or exceeds unity, you should expect strong buoyancy contributions to the flow. Conversely, if it is very small, buoyancy forces may be ignored in your simulation. In pure natural convection, the strength of the buoyancy-induced flow is measured by the Rayleigh number:

$$Ra = \frac{g\beta\Delta T L^3 \rho}{\mu\alpha} \tag{3.56}$$

where β is the thermal expansion coefficient:

$$\beta = -\frac{1}{\rho}\left(\frac{\partial\rho}{\partial T}\right)_p \tag{3.57}$$

and α is the thermal diffusivity:

$$\alpha = \frac{k}{\rho c_p} \tag{3.58}$$

Rayleigh numbers less than 10^8 indicate a buoyancy-induced laminar flow, with transition to turbulence occurring over the range of $10^8 < Ra < 10^{10}$.[117]

3.2.11 The Energy Equation

ANSYS Fluent solves the energy equation in the following form:

$$\frac{\partial}{\partial t}(\rho E) + \nabla\cdot(\vec{\nu}(\rho E + p)) = \nabla\cdot\left(k_{eff}\nabla T - \sum_j h_j\vec{J}_i + (\overline{\overline{\tau}}_{eff}\cdot\vec{\nu})\right) + S_h \tag{3.59}$$

where k_{eff} is the effective conductivity ($k + k_t$, where k_t is the turbulent thermal conductivity, defined according to the turbulence model being used), and $\vec{J}_i$ is the diffusion flux of species j. The first three terms on the right-hand side of Equation 3.59 represent energy transfer due to conduction, species diffusion, and viscous dissipation, respectively. S_h includes volumetric heat sources that you have defined but not the heat sources generated by finite-rate volumetric or surface reactions since species formation enthalpy is already included in the total enthalpy calculation.
In Equation 3.59,

$$E = h - \frac{p}{\rho} + \frac{\nu^2}{2} \tag{3.60}$$

where sensible enthalpy h is defined for ideal gases as

$$h = \sum_j Y_j h_j \tag{3.61}$$

and for incompressible flows as

$$h = \sum_j Y_j h_j + \frac{p}{\rho} \tag{3.62}$$

In Equation 3.61 and 3.62, Y_j is the mass fraction of species j and

$$h_j = \int_{T_{ref}}^{T} c_{p,j} dT \tag{3.63}$$

The value used for T_{ref} in the sensible enthalpy calculation depends on the solver and models in use. For the pressure-based solver T_{ref} is 298.15 K except for probability density function models in which case T_{ref} is a user input for the species. For the density-based solver T_{ref} is 0 K except when modeling species transport with reactions in which case T_{ref} is a user input for the species.[114]

3.3 Melting and Solidification

ANSYS Fluent can be used to solve fluid flow problems involving solidification and/or melting taking place at one temperature (for example, in pure metals) or over a range of temperatures (for example, in binary alloys). Instead of tracking the liquid-solid front explicitly, ANSYS Fluent uses an enthalpy-porosity formulation. The liquid-solid mushy zone is treated as a porous zone with porosity equal to the liquid fraction, and appropriate momentum sink terms are added to the momentum equations to account for the pressure drop caused by the presence of solid material. Sinks are also added to the turbulence equations to account for reduced porosity in the solid regions. ANSYS Fluent provides the following capabilities for modeling solidification and melting:

- calculation of liquid-solid solidification/melting in pure metals as well as in binary alloys;
- modeling of continuous casting processes (that is,“pulling” of solid material out of the domain);
- modeling of the thermal contact resistance between solidified material and walls (for example, due to the presence of an air gap);
- modeling of species transport with solidification/melting;
- postprocessing of quantities related to solidification/melting (that is, liquid fraction and pull velocities)

These modeling capabilities allow ANSYS Fluent to simulate a wide range of solidification/melting problems, including melting, freezing, crystal growth, and continuous casting.[108]

An enthalpy-porosity technique [118], [119] is used in ANSYS Fluent for modeling the solidification/melting process. In this technique, the melting interface is not tracked explicitly. Instead, a quantity called the liquid fraction, which indicates the fraction of the cell volume that is in liquid form, is associated with each cell in the domain. The liquid fraction is computed at each iteration, based on an enthalpy balance. The mushy zone is

a region in which the liquid fraction lies between 0 and 1. The mushy zone is modeled as a "pseudo" porous medium in which the porosity decreases from 1 to 0 as the material solidifies. When the material has fully solidified in a cell, the porosity becomes zero and hence the velocities also drop to zero.

3.3.1 Energy Equation

The enthalpy of the material is computed as the sum of the sensible enthalpy, h, and the latent heat, ΔH:

$$H = h + \Delta H \tag{3.64}$$

where

$$h = h_{ref} + \int_{T_{ref}}^{T} c_p dT \tag{3.65}$$

and

$h_{ref} =$ reference enthalpy
$T_{ref} =$ reference temperature
$c_p =$ specific heat at constant pressure

The liquid fraction, β, can be defined as

$$\begin{aligned} &\beta = 0 && \text{if } T < T_{solidus} \\ &\beta = 1 && \text{if } T > T_{liquidus} \\ &\beta = \tfrac{T - T_{solidus}}{T_{liquidus} - T_{solidus}} && \text{if } T_{solidus} < T < T_{liquidus} \end{aligned} \tag{3.66}$$

The latent heat content can now be written in terms of the latent heat of the material, L:

$$\Delta H = \beta L \tag{3.67}$$

The latent heat content can vary between zero (for a solid) and L (for a liquid).For solidification/melting problems, the energy equation is written as

$$\frac{\partial}{\partial t}(\rho H) + \nabla \cdot (\rho \vec{v} H) = \nabla \cdot (k \nabla T) + S \tag{3.68}$$

where

H enthalpy
ρ density
$\vec{v}$ fluid velocity
S source term

The solution for temperature is essentially an iteration between the energy equation 3.68 and the liquid fraction equation 3.66. Directly using Equation 3.66 [120] to update the liquid fraction usually results in poor convergence of the energy equation. In ANSYS Fluent, the method suggested by Voller and Swaminathan is used to update the liquid fraction.

3.3.2 Momentum Equations

The enthalpy-porosity technique treats the mushy region (partially solidified region) as a porous medium. The porosity in each cell is set equal to the liquid fraction in that cell. In fully solidified regions, the porosity is equal to zero, which extinguishes the velocities in these regions. The momentum sink due to the reduced porosity in the mushy zone takes the following form:

$$S = \frac{(1-\beta)^2}{(\beta^3+\varepsilon)} A_{mush}(\vec{\nu} - \vec{\nu_p}) \tag{3.69}$$

where β is the liquid volume fraction, ε is a small number (0.001) to prevent division by zero, A_{mush} is the mushy zone constant (for the simulations, the constant value was considered to be the default setting of 10^5), and $\vec{\nu_p}$ is the solid velocity due to the pulling of solidified material out of the domain (also referred to as the pull velocity).

The mushy zone constant measures the amplitude of the damping; the higher this value, the steeper the transition of the velocity of the material to zero as it solidifies. Very large values may cause the solution to oscillate.

The pull velocity is included to account for the movement of the solidified material as it is continuously withdrawn from the domain in continuous casting processes. The presence of this term in Equation 3.69 allows newly solidified material to move at the pull velocity. If solidified material is not being pulled from the domain, $\vec{\nu_p} = 0$.[114]

3.3.3 Turbulence Equations

Sinks are added to all of the turbulence equations in the mushy and solidified zones to account for the presence of solid matter. The sink term is very similar to the momentum sink term in Equation 3.69:

$$S = \frac{(1-\beta)^2}{(\beta^3+\varepsilon)} A_{mush}\varphi \tag{3.70}$$

where φ represents the turbulence quantity being solved (k, ε, ω, and so on), and the mushy zone constant, A_{mush}, is the same as the one used in Equation 3.69.[114]

3.4 Numerical Code Settings

This section concerns itself with briefly presenting more specific and pertinent settings for the numerical models pressure-velocity coupling methods and other features of Ansys Fluent that were used in this work.

SIMPLE and SIMPLEC In Fluent, the standard Semi-Implicit Method for Pressure Linked Equations (SIMPLE) algorithm and the Semi-Implicit Method for Pressure Linked Equations-Consistent (SIMPLEC) (SIMPLE-Consistent) algorithm can be used. SIMPLE is the default, but some solutions benefit from using SIMPLEC, specially due to the

increased under-relaxation that can be applied. For relatively uncomplicated problems (laminar flows with no other models) where convergence is limited by the pressure-velocity coupling, you can have a converged solution faster using SIMPLEC. With SIMPLEC, the pressure-correction under-relaxation factor is generally set to 1.0, which aids in convergence speed-up. However, in some problems, this increase in the pressure-correction under-relaxation to 1.0 can lead to instability due to high mesh skewness. In this case, it is needed one or more skewness correction schemes, employ a more conservative under-relaxation value (up to 0.7), or to use the SIMPLE algorithm. For complex, turbulent flows with additional physical models, SIMPLEC will improve convergence only if it is being limited by the pressure-velocity coupling. Often any limitations will be from one of the additional modeling parameters, in this context, SIMPLE and SIMPLEC will give similar convergence rates.[121]

PISO All transient flow calculations should be performed using the PISO technique with neighbor correction, especially if a large time step is desired. With a bigger time step and an under-relaxation factor of 1.0 for both momentum and pressure, PISO can continue to produce accurate results. In comparison to SIMPLE or SIMPLEC with optimal under-relaxation factors, PISO with neighbor correction does not offer any appreciable advantages for steady-state situations.

For both steady-state and transient calculations on meshes with a significant degree of distortion, PISO with skewness correction is advised.For all equations, under-relaxation factors of 1.0 or close to 1.0 are advised when using PISO neighbor correction. Set the under-relaxation variables for momentum and pressure so that they add to 1 if you use the PISO skewness correction as the only adjustment for highly distorted meshes (without neighbor correction) (e.g., 0.3 for pressure and 0.7 for momentum). Follow the under-relaxation guidelines for PISO neighbor correction listed above if you employ both PISO methods.

It is not required to turn off the default connection between neighbor and skewness fixes for the majority of situations. However, it is advised to disable the default coupling between neighbor and skewness repairs for significantly distorted meshes.[121]

COUPLED Coupled is the pressure-based coupled algorithm for Pressure-Velocity Coupling. In comparison to the pressure-based segregated algorithm, this solver has some advantages. For steady-state flows, the pressure-based coupled algorithm yields a more reliable and effective single phase implementation. For scenarios utilizing the periodic mass-flow, NITA (Non-Iterative Time Advancement setting), and multiphase Eulerian boundary conditions, it is not offered.[121]

First-Order Upwind Scheme In the momentum and energy equations, the convection term is discretized using the first-order upwind approach. Quantities at cell faces are determined when first-order accuracy is required by presuming that any field variable's

cell-center values represent a cell-average value and hold throughout the entire cell; the face quantities are the same as the cell quantities. As a result, when first-order upwinding is chosen, the face value ϕ_f is set to the upstream cell's cell-center value ϕ. Both the density-based and pressure-based solvers support first-order upwind.[121]

Second-Order Upwind Scheme Quantities at cell faces are computed using a multidimensional linear reconstruction technique when second-order accuracy is desired. This method uses a Taylor series extension of the cell-centered solution around the cell centroid to attain higher-order precision at cell faces. In order to compute the face value ϕ_f when second-order upwinding is chosen, the following expression is used:

$$\phi_{f,S} = \phi + \nabla\phi \cdot \vec{r} \tag{3.71}$$

where $\vec{r}$ is the displacement vector from the centroid of the upstream cell to the face centroid, and ϕ and ∇_ϕ are the cell-centered value and its gradient in the upstream cell. This equation needs the gradient ∇_ϕ in each cell to be determined. Finally, the gradient ∇_ϕ is constrained to prevent the introduction of any additional maxima or minima. Both the density-based and pressure-based solvers support first-order upwind.[121]

4

Methods

This chapter features, for the studied cases, a description of the inputs of the CFD models employed, regarding general information about the models themselves such as: boundary conditions, material properties, grid design, solution algorithms, solution monitors and any considerations and assumptions about the models. Considering the exploratory nature of the work developed here, a portion of the methodology will be iterative, dictating how the initial work development progresses, which in turn will affect the chosen methodology subsequently used to advance further with the work, until a set of basic working methods are selected to progress from. This chapter will elaborate upon the reasoning and methodology used and will help understand the work process as it progresses towards a solution.

4.1 Thermal Storage System

As mentioned, since this is a research and development work aiming to effectively build and design equipment that does not exist yet, there were a considerable number of unknown factors concerning its features, parameters, properties, etc. needed to design the thermal storage equipment. Information gathered from the literature based on the phase change materials and heat exchangers characteristics was used for the considerations applied to the first group of CFD simulations that would test out simplified models. Since this storing equipment is meant for residential dwelling applications, a set of energy building simulations concerning energy efficiency/behaviour of said buildings would acquire the information related to their heating (domestic hot water included) and cooling needs. These would come to provide the basic requirements for the energy storage set points and capacity that became the focus of this study, creating a storage component that would combine the considerations for the energetic needs of a specific building and the necessary thermal storage capacity to sustain it using only renewable energy resources and beneficial electric tariffs. The energy building simulations are not within the scope of the study presented in this work.

To exchange the energy stored in the PCMs for actual use in the building the basic factor of the heat exchanger would be its type and respective geometric parameters. The

simplest heat exchanger would be a pipe, within which would flow the heat transfer fluid, inserted into a mass of PCM. This however would severely limit the heat transfer ratio, so a reasonable step would be to apply a method to increase this ratio between the heat transfer fluid and PCM. Part of this work consisted on simulating several methods in order to ascertain the one that would benefit the most the increase of heat transfer ratio, testing fins, metallic foams and nanoparticles mixed with the PCMs. Another important consideration to bear in mind is that most PCMs have low thermal conductivity that significantly hinders the heat transfer process, so adding a method to increase this heat transfer is a requirement.

The chosen heat exchangers for this project were finned tubes (akin to HVAC finned coils), reason being that they have a good heat transfer coefficient potential while already being a well-proven type of exchanger and for being used ubiquitously in regular HVAC systems. The geometry also played well with the project basic concept of modular holding tanks being used to store energy at a desired temperature level with the adequate PCM surrounding the heat exchanger. Other heat exchanger types were not considered because of several factors such as complexity, ease of installation/application, technical incompatibilities, compactness, ease of manufacture, etc. In the specific case of plate heat exchangers, they were not considered because, although they have great heat transfer rates and are very compact, the heat transfer would take place between a liquid and a PCM that frequently switches between both liquid and solid state. The density variation that takes place between the phases can be significant in some PCMs, ranging between 5 and 30%, this density variation could compromise the sealing of the plates of the heat exchanger, prompting PCM leakage.

To simulate the heat exchangers, the ideal step would be to build the full 3D domain of a heat exchanger with generic dimensions and progressively test out different features and parameters. Nevertheless, this would require significant resources, both computationally to generate the geometry and respective adequately refined CFD mesh, and time wise since it would take an unreasonable amount of running time to obtain any kind of results.

As such in the starting phase, a prototypical segment of the considered domain was drawn using a simple, one meter long pipe (see Figure 4.1). This would be made out of three or four domains, the heat transfer fluid, the pipe and the PCM (alternatively, a medium with PCM plus nanoparticles or metallic foam could be used, with respective properties, in the PCM domain) and when four domains are considered, it means that fins were added to the geometry. This would be further simplified and turned into an axisymmetric 2D geometry (see Figure 4.2).

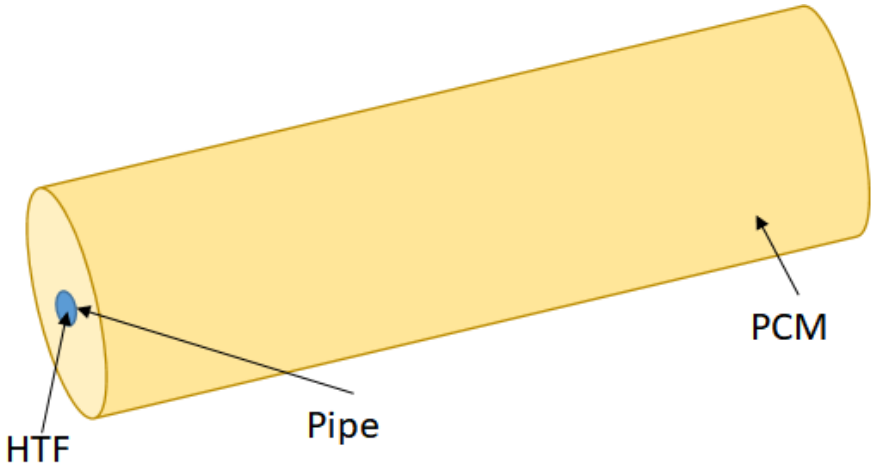

Figure 4.1: Simplified, 1 m long pipe with HTF, pipe and PCM domains.

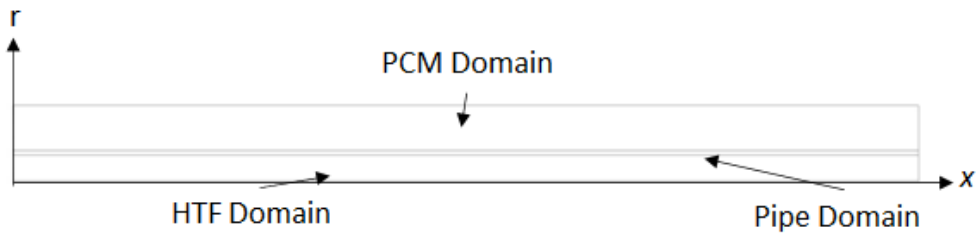

Figure 4.2: Simplified, 2D axisymmetric geometry.

4.1.1 Specific Heat Curve

Considering that the base for this endeavour to work successfully hangs on properly simulating PCM thermodynamic behaviour, a study was undertaken to study the effects of varying some of the material properties, specially the specific heat value. Given that PCMs work using latent heat, the code used to simulate has several ways to process the latent heat energy as well as the specific heat, several approaches were tested in order to verify which would be the best method to simulate it. The aim here was to ultimately know the best way to simulate PCM properties when close to the phase change, and to gain experience simulating with conditions never used before with an unknown material. In this stage, a model was built using Figure 4.2 geometry and tested with different thermodynamic properties such as density, thermal conductivity, phase change enthalpy and specially, specific heat.

It is worth noting that PCMs themselves are known to have properties that can vary depending on factors such as sample size and analysis method. This is due in part to the lack of standardized production methods and lack of certification procedures, however as these materials see more frequent applications this should stop being a concern. For example, the typical properties of a phase change material supplied by a commercial catalogue can

be, to an extent, different when undergoing an independent analysis. As mentioned in the Literature Review (Chapter 2), even samples from the same batch can have different behaviours/properties when tested microscopically, even though macroscopically they can have the same proper behaviour. Some of the PCMs considered for the simulations were tested for properties verification, some were not, for lack of resources, therefore the properties of such PCMs considered to be the ones being presented in the commercial catalogues.

4.1.2 Heat Transfer Methods

Following the previous phase, a group of simulations were performed to study how different methods of enhancing the heat exchange worked, comparing different parameters in an effort to direct the focus of the work. Starting from a basic axisymmetric construct of a pipe flowing heat transfer fluid (see Figure 4.2), the pipe itself and the storage medium (PCM), this would be the standard which all the following simulations in this stage will be compared to. The simulations considered heat transfer methods such as metallic foams with different porosities, nanoparticles, and fins.

In the case of metallic foams and nanoparticles the model was built using a combination of both the PCM and the foam/nanoparticles properties, in due proportion, and these equivalent characteristics were attributed to the whole PCM domain. Regarding the fins, they were effectively drawn in the geometry having a mesh, domain and properties of their own.

The PCM selected to be simulated was A53 (from PCM, products.inc catalogue), at this stage the reason for choosing this PCM relies solemnly on the phase change temperature being close to one of the storage temperatures considered and served as a starting point. For all the simulations, the HTF inlet temperature taken into consideration was 15ºC.

4.1.3 Sizing

Drawing from the conclusions taken from the previous simulation group this led to the following step, where a model based on the chosen heat exchanger type to be simulated was simplified. Starting from the general concept of the heat exchanger (Figure 4.3) that would have to be fitted into a specific storage volume, 1,5 m^3, that was stipulated by the project. From here, the geometry was simplified into blocks of influence of each of the single pipe circuits. Each circuit was then separated into circular sections of influence where the surface area is the same (see Figure 4.4).

Figure 4.3: Example of the typology of the heat exchanger considered. (This example shows a staggered tube arrangement.)[122]

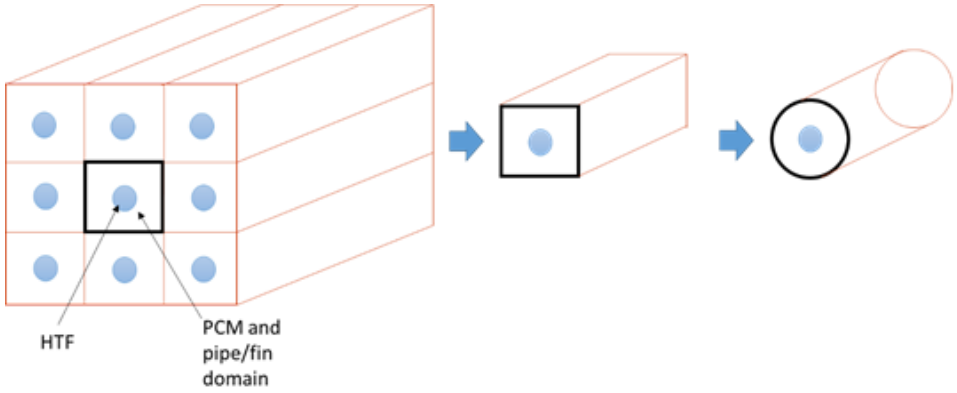

Figure 4.4: Typology of heat exchanger considered without collectors or curves and simplified with the axisymmetric geometry having the same cross section area of the 3D geometry.(The ilustrated simplication considers a simple square tube arrangement.)

It was specified that there would be three types of energy storage at a constant temperature. For ease of reference, they are called “cold” storage, “hot” storage and Domestic Hot Water (DHW) Storage, any additional thermal needs that cannot be met by the storage system are to be supplemented by a ground source heat pump. As their name implies each storage group will be aimed at storing energy at an approximately constant temperature to cool, heat and supply the necessary hot water to the residence. The temperatures are not necessarily restricted to a single specific value but can vary within an acceptable range, depending on the application it is for, the heat pump capacity and the available

PCMs that can be worked with at said range. For instance regarding the DHW storage, the minimal acceptable temperature considered was 45ºC, and taken into account that this set up would be required to heat up water coming in from the public water supply network that was estimated to be around 15ºC for at least 15 minutes, an adequate PCM would have to be able to meet conditions to achieve the required heating temperature and sufficient energy. Concerning the hot storage that would be used to heat the residence, the temperature considered should be able to heat to a comfortable temperature the interior of a building, this temperature was deliberated to be 22ºC, as per good HVAC practices. To achieve a satisfactory interior temperature and to minimise the ground sourced heat pump workload, and therefore increasing its efficiency, the minimum acceptable temperature for a 5 degree operation ΔT would be 39-40ºC. Regarding the cold storage that would be used to cool the building, the operating temperature should be able to cool the inside of the building's divisions at around 26ºC, as such its operation temperature was considered to be around 8-9ºC.

Each of the storage groups will work in tandem with a system that will both discharge it for home application usage and charge them to replenish the drained energy. In the concept of this work, the renewable energy sources will be solar panels and a ground sourced heat pump. Each of the storage systems will have a variation of the same operation method, in the DHW case, it will be a heat exchanger with three distinct circuits (within the heat exchanger), two closed circuits for charging the tank using solar collectors and the ground sourced heat pump. The third is an open circuit used for discharging, heating up water directly from the public network for domestic use. This circuit configuration allows the system to be in use while also being charged.
The hot storage will have two closed circuits. One for charging via solar collectors, exclusively. The other is to be used both for charging by the ground sourced heat pump, when needed and for discharging to use directly in the building's terminal units or in combination with the heat pump.
The cold storage will have just a single circuit that will be used both for discharge, to be used in the residence's terminal units and for charging via heat pump. Despite these differences between each storage group, they work exactly with the same principles.

With these considerations in mind, several parameters were simulated and tested for performance and results such as individual coils circuit length, fin height (also known as the spacing between pipes), HTF mass flow rate, fin pitch (spacing between each fin in a circuit) and heat exchanger materials. Although not effectively an heat exchanger parameter, another ponderation of the study that was also taken into consideration was the operation mode of the system (i.e. working in discharge or charge mode) to study how the distinct modes settings affected the phase change process of the PCM as each mode will effectively have different operative conditions.

The results from these simulations, through comparing values and eliminating non-relevant inputs, gave the required heat exchanger features to successfully achieve the desired performance. The concept was then tested out in laboratory to be verified first

with a pre-prototype simple circuit length and then later on at a full-scale replica of the storage that is to be installed in a location for field demonstration. The experimental results comparison with the numerical work yields reasonably good matches implying that the chosen approach and method is adequate to simulate this kind of storing system.

4.2 Ground Sourced Heat Pump Boreholes

The second part of the work regarding this project is to develop and improve the working of the boreholes heat exchangers by use of PCM in the boreholes themselves. Ground sourced heat pumps are known for their great thermal efficiency while operating with the same expansion cycle that regular HVAC systems use. This comes from the fact that the exterior energy source is the soil and not atmospheric air. Soil, unlike air, can maintain a very homogenous temperature throughout the year-round season cycle, while atmospheric air varies wildly even on a daily basis. The temperature stability allows for a great operative efficiency for both the heating and cooling mode of the heat pump, however the same soil that has such a great benefit also has a major drawback, thermal saturation. There is always a degree of thermal variation in the boreholes while a ground sourced heat pump is in operation, nevertheless if not properly designed or if overworked, a boreholes' energy can be sapped or unbalanced in the sense that the original soil temperature will change thus also changing the efficiency of the heat pump operating with the boreholes.

Since this project bears considerable dependence of a ground sourced heat pump, this part of the work will address the design and solutions for encapsulating PCM within a geothermal borehole in an effort to stabilize its temperature despite regular use, contributing to store some energy as well. Considering that geothermal energy tapping is an expensive technology, the considerations for the improvements will consider an effort to minimize any significant alteration to it, lest risk increasing significantly its cost.

In the first phase, the work focused in using encapsulation at a macroscopic scale, i.e. using closed pipe length to house PCM. To that end, a 2D approach was used to simulate a cross section of the borehole heat exchanger, testing out different boreholes heat exchanger types (coaxial, single U, double U) in combination with different encapsulation distributions of PCM (see Figure 4.5). These models were simulated to study the distribution of temperature along the borehole section in both charging and discharge mode, as well as to evaluate the elapsed time for the phase change to completely take place, for the operative conditions. Another initial focus of this study was to establish what area of effect the borehole had in the surrounding soil so that this information could be used when progressing to 3D modelling. Upon the conclusion of the previous simulations a 3D approach (see Figure 4.6) was used to effectively simulate operating boreholes with a model that took into consideration how a "on/off" ground sourced heat pump would operate versus how a variable ground sourced heat pump would operate. The results would then be compared in an effort to evaluate the best type of heat pump to be used in the installation.

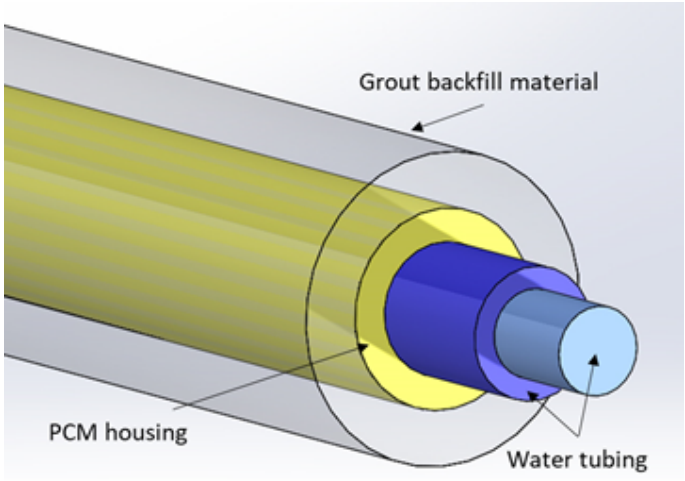

Figure 4.5: Example of PCM encapsulation in a borehole coaxial type.

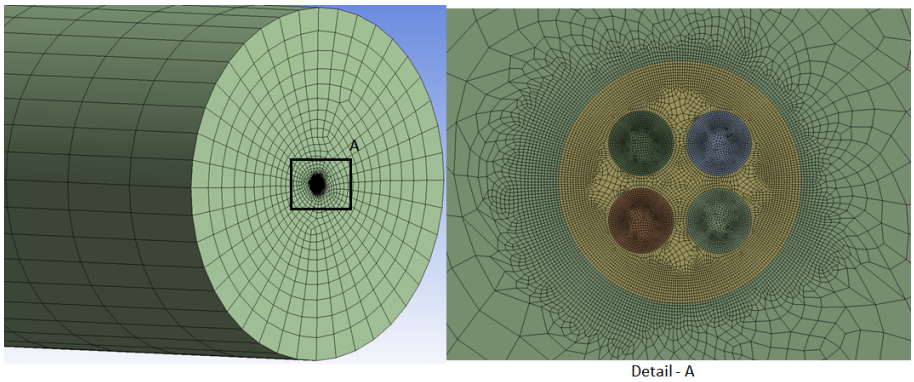

Figure 4.6: Mesh and computational domain outline.

4.3 CFD Models - Configuration and Inputs

The following section will address the construction and building of the CFD models, the basic assumptions and considerations for the 2D and 3D geometry, meshing and simulation model. This section will be further divided to focus separately on each of the applications developed in the line of this work. It is important to bear in mind that while there are applications of the individual technologies used for the system, the combination of such technologies was never done in such a way as it is presented in this work, therefore, there is no actual precedent for such a system. As previously mentioned, the work that this thesis rests on is a fraction, but ultimately the basis for a whole new heating, cooling and hot water producing system for residential dwellings and solutions for energy saving applications in agricultural-food industry. Aiming to combine thermal energy storage, solar and geothermal energy, to allow for bridging the gap of the frequent discrepancy between energy's supply and demand and storing energy for constant temperature processes. The general principle of this work is to design develop, validate and demonstrate a modular thermal storage system that can provide for all the thermal energy needs of a residential

building (heating, cooling and domestic hot water) and develop solutions for energy storing and saving for food production processes. To this end, Phase Change Materials (PCMs) would be stored/combined in tanks with heat exchangers, as well as with in geothermal boreholes to store energy at constant temperatures. All the different variables and requirements of the building applications would be run and optimized by a self-learning control system (this self-learning system is outside the scope of this work) that would manage all the components to garner the best performance possible. The ultimate end here being the implementation of the system into demonstration sites for validation. The thesis focuses on the development of the heat exchangers that interact directly with the PCMs that have their own challenges and the provided solution is at least one method to circumvent such issues.
For all presented cases in this work, the code used to simulate the solutions of the presented problems was Ansys Fluent v17.1.
The computing platform used for running the simulations was: CPU Xeon E3-1241 3.50GHz, RAM 16GB DDR3 1600MHz, GPU NVIDIA Quadro K2200 4GB.
It should be noted that all the cases in this work were run with a double precision solver setting.

4.3.1 Latent Heat Thermal Storage System Heat Exchangers

At the starting point of the development of the heat exchanger very few operational details were known beforehand. This meant that there were no strict reference points so a basic, all-purpose approach was chosen so that could be easily applied to any forthcoming inputs.

4.3.1.1 Domain Representation

For this application a 2D approach was selected as it was assumed that the heat transfer process could be modelled in such a way and it would allow for a greater range of mesh enhancements should a greater refinement be needed. For the heat exchanger type it was chosen an aluminium finned copper pipe that would be immersed in PCM inside a tank. While the tube array has a square distribution, one can make an approximation to a circular section with the same cross section area (Figure 4.7).

With this method the outer boundary of the physical domain is set between the halfway point between the pipes and set as an adiabatic boundary condition, with each finned tube being simulated individually, disregarding the influence of the surrounding pipes. The simplification considered here also bears in mind that the individual pipe domain be equated to a 2D axisymmetric section.
Upon consultation of commercial catalogues, a pipe dimension was selected with 10mm outside diameter and 8.6mm inside diameter, with 0.7mm pipe wall thickness (Figure 4.8). The fin thickness was considered 0.3mm and each fin was spaced 4.7mm apart, totalling 5mm spacing including the fin thickness. Regarding the fin height, or in other words, the halfway distance between the vicinity pipes, this feature is addressed separately as it is

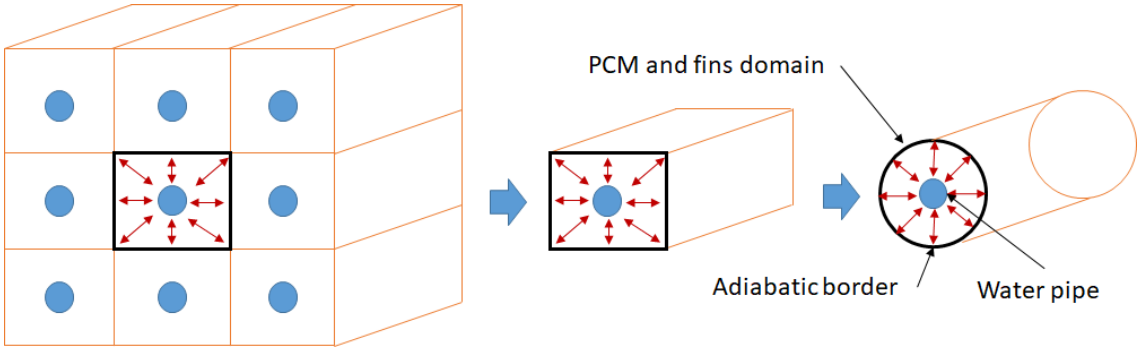

Figure 4.7: Geometric approximation for the simplification of the model. (Squared tube arrangment.)

one of the studied parameters along with the pipe length. The inlet and outlet radious equivalent dimensions are 4.3mm for the inner tube radius.

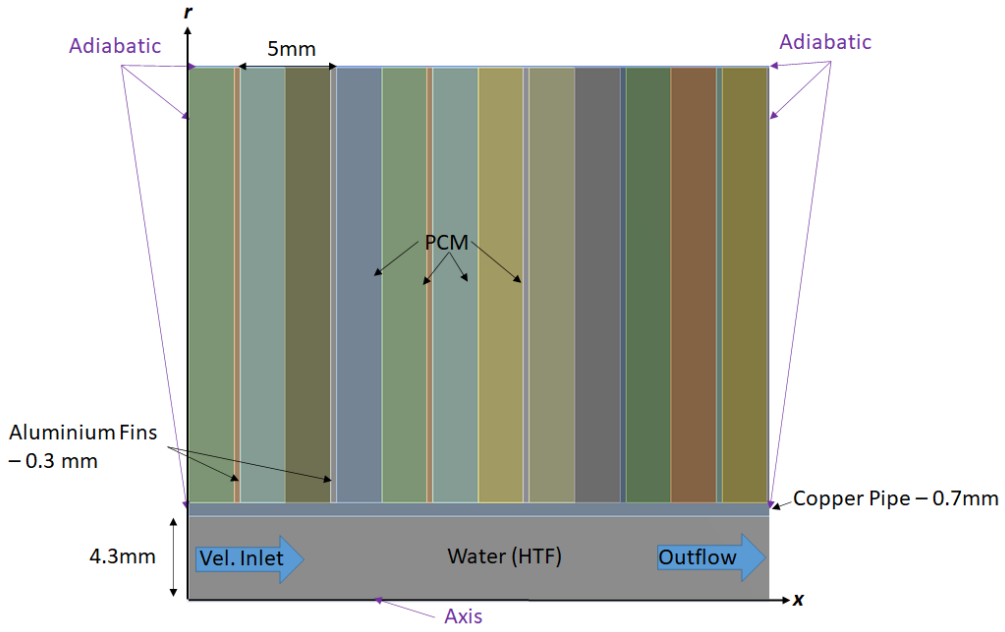

Figure 4.8: Model geometry dimensions, materials and boundary conditions.

There are four distinct materials used in the simulation: Copper, for the pipe; Aluminium, for the fins; Water as the heat transfer fluid and PCM for latent thermal storage, since PCM properties vary depending on its specific application it is not specifically scrutinized in this chapter and will be displayed later with better context, but the remaining materials properties that are consistently present in all the simulations are presented in Table 4.1 and displayed in Figure 4.8.

Table 4.1: Materials properties.

Property	**Aluminium**	**Copper**	**Water**
ρ [kg/m^3]	871	8978	998.2
Cp [J/kg.K]	271.9	381	4182
k [W/m.K]	202.4	387.6	0.6
μ [kg/m.s]	-	-	0.001003

4.3.1.2 Boundary Conditions and Initialization

There are four boundary conditions, presented in Figure 4.8*:

- Axisymmetric configuration that represents the Axis running through the centre of the water pipe;
- Inlet – Velocity Inlet, the velocity vector normal to the boundary, with constant velocity and temperature** as it would aim to mimic the operation of a heap pump, regulating the flow and temperature;
- Outlet – Outflow, matching the outlet flow to the inlet flow;
- All other boundaries were considered adiabatic walls as it was assumed that the remaining surroundings would not have significant effect on the studied domain.

* No temperatures are shown here as they are different for every process, even then within the same process there could be some variations, as such they are presented where more context is provided, while here the focus is only on the methods and set up of the model.

** In some cases, namely the cases that were run to check the verification of the CFD model when comparing with the experimental cases User Defined Functions (UDFs) were employed to describe the inlet temperature behaviour as closely as possible to what was registered in the experiments, aiming to ensure the closest possible match.

Hybrid initialization with the default features was chosen for all cases, the hybrid initialization employs a collection of recipes and boundary conditions interpolation methods, solving Laplace's equation to determine the velocity and pressure fields. All other variables including: temperature, turbulence, species, volume fractions, etc. will be automatically patched on domain averaged values or a particular interpolation recipe [121]. The initialized model was then patched with a temperature on all domains, its value would depend on the process being studied; if the process was discharge, the domain would be patched with a temperature slightly (approx. one degree) above the liquidus temperature of the PCM in use, if it was charge, it would be patched with a temperature slightly below the solidus temperature of the PCM.

4.3.1.3 Spacial Discretization

Given that the processes taking place in the heat exchanger through means of a working fluid and a latent heat storage medium, the following models were used throughout the development:

- Viscous models:
  - Laminar;
  - Transition - SST and kkl;
  - Turbulence - k-ε standard, RNG and Realizable;
- Energy;
- Solidification and Melting.

The different turbulent models were employed because of different flow rates tested throughout the work, particularly when comparing with experimental results, this is the same reason why different models/variations within the same turbulence models were used (RNG and Realizable), to ascertain what differences, if any, were between the use of such models comparatively to the standard defaults.

Wall Functions To ascertain if it is necessary to implement a wall function treatment, a y^+ check was done to the mesh that was selected to be used in all simulations after the dependence study. Immediately adjacent to the wall we have an extremely thin viscous sub-layer followed by the buffer layer and the turbulent core. The number of mesh points required to resolve all the details in a turbulent boundary layer would be prohibitively large, and normally the 'wall functions' are employed to represent the effect of the wall boundaries. A near-wall flow is taken to be laminar if $y^+ \leq$11,63. The wall shear stress is assumed to be entirely viscous in origin. If $y^+ >$11,63 the flow is turbulent, and the wall function approach is used. The criterion places the changeover from laminar to turbulent near-wall flow in the buffer layer between the linear and log-law regions of a turbulent wall layer. The exact value of $y^+ =$11,63 is the intersection of the linear profile and the log-law [114]. Given the emphasis on the heat exchange process in this case an analysis was run to check the y^+ value for the water flow (heat transfer fluid) and the pipe wall interaction (See Figure 4.9). Looking at the figure, it can be seen the y^+ value stays below the threshold of 11,36, thus it is not required an additional wall treatment function.

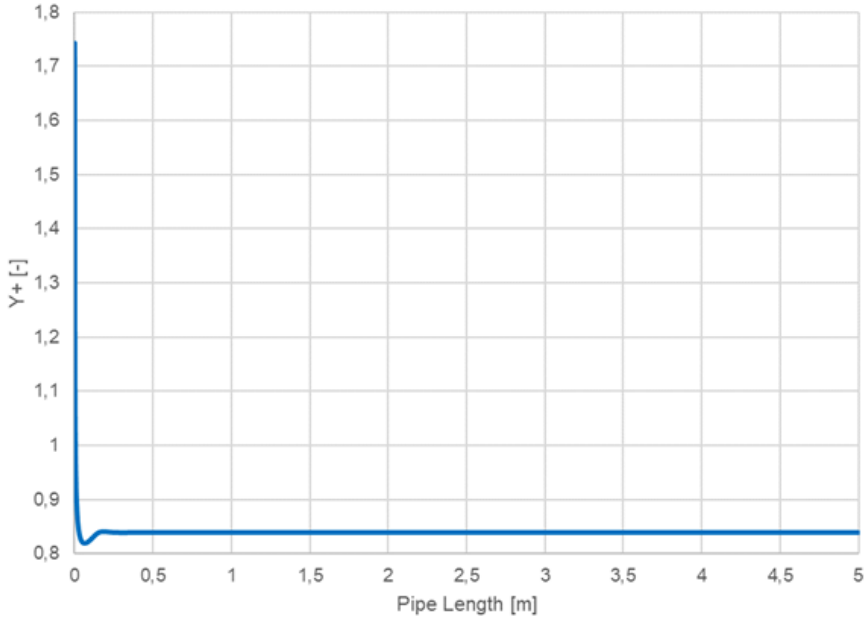

Figure 4.9: y^+ values for the interaction between the pipe wall and fluid (water, velocity inlet 0.1 m/s).

4.3.1.4 Mesh Design

Conscious effort was taken to achieve a reasonably good mesh for the model, specifically a structured, square-element grid. One of the influences for the simplification shown previously was that a 2D geometry with square geometric elements could provide a good starting point for a structured and square mesh. This would also allow for some room concerning the alteration of the mesh finesse should it be necessary as well as for the mesh-independence study. The resulting meshed body was, as seen in Figure 4.10, a structured, square mesh with low skewness, with 571200 elements and 579669 nodes. It can be noted in the figure that an inflation layer was added to the water domain in the interface with the pipe domain to improve interaction between the fluid and the solid wall where the heat transfer would take place.

A grid-dependency study was undertaken with a coarser (approx. 20% less elements) and finer (approx. 20% more elements) mesh, comparing some of the results of each simulation to ascertain matching results. As it can be seen on Figure 4.11, the results for the water outlet temperature and liquid mass fraction for each of the different degrees of mesh refinement show that all the lines mostly overlap with each other, with some slight deviations only present on the coarser mesh. This means that the mesh used for these models has a good definition.

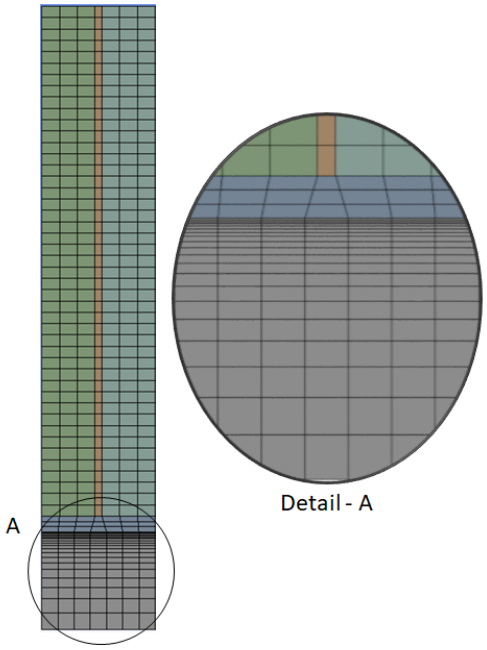

Figure 4.10: Grid section and inflation layer detail.

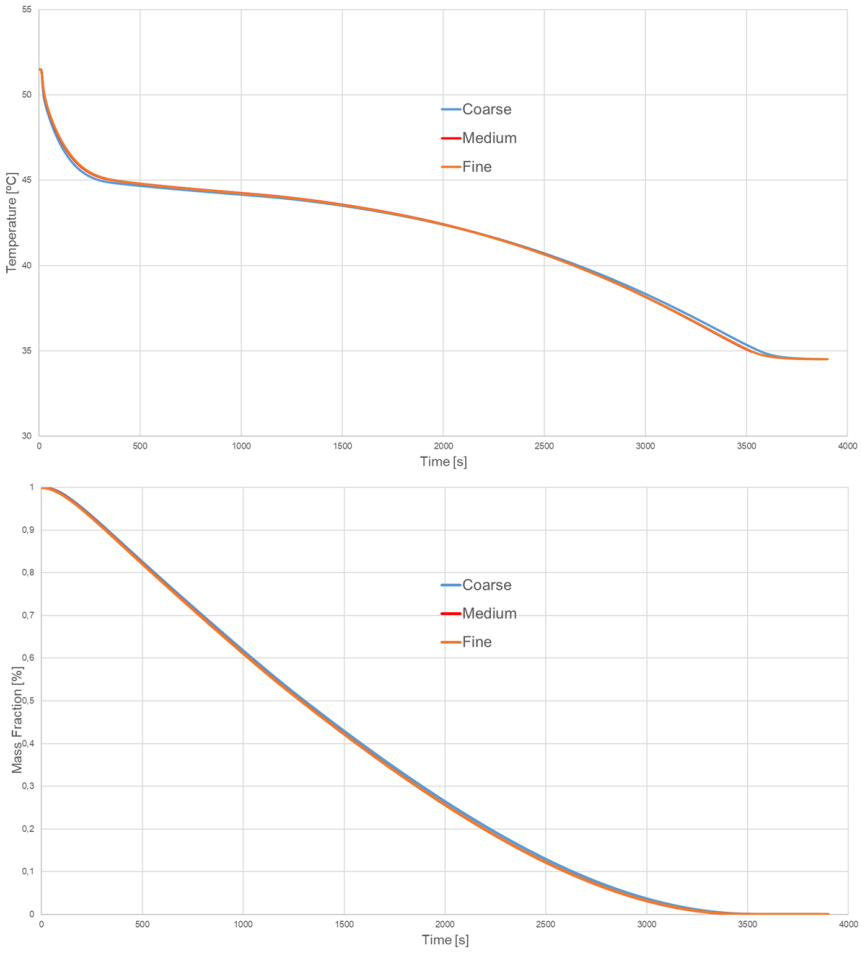

Figure 4.11: Independence test results for temperature and liquid mass fraction with an inlet velocity of 0.1m/s.

4.3.1.5 Solution Algorithms

General Settings For all the simulations the general settings were left with the defaults, with the solver Type set to "Pressure-Based" and Velocity Formulation set to "Absolute". As mentioned, the 2D Space was set to "Axisymmetric" and it had Gravity unchecked as it was assumed that given the close proximity of the fins, they would obstruct the vast majority of any natural convection that would take place if the fins were not so close together. The only exception being it the Time setting that would be set to "Transient" and this would be a process that would change over time.

Solution Methods The Scheme for the Pressure-Velocity coupling was set to "PISO" as it is highly recommended for all transient flow calculations.[121] For the Spatial Discretization, the Gradient was left with the default setting "Least Squares Cell Based". For the Pressure the setting was "PREssure STaggering Option (PRESTO)!" as in early simulation testing it provided seemingly better overall convergence times than the other methods. Momentum was set as default, "Second Order Upwind". Turbulent Kinetic Energy was set to default value "First Order Upwind". Turbulent Dissipation Rate was set as default "First Order Upwind". When first-order accuracy is desired, quantities at cell faces are determined by assuming that the cell-centre values of any field variable represent a cell-average value and hold throughout the entire cell; the face quantities are identical to the cell quantities. Thus, when first-order upwind is selected, the face value is set equal to the cell-centre value in the upstream cell.[121] When second-order accuracy is desired, quantities at cell faces are computed using a multidimensional linear reconstruction approach.[123] In this approach, higher-order accuracy is achieved at cell faces through a Taylor series expansion of the cell-centred solution about the cell centroid. Thus, when second-order upwind is selected, the face value is computed so that the cell centre discrete value and gradient of each cell-centre value and its gradient in the upstream cell times the displacement vector from the upstream cell centroid to the face centroid. This formulation requires the determination of the gradient value in each cell. Additionally, the gradient value is limited so that no new maxima or minima are introduced.[121] Overall, this makes the first order upwind the easiest interpolation scheme to converge, with only first order accuracy, while the second order upwind uses larger stencils for 2nd order accuracy, essential with tri/tet mesh or when flow is not aligned with grid, which can lead to a slower convergence. Given that the meshed used in this specific case is a fully squared and structured grid it was decided that, when used, a First Order Upwind interpolation scheme would provide adequate precision. Energy was also left as "Second Order Upwind".

Solution Controls (Under-Relaxation Factors) The under-relaxation factors for all the simulations were set to their default values: Pressure 0.3; Density 1; Body Forces 1; Momentum 0.7; Turbulent Kinetic Energy 0.8; Turbulent Dissipation Rate 0.8; Turbulent Viscosity 1; Liquid Fraction Update 0.9; Energy 1.

Iterative Convergence Regarding the convergence Residuals Monitors all were set to "Check Convergence" and all were left with the default setting of 1e-3 of "Absolute Criteria", with the exception of the Energy "Residual" that was set to 1e-12, the reasoning behind this lays in the fact that given the structured, squared mesh a very fast and possibly false convergence could be achieved, thus to prevent it this modification was made. The Residual Values were left as default with "Scale" that specifies whether or not to print or plot scaled residuals for each variable [121] and "Normalize" that specifies whether or not to normalize the printed or plotted residual for each variable by the value indicated as the Normalization Factor for that variable. The default Normalization Factor is the maximum residual value after the first 5 iterations, this was too, left as default. [121] The Convergence Criterion shows the residual value for which the solution of each variable will be considered converged, [121] was left as default "absolute", as well as all remaining features.

Time Discretization The setting for the Type was "Fixed" with a Time Step Size of 0,5 seconds, it was found in earlier tests that, with the used mesh, this time step size was a good compromise between accuracy and computational processing time.

NOTE: With the theoretical models and methodology presented so far the same methods were employed in the development of a heat exchanger and energy storage apparatus for food processing, the work for which is part of the academic published work developed in this thesis.

4.3.2 Ground Sourced Heat Pump Borehole Heat Exchangers

At the starting point of the development of the heat exchanger very few operational details were known beforehand. This meant that there were no strict starting points so a basic, all-purpose approach was chosen so that could be easily applied to any forthcoming inputs. For this heat exchanger specifically, the approach was slightly different than the on applied in the previous section. Since this section would involve borehole applications to start a 2D simulation was run to ascertain the diameter of the domain needed for the 3D simulations in order to make sure that the amount of soil would be unaffected by the borehole conditions.

4.3.2.1 Two-Dimensional Approach

Domain representation For this application a 2D approach was chosen initially as it was assumed that the heat transfer process could be modelled in such a way and it would provide valuable information concerning the soil domain when building a 3D model of a borehole. For the heat exchanger, given that the heat transfer process takes place radially and that the domain will have mostly uniform conditions it is reasonable to assume that a 2D quartered approach of the domain will simulate accurately the process. It should be noted that this model specifically represents a generic, horizontal slice of a typical borehole

with no soil variations in homogeneity. While there different borehole geometries like coaxial, single U and double U, the governing process between then and the surrounding soil is the same and since this stage of simulation is to determine the volume of the domain to be used in the 3D approximation any one geometry is adequate. For the example presented here a single U borehole ten square meters in section (Figure 4.12) was built to evaluate the domain effect on the borehole process with the given soil properties.

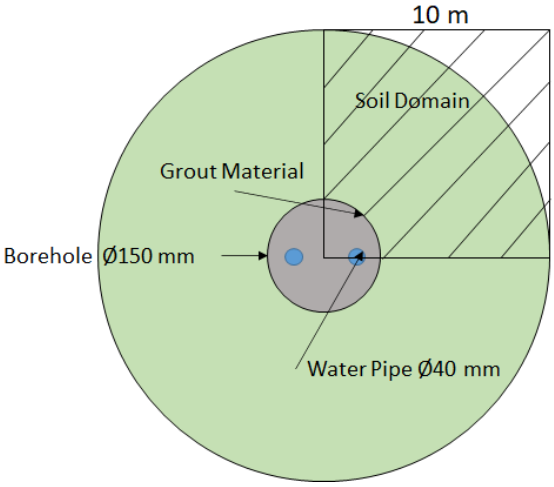

Figure 4.12: Borehole geometric approximation for the simplification of the 2D model.

For this example, the borehole dimensions were taken from the classic installation procedures from a drilling company. The borehole itself is filled with backfill grout material and has diameter of 150mm, the water pipes have a diameter of 40mm and are made of high-density polyethylene. There are three distinct materials used in the simulation: high-density polyethylene, for the tubing; back fill grout material, for filling the drilled boreholes and soil. The materials properties are presented in Table 4.2.

Table 4.2: Materials properties.

Property	**High-Density Polyethylene**	**Grout Material**	**Soil**
ρ [kg/m^3]	950	2250	1400
Cp [J/kg.K]	2000	1250	1000
k [W/m.K]	0.42	2.35	2

Boundary Conditions and Initialization There are three boundary conditions, illustrated in (Figure 4.13) and presented below:

- Constant temperature at water tube border (42,5ºC);
- Symmetry – Concerning the domain borders that would mirror the domain behaviour;
- Constant temperature at the outer border of the domain mimicking the soil infinite medium (18ºC).

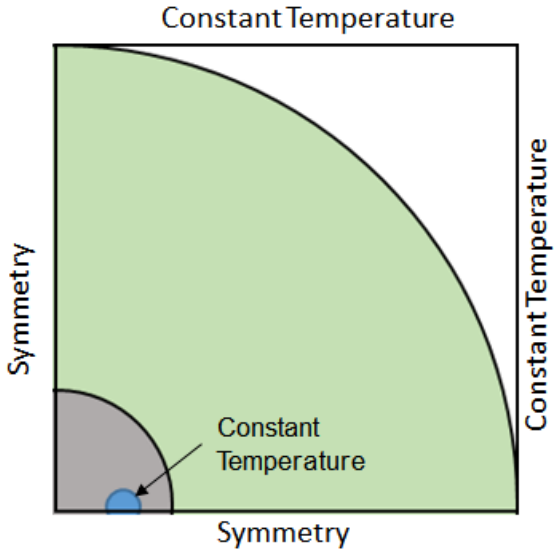

Figure 4.13: Borehole model boundary conditions.

Hybrid initialization with the default features was chosen, the hybrid initialization employs a collection of formulas and boundary conditions interpolation methods, solving Laplace's equation to determine the velocity and pressure fields. All other variables including: temperature, turbulence, species, volume fractions, etc. will be automatically patched on domain averaged values or a particular interpolation recipe.[121] The initialized model was then patched with a temperature on all domains, its value is 18°C to resemble a stabilized borehole at soil temperature before starting to be put in to work.

Spacial Discretization Given that the processes taking place in the heat exchanger by means of a working fluid and a latent heat storage medium the following models were used throughout the development:

Mesh Design Conscious effort was taken to achieve a reasonably good mesh for the model, specifically a structured, square-element grid. One of the influences for the simplification shown previously was that a 2D geometry with square geometric elements could provide a good starting point for a structured and square mesh. The resulting meshed body was, as seen in Figure 4.14, a structured, square mesh with moderate skewness, with 127000 elements and 128000 nodes. It can be noted in the figure that an inflation layer was added to the border between the water pipe and the boreholes grout material and the borehole and the soil domain to improve interaction between the fluid and the solid wall where the heat transfer would take place.

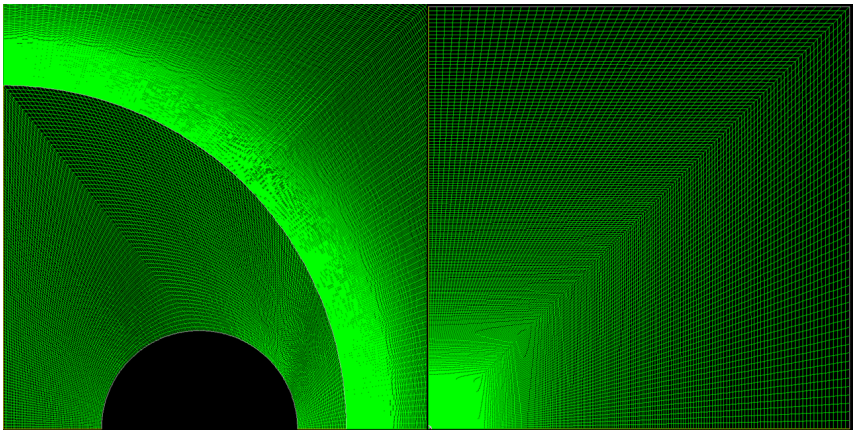

Figure 4.14: Domain grid and borehole detail.

Solution Algorithms

General Settings For all the simulations the general settings were left with the defaults, with the solver Type set to "Pressure-Based" and Velocity Formulation set to "Absolute". The 2D Space was set to "Planar" and it had Gravity unchecked as not only gravity is perpendicular to the plane being worked, the processes under scrutiny are not influenced by it. The Time configuration was set to "Transient" and this would be a process that would change over time.

Solution Methods The Scheme for the Pressure-Velocity coupling was set to "PISO" as it is highly recommended for all transient flow calculations.[121] For the Spatial Discretization, the Gradient was left with the default setting "Least Squares Cell Based". For the Pressure the setting was "Second Order" per default. Momentum was set as default, "Second Order Upwind". Energy was set as "Second Order Upwind".

Solution Controls (Under-Relaxation Factors) The under-relaxation factors for all the simulations were set to their default values: Pressure 0.3; Density 1; Body Forces 1; Momentum 0.7; Energy 1.

Iterative Convergence Regarding the convergence Residuals Monitors all were set to "Check Convergence" and all were left with the default setting of 1e-3 of "Absolute Criteria", with the exception of the Energy "Residual" that was set to 1e-12, the reasoning behind this lays in the fact that given the structured, squared mesh a very fast convergence could be achieved opening up room for false convergence as such the modification was chosen. The Residual Values were left as default with "Scale" that specifies whether or not to print or plot scaled residuals for each variable [121] and "Normalize" that specifies whether or not to normalize the printed or plotted residual for each variable by the value indicated as the Normalization Factor for that variable. The default Normalization Factor is the

maximum residual value after the first 5 iterations, this was too, left as default.[121] The Convergence Criterion shows the residual value for which the solution of each variable will be considered converged, [121] was left as default "absolute", as well as all remaining features.

Time Discretization The setting for the Type was "Fixed" with a Time Step Size of 60 seconds, it was found in earlier tests that, with the used mesh and given that the processes taking place were just solid-medium conduction, this time step size was a good compromise between accuracy and computational processing time.

Analysis In the mesh described in Figure 4.14 a measurement of temperatures was taken on the nodes along two lines, one that is diagonal to the domain and one that is horizontal, it can be seen on Figure 4.15.

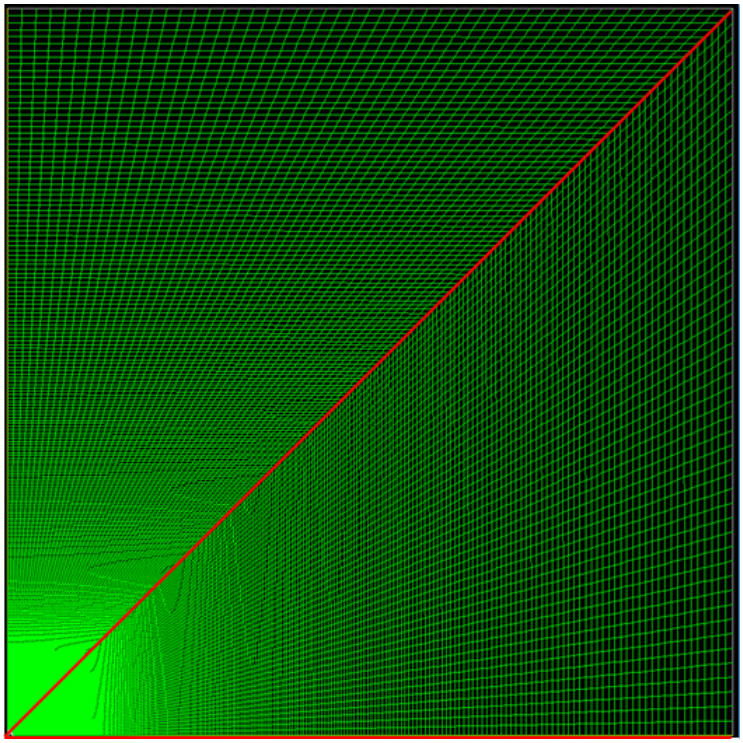

Figure 4.15: Domain control lines.

The model was simulated for 72 hours, while an actual ground sourced heat pump would not be likely to work for such an extended period of time under the same conditions, it served the purpose of observing how the process would affect the soil domain, regarding thermal saturation, allowing for an evaluation of the actual area that each borehole would influence when the heat pump was in operation.
The results yielded shown in Figure 4.16 that after approximately two meters there is no influence of the borehole on the surrounding soil after a continuous heat pump operation at constant 42,5ºC input temperature, as shown by the two overlapping lines.

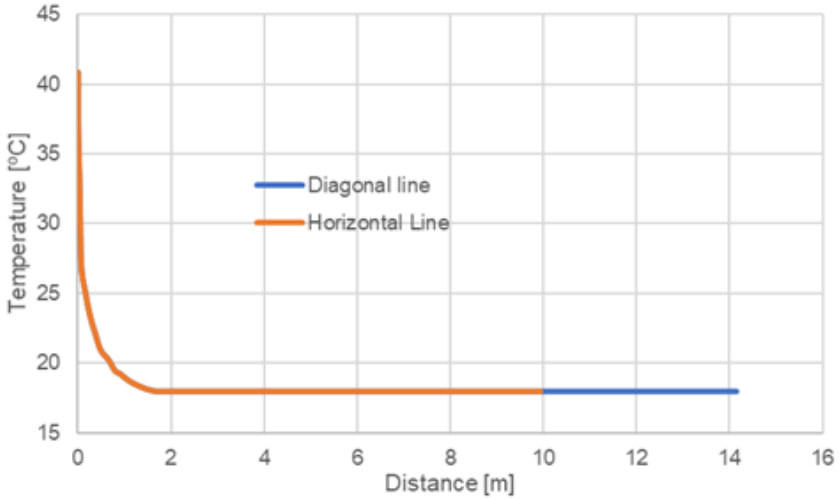

Figure 4.16: Temperatures along the domain control lines for a 72-hour run.

It is safe to assume then that, going forward to a 3D model, a reasonable radius for the domain to be studied should be three meters, providing a generous room for any unanticipated thermal influences that could take place in the simulations.

4.3.2.2 Three-dimensional Approach

Given the information gathered from the previous section, a full 3D model was built for a modified double U geometry borehole were one of the "U" circuits would be filled with PCM adequate for the borehole location and soil temperature, refined for the specific process that would be most relevant for the systems operation (see Figure 4.17). The other "U" circuit would work normally with water used for the heat pump. The length, or depth, of the boreholes would also vary per each location as it influences the heat exchanged between the system and the ground but the cross-section would be the same for all cases.

Domain representation For this approach a 3D approach was selected because it would require the ground volume to influence through the water lines to exchange heat. Additionally, this model cannot have a symmetric setting for the boundary conditions like the previous case as the pipes with PCM and water would not be able to be mirrored. Furthermore, the water circulation through its respective pipes would be made by means of User Defined Functions, in an effort to remove convergence issues that arose from using an actual geometric meshed body to connect the two water bodies together. The domain (see Figure 4.18) has 6 meters in diameter, at its centre the borehole has 150mm in diameter and all the pipes for water and PCM have 40mm.

There are four materials used in the simulation: high-density polyethylene, for the tubing; back fill grout material, for filling the drilled boreholes and soil. The materials properties are presented in Table 4.2. Since the PCM varies according to the soil's local

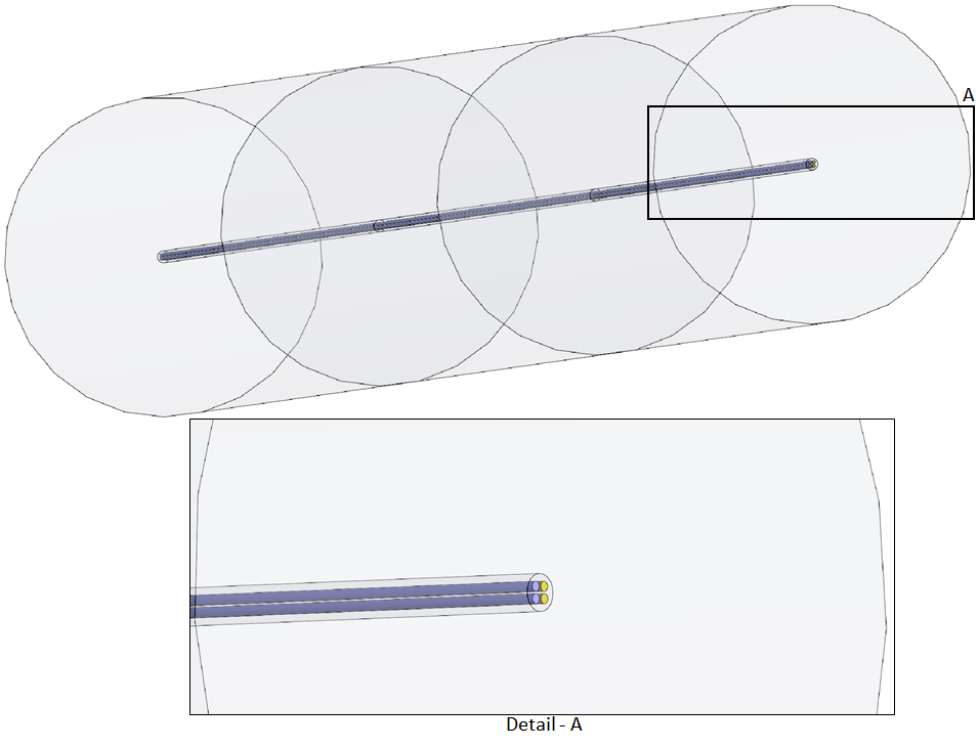

Figure 4.17: Domain of a modelled borehole and detail of the water and PCM pipes.

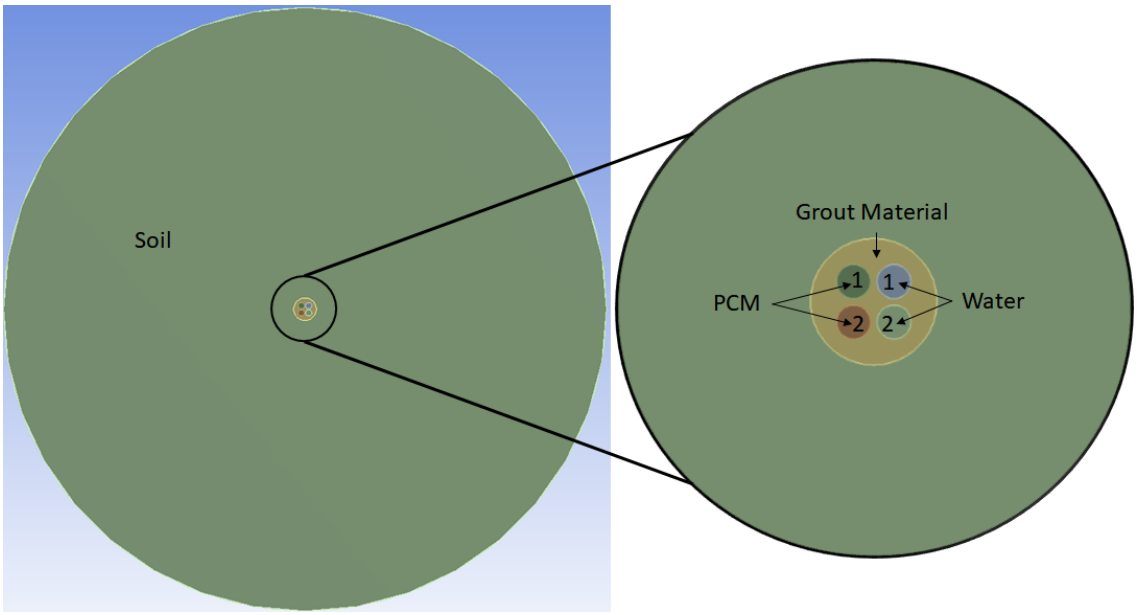

Figure 4.18: Geometric approximation of the domain zones of the model.

temperatures and with the process that is most favourable for the system, it will be presented further along where more context is provided.

Boundary Conditions and Initialization There are four boundary conditions, presented below*:

- Inlet1 (Entry to the water pipe 1) – Velocity Inlet with constant velocity and variable temperature input by means of a User Defined Function that combines temperature reading from Outlet2 and the input provided by the ground sourced heat pump, as it would aim to resemble the operation of a heap pump, varying the temperature accordingly;
- Outlet1 (Exit of the water pipe 1) – Outflow with User Defined Function to read the output values of the boundary;
- Inlet2 (Entry to the water pipe 2) – Inputs the information read on Outlet1 through a User Defined Function, acting as a connective pipe bend;
- Outlet2 (Exit of the water pipe 2) – Outflow with User Defined Function to read the output values of the boundary for input into Inlet1 closing the heat pump circuit;
- The outer edge of the soil domain is considered to be at a constant temperature of the soil of the demosite.

* No temperatures are shown here as they are different for every process and demosite, even then within the same process there could be some variations. Furthermore, two heat pump operation types were studied, On/Off and Variable (Inverter Technolology), as such they are presented where more context is provided, while here the focus is only on the methods and set up of the model.

Hybrid initialization with the default features was chosen for all cases, the hybrid initialization employs a collection of recipes and boundary conditions interpolation methods, solving Laplace's equation to determine the velocity and pressure fields. All other variables including: temperature, turbulence, species, volume fractions, etc. will be automatically patched on domain averaged values or a particular interpolation recipe.[121] The initialized model was then patched with a temperature on all domains, its value would depend on the process being studied and the soils natural temperature for each location.

Spacial Discretization Given that the processes taken place in the heat exchanger by means of a working fluid and a latent heat storage medium the following models were used throughout the development:

- Viscous models:

  - Turbulence - k-ε standard;

- Energy;
- Solidification and Melting.

Mesh Design Effort was taken to achieve a reasonably good mesh for the model, specifically a structured, hexahedral grid. The obtained mesh with 1076000 elements and 1088000 nodes was, unfortunately, not completely structured, although it was hexahedral in nature, as seen in Figure 4.19.

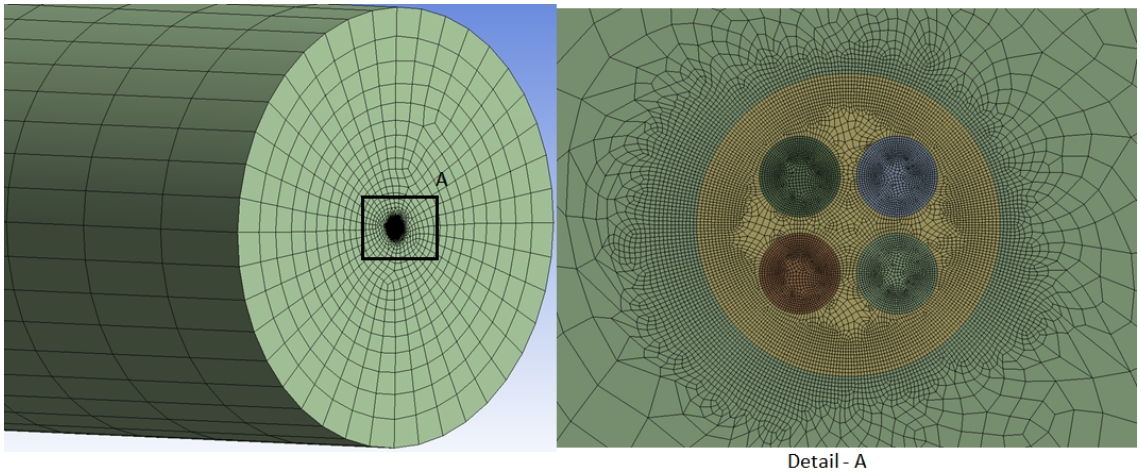

Figure 4.19: 3D model grid and detail.

Given that all the bodies present in the geometric were cylinders or curved surfaces, there are no straight lines thus restricting the generation of well-structured hexahedrons through all the mesh. This gave rise to some areas of the domains to have distorted elements with considerable skewness. It can be noted in the figure that an inflation layer was added to all the main heat transfer interfaces.

Solution Algorithms

General Settings For all the simulations the general settings were left with the defaults, with the solver Type set to "Pressure-Based" and Velocity Formulation set to "Absolute". Gravity was left as unchecked as it was assumed that no only it would not have a significant impact, but it would come at the cost of a significant computational time increase. The Time setting that would be set to "Transient" and this would be a process that would change over time.

Solution Methods The Scheme for the Pressure-Velocity coupling was set to "PISO" as it is highly recommended for all transient flow calculations.[121] For the Spatial Discretization,

the Gradient was left with the default setting "Least Squares Cell Based". For the Pressure the setting was "PRESTO!" as in early simulation testing it provided seemingly better overall convergence times than the other methods. Momentum was set as, "Second Order Upwind". Turbulent Kinetic Energy was configured to "Second Order Upwind". Turbulent Dissipation Rate was set to "Second Order Upwind". When first-order accuracy is desired, quantities at cell faces are determined by assuming that the cell-centre values of any field variable represent a cell-average value and hold throughout the entire cell; the face quantities are identical to the cell quantities. Thus, when first-order upwind is selected, the face value is set equal to the cell-centre value in the upstream cell.[121] When second-order accuracy is desired, quantities at cell faces are computed using a multidimensional linear reconstruction approach.[123] In this approach, higher-order accuracy is achieved at cell faces through a Taylor series expansion of the cell-centred solution about the cell centroid. Thus, when second-order upwind is selected, the face value is computed so that the cell centre discrete value and gradient of each cell-centre value and its gradient in the upstream cell times the displacement vector from the upstream cell centroid to the face centroid. This formulation requires the determination of the gradient value in each cell. Additionally, the gradient value is limited so that no new maxima or minima are introduced.[121] Overall, this makes the first order upwind the easiest interpolation scheme to converge, with only first order accuracy, while the second order upwind uses larger stencils for 2nd order accuracy, essential with tri/tet mesh or when flow is not aligned with grid, which can lead to a slower convergence. Given that the mesh used in this specific case is not squared, but a hybrid, unstructured grid it was decided that, when used, a Second Upwind interpolation scheme would provide adequate precision. Energy was left as "Second Order Upwind".

Solution Controls (Under-Relaxation Factors) This feature setting is configured the same way as for the first presented case.

Iterative Convergence Regarding the convergence Residuals Monitors all were set to "Check Convergence" and all were left with the default setting of 1e-3 of "Absolute Criteria", with the exception of the Energy "Residual" that was set to 1e-12, the reasoning behind this lays in the fact that given the structure of the hexahedral mesh a very fast convergence could be achieved, thus to prevent it this modification was made. The Residual Values were left as default with "Scale" that specifies whether or not to print or plot scaled residuals for each variable [121] and "Normalize" that specifies whether or not to normalize the printed or plotted residual for each variable by the value indicated as the Normalization Factor for that variable. The default Normalization Factor is the maximum residual value after the first 5 iterations, this was too, left as default [121]. The Convergence Criterion shows the residual value for which the solution of each variable will be considered converged, [121] was left as default "absolute", as well as all remaining features.

Time Discretization The setting for the Type was "Fixed" with a Time Step Size of 1 second, it was found in earlier tests that, with the used mesh, this time step size was a good compromise between accuracy and computational processing time.

5

Results and Discussion

The following chapter will address the results obtained from the numerical work and comparison with parallel experimental work, aiming to show clearly the evolving process to develop the solutions for heat exchanging, from start to finish. The figures and graphics displayed below are used as tools to characterize the geometries and specs while assessing the features of the studied cases in the selection process. The work that is shown here follows the structure established in the Methodology. Concerning the PCM tank heat exchanger, it starts by establishing base concepts and factors in order to progress studying relevant parameters towards the final application. Regarding the boreholes heat exchanger, the application first tries out the basic constructs then more elaborate configurations, advancing then to full-scale simulation.

5.1 Numerical Base Model

This section concerns the initial phase of numerical modelling performed in order to get acquainted with several features and concepts need to develop the work down the line. Features and parameters like metallic foams, nanoparticles and fins typology were tested in an effort to ascertain what would be the best method to implement.

The simulation work started out by studying the heat transfer process in transient condition on a 2D flat plate approximation. The first step was to verify the influence of the mesh sizing, discretization scheme, the density variation and the time step size concerning convergence and computational capacity need to run the simulations, while providing the general guidelines to design the heat exchangers. The geometry simulated in Figure 5.1 is a flat plate with 1.5mm thickness and three fins spaced 6mm, 0.6mm thick. Figure 5.2 also shows the wall boundary conditions applied in the CFD model, with an adiabatic top, symmetric sides and temperature input on the side of the flat plat of 5^{o}C above the PCM liquid temperature .

For the model, the PCM taken into consideration was commercial paraffin A53 while the flat plate and fins material was aluminium. The following Table 5.1 displays the properties of the materials used in the model, while Table 5.2 shows the computational

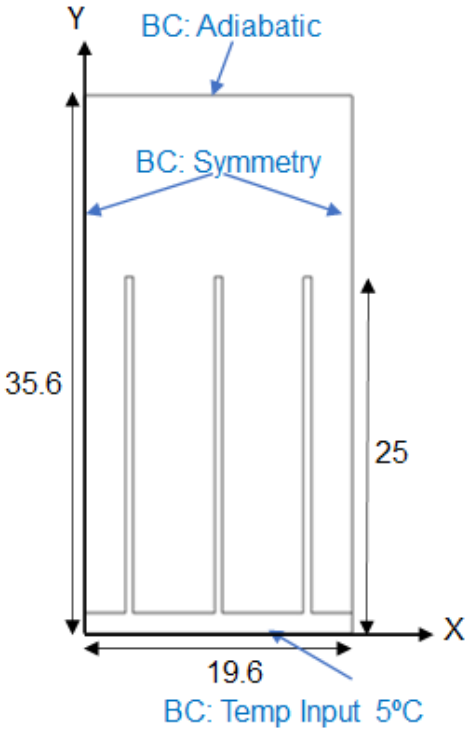

Figure 5.1: Flat plate 2D modelled geometry with boundary conditions (dimensions in mm).

details for the simulations.

Table 5.1: Materials properties.

Property	**Aluminium**	**PCM A53**
ρ [kg/m^3]	871	881.99
Cp [J/kg.K]	271.9	2220
k [W/m.K]	202.4	0.22
μ [kg/m.s]	-	1.9
β [1/K]	-	0.00048
Melting Latent Heat [J/kg]	-	162880
Solidus temperature [K/ºC]	-	325/51.85
Liquidus temperature [K/ºC]	-	326/52.85

It can be seen in Figure 5.2 that, with the employed mesh, the discretization scheme does not have ill effects on the computational results and for a time step size lower than 0.5 s the results are time step size independent. Regarding the simulated geometry the results showed that the density variation does have some effect over the heat transfer and consequently over the progression of the melting process, increasing the speed of the process when the fins are vertically aligned. Figure 5.2 shows how variable density has an effect on natural convection, increasing the heat transfer rate and speeding up the melting, comparatively to the case of constant density and of pure conduction. This can be taken

Table 5.2: Computational details of the simulations.

Case ID	Mesh Element Number	Discretization Scheme	Buoyancy Model	Solidification/ Melting	Time Step Size
A1	50910	First order upwind	Boussinesq	Melting	0.2
A2	100410	First order upwind	Boussinesq	Melting	0.2
A3	100410	First order upwind	No Bouyancy	Melting	0.2
A4	100410	Second order upwind	Boussinesq	Melting	0.2
A5	100410	Power Law	Boussinesq	Melting	0.2
A6	100410	Power Law	Boussinesq	Melting	0.5

to mean that, at least for the melting process, the actual speed of the phase change process would be slightly higher than what was estimated by numerical work, especially with low fin density. It was also possible to see that the PCM region beyond the fins changes at a slower pace when compared with the PCM in the fins vicinity. These results show that, in order to have an efficient heat transfer rate between the PCM and the heat exchanger, it is necessary a relatively high fin density and minimise the mass of PCM not in direct contact or not in close proximity with fins.

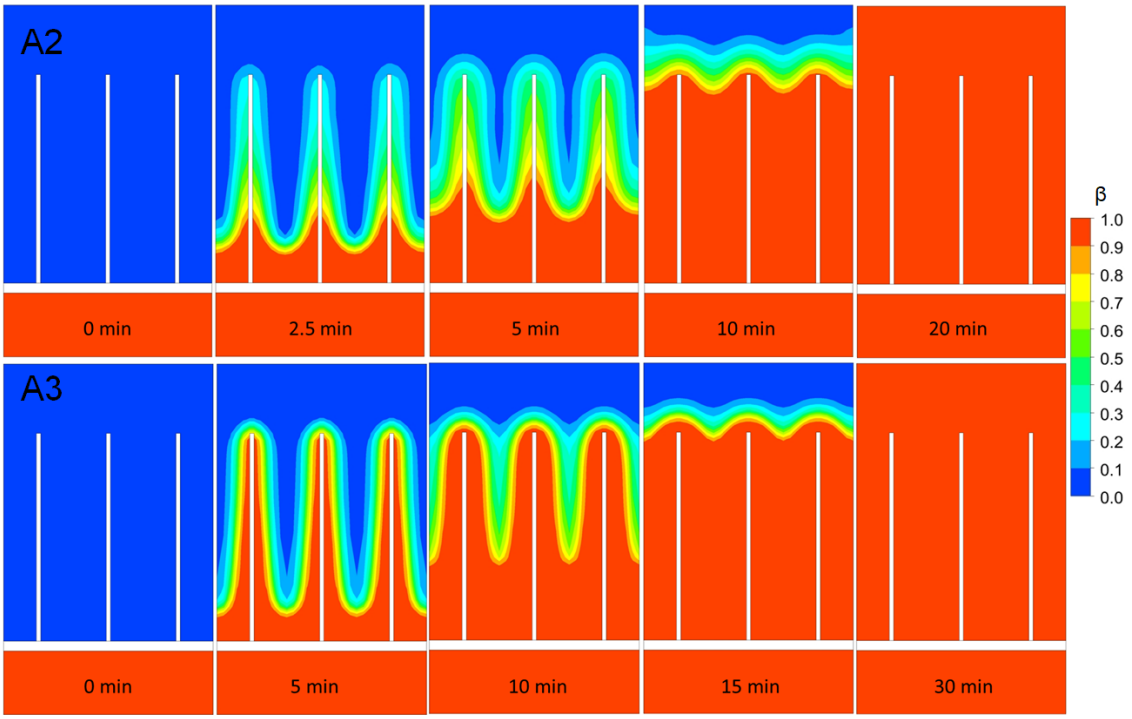

Figure 5.2: Results (cases A2 above and A3 below) comparison of mass fraction versus time, between variable and constant density.

To assess the phase change model in the software code and to understand how each of the considered parameters of the heat exchanger influenced the simulations, a group of simulations were performed on a simple shell and tube heat exchanger, based on work detailed in the literature.[10] In the referenced article, the experimental apparatus is made

up of two concentric pipes: one outer pipe made off Plexiglas, 44mm internal diameter, and the inner one made off stainless steel with 13mm internal diameter, 2.5mm thick. The pipes length is 400mm. The Plexiglas pipe would enable the visualization of the phenomena taking place during the experiments. The heat transfer fluid flows through the inner pipe to provide and remove heat, in the space annulus between the two pipes there is 480 g of PCM. 48 K-type 0.5mm calibrated thermocouples (± 0.1°C) were distributed at several angles (0°-90°-135°-180°-225°-270°) and at radial positions a ≈ 3mm, b ≈ 6mm and c ≈ 9mm at regular cross-sections intervals along the annulus central axis with metal pieces, see Figure 5.3. A data acquisition system logs all the temperatures and mass flow rate every 3 seconds.

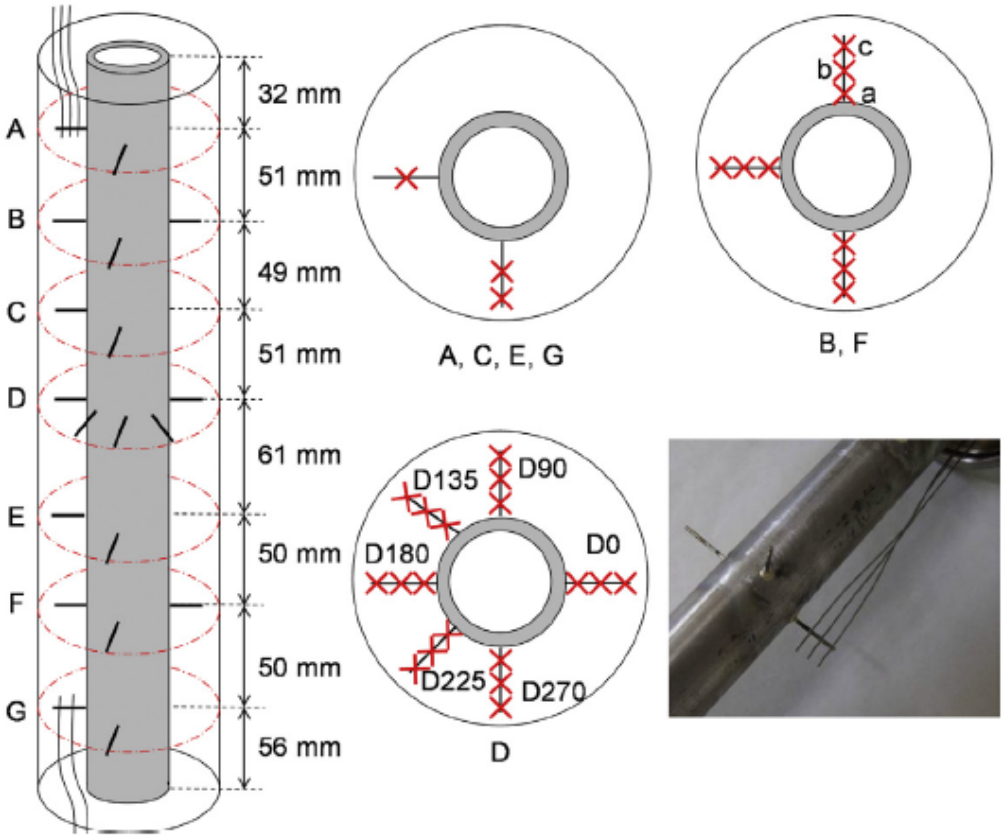

Figure 5.3: Experimental setup and thermocouple placement.[10]

Water was used as HTF, regulated by a micro-pump coupled with a Coriolis flowmeter to maintain the required flowrate. The average water velocity was kept constant at 0.01 m/s, corresponding to a Reynolds number lower than 2300 inside of the pipe (Laminar flow). The PCM used was a commercial paraffin RT35 with a melting temperature of 35°C, with physical properties provided by the manufacturer Rubitherm presented in Table 5.3. In Figure 5.4, it is possible to see the relation between Specific Heat (CP) and temperature. The integral of the CP curve between 28°C and 46°C provides the latent heat of the phase change, being the same for all the displayed curves, 157000J/kg.

Table 5.3: RT35 physical properties by Rubitherm.[10]

Property	Rubitherm data
T_m	35 ºC
ΔH_{sl}	157000 J/kg
ρ	880(sol.) / 760(liq) kg/m^3
β	0.001 1/K
CP	1800(sol)/2400(liq) J/kg.K
k	0.2 W/m.k
ν	3.3x10^{-6} m^2/s

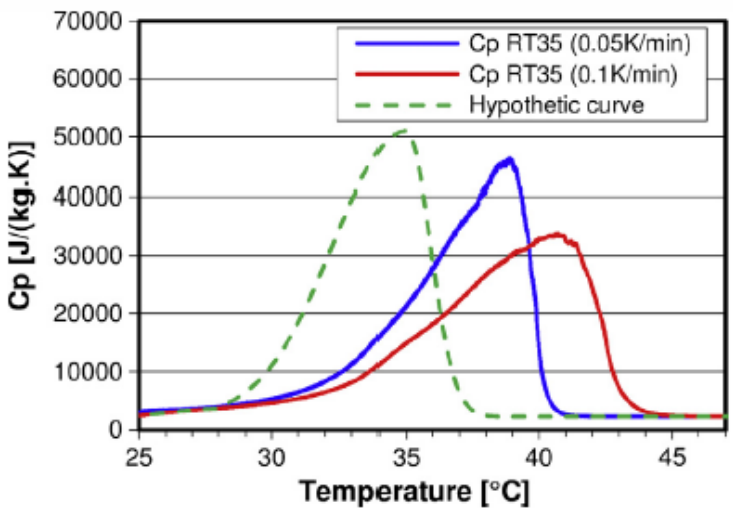

Figure 5.4: Specific heat measurement as a function of temperature obtained with a C80 calorimeter at different heating rates for the melting process.[10]

The simulations that were run in transient regime were performed using a 2D axisymmetric mesh with 90 radial cells and 100 axial cells, with a time step size of 0.5s. The time step size and mesh were the same used in referenced article [10] that already undergone a time step size and mesh independence test. Three zones were modelled: the PCM domain, the heat transfer fluid, and the pipe in between the first two. The algorithm used was SIMPLE to couple velocity and pressure fields while the natural convection for the liquid PCM was modelled with the Boussinesq approach, and the momentum and energy equations were discretized by second order upwind scheme and the pressure by PRESTO. The experimental apparatus was placed vertically where the HTF inlet was at the top, the simulations took this into consideration as well and established a constant water inlet temperature at 52ºC, the initial temperature of the solid PCM was 22ºC and the exterior wall of the Plexiglas was considered adiabatic. To ascertain the influence of modelling parameters a set of simulations were made to study the influence of the density variation with the Boussinesq approach, CP curve values, PCM liquidus and Solidus temperature on the computational model. Table 5.4 displays the relevant parameters under scrutiny of

this set of simulations.

Table 5.4: CFD simulations parameters.

Case ID	Solidus Temperature [ºC]	Liquidus Temperature [ºC]	ρ_0 [kg/m3] / T_0 [ºC]	Latent Heat Configuration
B1	28	37.85	880/28	ΔH = 157kJ/kg
B2	28	37.85	760/37.85	ΔH = 157kJ/kg
B3	28	37.85	760/37.85	CP curve 0.1 /K/min
B4	28	37.85	760/38	CP curve 0.1 /K/min
B5	30	37.85	760/37.85	CP curve 0.1 /K/min
B6	26	35.85	760/37.85	CP curve 0.1 /K/min; -2 K
B7	30	37.85	760/37.85	CP curve 0.1 /K/min; +2 K
B8	30	39.85	880/28	CP curve 0.05 /K/min
B9	30	39.85	760/37.85	CP curve 0.05 /K/min

In simulations B1 and B2 the energy was solved with the direct latent heat value, in the remaining cases the phase change latent heat value was considered approximately zero and the enthalpy was calculated based on the CP curve polynomial linear function. The difference between case B1 and B2 is that the value of the density in B1 is the density of the solid PCM at 301.15 K while in case B2 the liquid density at 311 K was used. Case B3 is akin to B2 but used the CP curve estimated for 0.1 K/min. In cases B4 and B5 the solidus temperature is increased one and two degrees respectively than in case B3. Regarding B6 and B7 the CP curve was shifted two degrees up and down respectively. Finally, B8 and B9 were run with 0.05 K/min CP curve and as with B1 and B2 with the solid and liquid density of PCM in the density term. The CP curves used in the numerical work are presented in Figure 5.5.

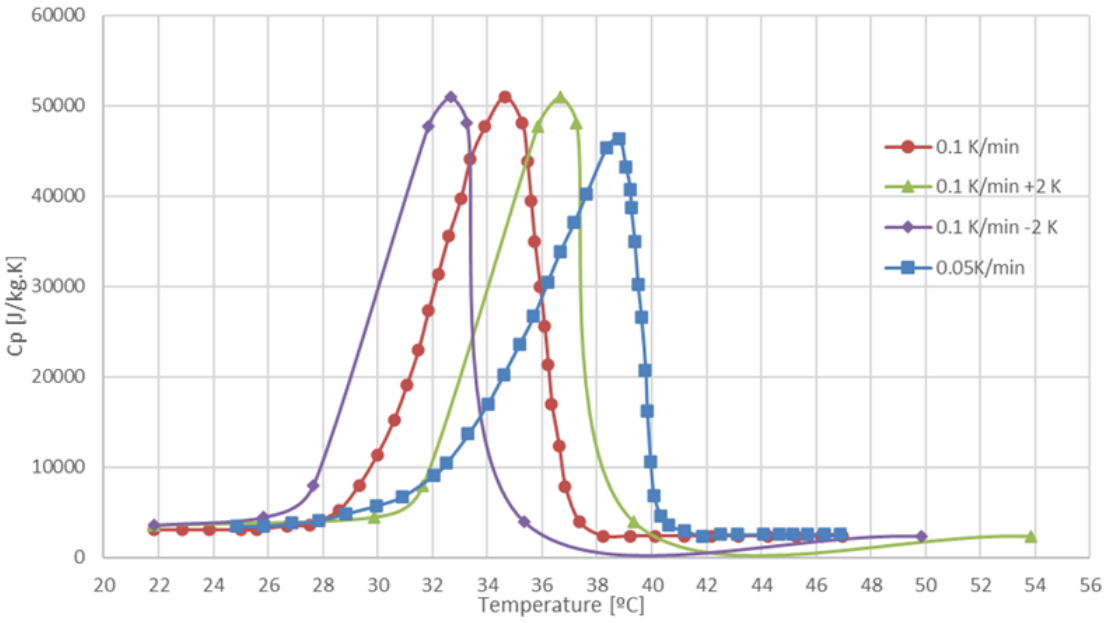

Figure 5.5: CP data used in the numerical simulations B3 to B6.

Figures 5.6 to 5.10 present the comparison between the predicted temperature and experimentally measured temperature at position a, b and c defined in the paragraph concerning Figure 5.3.

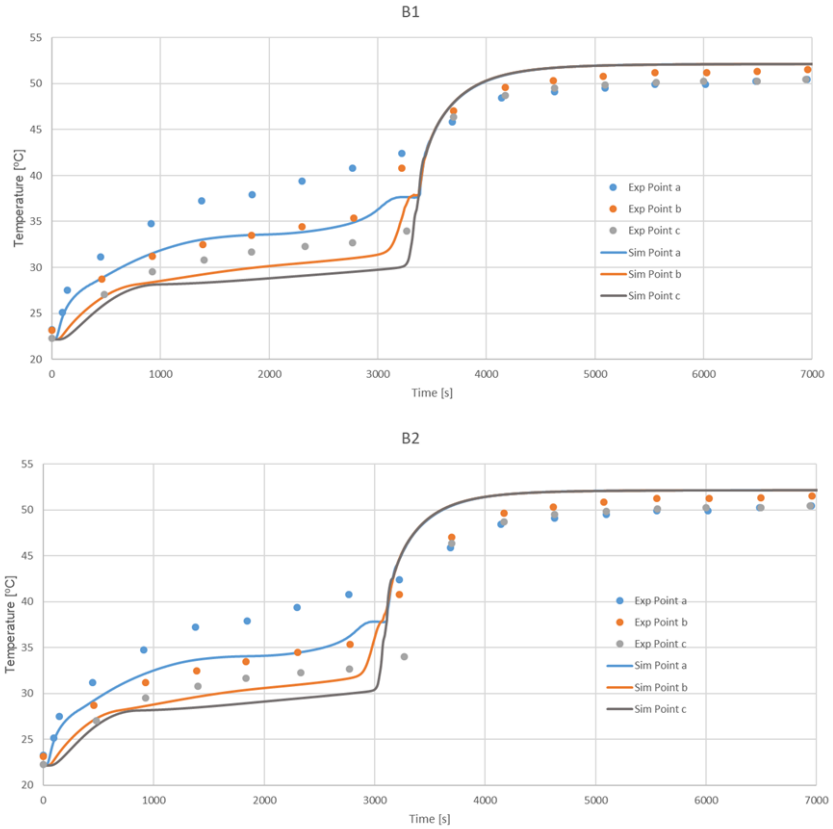

Figure 5.6: Experimental and simulated temperatures of cases B1 and B2.

The density variation and CP curves had an effect on the numerical results, concerning the solid density value for reference value, it has a better agreement with the experimental data when compared with the simulation run with the liquidus temperature density. It is also visible that integrating the phase change enthalpy in the CP curve provides better results and becomes the standard approach especially when predicting temperature before the melting process.
The results showed that increasing the solidus temperature and the CP curve improves the quality of the numerical results.

The computational data obtained with the 0.05 K/min CP curve (cases B8 and B9) shows a better agreement with the experimental data than the simulations that were run with the 0.1 K/min CP curve (cases B3 and B4). As seen on Figure 5.5 the 0.05 K/min CP curve is shifted forward for a higher temperature, when compared to the 0.1 K/min curve. Figure 5.11 shows that the numerical results are fairly influenced by the CP, the solidus temperature and the value of the density value used in the approximation. Ideally, the PCM properties have to be precisely defined in order to achieve the most accurate

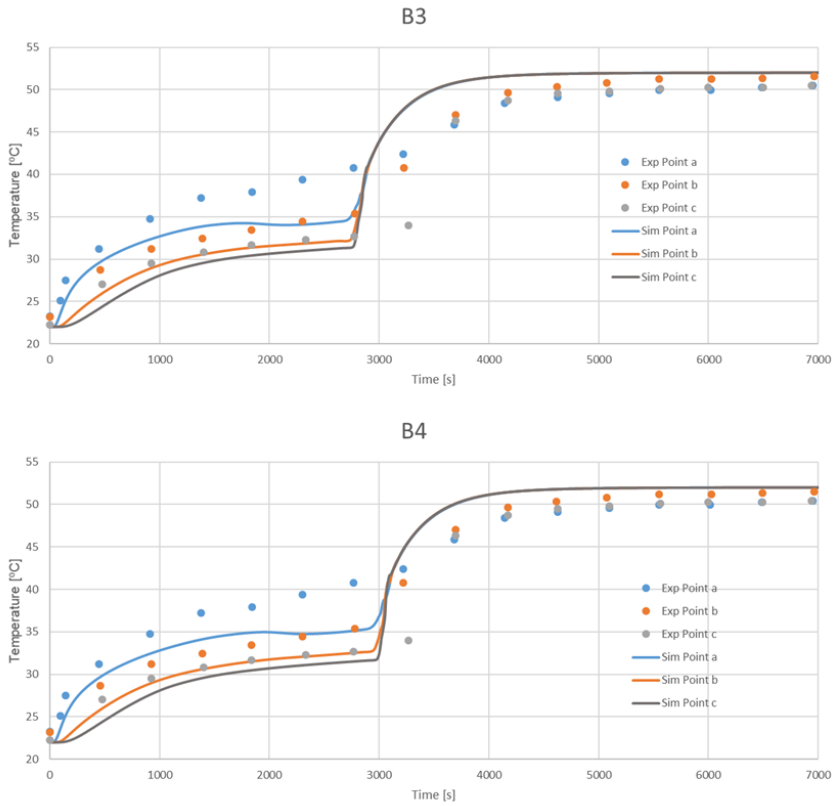

Figure 5.7: Experimental and simulated temperatures of cases B3 and B4.

results. However, acquisition of such PCM data properties goes beyond the scope and competence of the available resources and of the work developed in this thesis and so it is conditioned to the supplied information product by the manufacturer.

Section General Conclusions:

The boussinesq approach was ultimately discarded for the models presented in this work. The presence of fins in such a closely packed arrangement minimised the effect of any natural convection taking place. The PCM properties provided by the manufacturers are not accurate and do not mirror the materials actual behaviour, but sampling each material batch is unfeasible.

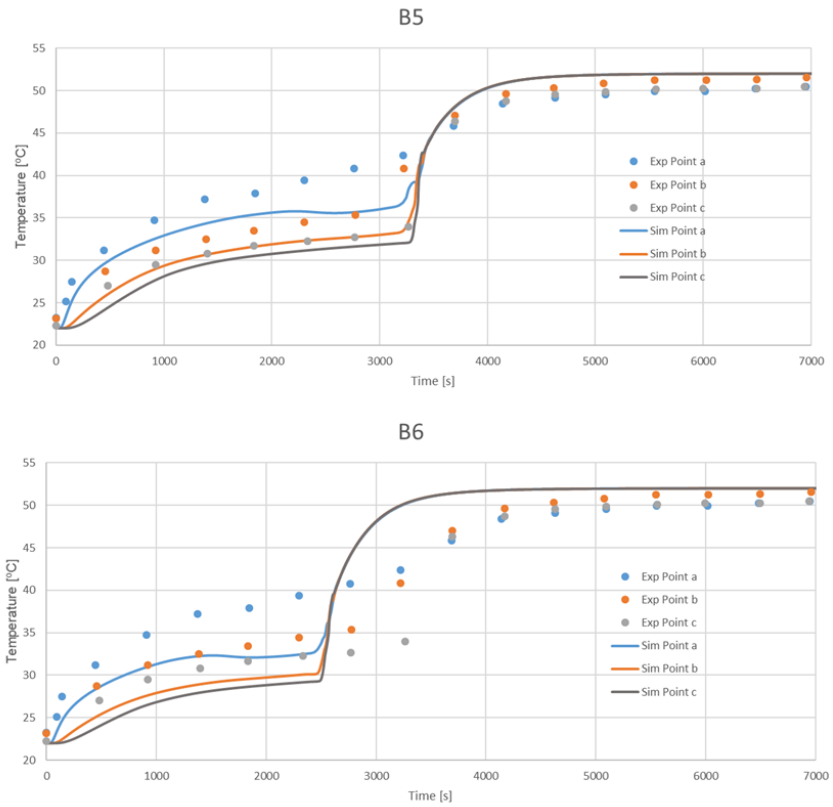

Figure 5.8: Experimental and simulated temperatures of cases B5 and B6.

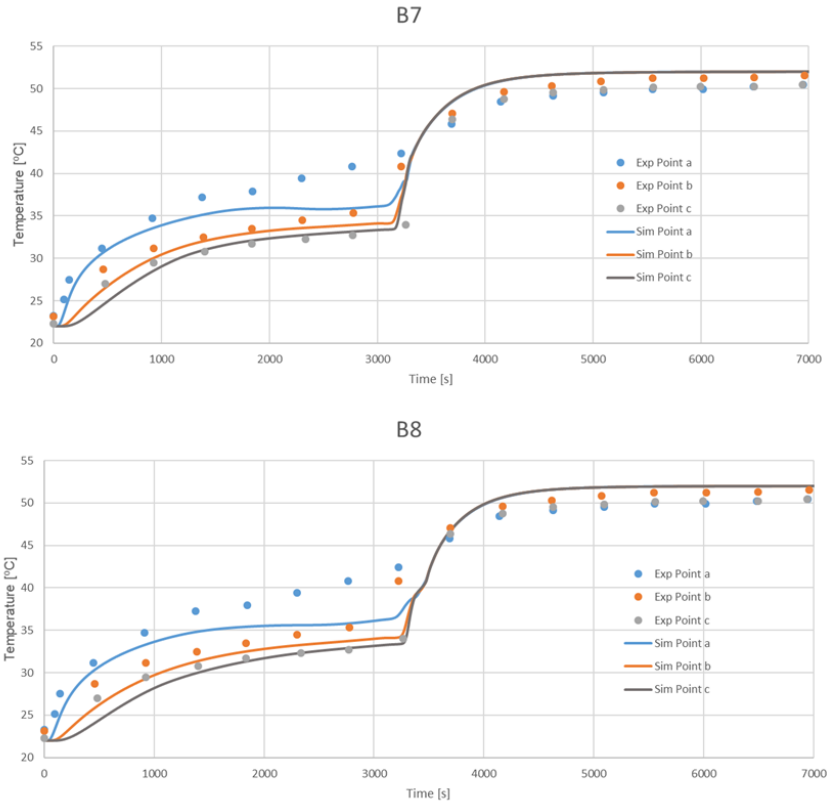

Figure 5.9: Experimental and simulated temperatures of cases B7 and B8.

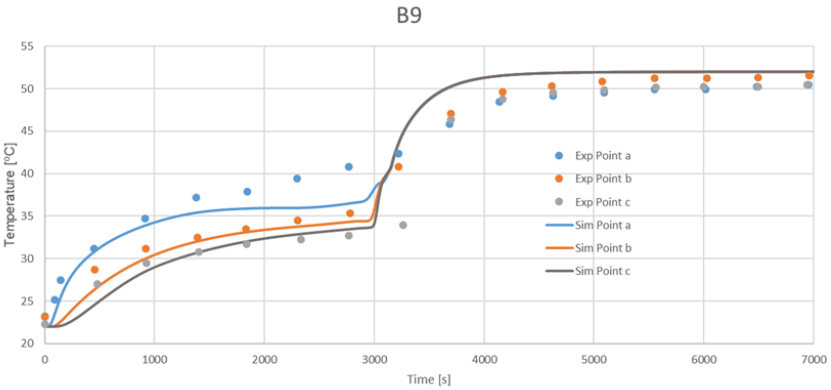

Figure 5.10: Experimental and simulated temperatures of case B9.

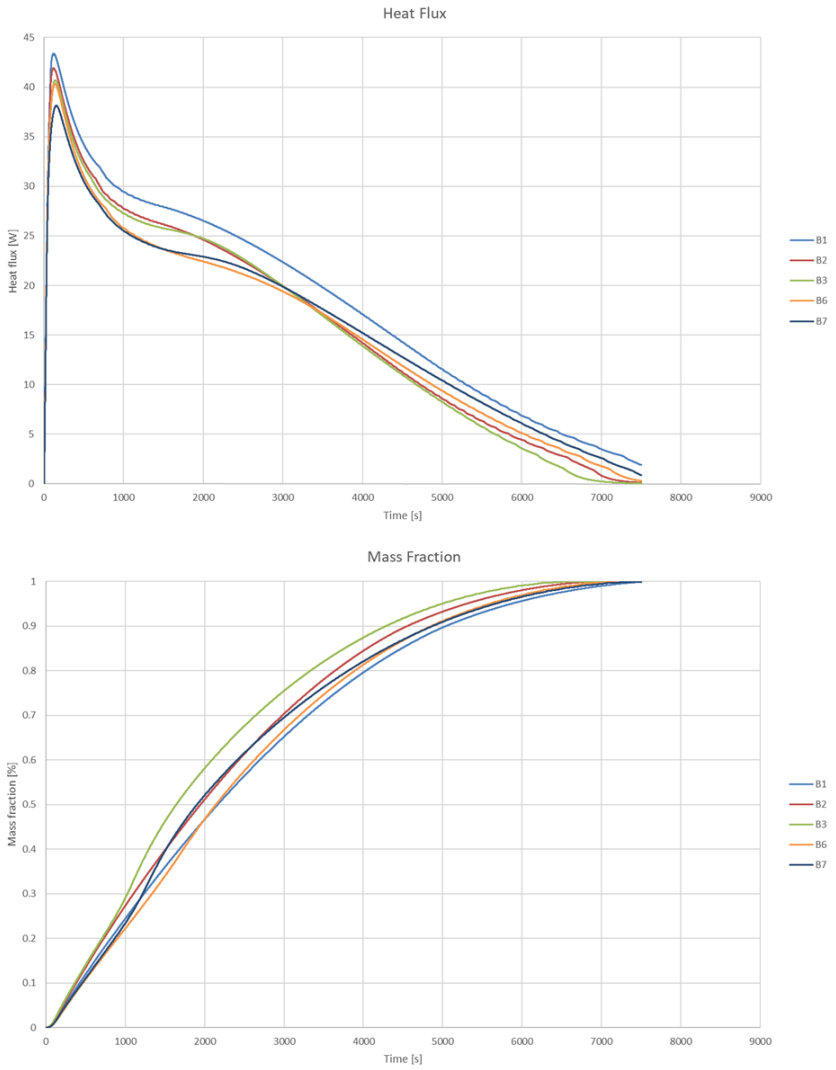

Figure 5.11: Heat fluxes and the PCM liquid mass fraction for cases B1, B2, B3, B6 and B7.

5.2 Numerical Study for PCM Heat Exchangers

This section's study will begin with the parameterization of the PCM heat exchangers features, focusing in the solidification/discharging process. The starting geometry chosen was two concentric pipes, one meter long, the inner tube has a 8.5mm internal diameter and 10mm exterior diameter. The exterior shell/tube has an internal diameter of 15mm, the exterior diameter is 16.5mm. The heat transfer fluid, water, will flow inside the inner pipe while the space in between the two tubes will be filled with the PCM. This geometry was selected taken into consideration the literature document from the previous section, while aiming to obtain a very compact make up to increase the heat transfer between the PCM and heat transfer fluid. This numerical work will simulate the basic geometry just described, an equivalent geometry with 16 longitudinal fins and another with 400 radial fins, a geometry with nanoparticles enhanced PCM (NPEPCM), a metallic foam-PCM medium with 95% porosity, an equal geometry except it is 1.5 meter long and a case with a lower mass flow of water relative to the first basic simulation. It is important to note that in this section the focus of the work is on the solidification process, i.e. drawing energy from what is stored in the PCM, as this is the process that will provide the necessary energy to work with the technical thermal storage solution, applying the energy to supply a dwelling thermal energy needs.

The simulated geometries can be seen in Figure 5.12. In all cases the temperature for all domains will be initialized at 55ºC (approx. one degree above the PCM liquidus temperature) while the water inlet temperature is set to 15ºC. The material properties can be seen in Table 5.5 and 5.6. The NPEPCM case considered a 30% increase of the PCM thermal conductivity due to doping with nanoparticles and assumed that the effect of the nanoparticles over the PCM properties is negligible. The aluminium foam case (with 95% porosity) was simulated with equivalent properties through mass ponderation considering the properties of both the PCM and Aluminium, making up the PCM domain with a foam/PCM medium combination. The average inlet water velocity will be constant at 0.15m/s for all cases, with one specific exception where a lower mass flow rate would be considered (0.1 m/s). In this group of simulations, the natural convection influence was also studied for the solidification process. With the results obtained, the cases with and without density variation were shown to have equal results. These results are in agreement with the literature, which reported that the natural convection, per rule, mostly only influences the liquefaction process, while the solidification is primarily driven by conduction, as layer upon layer freezes on top of each other when the PCM contacts the heat exchanger.

The results showed (Figures 5.13, 5.14 and 5.15) that there is a sudden drop in the water outlet temperature at approximately 10-15 seconds, this corresponds to the water inlet entry and first volume sweep of the circuit by the fluid up to the outlet. This is followed by a less sharp but continuous decrease of the water outlet temperature up to the end of the

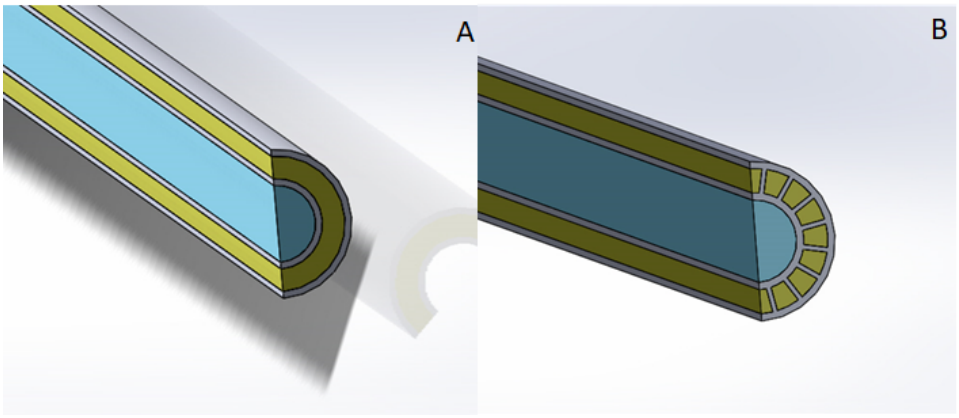

Figure 5.12: General geometries considered for the simulations. Image A ilustrates the geometry used for all the finless geometries, B shows the geometry employing longitudinal fins.

Table 5.5: Water and pipe material properties.

Property	**Water**	**Copper**
ρ [kg/m^3]	998.2	8978
Cp [J/kg.K]	4182	381
k [W/m.k]	0.6	387.6
ν [kg/m.s]	0.001003	-

Table 5.6: PCM properties and combinations properties.

Property	**A53**	**NPEPCM**	**Aluminium Foam - 95% porosity**
ρ [kg/m^3]	839	839	933
Cp [J/kg.K]	2220	2220	2023.43
k [W/m.k]	0.22	0.286	4.038
μ [kg/m.s]	0.007	0.007	0.007
ΔH_{sl} [J/kg]	162880	162880	139146
Solidus Temperature [K]/[ºC]	325.75/52.6	325.75/52.6	325.75/52.6
Liquidus Temperature [K]/[ºC]	326.75/53.6	326.75/53.6	326.75/53.6

melting process. It is discernible that the improvement of the PCM thermal conductivity by the nanoparticles considered have a marginal effect on the heat flux and water outlet temperature. The results also exhibit that the increased length of the heat exchanger from one meter to 1.5 meters and the decreased average water inlet velocity from 0.15 m/s to 0.1 m/s have a similar effect on the heat transfer process, albeit inversely. Comparatively to the base case these simulations showed an increase in the water outlet temperature up to the end of the PCM solidification process, however this increase is minimal. On the other hand, the performance of the geometry with both the longitudinal axial fins and radial fins and the 95% porosity aluminium foam, that have a similar behaviour, when

compared with the base case, having a significant increase of the heat flux and water outlet temperature.

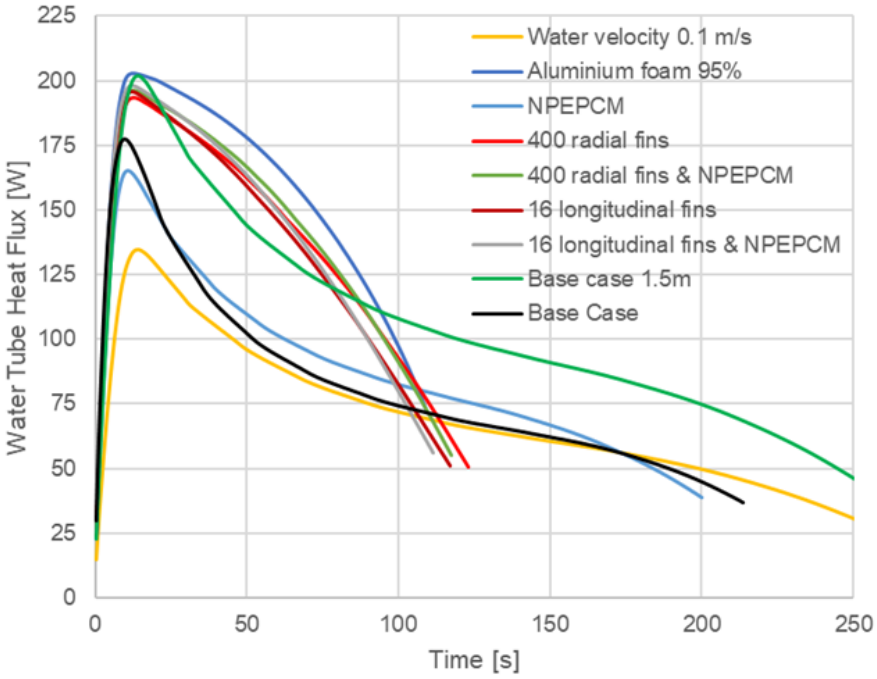

Figure 5.13: Heat flux versus time for the simulated cases.

Based on these results, a new group of simulations would be developed aiming to study geometry with other parameters such as a greater length and fins in order to achieve a good water outlet temperature for the desired purposes. The reason for choosing fins over metal foams, despite the later better thermal performance, lays with the fins simplicity and ubiquitous applications for heat exchanging in commercial systems, being easily found in the market as well as a tried and verified technical solution.

Section General Conclusions:
The finned tube heat exchanger was selected for the application. Despite good performance of nanoparticles and metallic aluminium foam, these were discarded because of their respective issues and limitations.

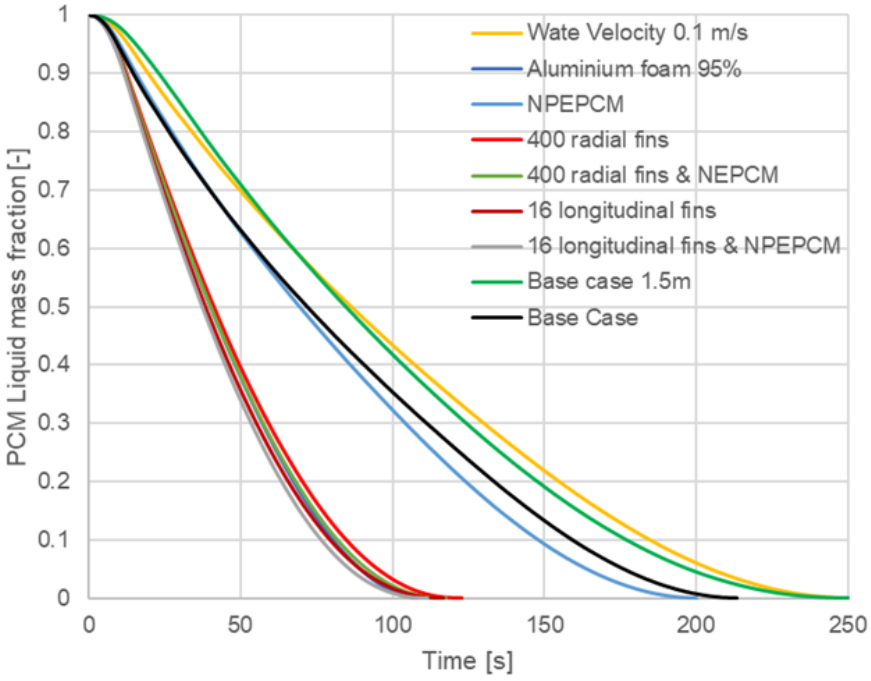

Figure 5.14: Liquid mass fraction versus time for the simulated cases.

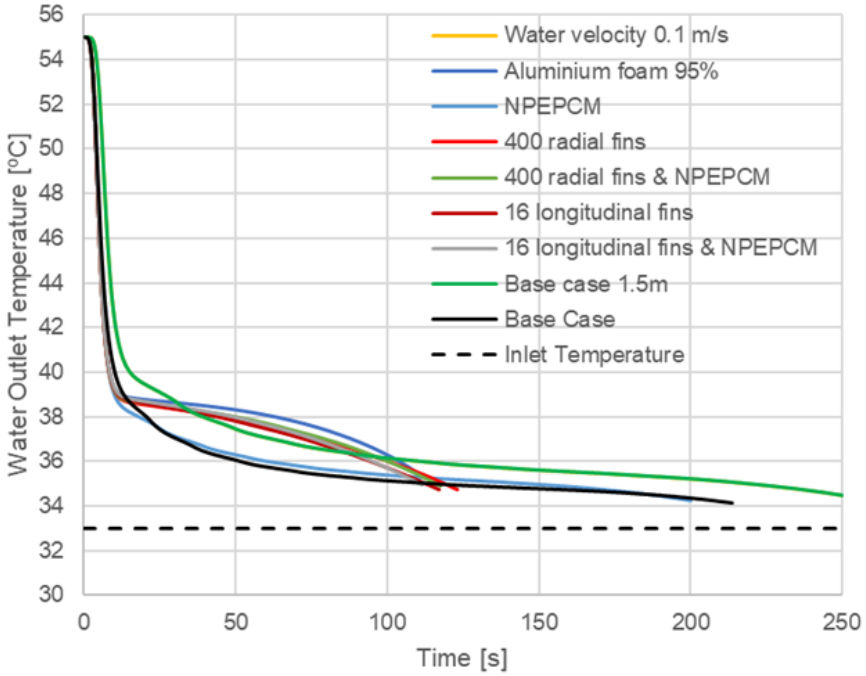

Figure 5.15: Water outlet temperature versus time for the simulated cases.

5.3 Storage Heat Exchanger Design

The following section will address the numerical work that was done to develop a functional heat exchanger to be used in tandem with a latent heat storing system. In order to ascertain the impact of the length of a single pipe circuit on the outlet temperature a set of simulations with three different lengths were run, 1.5m, 5m and 10m, Using an axisymmetric approximation of the geometry ilustrated in 5.12. Again, in this case the thermal process under scrutiny was the discharge process of the PCM, specifically A44 Table 5.7 displays the material properties. The boundary conditions were: water inlet temperature at 33ºC, velocity 0.15m/s; with the initialized temperature at 48ºC the remaining boundaries were either adiabatic or symmetric.

Table 5.7: A44 PCM properties.

Property	**A44**
ρ [kg/m^3]	800
Cp [J/kg.K]	2000
k [W/m.k]	0.24
ΔH_{sl} [J/kg]	250000
Solidus Temperature [K]/[ºC]	317/43.85
Liquidus Temperature [K]/[ºC]	318.5/45.35

As displayed in the results shown in Figures 5.16 to 5.17, there is a considerable increase of the heat flux and water outlet temperature between the length specifically comparing 1.5 m and 5 m (approx. 80% increase at the end of the phase change), but not so much between 5 m and 10 m (approx. 20% at the end of the phase change). Observing the 5 m case it is possible to see that the temperature difference is five degrees or above for the most of the discharge process, which is ideal for the solution trying to be achieved here since it is easily applicable to most general use heat exchangers, that usually work with a $\Delta T = 5$ºC. The results show that water outlet temperature drops considerably throughout the discharge process, it is possible to observe that the length of a single circuit is important to achieve a specific minimal outlet temperature for a given amount of time.

Another observation that can be gathered from the results is that while increasing the length from 5 to 10 m increases the heat flux and water temperature, it will also eventually drop below the desired minimum of five degrees difference. As the process takes place, the PCM will solidify in the first sections of the heat exchanger thus the water coming in will only start to heat up further down the pipe, decreasing the heat flux in those areas and contribute less to heat the water. This process reduces the effective area of the heat exchange with liquid PCM as the solidification takes place, becoming more widespread the longer the pipe is. In this a solidification front takes at the interface between the PCM and water pipe that hinders the heat exchange of the process over time. Another observation is that while the process is initially fast, as the solidified PCM layer increases the process slows down significantly, with the last third of the liquid PCM taking well over one third

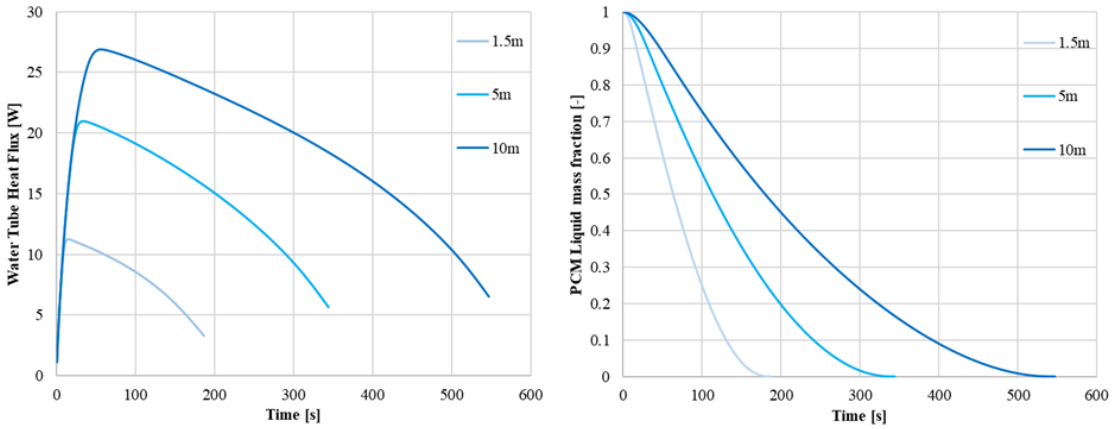

Figure 5.16: Heat flux versus time and Liquid mass fraction versus time.

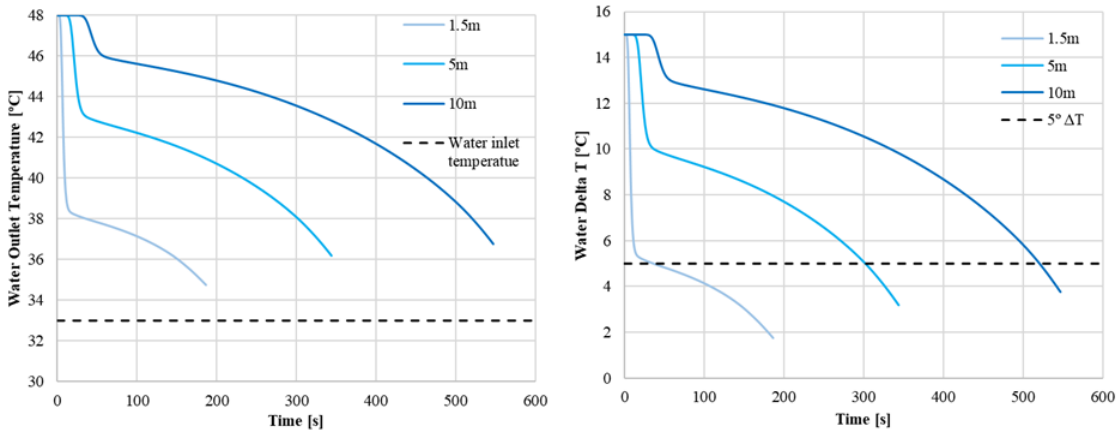

Figure 5.17: Water outlet temperature versus time and Water ΔT versus time.

of the total time for the phase change to occur.

Note: Henceforth a lot of plotted lines do not start exactly at "zero" seconds because there are numerical oscillations that are too large and non-relevant for the overall content because they are the product of the simulations iterations right after the initialization of all the domain at constant temperature up until the first time the volume of the heat transfer fluid (water) sweeps through the fluid domain. Because of this the first 150 seconds were removed as they did not take any effect on the overall process and it eliminated these abnormal peak values.

5.3.1 Parameter Characterization – Heating Discharge

Starting from the previously gathered information and bearing in mind project conditions, such a 150 l of total volume storage per tank. Since a 3D mesh would require a great computational capacity the previously successful 2D approach would be used again, that

would be in turn checked with experimental results to verify it. Due to the nature of the phase change process, the heat transfer is an almost isothermal phenomenon, consequently it is expected that with a finned tube heat exchanger array, the heat flux will take place in between the pipes area of influence. While the tube array has a square distribution, one can make an approximation to a circular section with the same cross section area (see Figure 4.7). In this manner, the limit boundary is set between the half-way point between the pipes and set as an adiabatic boundary condition, with each finned tube being simulated individually, disregarding the influence of the surrounding pipes. The simplification considered here also bears in mind that the individual pipe be equated to a 2D axisymmetric section, this simplications was ilustrated in Figure 4.7.

Upon consultation of commercial catalogues, a pipe dimension was selected with 10mm outside diameter and 8.6mm inside diameter. The fin thickness was considered 0.3mm and each fin was spaced 4.7mm apart (a total of 5mm spacing including the fin thickness), regarding the fin height or in other words, half the distance between the vicinity pipes will be addressed below as it will be one of the studied parameters along with the pipe length.

5.3.2 Heat Exchanger Individual Circuit Length

Given that, this heat exchanger is meant to be stored with in a modular tank that should have less than approx. 150l, the first parameter studied was length. As at this phase of work there were very few set demands and limitations the simulation was run with a water velocity input of 0.1m/s and for this specific case with a fin height of 12.5mm. However, one of the objectives for this device operation is for it to work paired with a ground-sourced heat pump as such some restrains were taken into consideration. One such restraint is that the minimum acceptable outlet temperature does not drop below 40ºC. This feature is intended to help the heat pump work with minimum load while achieving the desired output temperatures for the indoor terminal units, in the cases shown below (Figures 5.18 and 5.19) the temperature was set to be at minimum of 40ºC. Considering that overall, the heat exchanger principle is the same, the work developed for one operation mode (DHW production, heat or cooling) can be, considered valid for the other modes, at least from a qualitative standpoint.

In the analysis of the graphic results it is possible to see that the minimum water temperature stays above 40ºC between approx. 1.25 (5m) and 2.24 hours (10m) along the pipe, even though the complete discharge process takes almost 3 hours. While it cannot be expected that the water temperature always stay above 40ºC, most of the PCM should be drained of its stored energy when the temperature drops below the minimum. It is observable in the results that PCM liquid fraction stays approximately above 10%, while keeping the water temperature value above the limit. Considering that is impossible to achieve the desired temperature throughout all the phase change process a value of 10% liquid fraction can be allowed. Considering this and the narrow range for the mass fraction relation to the outlet temperature, the basic pipe length selected was 6 meters.

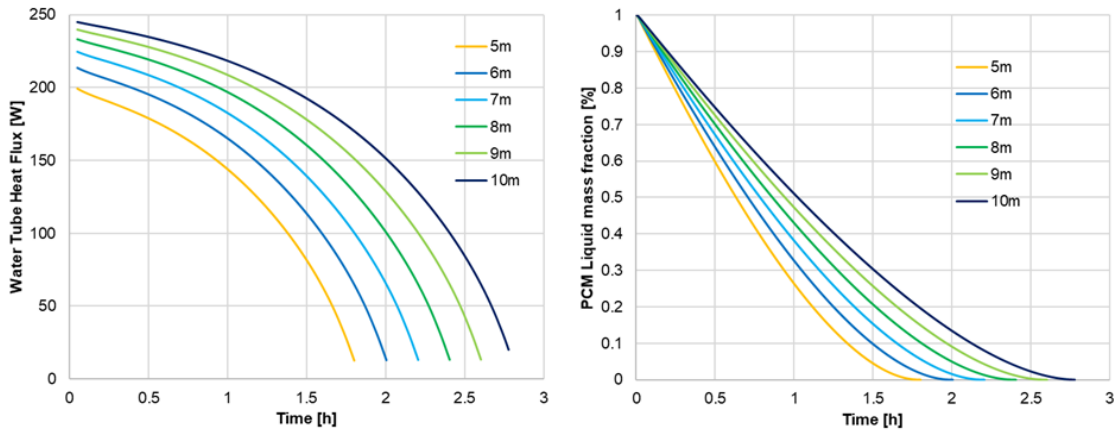

Figure 5.18: Heat flux and PCM liquid mass fraction for different pipe lengths.

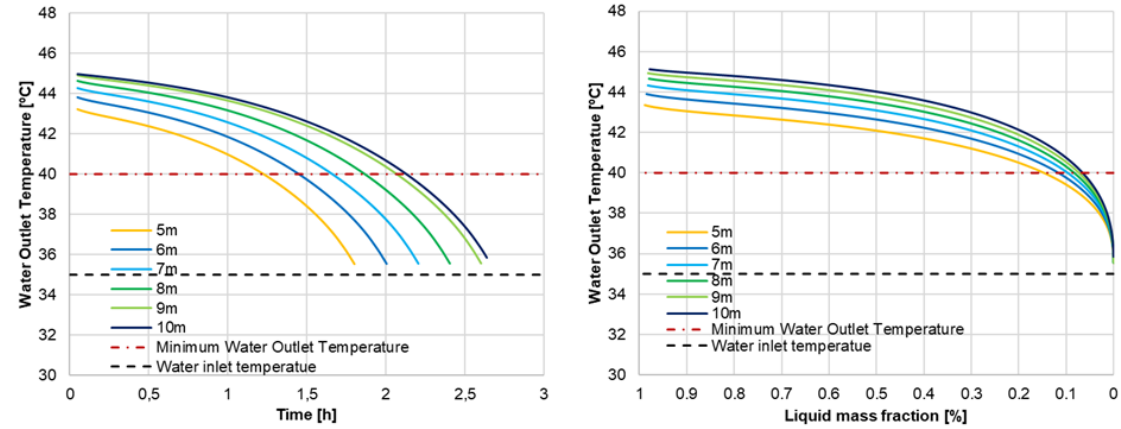

Figure 5.19: Water outlet temperature versus time and water outlet temperature over mass fraction for different pipe lengths.

Section General Conclusions:

The boussinesq approach was ultimately discarded for the models presented in this work. The presence of fins in such a closely packed

5.3.3 Fin Height

The height of the fins is the parameter concerning specifically the distance between circuit tubes, it gives the halfway distance between a pipe section and the surrounding pipes. The ideal configuration regarding this parameter would be for it to hold and provide energy for operating a cycle to acclimatize the building for a day with or without the ground-sourced heat pump and using low electrical tariffs for recharge. For this effect the simulation conditions were an inlet temperature of 35°C, water velocity 0.1m/s with A44, starting at 45°C and the process would be in discharge mode. As seen in Figures 5.20 and 5.21 four different fin heights were tested, 7.5mm, 12.5mm, 22.5mm and 45mm.

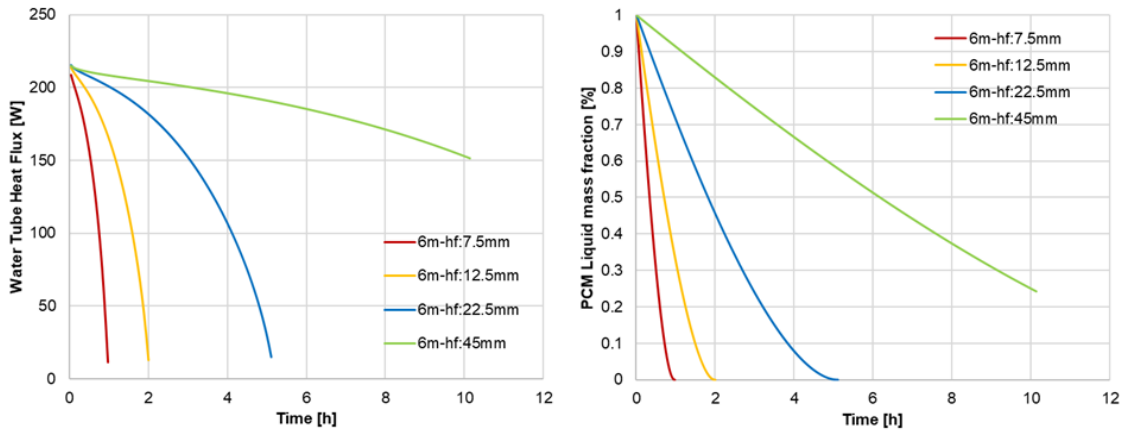

Figure 5.20: Heat flux and PCM liquid mass fraction (Note: The simulation with 45mm fin height stopped at 25% of the liquid mass fraction).

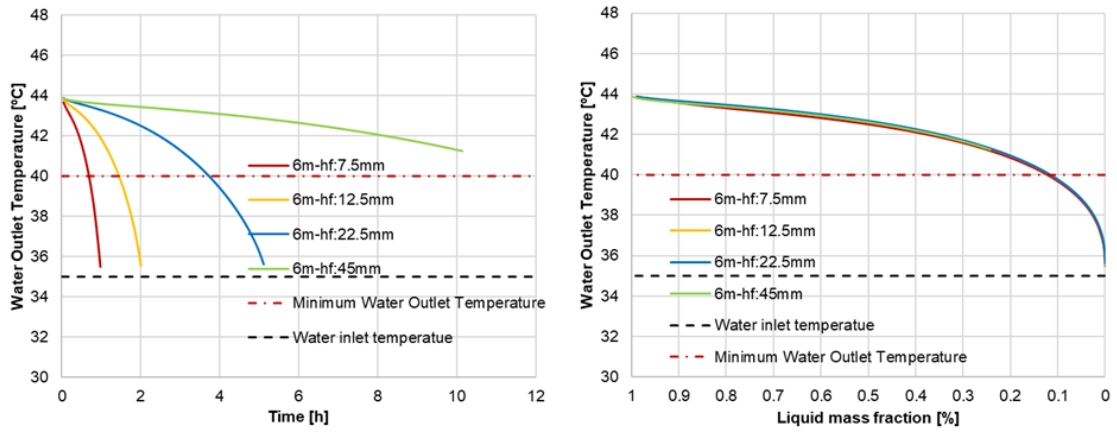

Figure 5.21: Water outlet temperature versus time and water outlet temperature over mass fraction.

Looking at the results one can discern that while the fin height of 7.5 and 12.5mm depletes their stored energy for the chosen mass flow very fast, the simulation with a fin height of 45mm holds temperature for a long time it would take too much energy to quickly recharge back the PCM. The height with 22.5mm was then chosen because it is a compromise between these limitations.

5.3.4 Fin Pitch

This parameter was considered in a more advanced phase of the parameterization stage, originally since the heat exchanger was chosen to be finned tube type, the immediate solution would be to choose from available HVAC interior units which have a fin pitch below 5mm. However, since this heat exchanger would handle a liquid that turns solid, this tight fin proximity while useful for heat transfer could be jeopardised by the expansion

and contraction of the PCM over the phase change process, not only that but with a high concentration of fins per pipe, it would also compete with the PCM for net volume. So, with no literary reference found in this specific regard, the default fin pitch chosen was 5mm, this was then later compared with a 10mm pitch, shown in the Figures 5.22 to 5.25, below. For these cases the boundary conditions were, an input temperature of 35ºC, water velocity 0.1m/s and 0.8m/s with A44, starting at 45ºC and the process would be in discharge mode with a fin height of 22.5mm.

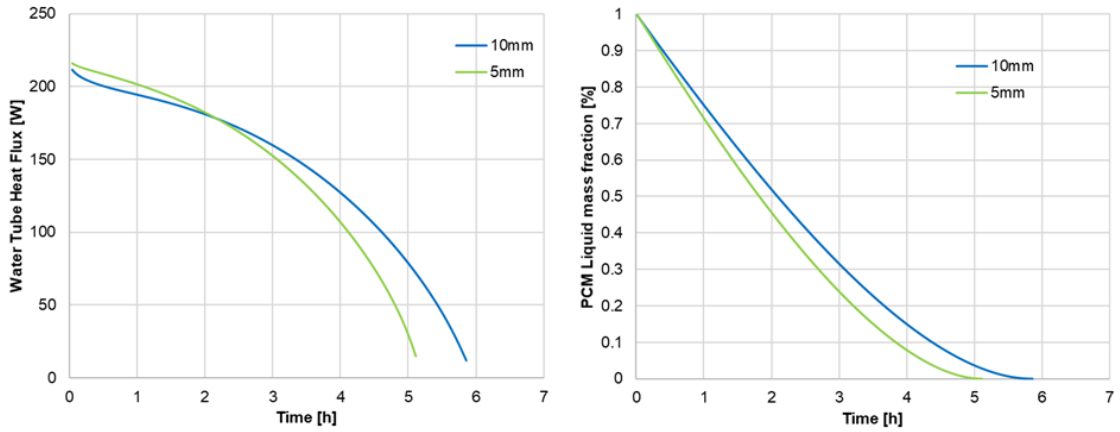

Figure 5.22: Heat rate and PCM liquid mass fraction for 0.1m/s.

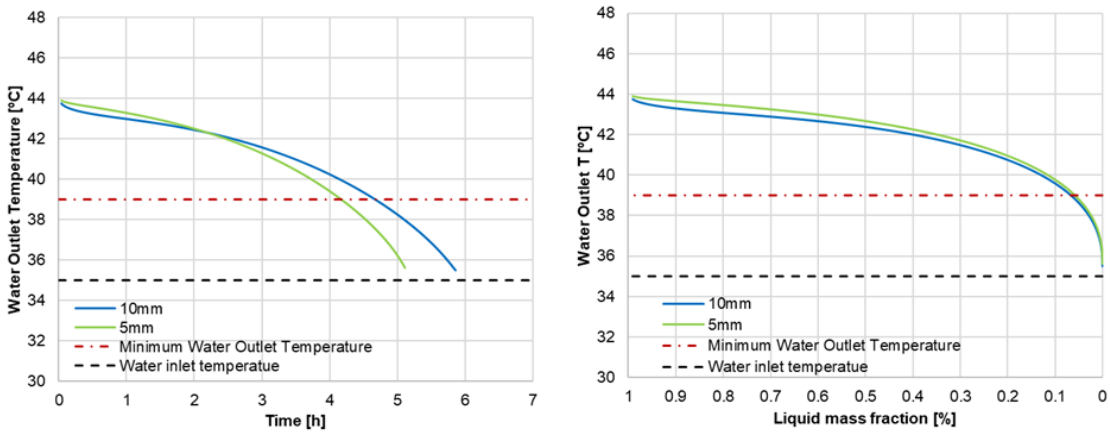

Figure 5.23: Water outlet temperature versus time and water outlet temperature over mass fraction for 0.1m/s.

Assessing the displayed results, it can be determined that while there is a time difference between the discharge processes, the difference is not of much relevance. While the pitch with 5mm has a higher heat flux and outlet temperature in the first half of the process and finishes earlier, the 10mm pitch process lasts longer but with a lower heat flux and outlet temperature (Figures 5.22 and 5.24). Additionally, the difference between the points at

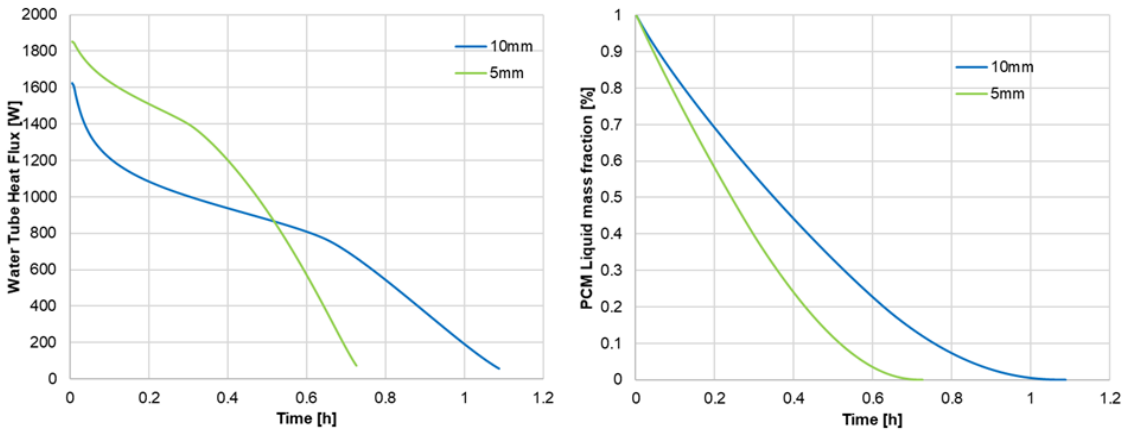

Figure 5.24: Heat flux and PCM liquid mass fraction for 0.8m/s.

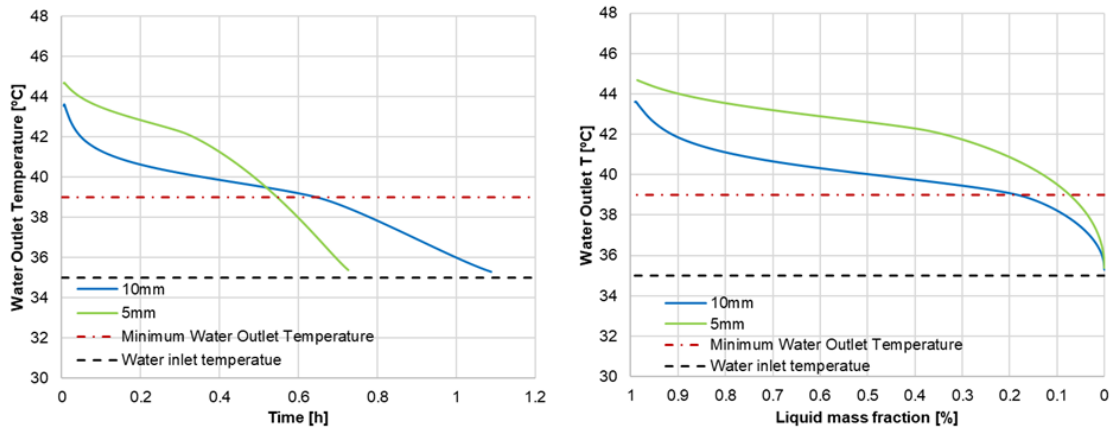

Figure 5.25: Water outlet temperature versus time and water outlet temperature over mass fraction 0.8m/s.

which the outlet temperature curves reaches the minimum water temperature line is small enough to not justify the change from 5 to 10mm. Furthermore the mass fraction value difference for the 0.1m/s velocity is practically non-existent, while for the velocity 0.8m/s the mass fraction for 5mm pitch stays above the minimum water outlet temperature almost up to the end of the phase change (approx. 8%) while the 10mm pitch drops below the minimum at around 20% (see Figures 5.23 and 5.25). Ultimately, the selected fin pitch was settled to 5mm, as it provided a water outlet temperature above the minimum temperature required with liquid mass fraction at aprox. 10% , versus aprox. 20% for the 10mm pitch, meaning it would generate less usefull energy.

Note: The 0.8m/s inlet velocity was comparison was added here because as the work progressed it was concluded that for the applications pondered here, 0.8m/s would equate to flow rates closer to actual practical commercial applications.

5.3.5 Material Influence

In this group of simulations, the focus will be to analyse the heat exchanger material influence on the performance of the heat transfer, specifically the evaluated materials would be the ones that typically the heat exchangers are manufactured out off, namely copper and aluminium and the typical combination being copper tube and aluminium fins (Figures 5.26 and 5.27). For these cases the boundary conditions were, inlet temperature of 35ºC, water velocity 0.075m/s, starting at 45ºC and the process would be discharge mode with A44 and the heat exchanger with a fin height of 22.5mm.

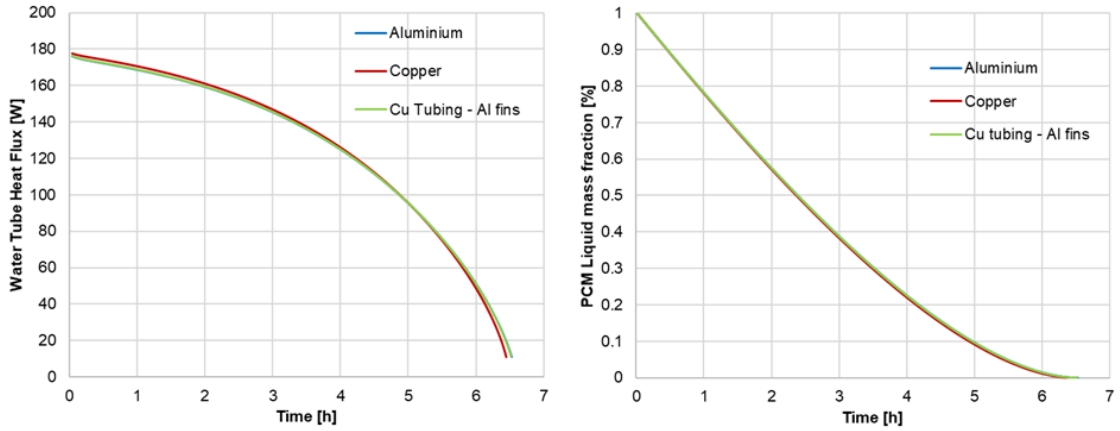

Figure 5.26: Heat flux and PCM liquid mass fraction versus time.

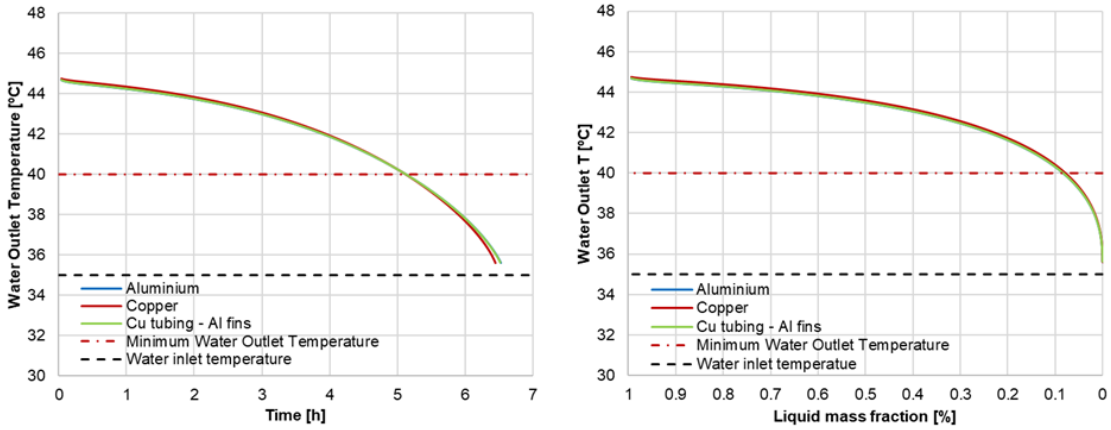

Figure 5.27: Water outlet temperature versus time and water outlet temperature over mass fraction.

It can be gathered from the overlapping results that, regarding the tested materials and combinations, there is practically no difference between using a typical copper tube-aluminium fin heat exchanger or a heat exchanger made completely out of either copper or aluminium, both metals have a high thermal conductivity leaving any heat transfer

limitation on the PCM and water flow side. This means that the heat exchanger could be built exclusively out of one of whatever combination is more beneficial for the manufacturer (for the simulated materials). For instance, considering that aluminium not only is over 3 times lighter than copper and it is per norm less expensive than the former, a heat exchanger that is fully made from aluminium, not only is less expensive but also lighter. This could be an important ponderation for this technology to be implemented both technically and cost wise. Note that this could have some manufacturing constraints concerning possibly the different processing and fabrication of the aluminium as material comparatively to copper.

5.3.6 Velocity and Flow Rate

This simulation set addresses the velocity and consequently the influence of the water flow within the heat exchanger as the heat transfer fluid. Considering all the studied parameters so far, it is discernible that considering the low thermal transfer coefficient of the PCM and the alternative solutions studied to minimize and apply, this is the only other parameter remaining that could be evaluated on the side of the heat transfer fluid being possibility the most relevant parameter concerning this heat exchanger. In the course of the work several velocities were tested, more than the ones presented here, some were considered initially because there were no specific guidelines for what flows would be used in the system. As the work progressed and more information and results regarding operation conditions, heating/cooling needs and heat pumps specs became available some values became more relevant than others, up until explicit values were used concerning the operation conditions for each demosite. Combining the velocities with the selected diameter for the exchanger tubes of 8.6mm interior diameter (Nominal diameter: 10mm), 22.5mm fin height, the water flow was obtained to match the desired operation conditions.

5.3.6.1 Heating Application

For the heating application, as previously, the PCM used here is A44. With regards to the geometric properties and the fluids properties, the flow Reynolds number contains all three basic flow types, laminar, transition and turbulent, with the heat transfer to increase with the increase of turbulence, Table 5.8 shows the Reynolds for each respective velocity and Ansys turbulence model used for the simulation.

Table 5.8: Simulation Reynolds and respective turbulence models.

Velocity [m/s]	**Mass flow [l/min]**	**Reynolds**	**Turbulence model**
0.05	2.09	640	Laminar
0.10	4.18	1280	Laminar
0.25	10.46	3200	kkl
0.49	20.49	6280	k-ε
0.80	33.46	10250	k-ε

Figures 5.28 to 5.31 exhibit the results of a range of velocities that cover the overwhelming majority of simulated velocities allowing for a reasonable assessment of how the heat exchanger works under such operation conditions. The boundary conditions: listed in Table 5.8 the cases the inlet velocity, for the discharging process the water inlet temperature was 35ºC and the simulation was initialized at 46ºC, mimicking a completely charged tank; for the charging process, three charging methods were employed: on two cases the charging inlet temperature considered would be 50 and 55ºC provided by the heat pump with an inlet velocity of 0.22m/s, the remaining case would use the solar system to heat the water with a variable input temperature function that is meant to emulate solar gains of nine solar collectors in a winter day (worst case scenario), the inlet velocity is 0.085m/s, being initialized at 42ºC representing a completely discharged tank.

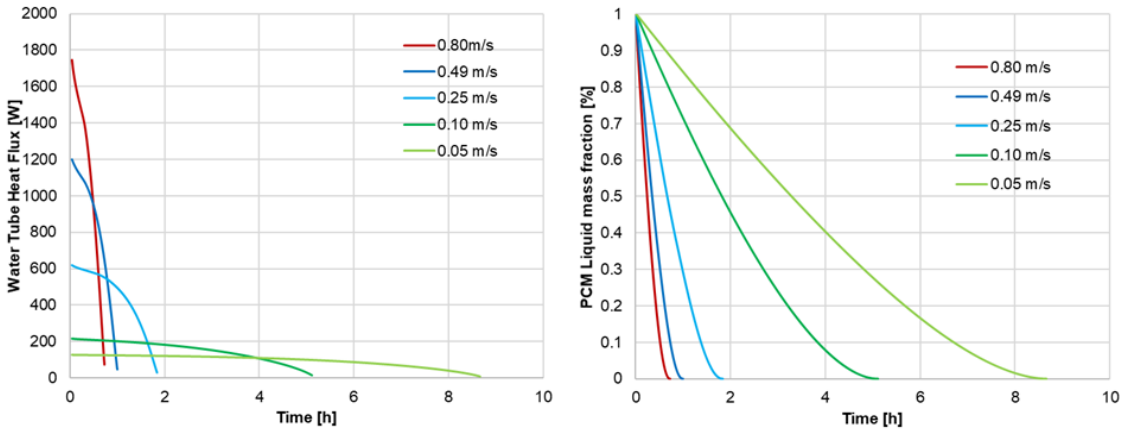

Figure 5.28: Heat flux and PCM liquid mass fraction versus time for the discharge process.

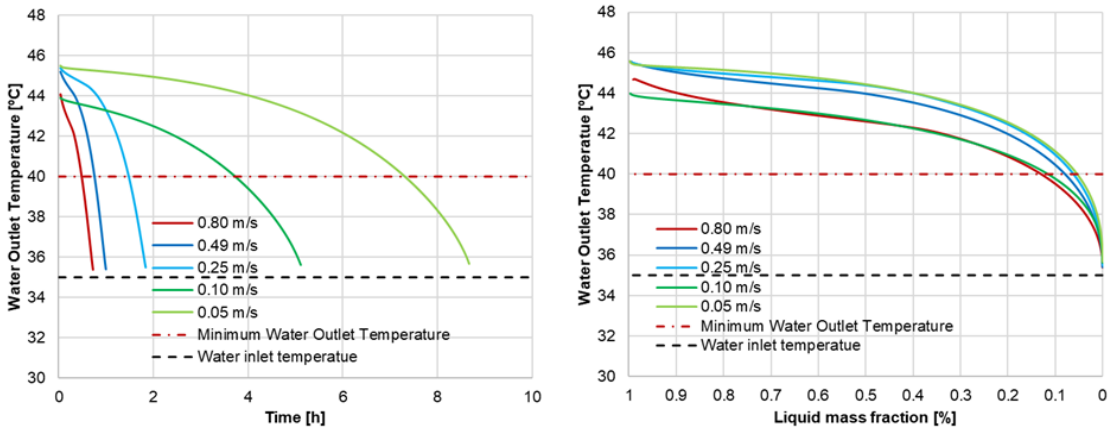

Figure 5.29: Water outlet temperature versus time and water outlet temperature over mass fraction for the discharge process.

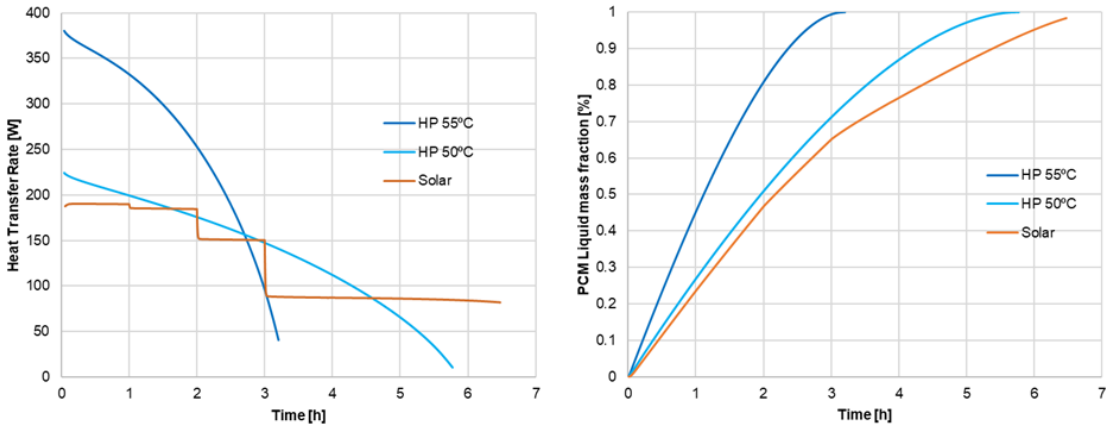

Figure 5.30: Heat flux and PCM liquid mass fraction versus time for the three charge processes.

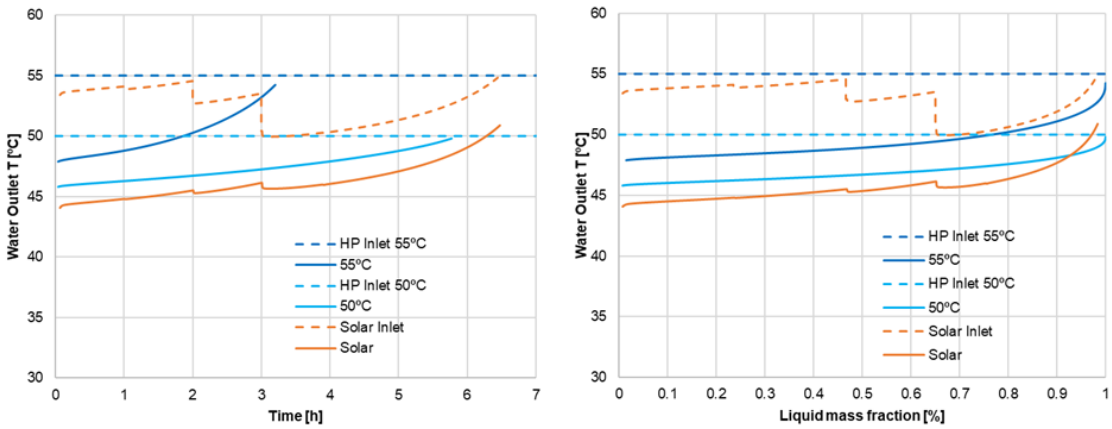

Figure 5.31: Water outlet temperature versus time and water outlet temperature over mass fraction for the three charge processes.

Assessing the displayed results for the discharge process it is possible to see, as expected, there is a significant influence of the heat transfer fluid velocity on the heat transfer rate, therefore the total amount of time to completely discharge (solidify PCM) is decreased as the flow velocity and Reynolds increase. Additionally, the figures show that as the velocity increases the outlet temperature of the heat transfer fluid decreases. Regarding the charge process, the solar system can be charged up to 75% in four hours, meaning that in a sunnier day it would be possible to completely charge the tanks. Concerning the charge through the heat pump at constant temperature it is discernible that for an inlet temperature of 50ºC it is possible to charge up to almost 90% in four hours, meanwhile for the 55ºC charge temperature setting its possible see that totality of the charge can be achieved in approximately three hours. This last condition however, is ill-advised as not only because it decreases any heat pump efficiency significantly to operate at 55ºC but

it would be dependent on the capacity of the installed heat pump and as such it would operate on these conditions sparingly. Table 5.9 lists the pertinent parameters selected for this application for the most important thermal process, discharge.

Table 5.9: List of selected parameters for this application discharge.

Parameter	**Unit**	**Value**
Length	m	6
Fin Height (Tube Spacing)	mm	22,5
Fin Pitch	mm	5
HX Material	-	Aluminium finned copper tube
Velocity (Mass Flow rate)	m/s	0,05-0,8

5.3.6.2 Cold Application

As the simulation concerning the heating solution provided seemingly promising results, the same methodology was applied to the cooling solution simulations. The cold application would cool the building resorting to tanks filled with PCM A9 (see Table 5.10) working with the systems Heat Pump. The model geometry was the same used for the previous chapter.

Table 5.10: A9 PCM properties.

Property	**A9**
ρ [kg/m^3]	800
Cp [J/kg.K]	2160
k [W/m.k]	0.24
ΔH_{sl} [J/kg]	185000
Solidus Temperature [K]/[ºC]	281/7.85
Liquidus Temperature [K]/[ºC]	282/8.85

For the presented cases below (Figures 5.32 and 5.33) both the charging and discharging process is shown with the following boundary conditions: in both cases the inlet velocity is 0.1m/s (4.18l/min), for the discharging process the water inlet temperature was 7ºC and the simulation was initialized at 11.85ºC, mimicking a completely charged tank; for the charging process, the water inlet temperature was 18ºC, being initialized at 6.85ºC representing a completely discharged tank.

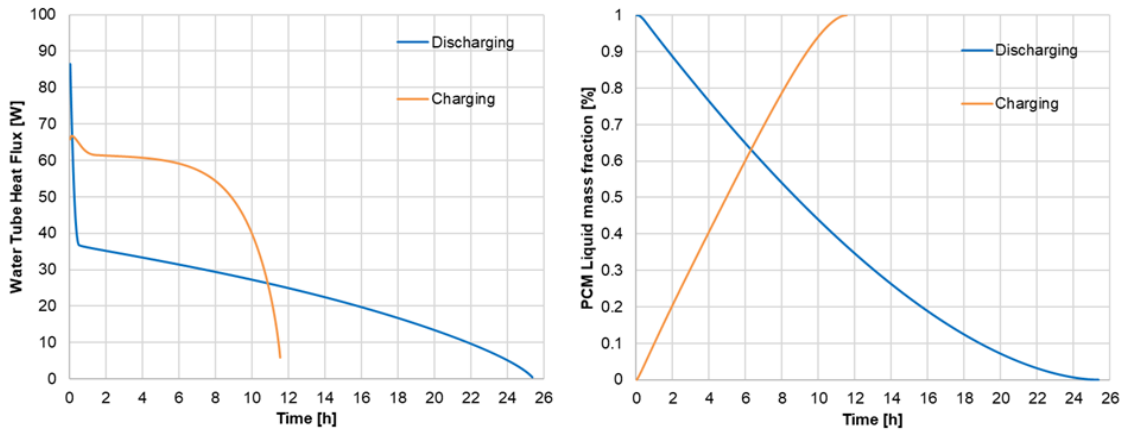

Figure 5.32: Heat flux and PCM liquid mass fraction versus time for the charge and discharge process.

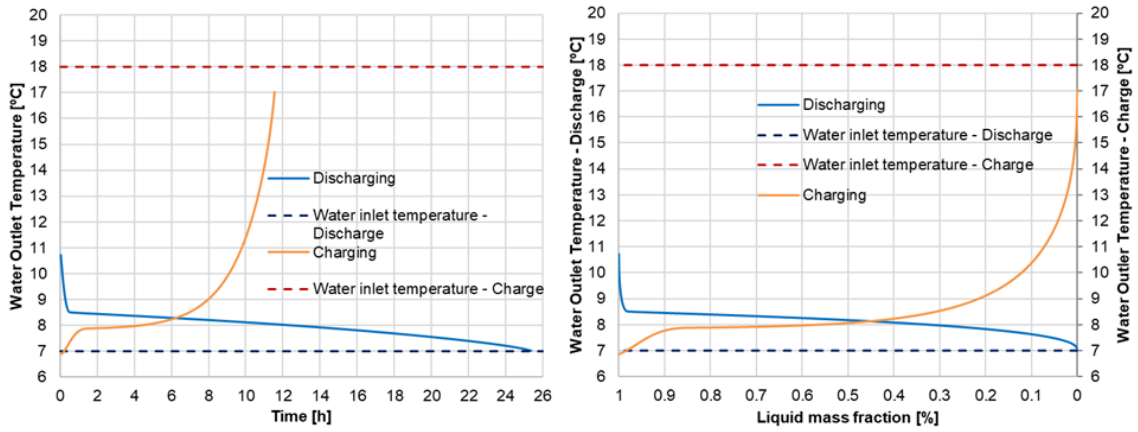

Figure 5.33: Water outlet temperature versus time and water outlet temperature over mass fraction for the charge and discharge process.

With regards to the results, it is observable that the model is adequate, qualitatively at least. The charging takes significantly less time than the discharging process, even though they have the same flow, this is because, concerning the charging, we have a much high ΔT than the discharge has, cutting significantly the total process time. Using the methodology and due to manufacturer suggestion, another simulation set was run considering a slightly different geometry, specifically with a fin height of 14.45mm. With this set of simulations some parameters where changed, like the inlet temperature for the discharge being 5ºC matching a typical operation feature for a cooling-mode chiller, Figure 5.34 and 5.35 show the results.

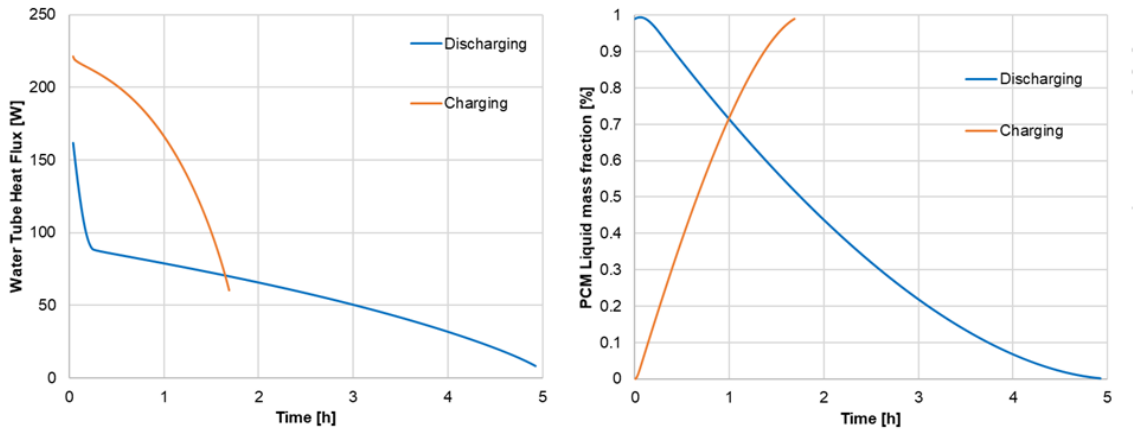

Figure 5.34: Heat flux and PCM liquid mass fraction versus time for the charge and discharge process.

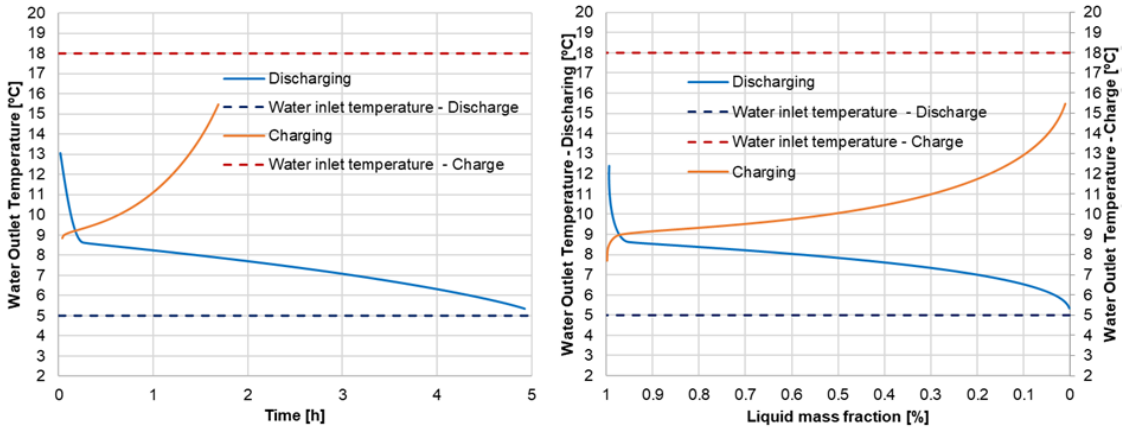

Figure 5.35: Water outlet temperature versus time and water outlet temperature over mass fraction for the charge and discharge process.

From the results it can be gathered that the tank can be discharged in five hours using a 5°C inlet temperature, while taking less than three hours to be completely charge under the shown conditions meaning it can be a viable application. Table 5.11 lists the pertinent parameters selected for this application for the most important thermal process, discharge.

Table 5.11: List of selected parameters for this application discharge.

Parameter	Unit	Value
Length	m	6
Fin Height (Tube Spacing)	mm	14.45
Fin Pitch	mm	5
HX Material	-	Aluminium finned copper tube
Velocity (Mass Flow rate)	m/s	0,1

5.3.6.3 Domestic Hot Water Application

For the domestic how water solution while the same overall methodology was used, since the actual process does not rely on stored heated water like a more conventional system but instead it would heat up the water instantaneously, the heat exchanger circuitry would be slightly different. In this specific application the heat exchanger would be composed by three interdependent but separated circuits; one circuit would connect the heat exchanger to the solar panel system for charging with a renewable heat source, another circuit would be connected to the ground sourced heat pump to provide heating to charge the PCM in any condition where the solar output was unable to charge the tank and the last circuit is directly connected to the public water network that would heat up the water that ultimately would be used in the home applications like showers, bathtubs and sinks, etc. Considering that this heat exchanger would have to heat water that would be close to the soil temperature in winter (worst case scenario) the major modification for the simulations in this section it's that instead of having the original six meters, it would require a greater heat exchange area to heat up the water, as so a longer circuit length was simulated. The simulation domain was increased to 18 meters long and the minimal permissible water outlet temperature is 45ºC so it can be used in DHW applications, this configuration however only applies to the discharge circuit (connected to the water network), the charging circuits have the same six meter length as in the previous cases. For this application the chosen PCM is A53 with the properties displayed in Table 5.12 so that it can store heat at a higher temperature matching the application.

Table 5.12: A53 PCM properties.

Property	**A53**
ρ [kg/m^3]	800
Cp [J/kg.K]	2160
k [W/m.k]	0.22
ΔH_{sl} [J/kg]	160000
Solidus Temperature [K]/[ºC]	324.2/51.05
Liquidus Temperature [K]/[ºC]	325.6/52.45

0.86 m/s (12 l/min), for the discharging process the water inlet temperature was 15ºC estimated to mimic the network water temperature and the simulation was initialized at 53ºC, mimicking a completely charged tank. For the charging process: the inlet velocity is 0.424m/s, the water inlet temperature would simulate the temperature from the solar system at 59ºC, being initialized at 50ºC representing a completely discharged tank. Figures 5.36 and 5.37 show the discharge results and Figures 5.38 and 5.39 display the charging results.

As depicted in the results, according to the simulation a single circuit 18 meters long has enough energy to provide water above 45ºC for over 15 minutes along the discharge process, considering bathing applications this feature is successful. While charging, using

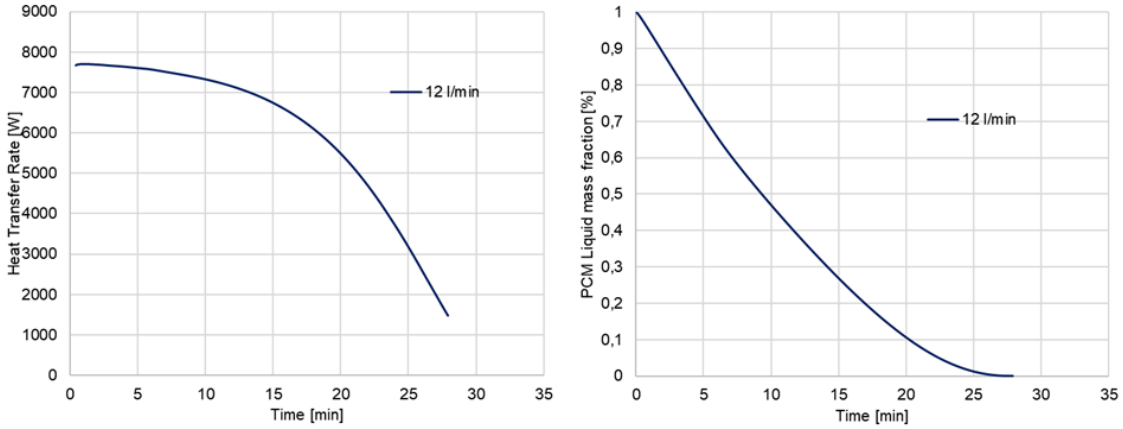

Figure 5.36: Heat flux and PCM liquid mass fraction versus time for the discharge process.

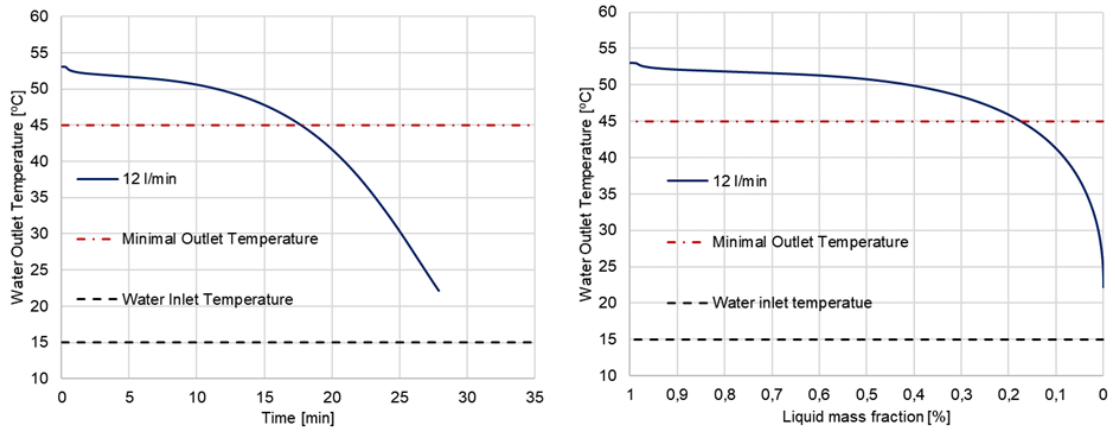

Figure 5.37: Water outlet temperature versus time and water outlet temperature over mass fraction for the discharge process.

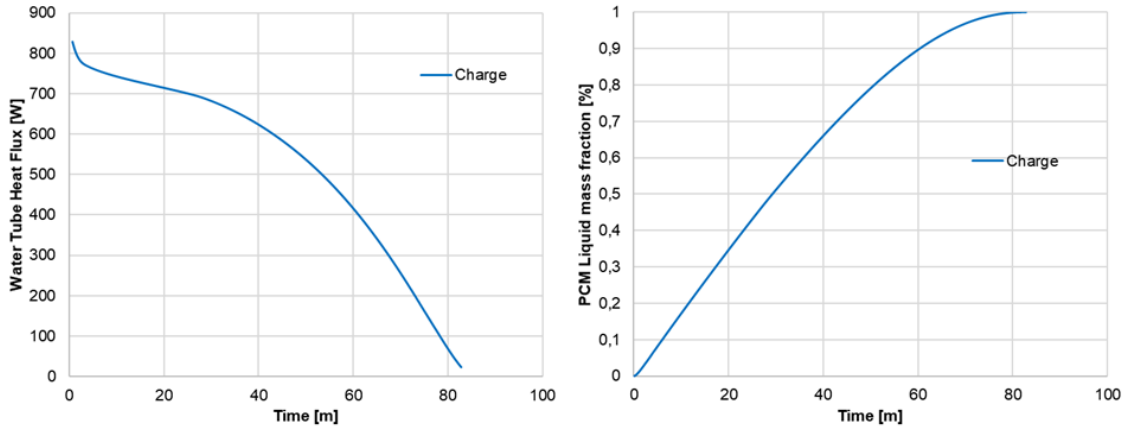

Figure 5.38: Heat flux and PCM liquid mass fraction versus time for the charge process.

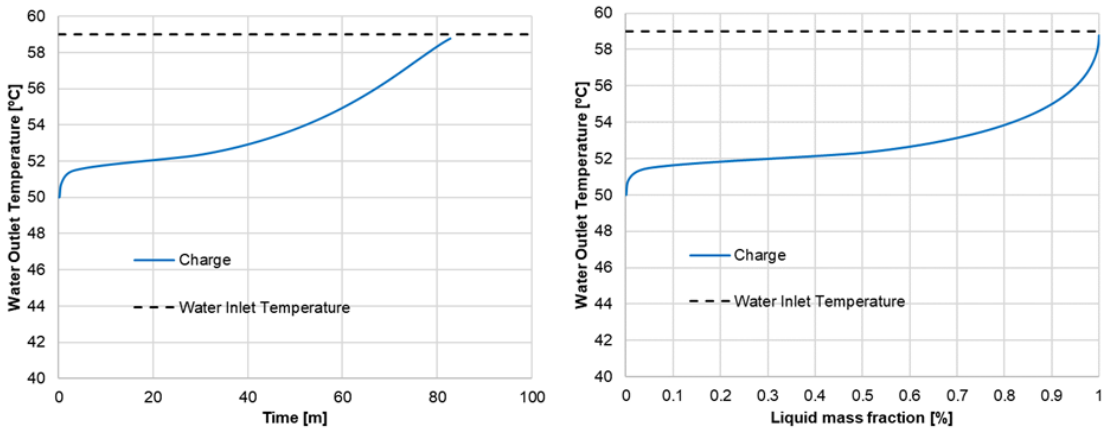

Figure 5.39: Water outlet temperature versus time and water outlet temperature over mass fraction for the charge process.

the solar system it can be achieved in less than 1.5 hours and be charged up to 50% in half an hour enabling the remainder of the solar availability be used to charge the heating tanks, allowing for some heat pump supplementation of the partial remaining heat charging needs. While the heat pump is also able to charge the tank in this case it was disregarded as the heat pump can reach a higher temperature level than the average solar system operation, in the worst case scenario. Following this another set of simulations were performed for the discharge process in order ascertain the tank behaviour with flow rates commonly used with in a domestic household, with results for the flows being 8, 10 and 12 l/min shown in Figures 5.40 and 5.41.

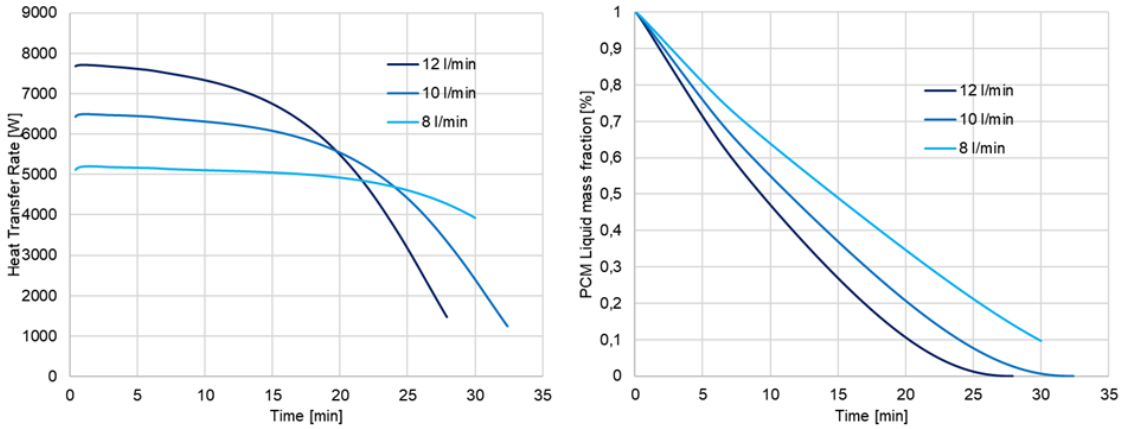

Figure 5.40: Heat flux and PCM liquid mass fraction versus time for the discharge process of the different flows.

From the results it can be gathered that the presented solution is adequate as all the flows show the outlet water temperature staying above 45ºC for over a mimimum of

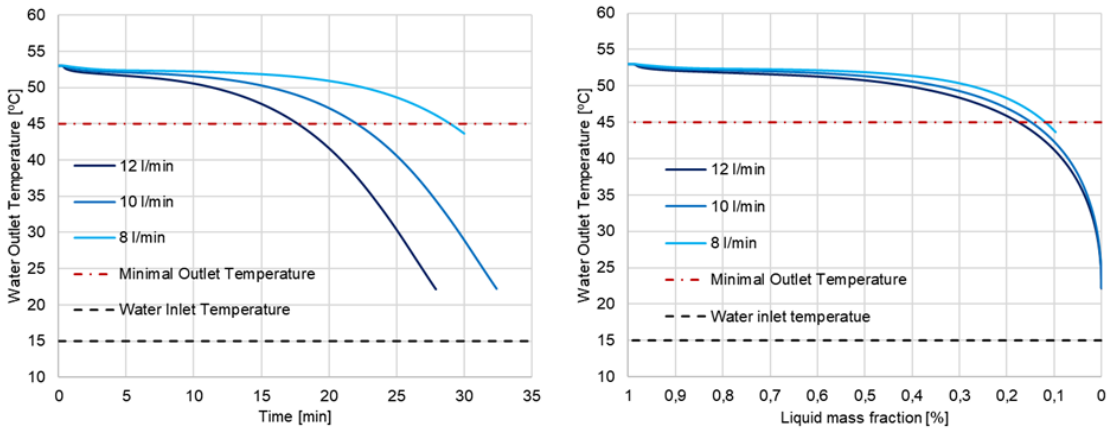

Figure 5.41: Water outlet temperature versus time and water outlet temperature over mass fraction for the discharge process of the different flows.

15 minutes with a total heat water volume of 210 l, 220 l and 230 l generated over that temperature for 8, 10 and 12 l/min respectively. These water volumes are higher than the storage in a conventional household application for a family of four that ranges typically with in 150 and 200 l.

Sections General Conclusions:

A single heat exchanger circuit was selected to be 6 m in length for the heating and cool applications, providing a balance between the quality and quantity of energy transferred. The circuit's inner diameter was based of a specs with 8,6 mm, with the fin thickness being 0.3 mm. The fin height (tube spacing) selected was 22,5 mm as it allowed for enough energy to be stored for the system to operate adequately whilst still being able to be recharged in a timely manner. The fin pitch employed was 5mm, is was chosen because it allowed for a more useful energy to be discharged out of the system. The heat exchanger's material, out of the tested materials, barerd no influence on its performance. The heat transfer fluid mass flow rate significantly impacts the heat transfer rate, as it increases (the velocity), outlet temperature of the HTF decreases. Table 5.13 lists the pertinent parameters selected for this application for the most important thermal process, discharge.

Table 5.13: List of selected parameters for this application discharge.

Parameter	Unit	Value
Length	m	12
Fin Height (Tube Spacing)	mm	22,5
Fin Pitch	mm	5
HX Material	-	Aluminium finned copper tube
Velocity (Mass Flow rate)	m/s	0,86

5.3.7 Pre-Prototype Verification

Using the information gathered from the previous sections, a pre-prototype was drawn and manufactured to verify the CFD model and simulations. The aim here is to verify the geometry, mesh and physical schemes solutions of the model built in CFD with an effective experiment to mimic as closely as possible the simulated conditions. In this effort a pre-prototype was built (Figure 5.42 to 5.44), the heat exchanger would be an aluminium finned copper tube 6 m long in total, external diameter 10mm and internal diameter 8.6 mm. The heat exchanger has 12 0.5m sections, with 100 fins (200 fins per meter), fin height 8.8mm, fin thickness 0.3mm and spaced 5mm apart as shown in Figure 5.43 in agreement with the simulated specifications.

Note: The experimental work, while it was performed in parallel and in accordance with what was presented here, it was made outside of the scope of this specific work, by another project partner, and thus could not be supervised nor executed by the author.

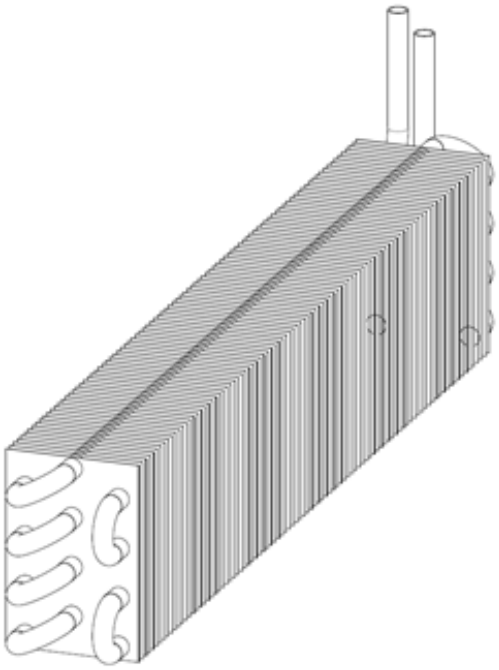

Figure 5.42: Pre-prototype outlined design. (Courtesy of NKUA) [122]

The heat exchanger would then be immersed in a A44 filled tank. The experimental setup would connect the heat exchanger to hot and cold reservoirs as show in Figure 5.45. Throughout the tank and heat exchanger an array of thermocouples, type-T, is placed to measure the temperature variation in the PCM-heat exchanger medium.

Three sets of discharge experiments were tested with three different flows, 30 l/h, 45l/h and 60 l/h (Details in Table 5.14). Comparing the results displayed in figures 5.46 to 5.48 it is possible to see that the 2D axisymmetric simplified approach is reasonably good, with the CFD model temperature outlet staying slightly beneath the experimental outlet, while maintaining the same overall qualitative behaviour. However, it is possible to see

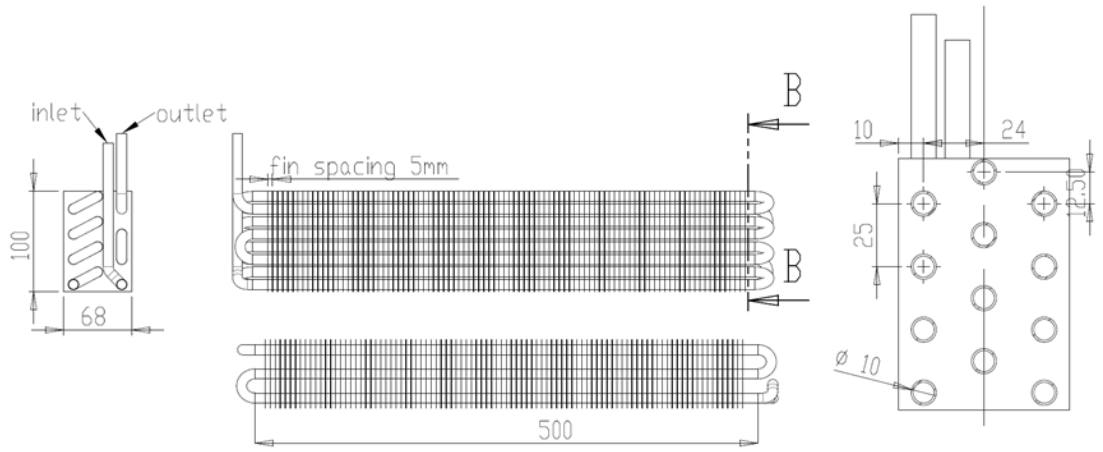

Figure 5.43: Geometric dimensions. (Courtesy of NKUA) [122]

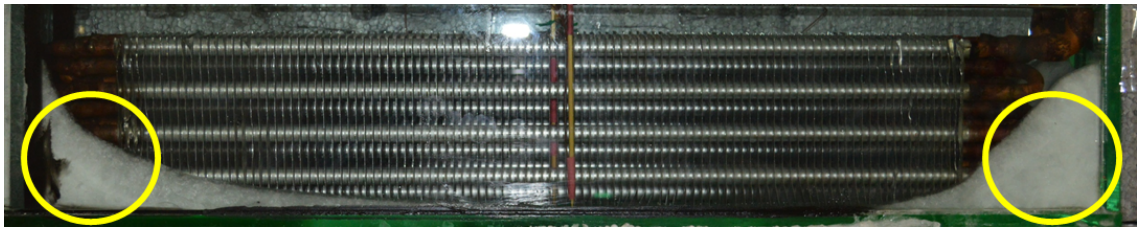

Figure 5.44: Heat exchanger pre-prototype within the experimental tank with highlighted PCM masses, after the discharge process is finished. (Courtesy of NKUA) [122]

a divergence of the plotted lines near the end of the phase change process, specifically in the Test 1 when the liquid mass fraction was about 13%, in Test 2 when the mass fraction approaches 15% and in Test 3 when the mass fraction was about 4%.

Table 5.14: Test conditions.

Test ID	**Volume flow [l/h]**	**Flow velocity [m/s]**	**Inlet Temperature [ºC]**	**Reynolds**
1	30	0.143	36	1830
2	45	0.215	36	2750
3	60	0.287	36	3670

The possible cause for the divergence of the curves lays with PCM deposits in area just outside of the heat exchanger fins (see Figure 5.44 highlights) and that are not able to exchange heat efficiently and provide an additional amount of stored energy that accounts to justify the experimental lines having a higher energy (higher average outlet temperature value) than the CFD model shows. One possible way to overcame this issue in future simulations could be using a thermal bridge calculating method to try and account for,

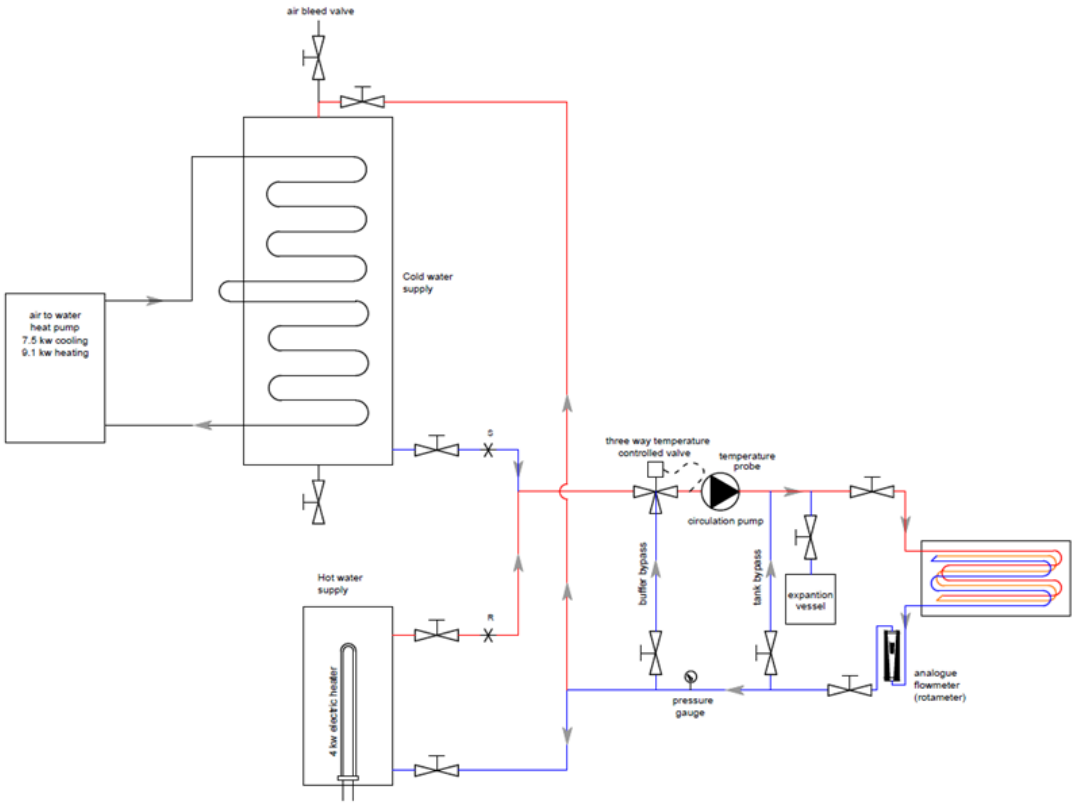

Figure 5.45: Experimental set up for the pre-prototype laboratory testing. (Courtesy of NKUA) [122]

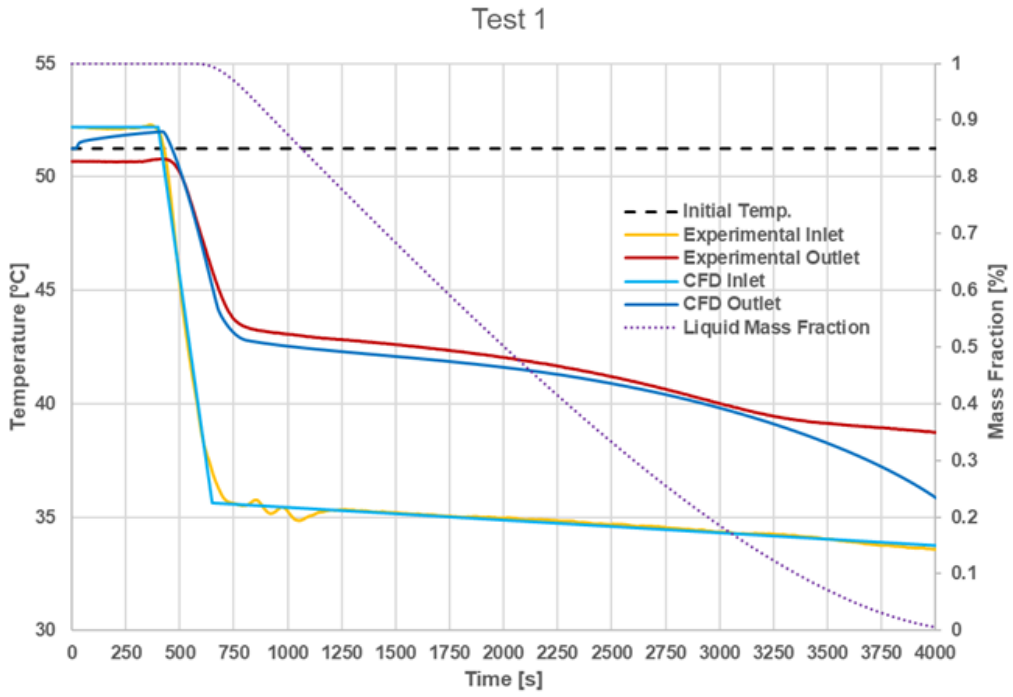

Figure 5.46: Experimental discharge test 1 - 30 l/h flow.

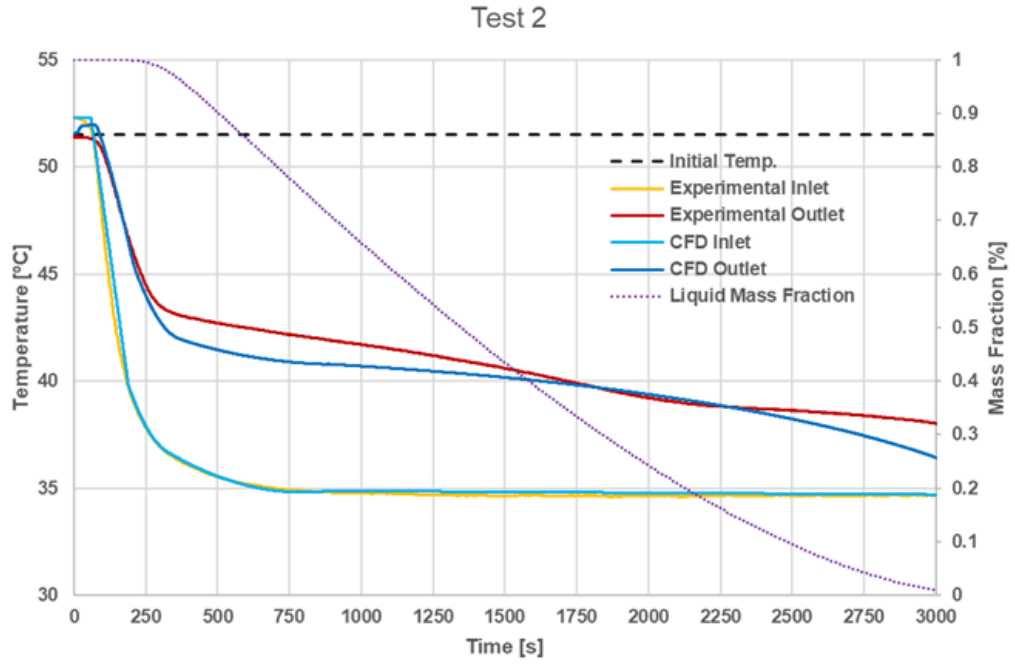

Figure 5.47: Experimental discharge test 2 - 45 l/h flow.

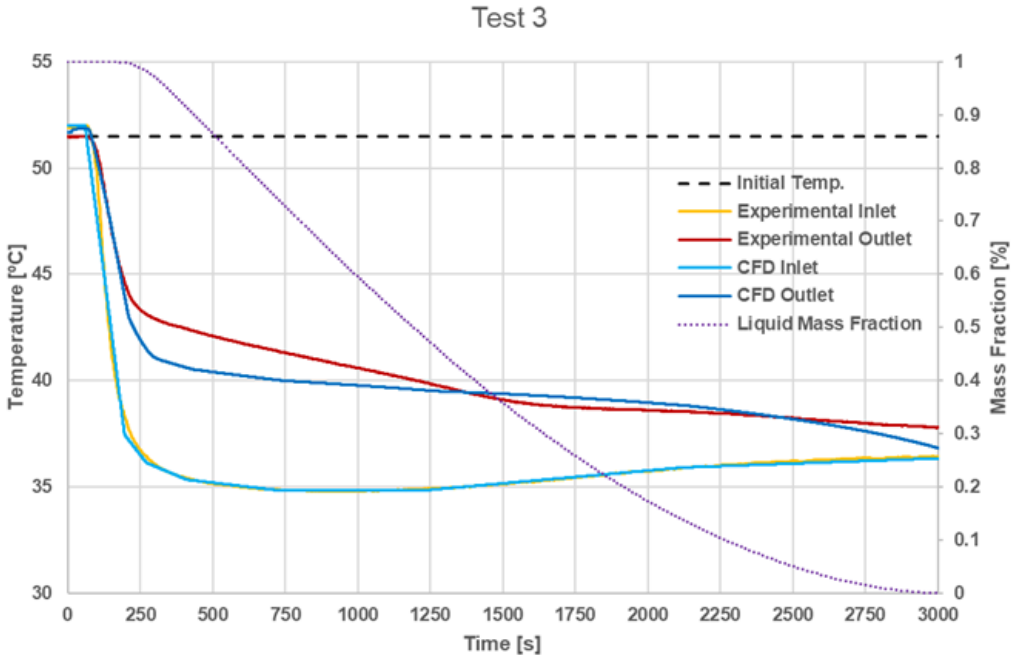

Figure 5.48: Experimental discharge test 3 - 60 l/h flow.

or to estimate, the deposited energy around the bend of the heat exchanger. As to the reason why the lines do not overlap as it would have been ideal there are several possible causes. Concerning the experiment specifically, there were issues maintaining a reasonably constant water inlet temperature for both cold and hot energy sources, possibly because of irregular water flow, while on the numerical model, the inlet temperature was considered as a constant averaged value. Another plausible experimental reason is that due to the processes studied taking place with in a relatively tight temperature range, the effective precision of the used thermocouples could be influencing the values obtained by the data acquisition system. Another issue here is that, as explained before, PCMs do not always behave exactly as the catalogued specifications stated, with thermophysical properties varying and with deviations in work temperatures that could extend beyond, or were not considered in, the configurations of the numerical model. Regarding the numerical model, it is important to remember that the CFD model is a 2D axisymmetric approximation to a 3D domain, this could influence the results. The greatest possible source of influence could come from the turbulence model. The mass flow rates studied in this experimental phase are either within the laminar flow region (Test 1) or within the transition flow region (Test 2 and Test 3). Literature as shown that the CFD turbulence models for transition flows have limitations regarding their accuracy therefore, the model used for transition modelling could be having a detrimental effect on the numerical results as most turbulence models assume high Reynolds numbers values. This does not imply that it can be advisable to use either laminar or turbulent models as it could also adversely affect the accuracy of the results from the simulated flows that take place in the transition region.[124] Further elaborating this point, Figure 5.49 plots a series of lines that are meant to compare different CFD turbulence models, from laminar, through transition and turbulent flows concerning their effects on the simulated outlet water temperature.

As mentioned before, most of the tested flow rates and velocities, for the used geometry, are within turbulent transition phase and like stated above, transition flows are not especially precise, but an effort was made to try and understand how the models behaved with in the transition interval. In Figure 5.49 one can see how all the models values vary to several degrees comparing with the experimental result, the laminar model shows a reasonable proximity with a visible deviation between approximately 250 and 1250 seconds, staying mostly below the experimental outlet line. The transition model, kkl shows a near identical behaviour to the laminar model while the SST model has more pronounced curvature and a behaviour more akin to the turbulent models with the results curve staying mostly above the experimental line. The turbulent models, standard k-ε model, the k-ε RNG model and k-ε Realizable model all have a nearly equal result with the most pronounced temperature curves comparatively to the experimental results. Overall, in these conditions, the models that seem to match the experimental results more closely are both the laminar model and the kkl transition model.

Another possible influence could come from the temperature considered initially as, like it was explained above, the variability of the water flow and temperature could have

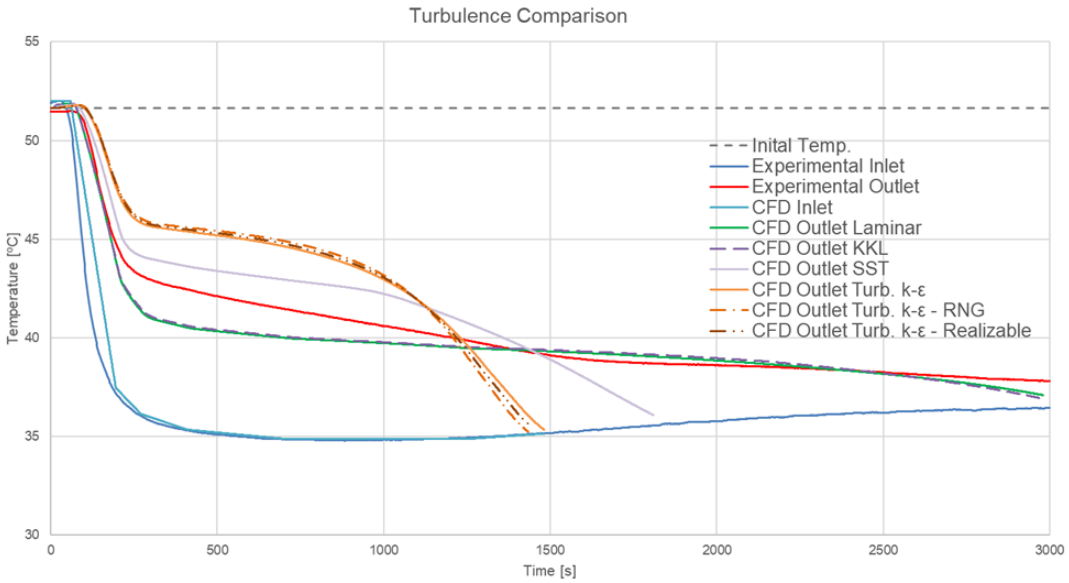

Figure 5.49: Experimental discharge test 3 - 60 l/h flow comparison between different turbulent models.

adulterated the actual behaviour of the experiment that the model could not precisely account for. Additionally, observing the temperature line for the numerical results its mostly always beneath the experimental line, so this could be used as a mean, when sizing a system with these components, to underestimate the effective energy leaving room for an added security for the energy stored, slightly oversizing a real-life system. Koukou et al [122] further corroborate the results through a parallel analysis of numerical simulation along with the laboratory work from a project partner involved in part of the experimental process described here. Nevertheless, considering all these possible causes for any difference between the experimental and numerical model results it still can be said that is a good approximation and from here on, the pre-prototype will be scaled to a prototype for installation in operational demosites.

Section General Conclusions:
Comparing the experimental work with the CFD showed that, for the specific cases, the laminar turbulence models showed best match, closely followed with the kkl transition model, as the mass flow of the experimental tests were in or close to the laminar-transition regime.

5.3.8 Tube spacing, Number of circuits, Circuit length and Pressure Drop

With the information resulting from the numerical work so far and the known limitations and objectives set for the system, a full-sized prototype was conceptualized and designed (see Figure 5.50), then a manufacturer was contacted to start the production, resulting in a working prototype for implementation in the demosites testing out the system.

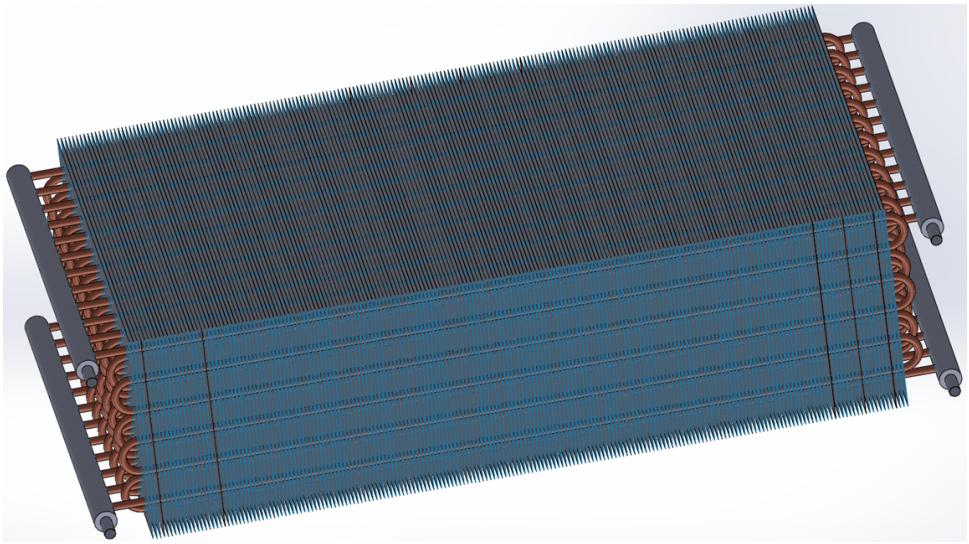

Figure 5.50: CAD render of the full-fledged heat exchanger prototype.

This set of simulations addresses the fin height (tube spacing), the number of circuits per heat exchanger and the length of each individual circuit and how these features might influence the heat exchanger behaviour. In this assessment, as in section 5.3.1.2, the fin height will become relevant because in this case the estimated volume for the heat exchanger prototype was considered and three geometries presented in Figure 5.51, detailed in Table 5.15, were considered for verification of the heat transfer process, defining the pipes arrangement inside the tank. In all geometries had a main dimension that was stipulated to be one meter with a total volume of 120 l, the other dimension would be arranged to meet the parameters of the geometry, by changing the tube spacing we can obtain the following configurations: six, four meter long circuits; eight, six meter long circuits and twelve, ten meter long circuits (see details in Table 5.16) effectively increasing the number of pipes in the tank and consequently varying the total flow of water for the same tank volume.
With these configurations and the aforementioned 5mm fin pitch, aluminium finned copper tube a series of Reynolds were simulated as shown in Table 5.16, as before since the most important process for the system is the discharge process all the presented cases are of this process.

Table 5.15: Geometries detail.

Geometry	**Pipe nº per Single Circuit length [m]**	**Gross Volume [l]**	**Pipe and Fins Volume [l]**	**Net Volume [l]**	**Volumetric Ratio**	**Tube spacing / Fin height[mm]**
Geometry 1	6 x 4 m	121	9.0	112.0	0.93	40.0
Geometry 2	8 x 6 m	114	10.4	103.6	0.91	27.5
Geometry 3	12 x 10 m	115	15.8	99.5	0.86	17.5

Table 5.16: Simulation cases for the established geometries.

Case ID	Geometry	Velocity [m/s]	Reynolds	Turbulence model	Number of circuits	Circuit length [m]	Heat exchanger flow [l/min]
C1	Geometry 1	0.8	10200	k-ε	6	4	16.70
C2				k-ε	4	6	11.20
C3				k-ε	3	8	8.36
C4				k-ε	2	12	5.58
C5		0.4	5100	kkl	6	4	8.36
C6				kkl	4	6	5.58
C7				kkl	3	8	4.18
C8				kkl	2	12	2.79
C9		0.2	2550	Laminar	6	4	4.18
C10				Laminar	4	6	2.79
C11	Geometry 2	1.2	15300	k-ε	4	12	16.70
C12		0.8	10200	k-ε	6	8	16.70
C13				k-ε	4	12	11.20
C14				k-ε	3	16	8.36
C15	Geometry 3	0.8	10200	k-ε	6	20	16.70

In Figure 5.52 it is possible to see some of the results from the simulations that, generally speaking, the smaller number of pipes there are, the longer the whole process will take to complete (the phase change). A greater number of pipes as in Geometry 3 allows for a greater heat transfer rate with a shorter process time with the PCM available volume being slightly smaller, the inverse is true. The results showcased in Figures 5.53 and 5.54 reveal that the heat exchanger behaviour is strongly influenced by the heat transfer fluid flow rate and the total number of pipes within the tank. The increase in the pipe number and the flow rate increases the transfer rate, however with a flow rate taking place above transition and within turbulent regimen the same number of pipes is independent of the tubes arrangement, on the other hand the laminar regime has a detrimental effect on the heat transfer, which can be seen in the comparison between C7 and C9.

Considering that in some of the cases there is a considerable rise in individual circuits for the whole heat exchanger, this could entail a significant increase in the pressure drop. Using the results from the cases above, an estimation was for the pressure drop each case would have and the resulting pump power needed to overcome, it as seen in Figures 5.55 and 5.56.

Observing the results, it can be gathered that, when the flow rate is the same, the pressure drop varies with the heat transfer fluid and so the shorter the individual circuit length is (meaning a higher total number of circuits) the smaller the pressure drop is, while the pumping power is exclusively dependent on the velocity, independent of the circuit arrangement.

Section General Conclusions:

The major influence of the heat transfer process is strongly influenced by the velocity and therefore the HTF mass flow rate and its turbulent regime and by extension, the total number of pipes in the tank and individual circuits. Furthermore , it can be gathered that, when the flow rate is the same, the pressure drop varies with the heat transfer fluid mass

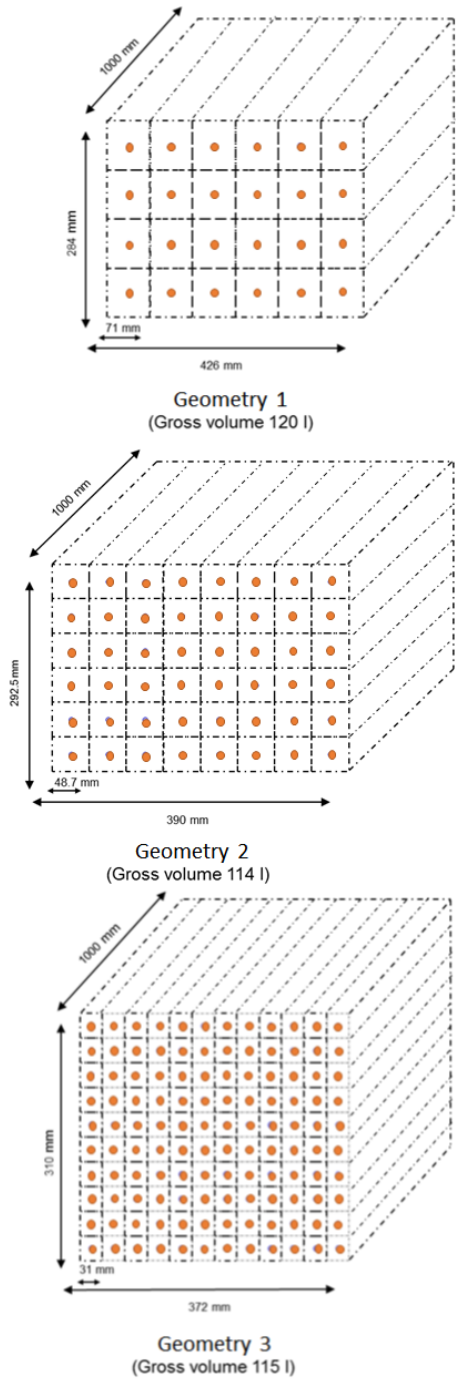

Figure 5.51: Simulated geometries (1,2 and 3) with a different number of circuits showing volume of influence of each pipe.(120l, 114l and 115l respectively)

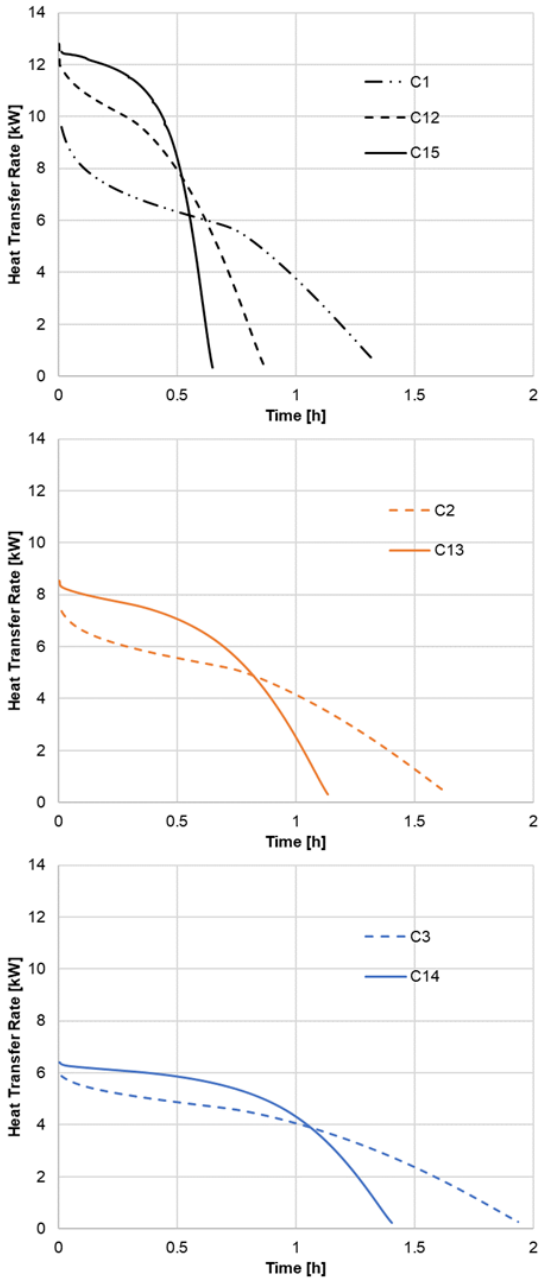

Figure 5.52: Heat transfer rate per heat exchanger for each of the three simulated geometries with different flow rates (16.70, 11.20 and 8.36 l/min).

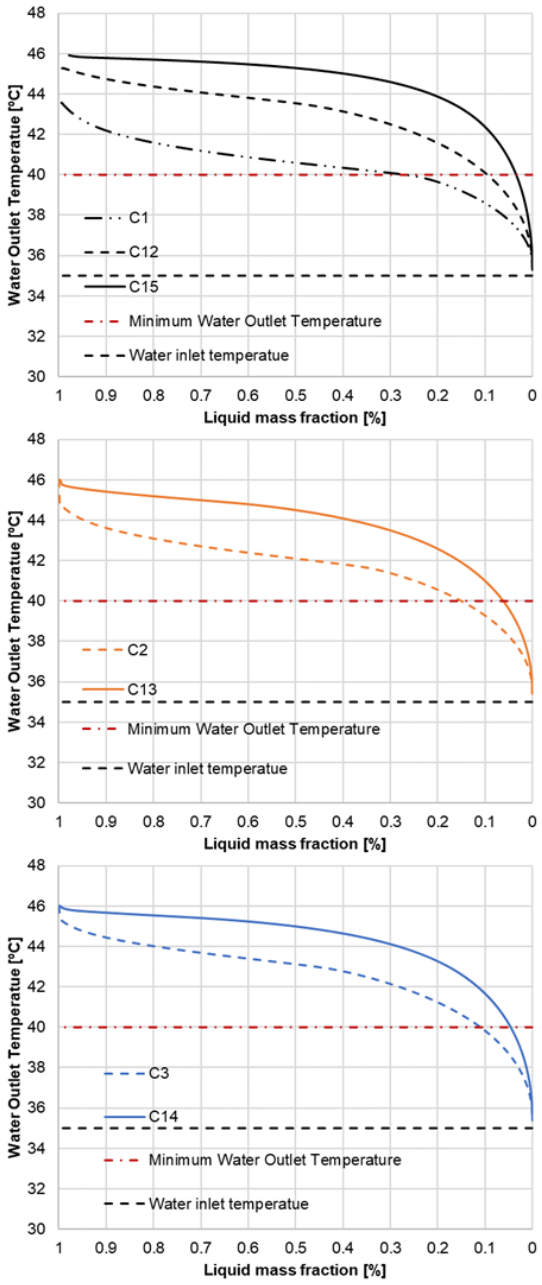

Figure 5.53: Heat transfer fluid discharge temperature vs liquid mass fraction per heat exchanger for each of the three simulated geometries with different flow rates (16.70, 11.20 and 8.36 l/min).

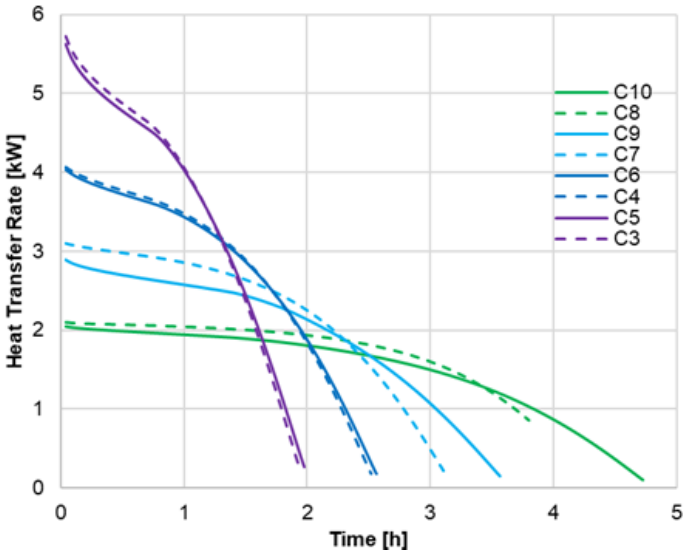

Figure 5.54: Heat transfer rate for Geometry 1 with different flow rates (8.36, 5.85, 4.18 and 2.79 l/min).

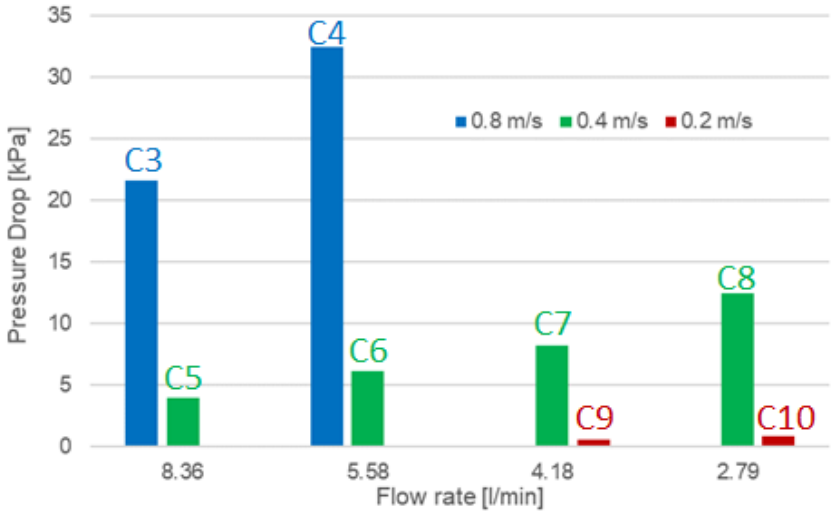

Figure 5.55: Pressure drop estimated for different flow rates (8.36, 5.85, 4.18 and 2.79 l/min).

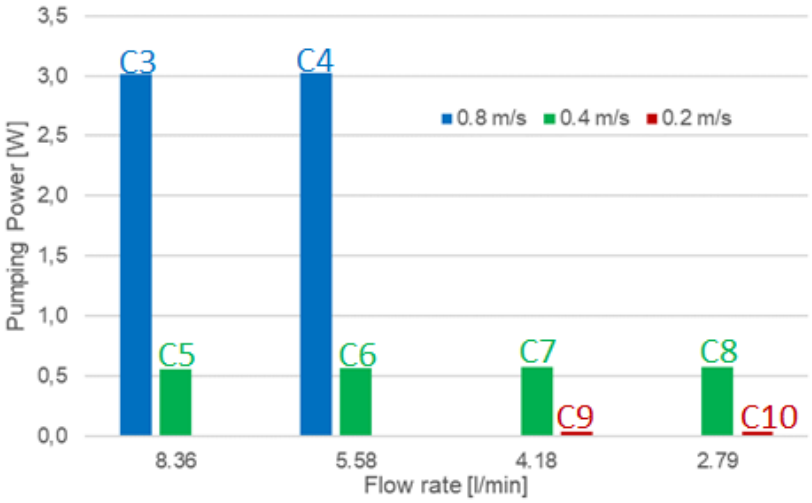

Figure 5.56: Pumping power loss estimated for different flow rates (8.36, 5.85, 4.18 and 2.79 l/min).

flow and so the shorter the individual circuit length is (meaning a higher total number of circuits) the smaller the pressure drop is.

5.3.9 Prototype Verification and Application

With the work developed so far, the prototypes were built to full-scale heat exchangers within a holding, storage tank (see Figures 5.57 and 5.58) and have undergone a series of experimental tests to be compared with a set of simulations with the CFD models, the following section shows the results of this comparison.

Figure 5.57: Heat exchanger full-scale prototype.(Photo courtesy of NKUA [122])

The design of the prototype heat exchanger was developed based on the previous chapther's results, showing that the main parameters that influence the heat transfer rate are the tube spacing (fin height) and the heat transfer fluid flow rate. The development considered these parameters but in order to avoid a customized design, the closest possible

Figure 5.58: Heat exchanger prototype holding tank (Photo courtesy of NKUA [122])

commercial standard solution was selected, aiming to avoid greater expenses by resorting to something already available on the market. The features comparison between the simulated CFD domain and the prototype are displayed in Table 5.17.

Table 5.17: Features for CFD domain and prototype.

CFD Domain	**Prototype**
Simulated domain – 6 m long pipe 2D axisymmetric mesh	Six single circuits 0.95 m, Total 5.7 m
Pipe Dint – 8.6mm; Dext – 10mm	Pipe Dint –7.94mm; Dext – 9.525mm
Domain diameter – 55mm (fin height 22.5mm/Square)	Diameter – 52.55mm (fin height 21.51mm/Staggered)
Fin thickness – 0.3mm	Fin thickness – 0.3mm
Fin pitch/spacing – 5mm (including fin thickness)	Fin pitch/spacing – 5mm (including fin thickness)
Total number of fins per length section – 200	Total number of fins per length section - 190
Simulated PCM – A44	PCM – A44

When comparing the results (Figures 5.59 to 5.64), it is possible to see some discrepancies with some being more significant than others. The numerical work was done following the 2D axisymmetric methodology that was previously established, for different geometries and operating conditions, based on the parallel experimental results. Note that all the results presented in this section, like before, display the values up until the end of the phase change process, be it discharge or charge. When comparing the results, it is possible

to see some differences, with some being more significant than others. It can be concluded that the heat transfer process is strongly influenced by flow rate of the heat transfer fluid and the total number of pipes within the tank. The heat transfer rate increases with the number of tubes and the heat transfer fluid flow. The numerical results also point out that for the same number of tubes, the heat transfer process is almost independent of the tubes arrangement. Concerning the pressure drop, the results showed that for the same flow rate the pressure drop is dependent on the heat transfer fluid velocity and consequently the shorter the circuit length is (implying higher circuit number) the smaller the pressure drop. However, the friction power loss is exclusively dependent on the heat transfer fluid velocity. It was also shown that increasing the fin density (reducing the fin pitch) increases the heat transfer rate for higher Reynolds numbers. The Reynolds number also seems to contribute to misalignment between the experimental and the numerical results, with emphasis on the simulations falling within the transition turbulence regime.

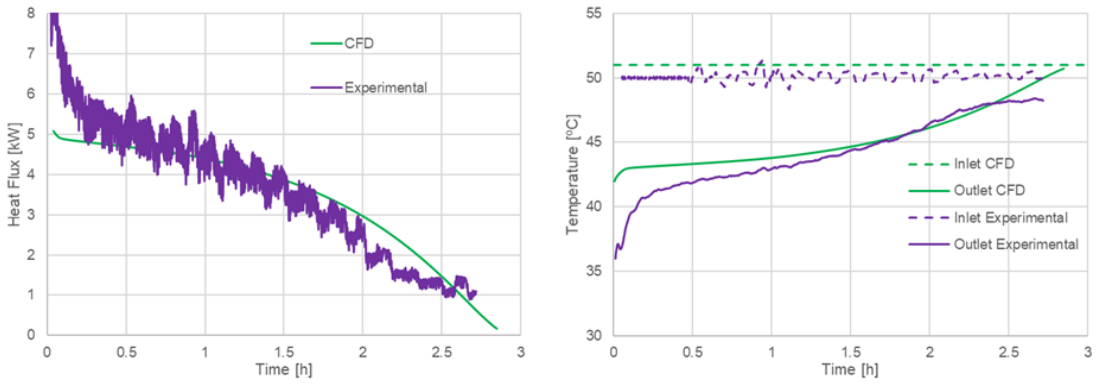

Figure 5.59: Comparison between CFD and experimental work for charging mode, flow rate 8.9 l/min, transition flow.

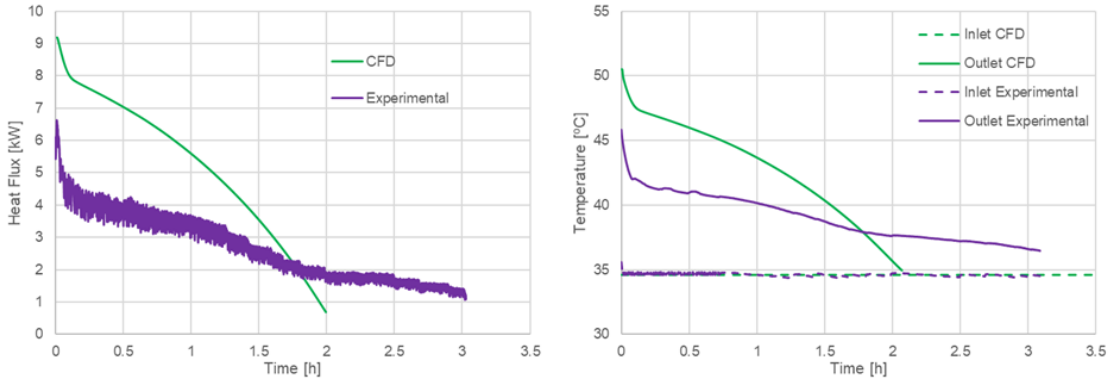

Figure 5.60: Comparison between CFD and experimental work for discharging mode, flow rate 8.9 l/min, transition flow.

The presented results cover distinct flow rate turbulent regimen (laminar-transition

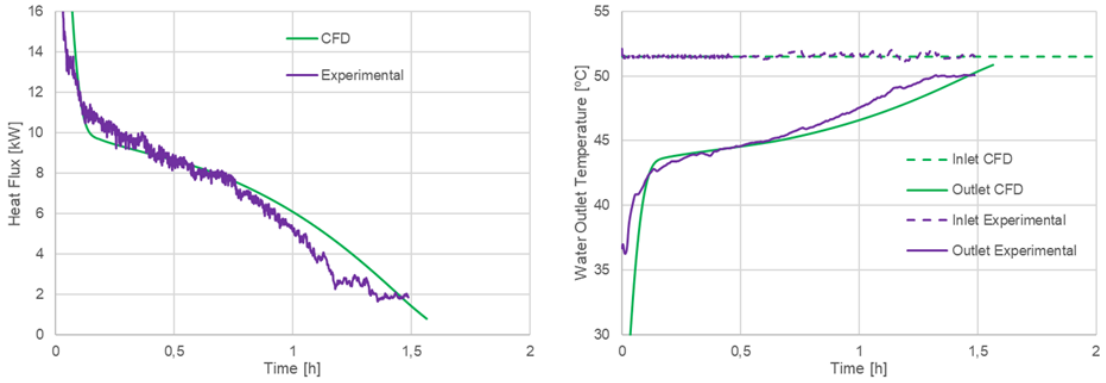

Figure 5.61: Comparison between CFD and experimental work for charging mode, flow rate 17.8 l/min, transition.

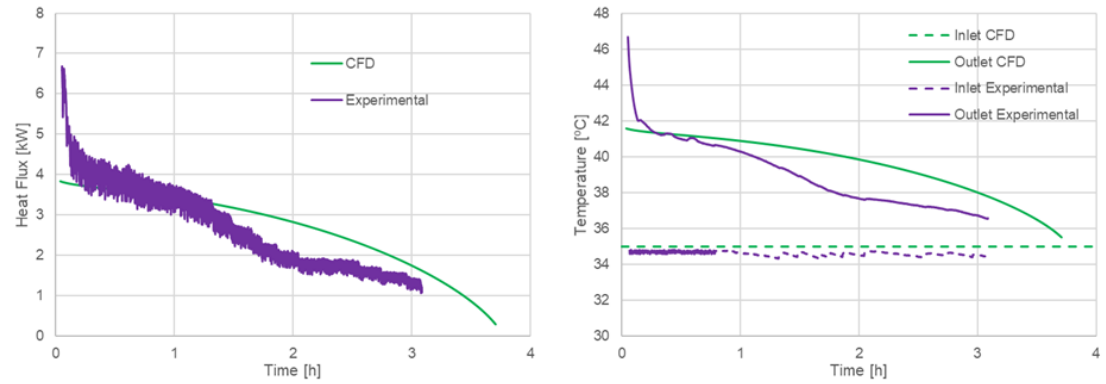

Figure 5.62: Comparison between CFD and experimental work for discharging mode, flow rate 8.3 l/min, laminar.

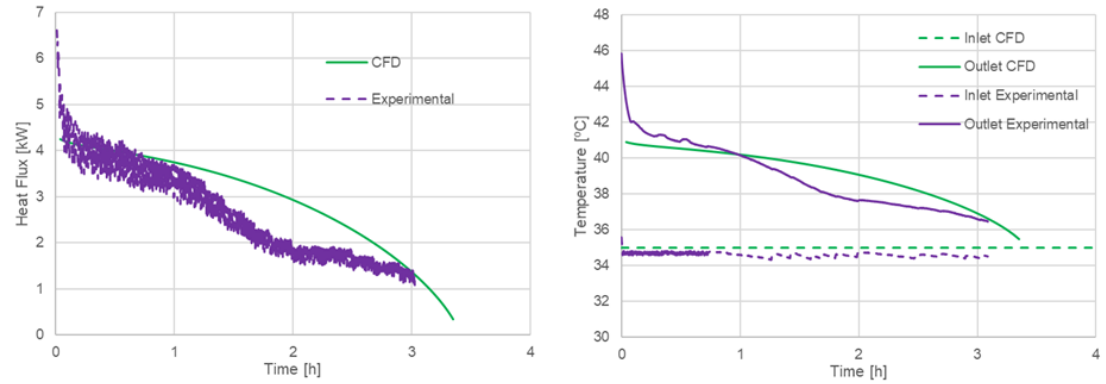

Figure 5.63: Comparison between CFD and experimental work for discharging mode, flow rate 10.3 l/min, laminar.

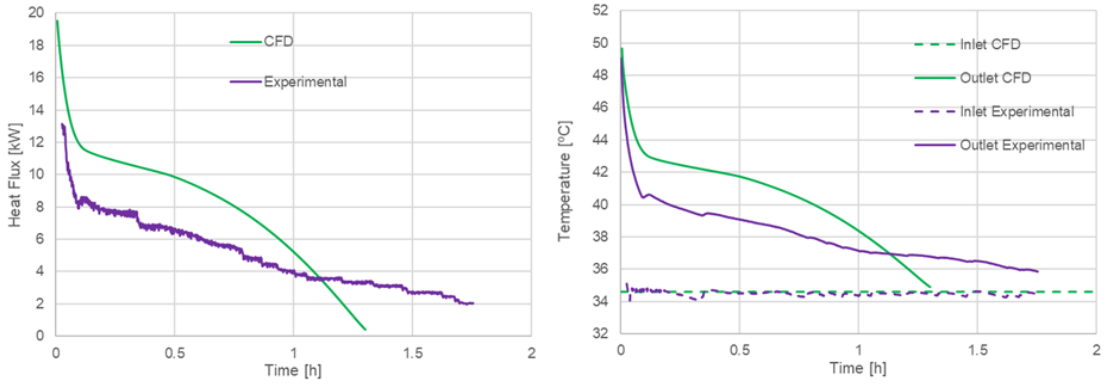

Figure 5.64: Comparison between CFD and experimental work for discharging mode, flow rate 20 l/min, transition.

and transition-turbulent regimes) due to the features of the demosites the shown values can both be used as there are a different number of PCM tanks, different climates, the heat pumps having different capacities, among other factors. Analysing these values, the expected behaviour seems to be, qualitatively at least, matching the CFD simulations. The flow rate bears a strong influence in the heat transfer rate over the phase change process. Judging from the Figures 5.60 and 5.64 it is possible to see that they have a poorer comparison between the experiments and the CFD, with significant mismatch between the curves. Possible reasons for these results could be related with process taking place in the transition regime and as such the results being detrimentally affected, another reason for this might be related with the specific batch of PCM own thermophysical features not being fully characterised resulting in a different behaviour in the experiments. Also, like mentioned in section 5.3.7, the prototype held some pockets of PCM mass (see Figure 5.44) that were not fully used as they were only present around voids near the bends of the heat exchanger, possibly causing variations in the logged experiment values that are not accounted for in the numerical work. On the other hand, Figures 5.59, 5.61, 5.62 and 5.63 seem to have much better matching values even though Figures 5.59, 5.62 and 5.63 having a slightly different inlet temperature. While there are conditions that can be considered not an adequate match it should be noted that the process is meant to be managed by a self-learning smart control system to achieve a greater benefit from the storage operation. Despite the simulations presented here being focused on the hot tank heat exchangers the same conclusions can be drawn for the cold and DHW tanks as the same process takes place, albeit at different temperatures.

Section General Conclusions:

The overall all comparison between experimental work versus CFD simulations show reasonable congruence with each other with some cases showing greater inconsistencies than others. The discrepancies can be explained by several considerations, one being explained by the fact that several cases were simulated within the turbulent transition and

such models are known to to be difficult to accurately modelled. Another reason is the PCM that is placed close to the heat exchangers circuit bends that has no fins and takes much longer to change phase skewing the real heat exchanger performance compared to the simulated model. One further reason is the PCMs' irregular, non-conforming, properties as well as experimental inherent inaccuracies.

5.3.10 Efficiency

In order to evaluate the overall performance to the heat exchanger behaviour, an effort was made to ascertain the efficiency of the heat exchanger. However due to the nature of the heat exchanging process there is not an actual constant temperature, as the phase change process progresses and the energy is depleted or replenished to the system, the temperatures involved vary over the time. As seen in Tay et al, the efficiency was estimated by dividing the temperature difference between inlet and outlet water temperatures by the maximum temperature difference possible to achieve within the system with the current temperatures, this difference is between the initial system temperature (initialisation temperature in the CFD work) and the water inlet temperature.[125] The values presented below in Figures 5.65 and 5.66 show an average value of the efficiency that fluctuates with the phase change, for these calculations the average water outlet temperature, inlet temperature and PCM average temperature were used, retrieved form the numerical work. The range of efficiency was calculated between 4.43 l/min and 33.50 l/min, covering simulations from laminar regime to full turbulent (see Table 5.18 and 5.19), as previously seen there is a heavy influence of the heat transfer fluid flow rate in the heat transfer process.

Table 5.18: Cases features for operating mode - Charge.

Case ID	Inlet Temperature [ºC]	Flow Rate [l/min]	Reynolds	Average Efficiency
D1	51	4.43	1540	0.63
D2	51	17.77	6110	0.74
D3	51	31.37	10700	0.60

Table 5.19: Cases features for operating mode - Discharge.

Case ID	Inlet Temperature [ºC]	Flow Rate [l/min]	Reynolds	Average Efficiency
D4	35	7.2	2200	0.55
D5	35	10.3	2800	0.46
D6	35	20.5	6700	0.81
D7	35	31.4	9800	0.70
D8	35	33.50	10800	0.67

Observing the results displayed in Figures 5.65 and 5.66, one can see three distinct trends for the process of charge and discharge in turbulent regime and for the discharge

in laminar regime. It is possible to see that as the flow rate increases, with in the same regime, efficiency starts to decrease with the same trending behaviour both for charge and for discharge. It can be gathered that, with a laminar flow, the heat transfer between the water and the heat exchanger is constrained by the heat transfer rate from the PCM to the heat transfer fluid. The average efficiency will decrease with the water flow rate because a greater flow rate does not make up for the increased convection, consequence of the increased Reynolds number. Looking at Figure 5.65 it is discernible that when the flow rate overtakes the laminar threshold, crossing over to the transition-turbulent regime, a significant increase in average effectiveness can be seen. This was caused by the increased convection, consequence of the turbulence induced by the new flow regime. While the high Reynolds number turbulence is important for the average efficiency for both modes of operation, Figure 5.66 shows that each mode as its own efficiency curves, with a higher average efficiency for the discharge process. As the turbulence increases the heat transfer rate between the stored PCM and the heat transfer fluid is not exclusively influenced by the convection of the water but also is dependent on the diffusivity with in the PCM-heat exchanger medium, resulting in efficiency decreasing despite increased flow rate, although this process is curbed in the laminar flows. The discrepancies between the different trends for the charge and discharge can be explained by the different thermal diffusivity between the liquid and solid phase of the PCM, further evidencing the relevance of the PCM diffusivity in turbulent flows.

Section General Conclusions:

The efficiency of the heat exchanger varies as the heat transfer progresses, and its dependant on the temperature and thermal conditions of the process taking place (charge and discharge) as well as the thermal diffusivity of the PCM in solid and liquid phases.

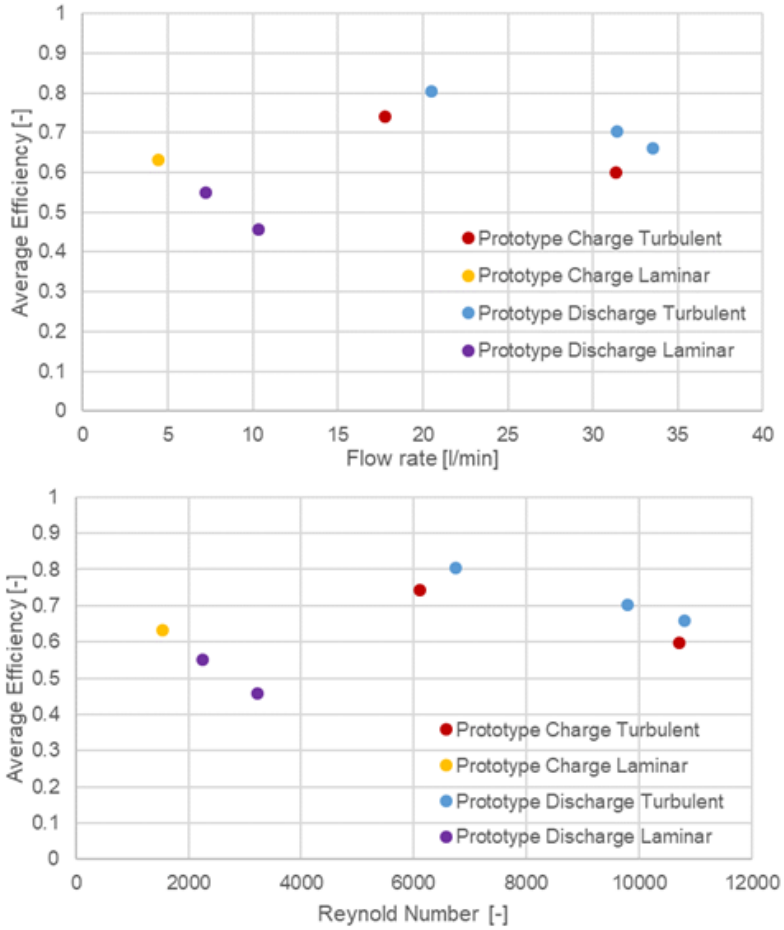

Figure 5.65: Average efficiency for flow rate and for Reynolds number for the different flow turbulence and operation modes.

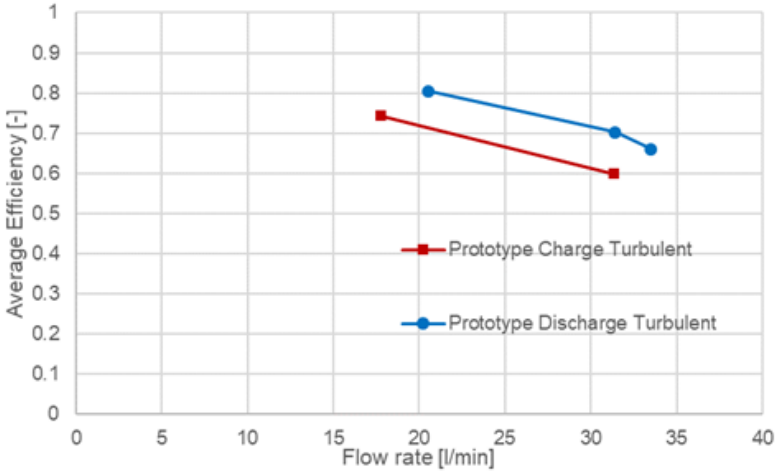

Figure 5.66: Average efficiency for turbulent flow rate for both operation modes.

5.4 Boreholes Heat Exchangers

5.4.1 Heat Exchanger Enhancement – 2D Geometric Study

This section will address the work that was developed for applications regarding PCM use in ground boreholes heat exchangers used in combination with ground-sourced heat pumps in order to increase the heat pump efficiency and decreasing the thermal inertia inherently consequent of the boreholes. The aim of these alterations is that (for the same amount of energy) either the boreholes could have a decreased length, thus decreasing the installation cost or if the boreholes were to have the same depth, they would also store more energy than a borehole with the same depth but with no PCM. In this section, there are two main stages of development. First stage is focused on 2D numerical work to verify the energy distribution in a borehole section, with and without PCMs, analysing its influence on how the borehole operates. The second stage progresses to a full 3D model of the boreholes with and without the PCM influence, operating with a ground-sourced heat pump, considering a regular on/off operated pump and inverter technology operation for the heat pump, checking if the inverter technology brings a greater saving comparatively with the on/off type. To this end, the PCM would be meant to be encapsulated, meaning it would be stored/encased within a solid medium of some kind. The considered means for encapsulating the PCM were: microencapsulated carbon powder, micro-encapsulated silica powder and micro-encapsulated hydrophobic silica powder.
While the original and ideal application of the PCM was to achieve an ideal homogenous mixture between it and the borehole filling back grout material (material akin to pourable concrete) Figure 5.67 Some simple and practical experiments revealed that when preparing the grout for injection in the boreholes (mixing the grout powder and water), the encapsulated PCM upon contact with water, would start to leech out of its encapsulation and segregating from the mix into the water (see Figure 5.68) not incorporating properly with the grout like in Figure 5.68 also rendering the mix a chunky, irregular compound with a lot of clumps.

The samples were poured into transparent beakers to assess how they settled over time as shown in Figure 5.69, the final total volume was disregarded as the same weight ratio between the grout and water was maintained in both batches. It was possible to see that while the regular mixture was set with a water excess, it dried soon within days of the pour. On the other hand the mixture with the encapsulated PCM not only it was difficult to pour, being chunky in texture and not fluid, it needed to be compacted forcibly and while it also had a layer of water on its top, there was also a thin film of PCM on top off it, akin to oil. In Figure 5.69 it is possible to see that while both samples had liquid layers after pouring in “A”, in “B”, where one month had elapsed, the PCM and water layer where still present as the PCM layer impeded the water underneath it to evaporate at the same rate as the regular sample. Both mixtures ended up hardening, however their mechanical properties were not tested nor were there such tests as it went beyond the scope

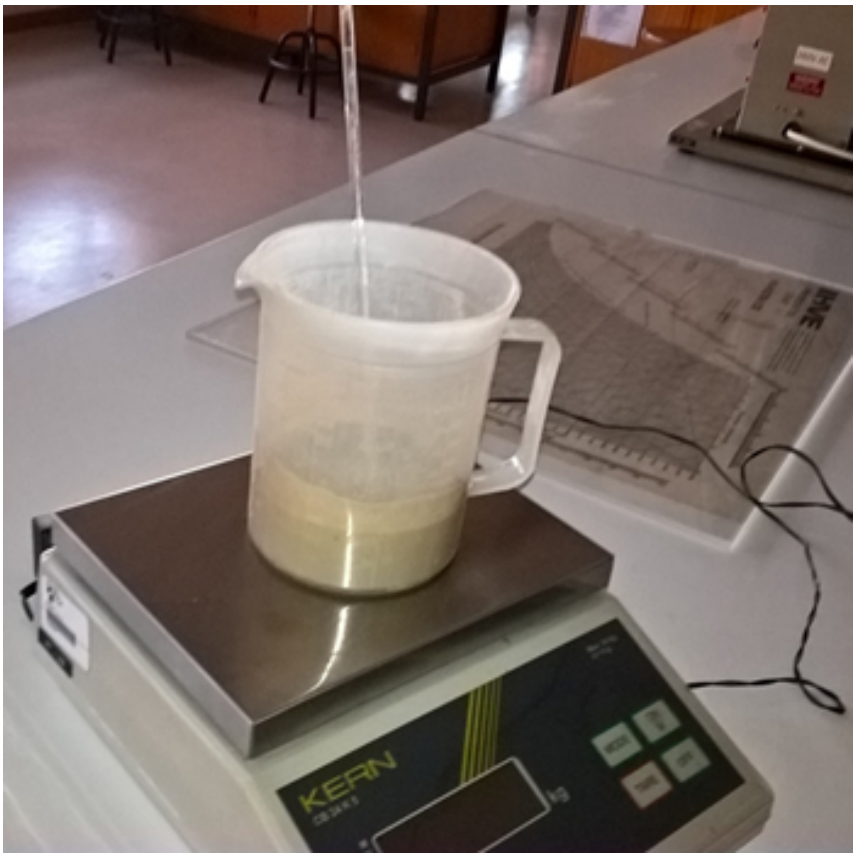

Figure 5.67: Mixed sample of regular grout material and water ready to pour.

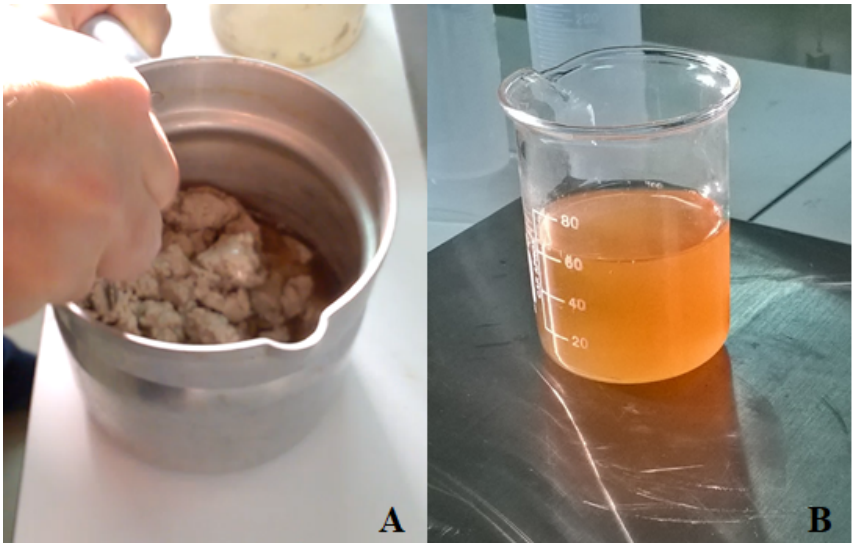

Figure 5.68: Sample taken from a mixture batch of grout material, water and microencapsulated PCM. Image A shows evidence of the heterogeneous mix unlike seen in Figure 5.67, with the PCM not staying within the designed encapsulation leeching into the water, as shown in B.

of this specific work. Despite the hardening, the PCM film was present for several months after the pour, this ultimately led to rejecting the direct addition of the microencapsulated PCM into the grout filling material as this posed a very significant danger of seeping into the soil surrounding the boreholes, tainting underground waters.

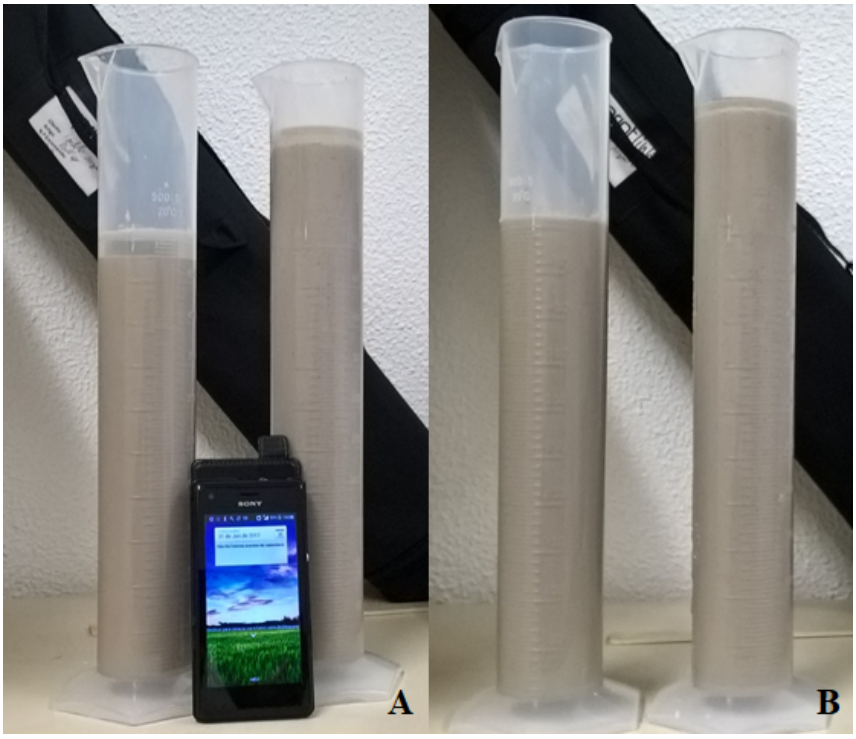

Figure 5.69: Image A showing the samples on the beakers on the pouring day (left regular grout and water mix – right grout, water and encapsulated PCM mix), both showing a liquid layer top of the mixture. B shows the samples after one month elapsed.

With this in mind, and considering project deadlines, in order to find a more adequate and timely solution, the work focus shifted to working with PCMs that were macroencapsulated. This encapsulation could come in various forms, but in an effort to simplify the process and decrease cost, the PCM was stored within the same type of pipes and/or material used for piping the water passing through the boreholes. In this effort, several geometries distributing the encapsulated PCM within the boreholes were designed and simulated to evaluate their behaviour. The geometries studied were modified versions of the most common typologies used in boreholes for geothermal applications, the coaxial design, single U design and double U design (See Figure 5.70). The modified geometries were made to add to the already defined features altering the base geometry to different degrees but trying to keep as most of the original features as possible, see Table 5.20, Figure 5.71 illustrates the different geometries.

With these geometries a series of simulations were run for a 72-hour period, this timeframe was chosen aiming to achieve a compromise between effective computational time and a reasonable time for the simulated domain (borehole and soil) to be affected by

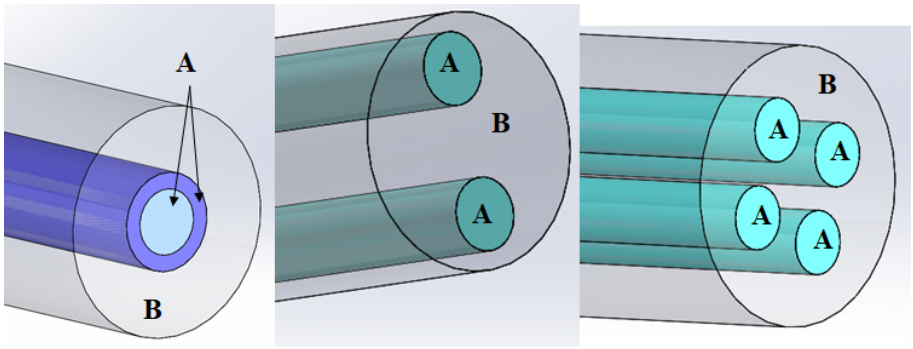

Figure 5.70: The three main boreholes typologies sections: Coaxial, Single U and Double U, respectively. A identifies the water circuit pipes, B identifies the fill back grout material, anything outside of its border is considered the surrounding soil.

Table 5.20: Cases geometry and features.

Case ID	Typology	Figurative Example	Description
E1	Coaxial	Fig.5.74 - E1	Modified coaxial typology. A – Water circuit. B – Grout material. C – PCM interior ring between the grout material and water pipes.
E2	Coaxial	Fig.5.74 - E1	Modified coaxial typology. A – Water circuit. B – PCM exterior ring between the grout material and soil. C – Grout material.
E3	Coaxial	Fig.5.74 - E3	Modified coaxial typology. A – Water circuit. B – Grout material. C – Sectioned PCM ring between the grout material and water pipes. D – High Density Polyethylene fins/separators.
E4	U	Fig.5.74 - E4	Modified single U typology. A – Water circuit. B – Grout material. C – PCM ring between the grout material and water pipes.
E5	U	Fig.5.74 - E5	Modified single U typology. A – Water circuit. B – Grout material. C – PCM cylinders within the grout material separating the water pipes.
E6	UU	Fig.5.74 - E6	Modified double U typology. A – Water circuit. B – Grout material. C – PCM cylinders distributed within the grout material in a cross disposition.

the heat provided by the heat pump. The aim here is to ascertain the energetic behaviour of these modified boreholes geometries and comparing the results. Since these simulations ran considering equal conditions in all cases (material properties are displayed in Table 5.21), varying only the geometry and distribution of the PCM in the boreholes, the boundary conditions for all cases were the same: constant heat pump water temperature input 42.5ºC on the water pipe wall and constant soil temperature 18ºC.

Analysing the plotted lines in Figure 5.72 it can be determined for the coaxial typology, the modification brought little benefit not surpassing in any of the cases the reference. Since in cases E1 and E2 the PCM formed an enclosing ring around the water pipes and in case E3 formed a segmented ring of PCM, the phase change of the material could be

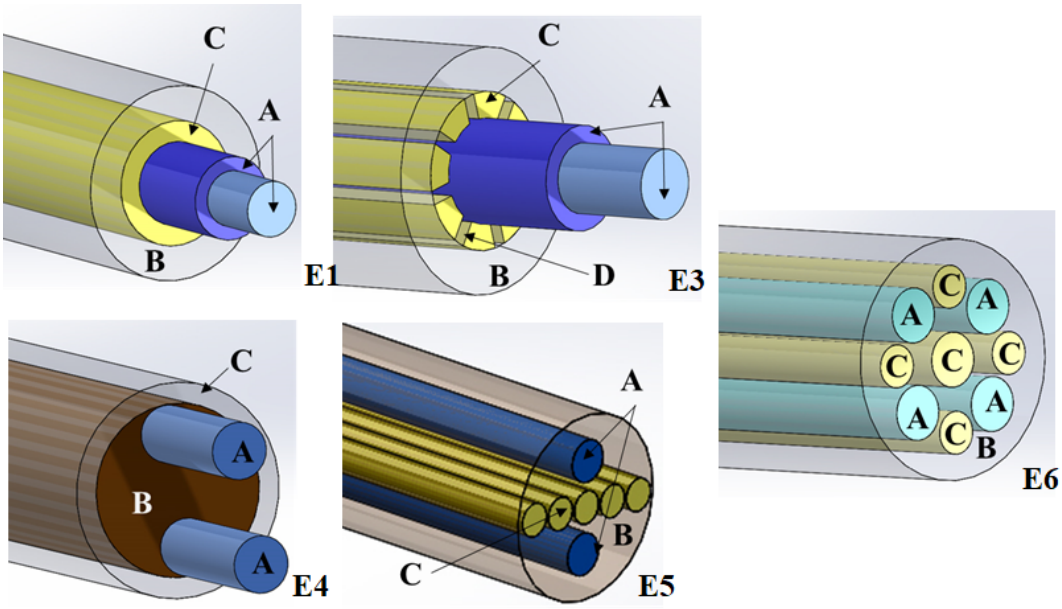

Figure 5.71: Figurative example of the typologies used.

Table 5.21: Materials properties.

Property	PCM	Grout Material	Soil	High Density - Polyethylene
ρ [kg/m^3]	889	2250	1400	950
Cp [J/kg.K]	2220	1250	1000	2000
k [W/m.k]	0.22	2.35	2.00	0.42
α [m^2/s]	1.12e-7	8.36e-7	1.14e-6	2.21e-7
ΔH_{sl} [J/kg]	162880	-	-	-
Solidus Temperature [ºC]	21	-	-	-
Liquidus Temperature [ºC]	21	-	-	-

acting as thermal damper, this combined with its low thermal conductivity can be limiting the actual amount of energy that is able to be injected into the surrounding domain.

Regarding the Single U typology, observing Figure 5.73, it can be determined that the modified configuration E4 had an initial gain in energy but after the 54-hour mark it started to hold less energy compared with the reference geometry, this could be consequence of the ring of PCM between the borehole and soil. This ring would initially insulate the borehole, keeping the energy within the grout material, increasing its temperature and by extension the temperature of the surrounding PCM as well, but since the PCM as greater heat transfer area, it started to lose energy to the soil. Geometry E5 had a very similar behaviour to the reference, being noteworthy to mention that effectively the geometry is very similar to the reference and as such the actual PCM absorbing heat from the source can be just one or the three (the centre cylinder and the two directly above and below it) closest to the centre of the borehole with the two remainder PCM cylinders being too far

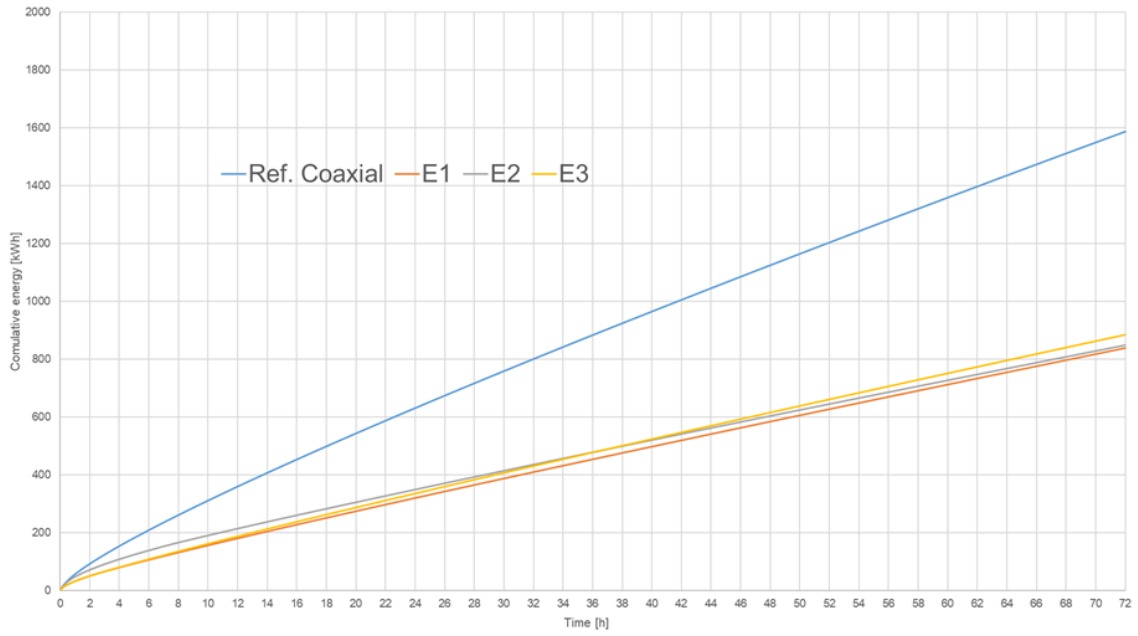

Figure 5.72: Coaxial geometries that were tested pitted against the reference geometry of the typology.

away for the heat to be conducted up to them in any significant manner.

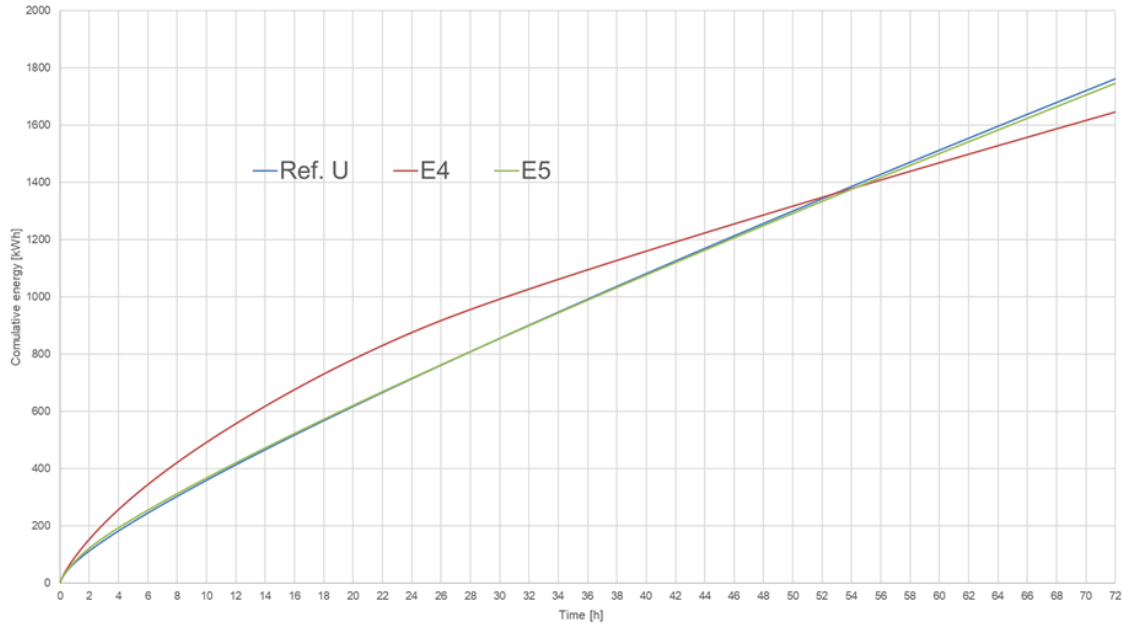

Figure 5.73: Single "U" geometries that were tested pitted against the reference geometry of the typology.

Concerning the Double U typology displayed in Figure 5.74 it is possible to see that the

configuration E6 as a better performance than the reference, showing the best prospective use. The PCM cross shaped disposition allows for a reasonable heat absorption while not completely isolating the boreholes from the surrounding soil.

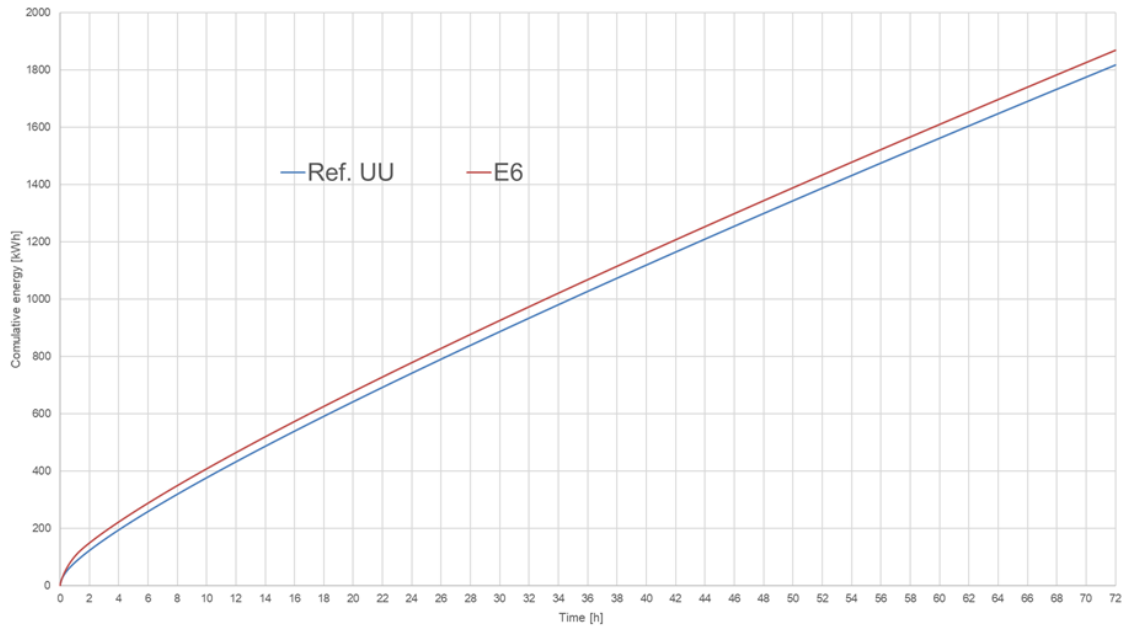

Figure 5.74: Double "U" geometries that were tested pitted against the reference geometry of the typology.

Despite some of the studied geometries having potential for the macroencapsulation of the PCM application in the boreholes, upon subsequent discussion with the involved partners it was decided that, considering that the geothermal boreholes being an already expensive technology using any kind of customized technique would significantly exacerbate its cost so, in an effort so simplify it was decided that the application would use a Double U configuration when only one water circuit would work, like a Single U, while the remaining circuit would be evacuated of the water and pumped full of the selected PCM for the demosite application.

Section General Conclusions:
Mixing micro-encapsulated PCMs with grout/water mix cause the PCM to separate from its encapsulation, diluting into the water, preventing the water to be as easily incorporated into the grout. This made for a chunky mix and not an ideal, flowing, runny mix. The leaked PCM could leech into local underground water tables. Macro-encapsulation studied, with complex and exotic dispositions and modifications of the PCM recipient, it was disregarded as it was an expensive solution with out any further modifications, any further alterations would further exacerbate the costs and complexity of the system.

5.4.2 Borehole 3D Simulation and Demosite Applications.

Following the results, conclusions and decisions made in the previous chapter a full 3D set of simulations was run with a cylindrical domain 4 meters in diameter and 90 meters deep to verify the performance of the geothermal boreholes using the PCM stored, comparing these results with a reference with no PCM. The simulations ran for a 24-hour period mimicking an on/off operating mode heat pump as well as an inverter operation heat pump with adaptable power adjustment. Another simulation using the inverter technology ran for a 48-hour period. The energy profiles for the 24 and 48 hour cycles were estimated based on the energy needs for a common family household from an energy simulation software (Design Builder), along with the COP of the heat pump, however these energy simulations are outside the scope of this work. The heating of the dwelling, in the 24 hour simulations, was considered to be completely provided by the geothermal heat pump. In the 48 hour cycle specifically, it contemplates a more complex heating system that integrates the geothermal heat pump, solar collectors and the thermal energy tanks sized previously in this work (hourly profiles in Figure 5.75). The considered simulation cases can be seen in Table 5.22, allowing to test out the influence of the a generic PCM that was selected, but in some cases with a different latent heat and phase change temperatures to verify how this specific characteristic would impact the objective of the work developed in this section.

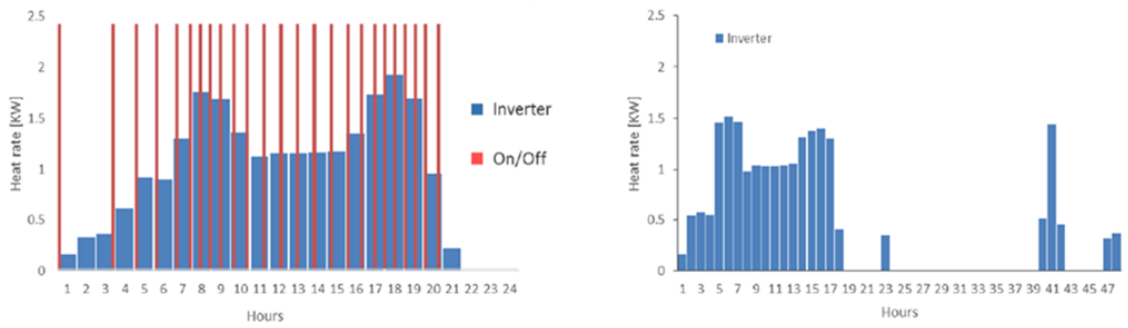

Figure 5.75: Energy demand profiles for 24 hours On/Off and 48 hours Inverter operation modes.

The results displayed in Figure 5.76 relates how the temperature typically is distributed in a borehole, the figure specifically shows a cross plane of the heat transfer fluid tubes for a 48 hour case but it illustrates how the general behaviour is affected by the operation mode. As a mean to measure the temperature evolution in the process, seven measuring points were created in the model registering the temperatures at three different depths at a relatively equal length of the 90 meters long borehole, at 15, 45 and 75 meters deep. Observing the results, it is possible to see that the heat transfer process has a fundamentally unidimensional linear behaviour, with the temperature gradients being effective in radial directions. On the other hand, for the heat transfer fluid and immediate adjacent regions,

Table 5.22: Cases features for operating mode - Discharge.

Case ID	Heat Pump Operation	PCM type	PCM Solidus Temperature [ºC]	PCM Liquidus Temperature [ºC]	PCM Latent Heat [kJ/kg]
F1	24h – On/Off	-	-	-	-
F2	24h - Inverter	-	-	-	-
F3	48h – Inverter	-	-	-	-
F4	24h – On/Off	PCM 1	15.5	16.5	200
F5	24h - Inverter	PCM 1	15.5	16.5	200
F6	48h – Inverter	PCM 1	15.5	16.5	200
F7	48h – Inverter	PCM 2	15.5	16.5	150
F8	48h – Inverter	PCM 3	15.5	16.5	250
F9	48h – Inverter	PCM 4	16.0	17.0	200

particularly in the borehole region, the temperature along the borehole axial direction can be seen to change, indicating that a 3D approach is a good tool to predict the heat transfer fluid temperature change over the operation cycle of the geothermal heat pump. It is to be noted that for the example on the figure how the temperature in the measured points is affected by the operation mode as it can be seen that the high and low peaks shown in Figure 5.76 follow the same behaviour of the operation cycle for 48 hours inverter mode in Figure 5.75.

The plotted lines displayed on Figure 5.77 show how the different operating modes and cycles affect the behaviour of the borehole. The figure shows graphics for the temperatures for the heat transfer fluid inlet and outlet, on the left column and for the PCM volume cylinders, on the right column. It is to be noted that, despite in these three cases (F1, F2 and F3) this volume being addressed as “PCM Average Temperature” it is actually filled with grout material, as these three cases have no PCM as seen in Table 5.22, the name here is misplaced but necessary to make it understandable that the very same volume would be changed and filled with PCM in cases F4 to F9 and that this would be same volume temperature studied, albeit with a distinct material. Comparing the results from F1 and F2 it is clear that while with the same time frame, the behaviour of the borehole is dissimilar, with case F1 on/off system having numerous and accentuated peaks and oscillations in the temperatures measured reaching low minimums but with case F2 the temperature has a much smoother evolution over time, with nearly no registered peaks, increasing the COP of the heat pump, despite operating on a partial load. The grout filled volume lines show the same qualitative behaviour as the work fluid, operating with in the same temperature range, with a less pronounced temperature drop at the 8 hour mark, unlike the on/off operation. Regarding case F3 the heat transfer fluid registers higher overall temperatures comparatively with F1 and F2 but still falling with in the same temperature range. These temperatures are important to select the PCM with the appropriate operation temperature to fill in the cylinders.

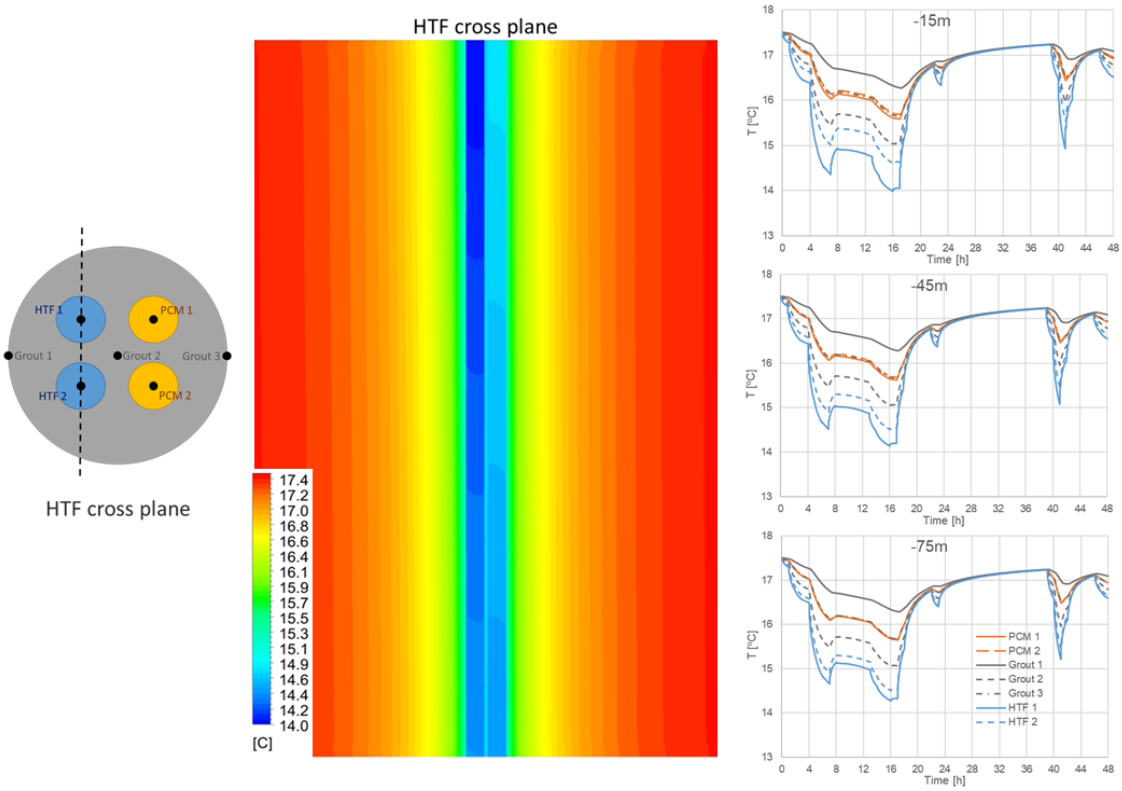

Figure 5.76: Temperature distribution of the borehole vertical section of the heat transfer fluid tubes with temperature results for 15, 45 and 75 meters deep in different points on the borehole.

Exhibited in Figure 5.78 for the cases F4, F5 and F6, are the inlet and outlet temperatures on the left column and the PCM volume average temperature along with the PCM liquid mass fraction showing how the phase change process progresses as well as the Solidus and Liquidus temperatures for the currently simulated PCM, that for the specific cases it is the same, PCM 1. The PCM temperature was selected based on the previously simulated cases. The results show that in all the cases F4 to F6, the PCM only partially changes phase, and while its stored energy is not completely used, it still allows for a stabilizing effect on the borehole. In spite of this, this effect as little impact on the overall temperature evolution of the inlet and outlet temperatures of the work fluid, being at almost the same temperatures as cases F1 to F3. Another related result is that despite the low effect it is proven that using the PCM in the boreholes brings a positive effect on thermal performance of the system. Further elaborating, it is possible to see that in all the three cases, when the system was not operating the PCM started to recharge from the surrounding soil, albeit not completely. In a system with thermal energy storage the time period possible for the geothermal heat pump to be shut down can be extended without disturbing the energy being delivered to the building. Therefore, the recovery time for the PCM can be extended when compared with a regular heating system with

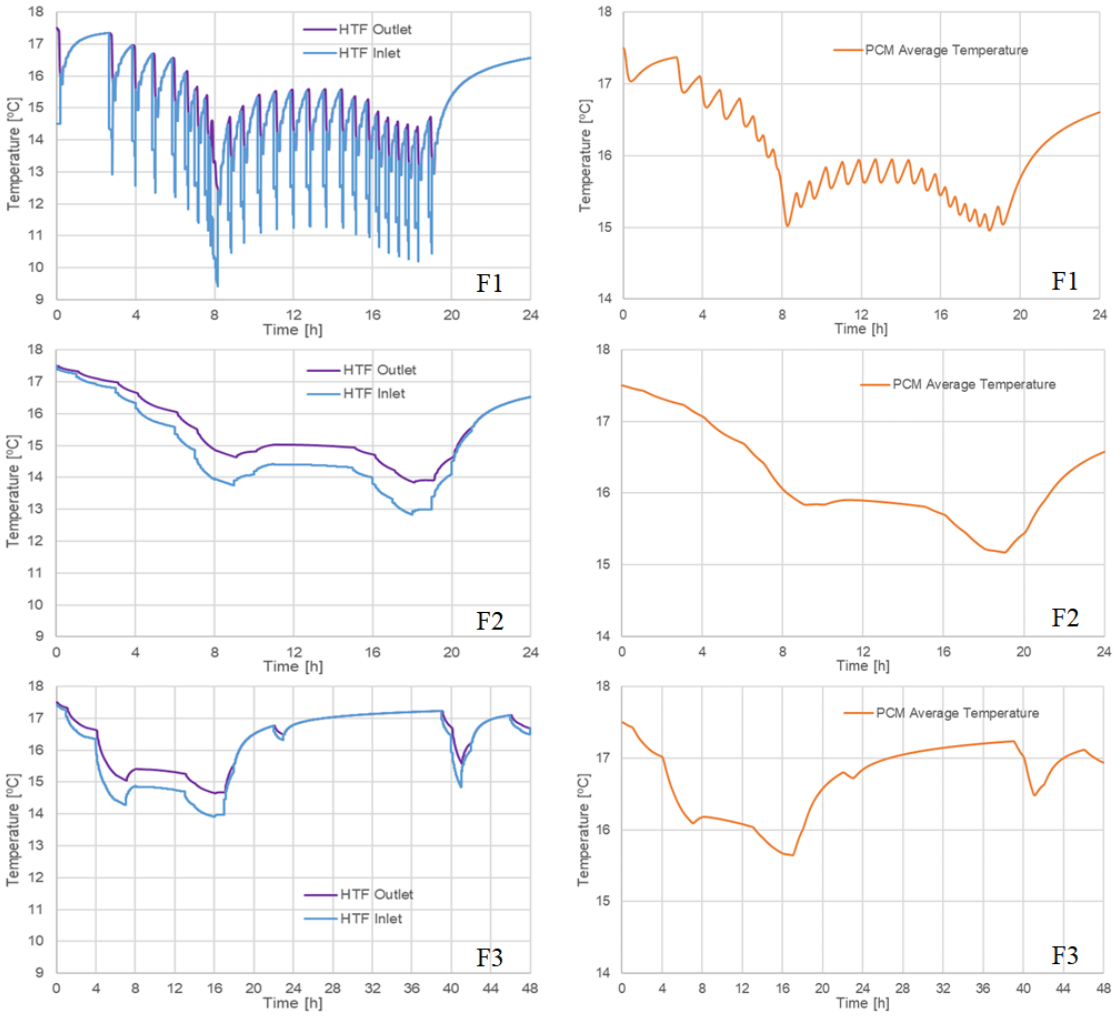

Figure 5.77: Inlet and outlet temperatures of the heat transfer fluid and temperature of the grout filled material that will be switched later to be filled with PCM for cases F1, F2 and F3.

no thermal storage. Another relevant conclusion that can be drawn from these simulated cases is that the inverter technology makes for a much smoother operation, keeping the PCM temperature from needlessly dropping too sharply, depleting its stored energy.

Figure 5.79 showcases for the simulations F7, F8 and F9, the inlet and outlet temperatures on the left column and the PCM volume average temperature along with the PCM liquid mass fraction showing how the phase change process progresses as well as the Solidus and Liquidus temperatures for the simulated PCM. For the specific cases, the PCM tested were PCM 2, 3 and 4. PCM 2 has the same Solidus and Liquidus temperatures as PCM 1 but considers a 25% lower latent heat capacity, 150kJ/kg. PCM 3 has the same Solidus and Liquidus temperatures as PCM 1 but considers a 25% higher latent heat capacity, 250kJ/kg. PCM 4, on the other hand, has the same latent heat as PCM, 200kJ/kg but the Solidus and Liquidus temperatures were risen 0.5ºC, becoming 16 and 17ºC respectively.

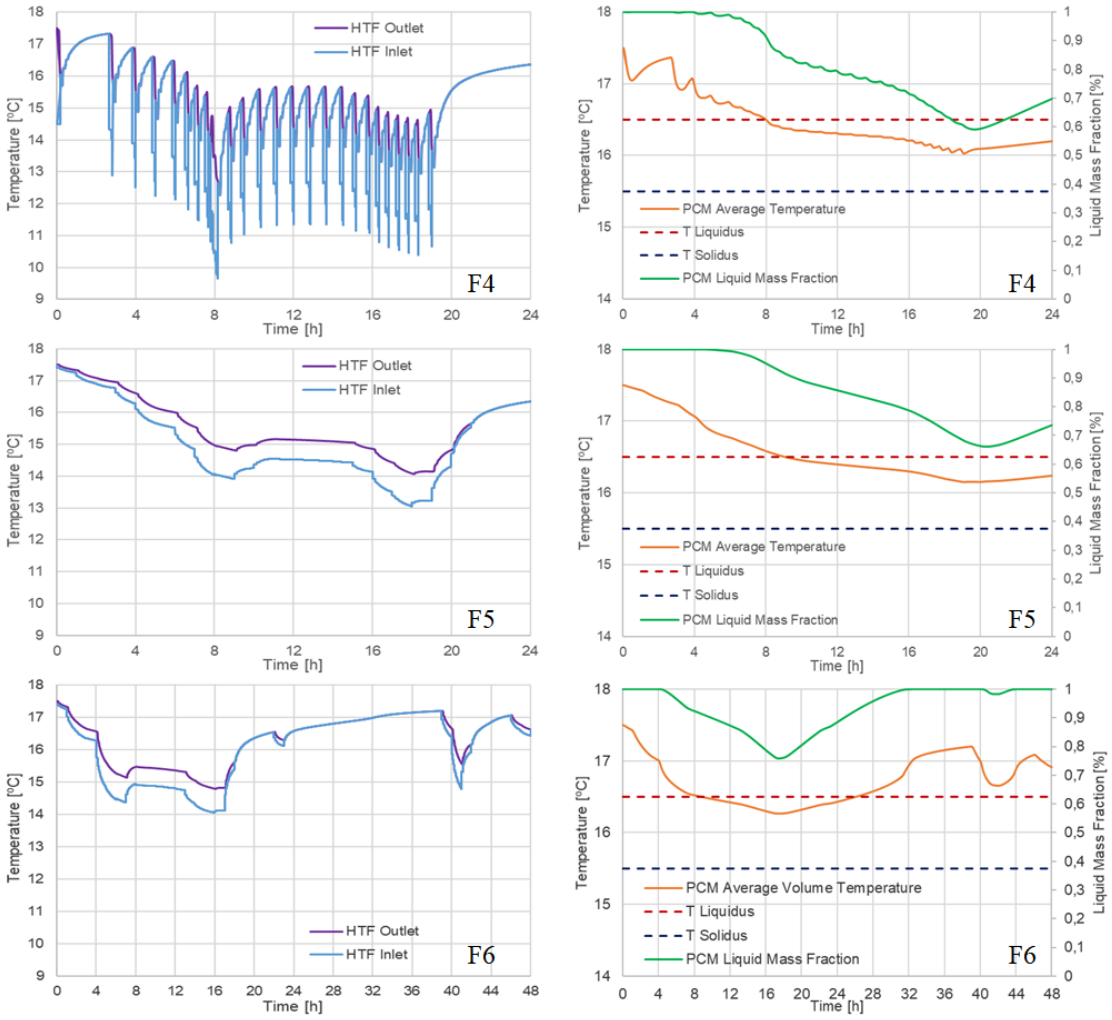

Figure 5.78: Inlet and outlet temperatures of the heat transfer fluid and PCM volume average temperature and liquid mass fraction for cases F4, F5 and F6.

Observing the results for F7 and F8 it is possible to see how the difference in latent heat, and as such the energy storage capacity influences the PCM behaviour with the mass fraction and average temperature shifting up or down when the latent heat increases or decreases respectively, with the case F7, that has lower latent heat, changes the PCM phase up to around to 70% while in F8, that has higher latent heat, only changes up to less than 80%. Nevertheless, these alterations do not seem to have a significative influence in the inlet and outlet temperatures, shifting the overall temperatures about 0.5ºC. Case F9, by shifting the PCM operational range temperature up half a degree obtained more noticeable results, both with concerning the PCM behaviour and energy extracted from it, as well as moving up the heat transfer fluid temperatures.

Figure 5.80 displays a comparison between cases F6, F7 and F8, comparing the effect of PCM 1, PCM 2 and PCM 3, that have the same operating temperatures for the phase change of the PCM but have a latent heat 25% below (F7) and 25% above (F8) PCM 1, to

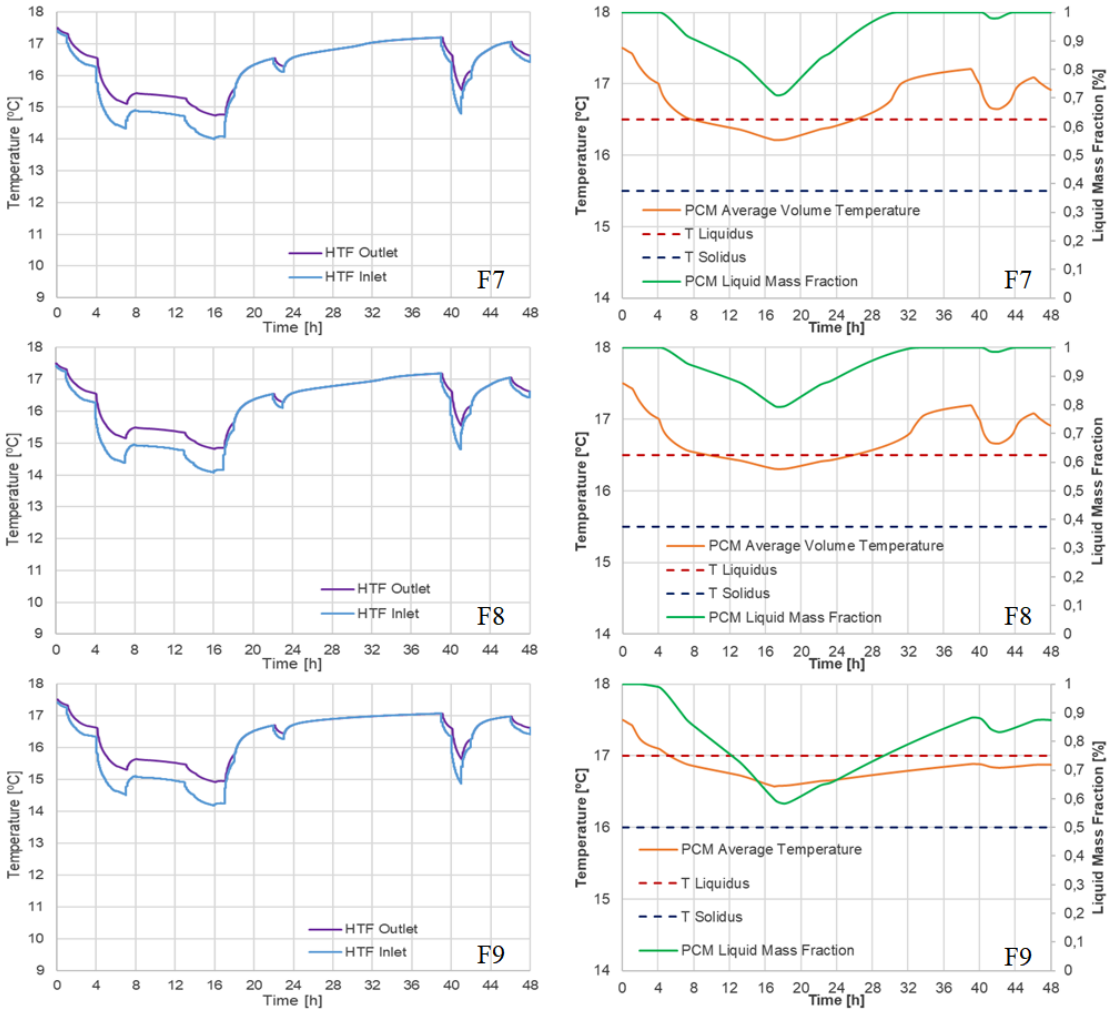

Figure 5.79: Inlet and outlet temperatures of the heat transfer fluid and PCM volume average temperature and liquid mass fraction for cases F7, F8 and F9.

ascertain what difference it has on the overall system. The results indicate that the latent heat has an effect on the PCM that solidifies during the heat pump operation cycle, but like seen on Figure 5.79 it has minimal impact on the overall temperatures of the heat transfer fluid temperatures along with the PCM average temperature. The solidified fraction of PCM is proportional to the latent heat increase or decrease, with the lowest liquid mass fraction reaching around 0.7 for case F7, that has the lowest latent heat. Overall, in the shown cases the PCM never completely solidifies when the heat pump is operating and the temperatures on display are minimally influenced.

In Figure 5.81 it is displayed a comparison between cases F6 and F9, comparing the influence of PCM 1 and PCM 4, that have the same latent heat but a different operating temperature range, being 0.5ºC higher in F9 than it is in F6. Studying the results, the increase in 0.5ºC for the PCM operation range (case F9) increases the mass of material that solidifies and the overall temperatures of the borehole stabilized at a higher temperature.

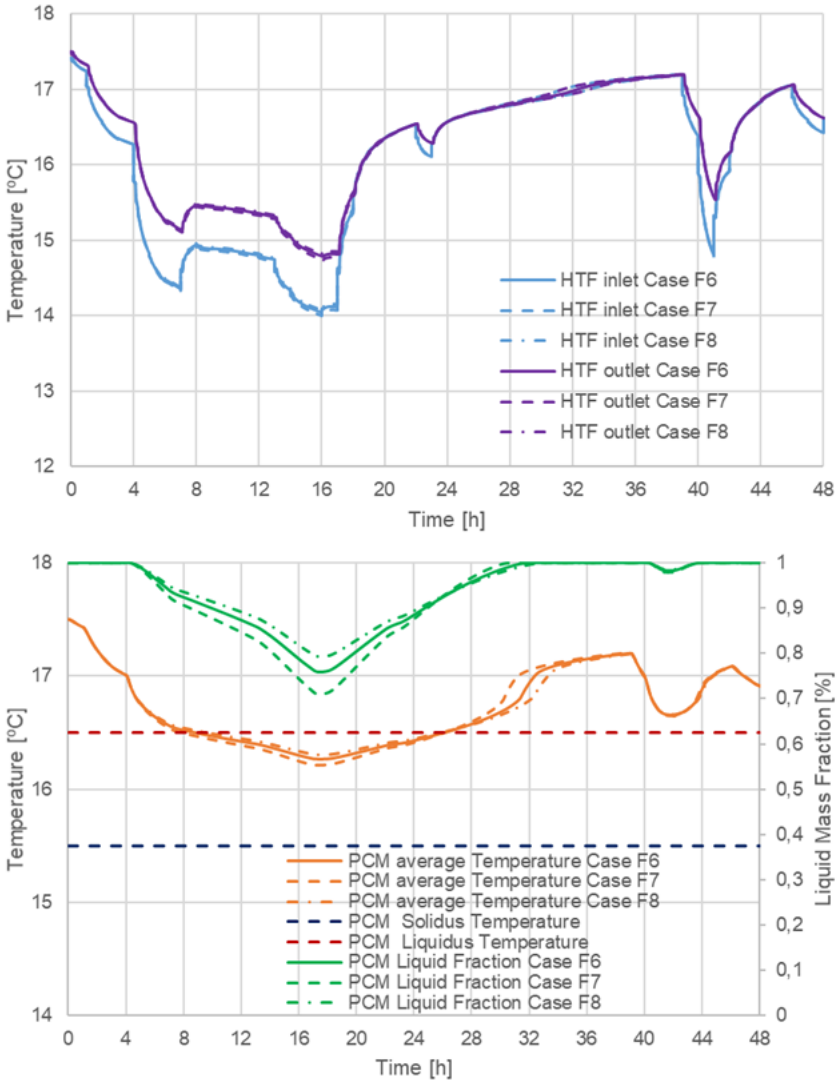

Figure 5.80: Comparison of the inlet and outlet temperatures of the heat transfer fluid and PCM volume average temperature and liquid mass fraction for cases F6, F7 and F8.

The inlet and outlet temperatures on the work fluid are higher, which translates to an increase in the geothermal heat pump performance as the temperature to be reached isn't as low as the in case F6. However, the results also show that in case F9, the PCM is not able to reach the initial condition (recharged from the surrounding soil), pointing out the drawback of increasing the material operating temperature range. Ideally the PCM should be able to be cyclically recharged by the soil, over each operating cycle.

Figure 5.82 showcases a simple comparison for cases F3 and F9, effectively comparing a 48 hour inverter heat pump operation cycle with no PCM in the borehole (F3) with a case that has the same operation cycle with PCM 4 (F9). Analysing the results displayed show the advantage of integrating PCM in a borehole heat exchanger, the PCM increases the inertia of the borehole, stabilizing its temperature when the geothermal heat pump is running. Generally, the temperatures registered for the heat transfer fluid are higher with

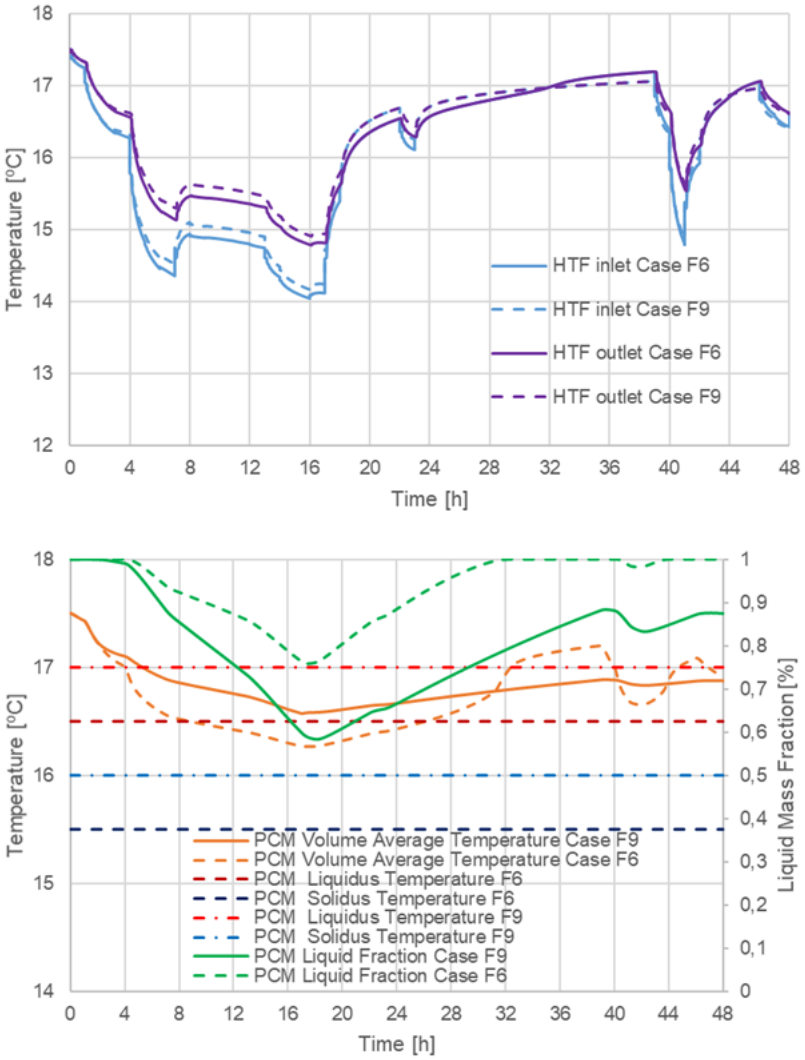

Figure 5.81: Comparison of the inlet and outlet temperatures of the heat transfer fluid and PCM volume average temperature and liquid mass fraction for cases F6 and F9.

PCM in place, this contributes for the heat pump having an improved energy performance when in operation.

Overall, it can be gathered from the results in this section that using the inverter technology smooths out the heat transfer fluid temperatures in the borehole, decreasing the fluctuations and peaks present in an on/off system, contributing for a more efficiently run geothermal heat pump. The PCM not only stabilizes the temperatures in the borehole but also at an higher baseline, allowing for a longer system operation without relying solely on the heat pump to heat the dwelling. The latent heat of the PCM influences the mass fraction that is solidified, with a proportional behaviour between the mass that changes phase and the latent heat capacity. Furthermore, a higher PCM temperature operation range helps stabilizing the temperatures at a higher baseline, but this incurs a drawback that prevents the material to fully recover in the heat pump down time. While

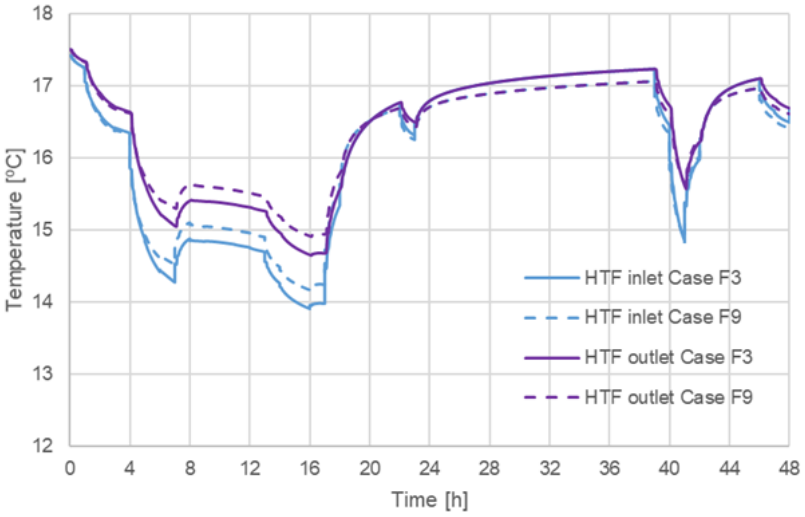

Figure 5.82: Comparison of the inlet and outlet temperatures of the heat transfer fluid for cases F3 and F9.

it underperformed for the studied parameters, it is clear that the PCM application in the borehole provides a stabilization action of the temperatures registered, with a strong influence of the its temperature operational range, this improves the energy performance of the heat pump and thus of all the system. Concerning the usage of alternative PCM encapsulations (micro and nano-encapsulations) for mixing with grout material, it would seem that at its the current state, this solution is not fully ready for implementation. However, the potential use for this application poses an attractive prospect as it has a simple implementation method and can provide a great benefit to the operating heating and/or cooling systems that relies on it, provided that is well design for the purpose and soil conditions, so further work should be carried out to develop this technology for implementation in a future solution. The macro-encapsulation choice of using the Double U typology adapted to have only one circuit with heat transfer fluid and the other with the PCM was used here as this is a typology widely used and has the lowest risk for its cost effectiveness. The work results of this particular section show good agreement with recent literature conclusions.[126]

Section General Conclusions:

Overall the concept being studied showed that the suggested modifications worked in the sense that is stabilised the soil temperature and did store some thermal energy, however it underperformed requiring significant further developments.

6

Conclusions and Future Developments

The objective for the work developed in the theme of this thesis was to develop a functional latent heat based thermal storage system. The study used a CFD tool to develop two distinct applications: (i) heat exchangers part of a thermal storage tank that would hold PCMs at a specific temperature needed for heating, cooling and supply of domestic hot water to a dwelling. (ii) heat exchangers meant to be applied within geothermal boreholes in combination with encapsulated PCMs.

The storage tanks heat exchangers parameterization was studied in chapter 5.3. Given the non-existing technical precedent, the parametric study stared of with a very general evaluation of geometric features influence such as tubing length and fin characteristics. It progressed then to heat exchanger materials and heat transfer fluid parameters such as velocity/flow rate, and considering operation modes of the system, charging and discharging the tanks, especially concerning the discharge as this would be the mode that would be responsible for supplying the dwelling with the thermal conditions from each of the tanks. The established parameters from the CFD studies led to the manufacture of a pre-prototype that went on to be experimentally tested with reasonable results that indicated that the numerical model gave a good approximation of the physical processes taking place. With the successful pre-prototype testing successful, a full-scale prototype for demosite installation was built and these were simulated testing parameters such as flow rate and heat exchanger circuitry, pressure drop and overall efficiency. As it was presented, several parameters were evaluated, the selection of such features came from preconceptions and expectations such as regular domestic applications for heating, cooling and domestic hot water usage, in an effort to easily retrofit in existing buildings. Other considerations that came into play were the heat pumps operative features and heat exchangers circuit length and circuit number, as well as operational temperatures both for the geothermal heat pump, the selected PCMs and indoor conditions. The displayed parameters were therefore shown because they presented a good expectation for the operational range for the heat exchangers combined with the system.

Other inferences regarding the PCM behavior in the tank heat exchanger are that when it starts taking place, the discharge (or solidification) creates a solid layer of material between the pipe/fins and the still liquid PCM that hinders the convective exchange making the heat transfer process happen mostly through conduction, that is dependent on the thermal conductivity of the PCM which is considered low, decreasing the heat transfer rate, thus increasing the time for the process. This was minimized with the usage of the finned tubes for the heat exchanger build, resulting in the greater limitation laying on the waterflow side and its turbulence regime. On the other hand, the charge process (or melting) has the tendency to be slightly faster than it was simulated due to minuscule convective currents that might take place but this effect is mitigated due to the close packing of the fins and, in the specific applications of the charge process, it uses a generally higher temperature difference than the discharge process does.
Further deductions for the tanks heat exchangers regarding the experimental versus numerical work deviations can be credited to several reasons, such as any experimental imprecisions like having slightly different temperatures and heat rates. Another cause for deviation is effective operative PCM properties between what it was considered to be (from the manufacturer available information) and what actually is when in effective experimental use, as it was found there can be some discrepancies between the manufacturers values used in the simulations and the actual material properties. Additionally, because of the way the prototypes were built they house PCM that is not directly surrounding fins, this superfluous material was not considered when the numerical simulations were run, throwing off the measurements, contributing its share for the discrepancies between experiments and simulations.
Effectively the application developed allowed for storing and shifting the energy needs of a dwelling from the time that renewable energy is available and cheaper, but demand is low, to a more convenient time when availability is low, but demand and cost are high. The energy is stored in a form of a temperature level in the tanks where the PCMs and heat exchangers studied in this section are housed.
An additional noteworthy mention; while it was originally considered for the these applications to also use solutions with hydrated salts and some work was done on this front, they were eventually discarded at the point when the first geometry parameters were still being studied and the work effort for the organic PCMs that was presented here was far greater than what was developed for the hydrated salts. The reasons for being rejected were that despite being cheaper and, generally, having better thermal properties than the organic PCMs, the overall disadvantages far outpaced their worth for the work developed. The hydrated salts, as the name implies, are a combination of salts (solid) mixed with a portion of water in the liquid state. When releasing and absorbing heat a phase separation could take place, this would require an expensive and complicated modification for the heat exchanger, this phase separation could also lead to an undesired supercooling effect on the material of about 2 to 4ºC, shifting the material operational range. Another issue with the salts is that they are highly corrosive for metals and would eventually damage/destroy

the heat exchanger as well as its holding tank. A protective coating solution was developed successfully at a small scale that would not hinder the heat exchanging between the heat exchanger and the PCM (this was done outside of the scope of this thesis), however the equipment needed to bring this technology to full workable scale was prohibitively expensive to build and develop with the available funds so, for the time being it was dropped.

Chapter 5.4 studied the approach to develop heat exchangers meant to be combined with geothermal boreholes. The original intent of the project was to combine nano or micro-encapsulated PCMs with the boreholes fill back grout material. Upon experimental testing it was verified that not only the encapsulated PCM did not mix homogenously with the grout material and water for filling the borehole but it also leached out, when in contact with water and as such it was not feasible to apply it to boreholes for fear of phreatic water lines being tainted, moreover it took longer than the original mix for it to completely solidify. Because of this, nano and micro-encapsulation were discarded from the original application and the focus shifted then to finding a solution using macro-encapsulation. In this effort several geometric concepts were designed and tested with varying degrees of success. However, given the relatively expensive technology that is geothermal borehole drilling and installation, a simpler approach was ultimately preferred for a prototypical installation, using only a regular Double U typology for boreholes where one of the two water circuits was filled with PCM. Overall this simple approach yielded positive but underperforming results, still, it allowed for the systemsof geothermal heat pump to have a higher efficiency than it would otherwise have.
These applications in tandem with renewable energy sources and combined with a self-learning, smart control system that manages the system with inputs such as user/occupation profiles and schedules, climate screening and forecasting and indoor setpoints make for a thermal supply needs system that can save between 15 and 30% energy annually. With versatility to be installed in a new building or to be retrofitted in an existing structure using common terminal indoor units. This translates to an increase in energy efficiency and share of renewable energy sources share in the energy mix and making the energy grid more flexible and decreasing the energy tariffs. All in all, this work showed that a good numerical method for these applications was developed and could be used for further progress. It is also important to emphasize the relevance of the control system, that while completely outside of the scope of this work, as it is responsible to combine the complex behaviors of the availabilities and needs of the dwelling thermal energy uses, coordinating an array of numerous input and output variables in the thermal system, without which the good performance of the system cannot be guaranteed.
Steps for future developments can be, for instance optimizing some features of the system or further developing concepts and applications that were partially developed but not fully applied or grown into fully workable solutions. One such improvement is the increase of thermal conductivity of PCMs through means other than exclusively “area based” heat

exchangers that increase the surface area of contact for the heat transfer between media, to that end, for instance, using nanoparticles that can be mixed and used without restrictions or limitations with the PCMs in their storage tanks that would improve their thermal qualities with minimal loss of latent heat capacity and consequent thermal storage capacity. Another development for the tank heat exchanger would be to effectively develop an equipment capable of coating a full-sized metal heat exchanger, with a protective layer, in a way that would help make it possible for the solution with hydrated salts to become viable once more and given that the Hydrated salts are less expensive than organics make the setup have a more competitive price/implementation.

An additional progress in the PCM encapsulation technology would be improving it, reducing the possibility of encapsulation content leaching, preferably removing altogether, and reducing its manufacturing costs, to allow for more easily applying the materials in cases such as the geothermal boreholes as this would not only increase the overall thermal storage capacity of the system but allow for the boreholes to effectively be less deep, as their heat bearing capacity would be increased with the PCM addition, thus decreasing the installation cost of this expensive technology, additionally contributing to increasing the geothermal heat pump thermal efficiency, by working at less extreme temperatures and with fewer fluctuations, smoothing out the pumps operation.

Other improvement that could be put into place using PCM in boreholes, would be using the general method presented in this work, but macroencapsulating the material in significantly larger tubes. This however, could further increase the boreholes installation costs and be dependent on drilling technology development but further numerical work is needed to effectively verify if it is worthwhile.

These developments and considerations rely on PCM manufacturers to not only improving the technology behind some of their applications but more importantly to make PCM undergo homogenous, standardized production and verification norms to ensure that not only all batches of PCMs bear the same thermo-physical properties consistently, but also have verified properties that actually match the manufactures claims. As it was seen throughout the work in the thesis and can be read in subject literature that these properties not always have or behave as stated by the manufacturers and that can have a detrimental impact on the behavior of the system dependent on PCM and in numerical models results based of off them. These features alone could increase the systems performance as they would allow for better simulation models to be developed, being more accurate predicting the behavior for such systems with these materials. Overall, the solutions developed throughout this work show the versatility and multi-applicability of PCMs, in areas as diverse as construction/buildings thermal process and agricultural processes, that have attractive features and a great potential for thermal energy storage and respective applications and, when combined with a CFD tool, provide a valuable instrument in the development of new energy efficient systems.

Bibliography

[1] C. Europeia. *Comunicação da Comissão ao Parlamento Europeu, Ao Concelho, Ao Comité Económico e Social Europeu e ao Comité das Regiões*. Tech. rep. introducao. COMISSÃO EUROPEIA, 2011 (cit. on p. 1).

[2] P. EUROPEU. *DIRECTIVA 2010/31/UE do Parlamento Europeu relativa ao desempenho energético dos edifícios*. Tech. rep. introducao. Jornal Oficial da União Europeia, 2010 (cit. on p. 3).

[3] P. Torcellini et al. *Zero Energy Buildings: A Critical Look at the Definition*. Conference Paper 550-39833, 2006 (cit. on p. 3).

[4] L. M. Bal, S. Satya, and S. Naik. "Solar dryer with thermal energy storage systems for drying agricultural food products: A review". In: *Renewable and Sustainable Energy Reviews* 14 (2010). chp2.1, pp. 2298–2314 (cit. on p. 9).

[5] A. de Gracia and L. Cabeza. "Phase change materials and thermal energy storage for buildings". In: *Energy and Buildings* (2015). chp2.1 (cit. on p. 11).

[6] A. Caron-Soupart et al. "Performance analysis of thermal energy storage systems using phase change material". In: *Applied Thermal Engineering* 98 (2016). chp2.2, pp. 1286–1296 (cit. on p. 12).

[7] A. A. R. Darzia, M. Jourabian, and M. Farhadic. "Melting and solidification of PCM enhanced by radial conductive fins and nanoparticles in cylindrical annulus". In: *Energy Conversion and Management* 118 (2016). chp2.2, pp. 253–263 (cit. on p. 13).

[8] M. Torlak, A. Teskeredžić, and N. Delalić. "MODELING AND SIMULATION OF HEAT STORAGE IN PHASE-CHANGE MATERIALS BASED ON COMPUTATIONAL FLUID DYNAMICS". In: *Trends in the Development of Machinery and Associated Technology*. chp2.2. 2013 (cit. on p. 14).

[9] M. Medrano et al. "Experimental evaluation of commercial heat exchangers for use as PCMthermal storage systems". In: *Applied Energy* 86 (2009). chp2.2, pp. 2047–2055 (cit. on p. 14).

[10] M. Longeon et al. “Experimental and numerical study of annular PCM storage in the presence of natural convection”. In: *Applied Energy* 112 (2013). chp2.2, pp. 175–184 (cit. on pp. 15, 78–80).

[11] J. N. Chiu and V. Martin. “Submerged finned heat exchanger latent heat storage design and its experimental verification”. In: *Applied Energy* 93 (2012). chp2.2, pp. 507–516 (cit. on p. 16).

[12] A. Castell et al. “Maximisation of heat transfer in a coil in tank PCM cold storage system”. In: *Applied Energy* 88.11 (2011). chp2.2, pp. 4120–4127 (cit. on p. 16).

[13] M. O. et al. “Numerical study for enhancing the thermal conductivity of phase change material (PCM) storage using high thermal conductivity porous matrix”. In: *Energy Conversion and Management* 46.6 (2005). chp2.2, pp. 847–867 (cit. on p. 16).

[14] M. N. A. Hawlader, M. S. Uddin, and H. J. Zhu. “Encapsulated phase change materials for thermal energy storage: Experiments and simulation”. In: *International Journal of Energy Research* 26.2 (2002). chp2.2, pp. 159–171 (cit. on p. 17).

[15] R. Baetens et al. “Gas-filled panels for building applications: A state-of-the-art review”. In: *Energy and Buildings* 42.11 (2010). chp2.3, pp. 1969–1975 (cit. on pp. 17, 18).

[16] T. Whiffen and S. Riffat. “A review of PCM technology for thermal energy storage in the built environment: Part I”. In: *International Journal of Low-Carbon Technologies* 8.3 (2013). chp2.3, pp. 147–158 (cit. on pp. 17, 21).

[17] I. Dincer and M. A. Rosen. *Thermal Energy Storage: Systems and Applications 2nd Edition*. chp2.3. Wiley and Sons, 2011 (cit. on p. 17).

[18] M. Ltd. *Monodraught Cool-Phase Mark 2 Brochure*. chp2.3. High Wycombe, 2011 (cit. on p. 17).

[19] A. Sharma et al. “Review on thermal energy storage with phase change materials and applications”. In: *Renewable and Sustainable Energy Reviews* 13.2 (2009). chp2.3, pp. 318–345 (cit. on pp. 17, 23).

[20] B. P. Jelle, C. Breivik, and H. D. Rokenes. “Building integrated photovoltaic products: A state-of-the-art review and future research opportunities”. In: *Solar Energy Materials and Solar Cells* 100 (2012). chp2.3, pp. 69–96 (cit. on p. 17).

[21] B. P. Jelle and C. Breivik. “State-of-the-art Building Integrated Photovoltaics”. In: *Energy Procedia* 20 (2012). chp2.3, pp. 68–77 (cit. on pp. 17, 24).

[22] B. P. Jelle and C. Breivik. “The Path to the Building Integrated Photovoltaics of Tomorrow”. In: *Energy Procedia* 20 (2012). chp2.3, pp. 78–87 (cit. on p. 17).

[23] R. Baetens et al. “Vacuum insulation panels for building applications: A review and beyond”. In: *Energy and Buildings* 42.2 (2010). chp2.3, pp. 147–172 (cit. on p. 18).

[24] R. Baetens, B. P. Jelle, and A. Gustavsen. "Properties, requirements and possibilities of smart windows for dynamic daylight and solar energy control in buildings: A state-of-the-art review". In: *Solar Energy Materials and Solar Cells* 94.2 (2010). chp2.3, pp. 87–105 (cit. on p. 18).

[25] R. Baetens, B. P. Jelle, and A. Gustavsen. "Aerogel insulation for building applications: A state-of-the-art review". In: *Energy and Buildings* 43.4 (2011). chp2.3, pp. 761–769 (cit. on p. 18).

[26] T. Gao et al. "Monodisperse Hollow Silica Nanospheres for Nano Insulation Materials: Synthesis, Characterization and Life Cycle Assessment". In: *ACS Applied Materials and Interfaces* 5.3 (2013). chp2.3, pp. 761–767 (cit. on p. 18).

[27] B. Jelle, A. Gustavsen, and R. Baetens. "The path to the high performance thermal building insulation materials and solutions of tomorrow". In: *Journal of Building Physics* 34.2 (2010). chp2.3, pp. 99–123 (cit. on p. 18).

[28] B. P. Jelle. "Traditional, state-of-the-art and future thermal building insulation materials and solutions - Properties, requirements and possibilities". In: *Energy and Buildings* 43.10 (2011). chp2.3, pp. 2549–2563 (cit. on p. 18).

[29] S. E. Kalnaes and B. P. Jelle. "Vacuum insulation panel products: A state-of-the-art review and future research pathways". In: *Applied Energy* 116 (2014). chp2.3, pp. 355–375 (cit. on p. 18).

[30] S. L. et al. "Synthesis of Hollow Silica Nanospheres by Sacrificial Polystyrene Templates for Thermal Insulation Applications". In: *Advances in Materials Science and Engineering* (2013). chp2.3, pp. 1–6 (cit. on p. 18).

[31] T. M.J. "Vacuum Insulation Panels Applied in Building Constructions". chp2.3. PhD thesis. Technische Universiteit Delft, 2010 (cit. on p. 18).

[32] F. Agyenim et al. "A review of materials, heat transfer and phase change problem formulation for latent heat thermal energy storage systems (LHTESS)". In: *Renewable and Sustainable Energy Reviews* 14.2 (2010). chp2.3, pp. 615–628 (cit. on p. 18).

[33] S. N. AL-Saadi and Z. Zhai. "Modeling phase change materials embedded in building enclosure: A review". In: *Renewable and Sustainable Energy Reviews* 21 (2013). chp2.3, pp. 659–673 (cit. on p. 18).

[34] R. Baetens, B. P. Jelle, and A. Gustavsen. "Phase change materials for building applications: A state-of-the-art review". In: *Energy and Buildings* 42.9 (2010). chp2.3, pp. 1361–1368 (cit. on pp. 18, 21).

[35] L. F. Cabeza et al. "Materials used as PCM in thermal energy storage in buildings: A review". In: *Renewable and Sustainable Energy Reviews* 15.3 (2011), pp. 1675–1695 (cit. on pp. 18, 23).

[36] A. M. Khudhair and M. M. Farid. “A review on energy conservation in building applications with thermal storage by latent heat using phase change materials”. In: *Energy Conversion and Management* 45.2 (2004). chp2.3, pp. 263–275 (cit. on p. 18).

[37] F. Kuznik et al. “A review on phase change materials integrated in building walls”. In: *Renewable and Sustainable Energy Reviews* 15.1 (2011). chp2.3, pp. 379–391 (cit. on p. 18).

[38] S. A. Memon. “Phase change materials integrated in building walls: A state of the art review”. In: *Renewable and Sustainable Energy Reviews* 31 (2014). chp2.3, pp. 870–906 (cit. on p. 18).

[39] E. Osterman et al. “Review of PCM based cooling technologies for buildings”. In: *Energy and Buildings* 49 (2012). chp2.3, pp. 37–49 (cit. on p. 18).

[40] M. Pomianowski, P. Heiselberg, and Y. Zhang. “Review of thermal energy storage technologies based on PCM application in buildings”. In: *Energy and Buildings* 67 (2013). chp2.3, pp. 56–69 (cit. on p. 18).

[41] N. Soares et al. “Review of passive PCM latent heat thermal energy storage systems towards buildings’ energy efficiency”. In: *Energy and Buildings* 59 (2013). chp2.3, pp. 82–103 (cit. on p. 18).

[42] P. Tatsidjodoung, N. L. Pierres, and L. Luo. “A review of potential materials for thermal energy storage in building applications”. In: *Renewable and Sustainable Energy Reviews* 18 (2013). chp2.3, pp. 327–349 (cit. on p. 18).

[43] A. Waqas and Z. U. Din. “Phase change material (PCM) storage for free cooling of buildings—A review”. In: *Renewable and Sustainable Energy Reviews* 18 (2013). chp2.3, pp. 607–625 (cit. on p. 18).

[44] D. Zhou, Y. Tian, and C. Y. Zhao. “Review on thermal energy storage with phase change materials (PCMs) in building applications”. In: *Applied Energy* 92 (2012). chp2.3, pp. 593–605 (cit. on pp. 18, 19).

[45] Z. N., M. Z., and W. S. “Dynamic characteristics and energy performance of buildings using phase change materials: A review”. In: *Energy Conversion and Management* 50.12 (2009). chp2.3, pp. 3169–3181 (cit. on p. 18).

[46] T.-C. Ling and C.-S. Poon. “Use of phase change materials for thermal energy storage in concrete: An overview”. In: *Construction and Building Materials* 46 (2016). chp2.3, pp. 55–62 (cit. on p. 18).

[47] F. Kuznik, J. Virgone, and J.-J. Roux. “Energetic efficiency of room wall containing PCM wallboard: A full-scale experimental investigation”. In: *Energy and Buildings* 40.2 (2008). chp2.3, pp. 148–156 (cit. on p. 18).

[48] J. Schröder and K. Gawron. “Latent heat storage”. In: *International Journal of Energy Research* 5.2 (1981). chp2.3, pp. 103–109 (cit. on p. 19).

[49] D. J. *Latent Heat Storage in Concrete*. Technische Universitat Kaiserslautern. chp2.3. 2008 (cit. on pp. 19, 20).

[50] M. K. Rathod and J. Banerjee. "Thermal stability of phase change materials used in latent heat energy storage systems: A review". In: *Renewable and Sustainable Energy Reviews* 18 (2013). chp2.3, pp. 246–258 (cit. on p. 20).

[51] B. D and S. RL. "On thermal energy storage and energy conversion". In: chp2.3. 1994 (cit. on pp. 21, 23, 25, 26).

[52] E. Conversion and Management. "A review on phase change energy storage: materials and applications". In: *Energy Conversion and Management* 45.9 (2004). chp2.3, pp. 1597–1615 (cit. on pp. 21, 22).

[53] S. M. Hasnain. "Review on sustainable thermal energy storage technologies, Part I: heat storage materials and techniques". In: *Energy Conversion and Management* 39.11 (1998). chp2.3, pp. 1127–1138 (cit. on p. 21).

[54] A. Sharma et al. "Review on thermal energy storage with phase change materials and applications". In: *Renewable and Sustainable Energy Reviews* 13.2 (2009). chp2.3, pp. 318–345 (cit. on pp. 22, 23).

[55] S. E. Kalnaes and B. P. Jelle. "Phase change materials and products for building applications: A state-of-the-art review and future research opportunities". In: *Energy and Buildings* 94 (2015). chp2.3, pp. 150–176 (cit. on pp. 22, 24, 26, 28, 30–33).

[56] M. H. and C. L. *Heat and cold storage with PCM*. chp2.3. Springer, 2008 (cit. on p. 23).

[57] D. JA. *The Analytical Chemistry Handbook*. chp2.3. McGraw Hill, Inc., 1995 (cit. on p. 23).

[58] D. Buddhi et al. "A simplification of the differential thermal analysis method to determine the latent heat of fusion of phase change materials". In: *Journal of Physics D: Applied Physics* 20.12 (1987). chp2.3 (cit. on p. 23).

[59] Z. Zhang et al. "Preparation and thermal energy storage properties of paraffin/expanded graphite composite phase change material". In: *Applied Energy* 91.1 (2012). chp2.3, pp. 426–431 (cit. on p. 23).

[60] Z. Y. and J. Y. "A simple method, the T-history method, of determining the heat of fusion, specific heat and thermal conductivity of phase-change materials". In: *Measurement Science and Technology* (1999). chp2.3 (cit. on p. 23).

[61] J. H. Peck et al. "A study of accurate latent heat measurement for a PCM with a low melting temperature using T-history method". In: *International Journal of Refrigeration* 29.7 (2006). chp2.3, pp. 1225–1232 (cit. on p. 23).

[62] A. F. Regin, S. C. Solanki, and J. S. Saini. "Heat transfer characteristics of thermal energy storage system using PCM capsules: A review". In: *Renewable and Sustainable Energy Reviews* 12.9 (2008). chp2.3, pp. 2438–2458 (cit. on p. 23).

[63] D. Feldman, M. A. Khan, and D. Banu. "Energy storage composite with an organic PCM". In: *Solar Energy Materials* 18.6 (1989). chp2.3, pp. 333–341 (cit. on pp. 24, 25).

[64] D. Feldman et al. "Fatty acids and their mixtures as phase-change materials for thermal energy storage". In: *Solar Energy Materials* 18.3 (1989). chp2.3, pp. 201–216 (cit. on pp. 24, 25).

[65] G. Lane. *Phase change thermal storage materials, Hand Book of Thermal Design*. chp2.3. McGraw Hill Book Co., 1989 (cit. on p. 24).

[66] A. Sarı, H. Sarı, and A. Önal. "Thermal properties and thermal reliability of eutectic mixtures of some fatty acids as latent heat storage materials". In: *Energy Conversion and Management* 45.3 (2004). chp2.3, pp. 365–376 (cit. on p. 24).

[67] L. Shilei, Z. Neng, and F. Guohui. "Eutectic mixtures of capric acid and lauric acid applied in building wallboards for heat energy storage". In: *Energy and Buildings* 38.6 (2006). chp2.3, pp. 708–711 (cit. on p. 24).

[68] L. GA and R. HE. "Encapsulation of heat of fusion storage materials." In: *In: Proceedings of the second southeastern conference on application of solar energy*. chp2.3. 1976 (cit. on p. 25).

[69] T. M. "Thermal storage for solar heating and cooling". In: *In: Proceedings of the workshop on solar energy storage sub-systems for heating and cooling of buildings*. chp2.3. 1975 (cit. on p. 25).

[70] A. Rudd. "Phase-Change Material Wallboard for Distributed Thermal Storage in Buildings". In: *ASHRAE Transactions* 99.2 (1993). chp2.3, pp. 339–346 (cit. on p. 25).

[71] D. Feldman and D. Banu. "DSC analysis for the evaluation of an energy storing wallboard". In: *Thermochimica Acta* 272.1-2 (1996). chp2.3, pp. 243–251 (cit. on p. 25).

[72] A. K. Athienitis et al. "Investigation of the thermal performance of a passive solar test-room with wall latent heat storage". In: *Building and Environment* 32.5 (1997). chp2.3, pp. 405–410 (cit. on p. 25).

[73] T. Stovall and J. Tomlinson. "What are the potential benefits of including latent storage in common wallboard?" In: *Journal of Solar Energy Engineering* 117 (2008). chp2.3, pp. 318–325 (cit. on p. 25).

[74] D. R. Biswas. "Thermal energy storage using sodium sulfate decahydrate and water". In: *Solar Energy* 19.1 (1977). chp2.3, pp. 99–100 (cit. on p. 25).

[75] B. Carlsson, H. Stymne, and G. Wettermark. "An incongruent heat-of-fusion system—CaCl 2 · 6H 2 O—Made congruent through modification of the chemical composition of the system". In: *Solar Energy* 23.4 (1979). chp2.3, pp. 343–350 (cit. on pp. 25, 26).

[76] A. V and S. A. D. "Mathematical modeling of melting and freezing process". In: *Washington, DC: Hemisphere Publishing Corporation* (1992). chp2.3 (cit. on p. 26).

[77] F. S. "Heat storage units using a salt hydrate as storage medium based on the extra water principle". In: *Technical University of Denmark* (1982). chp2.3 (cit. on p. 26).

[78] N. Shukla, A. Fallahi, and J. Kosny. "Performance characterization of PCM impregnated gypsum board for building applications". In: *Energy Procedia* 30 (2012). chp2.3, pp. 370–379 (cit. on p. 26).

[79] P. M. et al. "A new experimental method to determine specific heat capacity of inhomogeneous concrete material with incorporated microencapsulated-PCM". In: *Cement and Concrete Research* 55 (2014). chp2.3, pp. 22–34 (cit. on p. 27).

[80] J. Kosny. *Opportunities to apply phase change materials to building enclosures in: Building America: Introduction.* PP-Presentation, Cambridge, MA,USA. chp2.3. Nov. 2011 (cit. on p. 27).

[81] N. Soares et al. "Thermophysical characterization of paraffin-based PCMs for low temperature thermal energy storage applications for buildings". In: *Energy* (2023), p. 126745. ISSN: 0360-5442. DOI: https://doi.org/10.1016/j.energy.2023.126745. URL: https://www.sciencedirect.com/science/article/pii/S0360544223001391 (cit. on p. 27).

[82] B. P. Jelle. "Accelerated climate ageing of building materials, components and structures in the laboratory". In: *Journal of Materials Science* 47.18 (2012). chp2.3, pp. 6475–6496 (cit. on p. 28).

[83] B. Jelle et al. "Robustness classification of materials, assemblies and buildings". In: *Journal of Building Physics* 37 (2013). chp2.3, pp. 213–245 (cit. on p. 28).

[84] B. Zalba et al. "Free-cooling of buildings with phase change materials". In: *International Journal of Refrigeration* 27.8 (2004). chp2.3, International Journal of Refrigeration (cit. on p. 28).

[85] H. C.K. and B. Robert. "Modeling of phase change material peak load shifting". In: *Energy and Buildings* 39 (2007). chp2.3 (cit. on p. 28).

[86] Y. Sun et al. "Peak load shifting control using different cold thermal energy storage facilities in commercial buildings: A review". In: *Energy Conversion and Management* 71 (2013). chp2.3, pp. 101–114 (cit. on p. 28).

[87] Tate. *EcoCore*. Dec. 2013. URL: http://www.tateinc.com/products/ecocore.aspx (cit. on p. 29).

[88] L. Lan, P. Wargocki, and Z. Lian. "Quantitative measurement of productivity loss due to thermal discomfort". In: *Energy and Buildings* 43.5 (2011). chp2.3, pp. 1057–1062 (cit. on p. 29).

[89] O. A. Seppanen and W. Fisk. "Some Quantitative Relations between Indoor Environmental Quality and Work Performance or Health". In: *HVAC and Research* 12.4 (2006). chp2.3, pp. 957–973 (cit. on p. 29).

[90] E. Shaw. "Thermal Comfort: analysis and applications in environmental engineering, by P. O. Fanger. 244 pp. DANISH TECHNICAL PRESS. Copenhagen, Denmark, 1970. Danish Kr. 76, 50". en. In: *Royal Society of Health Journal* 92.3 (June 1972), pp. 164–164. ISSN: 0035-9130. DOI: 10.1177/146642407209200337. URL: http://journals.sagepub.com/doi/10.1177/146642407209200337 (visited on 01/23/2023) (cit. on pp. 29, 30).

[91] *ANSI/ASHRAE Standard 55-2013: Thermal Environmental Conditions for Human Occupancy*. ASHRAE standard. ASHRAE, 2013. URL: https://books.google.pt/books?id=AGxFjwEACAAJ (cit. on p. 30).

[92] Q. Al-Yasiri and M. Szabó. "Incorporation of phase change materials into building envelope for thermal comfort and energy saving: A comprehensive analysis". In: *Journal of Building Engineering* 36 (2021), p. 102122. ISSN: 2352-7102. DOI: https://doi.org/10.1016/j.jobe.2020.102122. URL: https://www.sciencedirect.com/science/article/pii/S2352710220337542 (cit. on p. 31).

[93] L. Georgiou et al. "Numerical and environmental analysis of post constructive application of PCM coatings for the improvement of the energy performance of building structures". In: *Construction and Building Materials* 364 (2023), p. 129984. ISSN: 0950-0618. DOI: https://doi.org/10.1016/j.conbuildmat.2022.129984. URL: https://www.sciencedirect.com/science/article/pii/S0950061822036406 (cit. on p. 31).

[94] R. Ansuini et al. "Radiant floors integrated with PCM for indoor temperature control". In: *Energy and Buildings* 43.11 (2011). chp2.3, pp. 3019–3026 (cit. on p. 31).

[95] H. Babaei, J. M. Khodadadi, and P. Keblinski. "Improvement in thermal conductivity of paraffin by adding high aspect-ratio carbon-based nano-fillers". In: *Physics Letters A* 377.19 (2013). chp2.3, pp. 1358–1361 (cit. on p. 32).

[96] G. Evola, L. Marletta, and F. Sicurella. "A methodology for investigating the effectiveness of PCM wallboards for summer thermal comfort in buildings". In: *Building and Environment* 56 (2013). chp2.3, pp. 517–527 (cit. on p. 32).

[97] L. Fan and J. M. Khodadadi. "Thermal conductivity enhancement of phase change materials for thermal energy storage: A review". In: *Renewable and Sustainable Energy Reviews* 15.1 (2011). chp2.3, pp. 24–46 (cit. on p. 32).

[98] J. P. et al. “Improvement of the thermal conductivity of a phase change material by the functionalized carbon nanotubes”. In: *Chemical Engineering Science* 81 (2012). chp2.3, pp. 140–145 (cit. on p. 32).

[99] J. J. et al. “Preparation and performances of bulk porous Al foams impregnated with phase-change-materials for thermal storage”. In: *Progress in Natural Science: Materials International* 22 (2012). chp2.3, pp. 440–444 (cit. on p. 32).

[100] J.-l. SONG et al. “Thermophysical properties of high-density graphite foams and their paraffin composites”. In: *New Carbon Materials* 27.1 (2012). chp2.3, pp. 27–34 (cit. on p. 32).

[101] S. Yu et al. “Bio-based PCM/carbon nanomaterials composites with enhanced thermal conductivity”. In: *Solar Energy Materials and Solar Cells* 120 (2014). chp2.3, pp. 549–554 (cit. on p. 32).

[102] Y. Zhong et al. “Heat transfer enhancement of paraffin wax using graphite foam for thermal energy storage”. In: *Solar Energy Materials and Solar Cells* 94.6 (2010). chp2.3, pp. 1011–1014 (cit. on p. 32).

[103] M. M. Sedeh and J. M. Khodadadi. “Thermal conductivity improvement of phase change materials/graphite foam composites”. In: *Carbon* 60 (2013). chp2.3, pp. 117–128 (cit. on p. 32).

[104] N. K., N. T., and M. P. “A review on fire protection for phase change materials in building applications”. In: chp2.3. Taylor and Francis Group, 2012. Chap. From Materials to Structures: Advancement Through Innovation (cit. on p. 32).

[105] F. Ascione et al. “Energy refurbishment of existing buildings through the use of phase change materials: Energy savings and indoor comfort in the cooling season”. In: *Applied Energy* 113 (2014). chp2.3, pp. 990–1007 (cit. on p. 33).

[106] J. Kosny, N. Shukla, and A. Fallahi. *Cost Analysis of Simple Phase Change Material-Enhanced Building Envelopes in Southern U.S. Climates*. chp2.3. U.S. Department of Energy. Jan. 2013 (cit. on p. 33).

[107] A. Pasupathy and R. Velraj. “Effect of double layer phase change material in building roof for year round thermal management”. In: *Energy and Buildings* 40.3 (2008). chp2.3, pp. 193–203 (cit. on p. 33).

[108] A. Corp. *ANSYS Fluent Theory Guide, Release 17.1*. chp3 math. AnSys Corp., 2017 (cit. on pp. 34, 39, 42, 43, 45).

[109] G. K. Batchelor. *An Introduction to Fluid Dynamics*. chp3 math. Cambridge Univ.Press. Cambridge, England, 1967 (cit. on p. 35).

[110] D. K. Walters and D. Cokljat. “A three-equation eddy-viscosity model for reynolds-averaged navier-stokes simulations of transitional flows”. In: *Journal of Fluids Engineering* 130 (2008). chp3 math (cit. on pp. 35, 39).

[111] B. E. Launder and D. B. Spalding. *Lectures in Mathematical Models of Turbulence*. chp3 math. Academic Press, London, England, 1972 (cit. on pp. 40, 41).

[112] V. Yakhot and S. A. Orszag. "Renormalization Group Analysis of Turbulence I Basic Theory". In: *Journal of Scientific Computing* (1986). chp3 math (cit. on p. 40).

[113] T. Shih et al. "A New k-epsilon Eddy-Viscosity Model for High Reynolds Number Turbulent Flows - Model Development and Validation". In: *Computers Fluids* 24.3 (1995). chp3 math, pp. 227–238 (cit. on pp. 40, 42).

[114] H. K. Versteeg and W. Malalasekera. *An Introduction to Computational Fluid Dynamics, THE FINITE VOLUME METHOD, 2ed*. chp4.1. Pearson, 2007 (cit. on pp. 40, 45, 47, 61).

[115] . A. Orszag et al. "Renormalization Group Modeling and Turbulence Simulations". In: *In International Conference on Near- Wall Turbulent Flows, Tempe, Arizona*. chp3 math. 1993 (cit. on p. 41).

[116] B. J. *Theorie de lecoulement tourbillonnant et tumultueux des liquides dans les lits rectilignes a grande section*. chp3-math. Gauthier-Villars et fils, 1897 (cit. on p. 43).

[117] T. L. Bergman, A. S. Lavine, and F. P. Incropera. *Fundamentals of Heat and Mass Transfer*. eng. 7th ed. OCLC: 958564570. Somerset: Wiley, 2011. ISBN: 9781118137253 (cit. on p. 44).

[118] V. R. Voller. *Modeling Solidification Processes*. Tech. rep. chp3 math. CAAmerican Metallurgical Society, 1987 (cit. on p. 45).

[119] V. R. Voller and C. Prakash. "A Fixed-Grid Numerical Modeling Methodology for Convection-Diffusion Mushy Region Phase-Change Problems". In: *Int. J. Heat Mass Transfer* 30 (1987). chp3 math, pp. 1709–1720 (cit. on p. 45).

[120] V. R. Voller and C. R. Swaminathan. "Generalized Source-Based Method for Solidification Phase Change". In: *Heat Transfer B* 19.2 (1991), pp. 175–189 (cit. on p. 46).

[121] AnsysCorp. *ANSYS FLUENT User's Guide, Release 13.0*. chp4. Ansys Corp, 2012 (cit. on pp. 48, 49, 60, 64, 65, 67–69, 72–74).

[122] M. K. Koukou et al. "Experimental and computational investigation of a latent heat energy storage system with a staggered heat exchanger for various phase change materials". In: *Thermal Science and Engineering Progress* 7 (2018). chp5, pp. 87–98 (cit. on pp. 54, 109–111, 114, 121, 122).

[123] T. J. Barth and D. Jespersen. *The design and application of upwind schemes on unstructured meshes*. Tech. rep. chp4. Aerospace Sciences Meeting, 1989 (cit. on pp. 64, 74).

[124] A. Corp. *Transition Flow*. 2017. URL: https://www.sharcnet.ca/Software/Ansys/17.0/en-us/help/flu_ug/flu_ug_sec_turb_rans.html (cit. on p. 113).

[125] N. Tay, M. Belusko, and F. Bruno. "An effectiveness-NTU technique for characterising tube-in-tank phase change thermal energy storage systems". en. In: *Applied Energy* 91.1 (Mar. 2012), pp. 309–319. ISSN: 03062619. DOI: 10.1016/j.apenergy.2011.09.039. URL: https://linkinghub.elsevier.com/retrieve/pii/S0306261911006441 (visited on 01/20/2023) (cit. on p. 126).

[126] W. Yang et al. "Experimental and numerical investigations on the thermal performance of a borehole ground heat exchanger with PCM backfill". In: *Energy* 174 (2019). chp5, pp. 216–235 (cit. on p. 144).

I

Annex 1 - Scientific production

During the course of this PhD three articles were authored or co-authored by the candidate in two peer-reviewed publications. Furthermore, the author participated in several national and international oral presentations showcasing the results of the work developed so far as well as working in international projects within the scope of the thesis. With the theoretical models and methodology presented in this work, the same methods were employed in the development of a heat exchanger and energy storage apparatus for food processing, the work for which is part of the academic work developed in this thesis

I.1 Peer-reviewed publications

- C. Simão, J. Murta-Pina, **J. Pássaro**, L. Coelho, R. Lopes, F. Reboredo, T. Jorge, D. Lemos; Prospects for the Improvement of Energy Performance in Agroindustry Using Phase Change Materials; Springer 2021.
  (https://doi.org/10.1007/978-3-030-45124-0_26)

- **J. Pássaro**, A. Rebola, L. Coelho, J. Conde, G.A. Evangelakis, C. Prouskas, D.G. Papageorgiou, A. Zisopoulou, I.E. Lagaris; Effect of fins and nanoparticles in the discharge performance of PCM thermal storage system with a multi passages finned tube heat exchanger; Applied Thermal Engineering; 2022.
  (https://doi.org/10.1016/j.applthermaleng.2022.118569)

- C. Simão, J. Murta-Pina, J. Oliveira, **J. Pássaro**, L. Coelho, D. Ferreira, F. Reboredo, T. Jorge P. Figueiredo; A Case Study for Decentralized Heat Storage Solutions in the Agroindustry Sector Using Phase Change Materials; AgriEngineering 2022.
  (https://doi.org/10.3390/agriengineering4010018)

- **J. Pássaro**, A. Rebola, L. Coelho, J. Conde; Numeric Study of Geothermal Borehole Heat Exchanger Enhancement via Phase Change Material Macro Encapsulation; International Journal of Thermofluids, Part of special issue: Sustainable Energy and

Environmental Protection 2021.
(https://doi.org/10.1016/j.ijft.2022.100245)

I.2 Oral presentations

- "Semana da Engenharia Mecânica", Novembro 2021, EST-IPS, Setúbal, Portugal **Regional Event. - Online**
- "Semana da Engenharia Mecânica", Novembro 2020, EST-IPS, Setúbal, Portugal **Regional Event. - Online**
- "Semana da Engenharia Mecânica", Novembro 2019, EST-IPS, Setúbal, Portugal **Regional Event.**
- "The TESSe2b project: Thermal Energy Storage Systems for Energy Efficient Buildings" and "Presentation of the SCORES Project (H2020)", 8th TESSe2b project workshop, 18th September of 2019, Anfiteatro 2, ESTSetúbal/IPS, Setúbal, Portugal. **International Event.**
- "The TESSe2b project: Thermal Energy Storage Systems for Energy Efficient Buildings" and "Presentation of the SCORES Project (H2020)", 7th TESSe2b project workshop, 12th June 2019, Hotel Gromada, Plac Powstańców Warszawy, Poland. **International Event.**
- "The TESSe2b project: Thermal Energy Storage Systems for Energy Efficient Buildings" and "Presentation of the SCORES Project (H2020)", 6th TESSe2b project workshop, 10th April 2019, Hotel Europa, Graz, Austria. **International Event.**
- "The TESSe2b project: Thermal Energy Storage Systems for Energy Efficient Buildings" and "Presentation of the SCORES Project (H2020)", 5th TESSe2b project workshop, 24th January 2019, Room C10, Second Floor, Sustainable Research Building, University of Nottingham, U.K. **International Event.**

I.3 Participation in international and national research projects

- TESSe2b project - Thermal Energy Storage Systems for Energy Efficient Buildings. An integrated solution for residential building energy storage by solar and geothermal resources, Horizon 2020, Grant agreement ID: 680555.
- SCORES project - Self Consumption Of Renewable Energy by hybrid Storage systems, Horizon 2020, Grant agreement ID: 766464.
- CFD4CHEESE - Application of computational fluid dynamics in the optimization of traditional cheeses ripening conditions; Portugal 2020.